Fall 12-1-2020

Practical Adhesion Measurements in Organic Coatings; Advancing Understanding and Mechanical Methods Development

Diana Gottschalk

PRACTICAL ADHESION MEASUREMENTS IN ORGANIC COATINGS; ADVANCING UNDERSTANDING AND MECHANICAL METHODS DEVELOPMENT

by

Diana Gottschalk

A Dissertation
Submitted to the Graduate School,
the College of Arts and Sciences
and the School of Polymer Science and Engineering
at The University of Southern Mississippi
in Partial Fulfillment of the Requirements
for the Degree of Doctor of Philosophy

Approved by:

Dr. James W. Rawlins, Committee Chair
Dr. Derek L. Patton
Dr. Sergei I. Nazarenko
Dr. Robson F. Storey
Dr. Robert Y. Lochhead

December 2020

Published by the Graduate School

ABSTRACT

"Adhesion" can be considered either a mechanical or chemical phenomenon. The mechanical interpretation describes the difficulty of separating surfaces and is useful for quantifying performance within applications that depend on bulk and interfacial properties. Chemical adhesion describes interfacial resistance to chemical attack and does not depend on bulk properties. Predicting chemical failure through mechanical measurement is confounded by the influence of bulk properties. However, the prospect is attractive because of the robust tolerance for sample geometries, allowing experiments to resemble an end-use system. The present work's primary goal was to elevate mechanical methods to provide a detailed interfacial characterization of industrially relevant samples.

Bulk mechanical property effects on 90° peel tests were addressed by leveraging mechanical properties' predictability relative to the T_g. Characterization of peel forces of three epoxy-amine coatings with various T_gs at four test temperatures demonstrated the extent of the temperature dependence of adhesion. Framing the results relative to each coating's T_g uncovered a universal peel force maximum at T_g-20°C and identified that chain mobility is as vital to interfacial strength as functional group compatibility.

Pull-off adhesion results can be difficult to interpret from the minimal information provided by peak stress values. One quantity represents the entire pull-off testing procedure. Performing pull-off on a load frame provides stress-strain curves with each pull to describe how a coating responds to the tensile load and what defects are present that can lead to peak stress data sets with high variation. This analysis technique was applied to deciding on an appropriate adhesive and scoring method for the present coating-substrate system.

Predicting adhesion is an important step toward predicting coating performance. A model describing pull-off peak stress as a function of coating thickness was found to be inaccurate for a number of literature examples. A critical modulus was defined where coating film yielding occurred at lower stresses than interfacial failure leading to increases in pull-off peak stress with thickness, in contrast to predictions. Similar effects were induced through solvent trapping. These findings are essential for defining relationships between mechanical test results and interfacial parameters to understand coating performance.

ACKNOWLEDGMENTS

I am profoundly grateful for all those who never stopped believing in me. From Dr. Rawlins for being my advisor and providing the environment and endless opportunities for growth, but also for seeing ambition and tenacity through the former Ph.D. drop-out. To my ever-changing committee of Dr. Daniel Savin, Dr. Paige Buchanan, Dr. Sergei Nazarenko, Dr. Derek Patton, Dr. Robert Lochhead, and Dr. Robson Storey, for their flexibility and integrity over this extended journey.

To all members of the Thames-Rawlins Research Group, whose contributions big and small were greatly appreciated. Most importantly are the present members, who have been a part of my graduate career the longest. Richard Ferguson, who has been an unparalleled supervisor and is most responsible for what my project became and the current prevalence of pull-off methods in the group. Dr. Dwaine Braasch for training my eye for detail and how to overcome experimental hurdles. Michael Blanton for being the most patient person on Earth. Dr. Ethem Kaya for being the perfect lab-mate. Dr. Eric Williams for always being honest and helpful. And the fellow graduate students Mark Early, Jessica Davison, and Chris Scanlon, who have lifted me up more times than I can count and have been truly inspirational coworkers.

I want to acknowledge my first-year class because however small and strange it was, it included my biggest allies, Steven Wand and Vivek Vasagar, who have gone on to be very successful and have been integral to my own achievements. I also could not have gotten this far without my undergrads and high schoolers. Sam Lucas, John-Gabe Robinson, Russell Vick, Lucia Lang, Cody Shaw, and Peyton Warren collected much of this data and much more, which I hope to highlight in future work.

Finally, I want to acknowledge the funding that made this research possible. The United States Air Force Academy (FA7000-10-2-0014, FA7000-12-2-0016, and FA7000-13-2-0022) through funding by the Department of Defense and collaborative efforts for Corrosion Prevention and Understanding via the Technical Corrosion Collaboration working group comprised of The University of Virginia, The University of Hawaii, The Ohio State University, the Air Force Academy, The University of Akron, The University of Southern Mississippi, the Air Force Institute of Technology, the Naval Postgraduate School, and the US Naval Academy. Additionally, the NSF research traineeship INTERFACE program (Award DGE-1449999)

DEDICATION

To Brad & Cathie Gottschalk, and Bobby Wilson.

My victories are their victories.

TABLE OF CONTENTS

LIST OF TABLES

LIST OF ILLUSTRATIONS

CHAPTER I – MOTIVATION AND BACKGROUND

1.1 Motivation

Adhesion has been considered important in all facets of decorative, protective, and functional polymer-based coatings technology. Unfortunately, current scientific understanding and quantification of why, how, and when adhesion is attained, retained, and lost during the service life of a given coating or coating system remains poor. Adhesion has to perform the basic function of keeping the coating-substrate system together and holding pigments, fillers, and additives in place to perform their functions, and yet, adhesion also has been shown to play a critical role with respect to corrosion resistance[1–5] and durability.[6] In consumer and industrial use cases, it is tempting to formulate and engineer coatings based solely on the function of the bulk. For example, designing the film to achieve a desired hardness, permeability, or appearance ignores the performance of the substrate interface. Using such an approach relegates adhesion to an afterthought and simply meeting the minimal criteria of supporting its own weight. Coating design that excludes adhesion is costly in the long term and neglects the active role the interface can plan in protection and performance retention. Studying and understanding the adhesion is important to better predict performance and design interfaces. The ability of a film to resist interfacial hydrolysis is expected to correlate with corrosion protection, but many coating environments are dynamic, experiencing a range of temperatures and relative humidity, making interfacial toughness hard to rate and compare. What's more, the interfacial criteria to minimize hydrolysis is largely unknown. Polar and acid-base interactions form strong bonds between the functional groups on polymers and substrates, but water could potentially form stronger interactions

between both moieties. As a result, there is a debate surrounding the importance of interfacial interaction strength over high molecular levels of interfacial conformity in resisting hydrolysis. Our research was motivated by the need to establish more quantifiable interfacial structure-property and property-performance relationships for protective organic coatings. Adhesion measured at ambient laboratory conditions is considered to be the most commonly measured adhesion performance parameter and yet results in a limited layer of understanding. Consider that the same system and adhesion developed, retained, and lost in the wet state was often the primary mode to prevent the spread of corrosion. Wet adhesion has been shown to be much more complicated to predict and measure, especially when the wet state was simplistically defined. Wet adhesion is a function of environmental severity, and therefore, location, time, and season must be accurately reported to produce meaningful and generally useful adhesion data. Unfortunately, adhesion has been generally analyzed in an oversimplified and rudimentary way even though improved adhesion has been the primary goal of much research and development efforts. Findings from adhesion driven studies lose impact because questions like 'which type of adhesion,' 'under what conditions,' 'as measured by what methods' and 'on which substrate' along with other dependent variables such as thickness, degree of cure, number of layers and application method are not considered.

The simple, rapid, and most common adhesion test methods were developed mainly as *in situ* quality control checks and have become the industry standard for most surface coatings adhesion measurements. Within that context, adhesion measurement methods intended for in-use surface coatings must be practical, and yet we felt the need to further develop the basis for scientific understanding of the overall process of

attainment, retention, and loss of adhesion from polymeric materials enduring a variety of environmental conditions. A brief review of the most common methods was presented here to provide context for the subsequent research and results of our adhesion measurements.

The crosshatch tape test is the most widely employed adhesion testing method for protective and decorative coatings. Crosshatch adhesion testing is seen in both industrial settings,[7,8] as production qualification, and in scientific studies as the basis to discern between different combinations of raw materials, substrates, conditions, other variables, or systems.[9–14] The crosshatch test is performed by cutting a small array of squares into and through the coating, applying strong adhesive tape to the top side of the cut squares, and ripping the tape away.[15] Requiring almost no tools or instruments, the test's simplicity is the method's strength, and yet, this method has often been utilized in scholarly journals as the basis for understanding. At best, crosshatch adhesion results translate to adhesion attainment under limited very conditional specifics (number of squares missing after tape-peel, differences in adhesion of the tape to the top side of the coating, differences in adhesion on the basis of; cutting through the coating technique, coating thickness, coating degree of conversion, solvent, waxy surface modifications, topography, bulk differences, wetting and substrate preparation related variables, the timing of when testing was performed relative to when the film was applied, application method) and consistently lack depth towards gains in adhesion science. There is no way to ensure that any two executions of the method will be performed with the same force or peel angle, both of which affect force transferred to the interface, and the method is

inherently qualitative, making it a poor foundation for scientific gain or the basis for conclusions.

Other prolific methods of coating adhesion measurement are peel and pull-off. These methods offer superior analytical power over crosshatch by being quantitative, but the techniques have sub-standard connotations associated with them because of how collected adhesion values are shared without much appreciation for the underlying process and the associated dependent variables. There are many modifications that can be made to the performance of peel (rate, angle, geometry)[16–18] and pull-off (adhesive, dolly geometry, instrumentation)[19–21] experiments that have been demonstrated to affect the numerical outcome and yet are rarely disclosed alongside measurements in the literature. As a result, the literature is filled with data from peel and pull-off experiments whose variability and uncertainty render the results difficult to utilize as a foundation of knowledge. The lack of scientific adhesion characterization and poorly defined basic connectivity between literature results motivated the validation, promotion, and gain of scientific understanding of the relationships between raw material composition and interfacial strength and mechanical measurements of adhesion.

The cutting edge of coating science includes detailed methods, accurate instrumentation, high levels of inquiry, and detailed foundations for the variables which are important, independent, dependent, and interdependent. In the most recent issue of Progress in Organic Coatings, there are complex rheological and spectroscopic studies with detailed sample preparation, data analysis, and modeling.[22–24] Coating science as a whole is not struggling to modernize, but adhesion results are not receiving the same level of attention. Pull-off data reports a single peak pull-off stress for each applied

dolly, with little statistical much less in-depth mechanistic analysis and most often no consideration for the polymeric material's cure, physical state, residual solvent, or environmental conditions. There are discrepancies in the advancement between mechanical adhesion methods and other forms of coatings research. The central hypothesis of this dissertation was that by putting the adhesion mechanical testing methods through the same analytical rigor, the scientific community would gain a greater understanding of the process of adhesion attainment, retention, and loss that was and continues to be absent in the open literature during our inquiry and research.

1.2 Types of adhesion

Adhesion manifests on multiple size scales. The adhesion described in the context of thermodynamics (surface energies and sorption strength) is very different from adhesion at the macroscale. Adhesives and adhesive joints depend on both thermodynamic interfacial affinity between the adhesive material and the substrate and the mechanical properties required to maintain the bonds in response to external stimuli. Calling both phenomena "adhesion" is misleading to an outside observer and makes progress in adhesion science difficult from the outset. The difference in the dependent variables makes comparing conclusions between sub-disciplines misguided. Chemical and morphological changes to the coating that alter the interface will also alter the bulk, and a modification that improves joint durability will not necessarily equate to an improvement in cathodic delamination resistance. In reality, molecular affinity or chemical adhesion is only one of the variables involved in determining the difficulty of separating two surfaces; alternatively, the separation of surfaces can be referred to as practical adhesion.[25]

The protective ability of polymer-based coatings has been suggested to be rooted in good adhesion, and performance is suspected to directly correlate with the quality of a coating-substrate adhesive bond. Strong interactions between functional groups within the coating and substrate resist deadhesion by hydrolysis and subsequent substrate dissolution. To the same end of resisting corrosion, high packing in the interphase region increases the resistance to ion transfer across the substrate surface. It has been proposed by the author that poor correlation between adhesion measurements and corrosion typically occurs because of the contradiction between what was quantified in adhesion versus corrosion experiments. Intimate polymer to metal (primary or secondary) bonding drives corrosion resistance and protection from interfacial hydrolysis and cathodic delamination. Mechanical measurements of adhesion suffer from having no clear protocol for separating the effects of bulk properties and interfacial forces on the results. The complex relationship between mechanical results and coating properties allows for changes in bulk properties to be interpreted as changes in interfacial strength, thereby skewing the results. Scantlebury et al. sought to correlate wet adhesion with the interfacial performance by measuring pull-off adhesion and cathodic delamination rate of a single polymeric material and substrate while varying between different pretreatments. A silane treated system achieved high adhesion at all immersion times but demonstrated **low** resistance to cathodic delamination because silane films, albeit hydrolytically stable, were shown to have poor resistance to the pH changes that occur during cathodic delamination.[26] Pull-off experiments after exposure to a basic solution instead of deionized water would have shown a better correlation. Conversely, a phosphate treated substrate had poor adhesion but exceptional resistance to cathodic delamination. This

result demonstrates another issue with the way adhesion data are analyzed. The location of failure for phosphate samples after pull-off testing was at the pretreatment-coating interface, but corrosion acts on the pretreatment-substrate interface. Without considerations of these additional variables, the authors poorly described the system and conveyed inaccurate conclusions.

Researchers have utilized cohesive energy density (CED) calculations to calculate absolute or relative adhesion outcomes, and yet, the CED values alone have failed to predict differing results for corrosion protection. Clearly, the variables involved in establishing, retaining, losing, and possibly regaining adhesion through interfacial forces are extremely complex and change as a function of time, conditions, and the system's history. If a lower strength functional group (as defined by CED or pK_a/pK_b values) were able to achieve greater mobility and, in turn, substrate wetting at a molecular level, then the conceptually weaker material would conditionally result in better adhesion than a higher CED functional group. Additionally, thermoplastic and thermosetting polymer architectures have often been cited as possessing adhesion that is stronger or weaker depending upon the basis of the argument (a form of scientific convenience), and yet the basis of thinking has not resulted in any improvement in understanding of the true adhesion, substate, polymer, and environmental condition relationships.[2]

Practical adhesion is a function of the interfacial factors affecting chemical adhesion and mechanical adhesion, with influence from bulk coating properties like modulus. A review of the main variables involved in determining practical adhesion has been summarized in Figure 1.1. Currently, the known components of interfacial strength are adsorption or chemical attraction, mechanical adhesion, covalent bonding, and

interdiffusion. Interfacial strength benefits from substrate roughness, increasing surface area, and by extension, interaction density up to the point where it increases the distance between interfacial atoms, i.e., loss of conformity. Deformation of coating material in the process of a mechanical adhesion experiment can account for the discrepancy between interfacial strength and practical adhesion. A given coating system's deformability depends on variables such as coating mechanical properties, deformation rate, film thickness, and in the case of thermosetting materials, variables like the degree of conversion in advance of vitrification or % solvent trapped at vitrification. The complex interplay of many characteristics determines the difficulty of separating surfaces, which can't be predicted from intermolecular force data alone as of today. The ways bulk properties and mechanisms dictate the interfacial morphology has also been poorly addressed. All the different types of adhesion, adhesion failure, and adhesion testing ultimately convolute the science of adhesion.

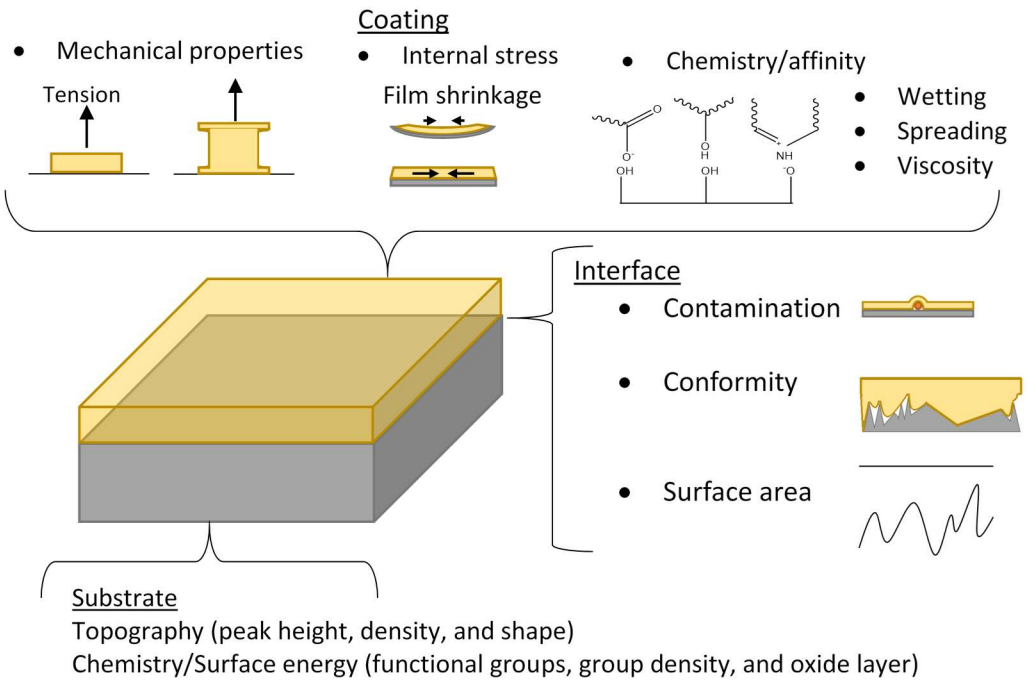

Figure 1.1 Factors affecting practical adhesion

1.3 Importance of mechanical measurement methods

Brute force methods like pull-off give rise to prejudices against mechanical techniques as being unscientific. Whereas spectroscopic and microscopic methods of probing adhesion and interfaces which require finesse and delicacy align them more readily with scientific inquiry.[27,28] Such inequality is a man-made bias and an unnecessary limitation; enough literature, mathematics, and knowledge surrounding mechanical engineering are available that mechanical-based adhesion testing methods should be considered and studied at the same level as, for example, electrochemical properties.

Practical adhesion measurements have value with respect to understanding failures resulting directly from mechanical forces experienced during use and towards understanding commercially relevant interfaces. Advancing the level of detail and

accuracy of measurements of interfacial variables traditionally requires simplification of the sample system. X-ray photoelectron spectroscopy (XPS) is a powerful method for determining atomic binding energies. The incident x-ray beam has a high penetration depth on the order of millimeters, but the photoelectrons generated by the x-rays can only travel through solid material for several nanometers before losing their kinetic energy.[29] Analysis of interfaces via XPS, therefore, requires an unrealistically thin coating that must be applied by obscure methods, and the results would not be directly applicable to most commercial protective coatings. In another example, coatings can be applied to the crystal of an attenuated total reflection (ATR) infrared spectrometer giving direct access to the interface without having to probe through the coating, but the interface that forms between an ATR diamond or ZnSe crystal is not relevant to the vast majority of interfaces encountered in practical coating systems. Finally, an industrially relevant interface can be accessed through cryofracture or cross-section microtoming and analyzed by atomic force microscopy, but the sample preparation required is extreme, prohibitive, and potentially damaging. In these cases, data collected on a simplified system must be extrapolated to a practical system. Having a measured quantity for molecule-substrate interaction or interfacial interaction density must then be extrapolated to macroscale coating-substrate interaction. It is not unreasonable to conclude that practical adhesion measurements resulting in complicated data on a full-scale system can be extrapolated to an interfacial attribute using material relationships and deliver meaningful chemical adhesion information.

1.4 Contradictions in practical adhesion literature

A problem plaguing the adhesion science community and the advancement of mechanical methods of adhesion measurement is inconsistencies in the literature. While contradictions can sometimes be accounted for by differences in methodologies among the studies, others highlight the incomplete picture of coating adhesion relationships. When studies find contradicting results, the reputation of the methodologies suffers instead of sparking interest in identifying the underlying phenomenon causing the contradiction.

Results obtained from pull-off tests performed with or without sectioning off the test area underneath the applied dolly could each be considered invalid as a direct result of contradictory reports. The thinking that cutting into the coating will interfere with and damage the interface resulting in erroneous adhesion measurements, is valid. However, ignoring the effect that keeping the coating intact has on the data is not the answer. Turunen found that if the area under the dolly is not isolated, then stress concentrates at the dolly interface instead of the substrate and is distributed through coating volume outside the area of interest.[30] Their method of isolating the test area by lithography is not an option for most coatings. No investigations have been made on how to overcome these difficulties, only dismissal and mounting distrust of the method.

One of the only attempts at predicting practical adhesion and applying a scientific approach to pull-off testing was made by Croll in 1980.[31] The relationships he defined between thickness and peel strength and pull-off stress can be seen in Figure 1.2 and Figure 1.3, respectively. The studies were motivated by research into internal stress present in coatings, and therefore the predictive equations relied very heavily on internal

stress. In examples of coatings where factors other than internal stress influence adhesion performance, the internal stress-driven relationship was not shown to be consistent. As shown in Figure 1.4, a ballast tank coating was shown to increase in peak pull-off stress from 12 MPa at 150 µm to 14.5 MPa at 1,000 µm.[32] The results were repeatable with and without scoring around the dolly to isolate the sample area. Applications of constant water immersion tend towards coatings with low moduli (less than 1 GPa), which is the case for most ballast tank coatings and implies yielding of the coating occurs within the pull-off test, causing increases in peak stress with thickness.

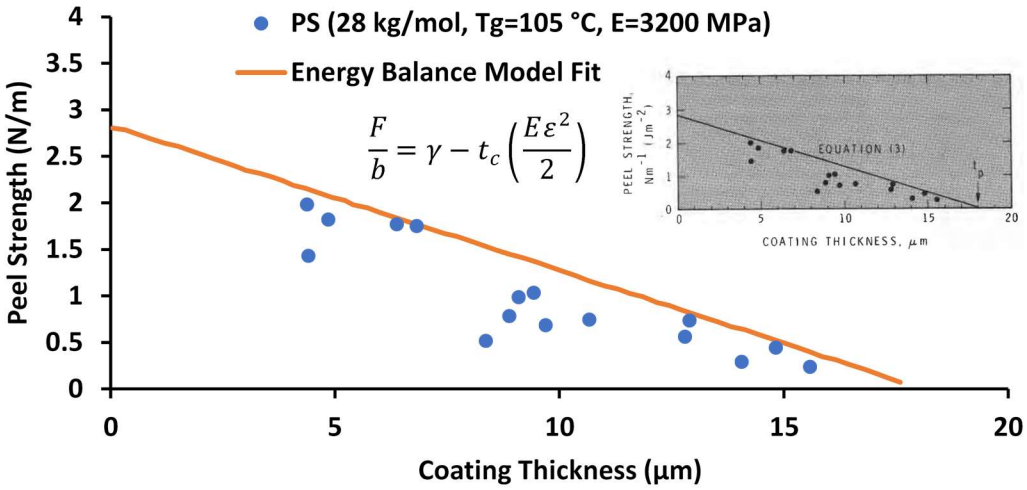

Figure 1.2 Peel strength of polystyrene (PS) modeled by the energy balance predictive equation

Films were applied by drawdown at 10 wt% solids in toluene and dried for 2-3 weeks.

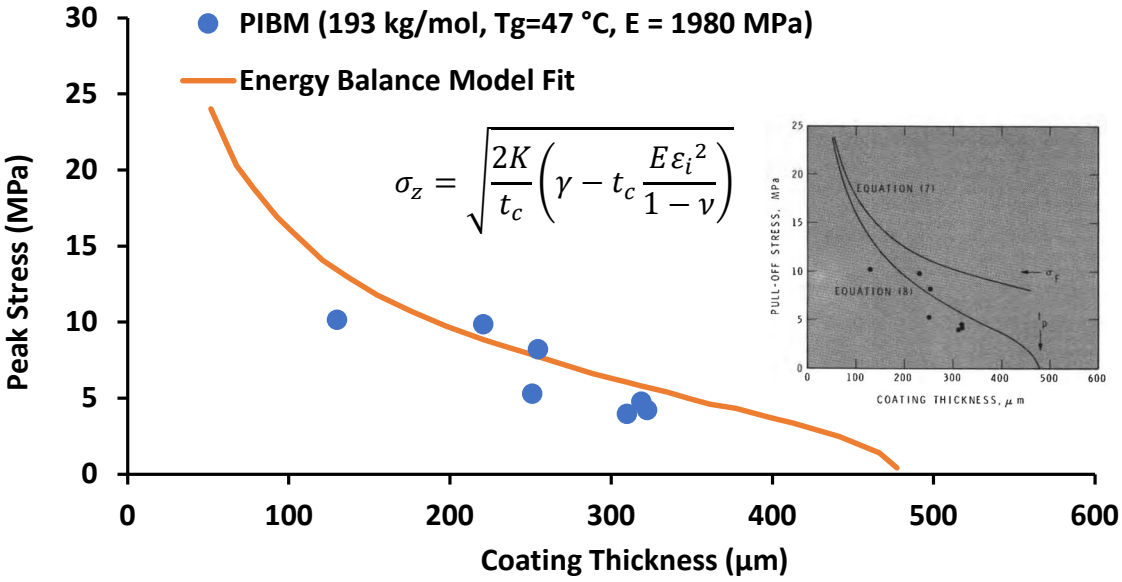

Figure 1.3 Pull-off stress of poly(isobutyl methacrylate) (PIBM) modeled by the energy balance predictive equation

Films were applied by a manual drawdown in two layers, one 10 wt% solid and then a higher solids layer to achieve well adhered thick films. Coatings were dried for nine months.[31]

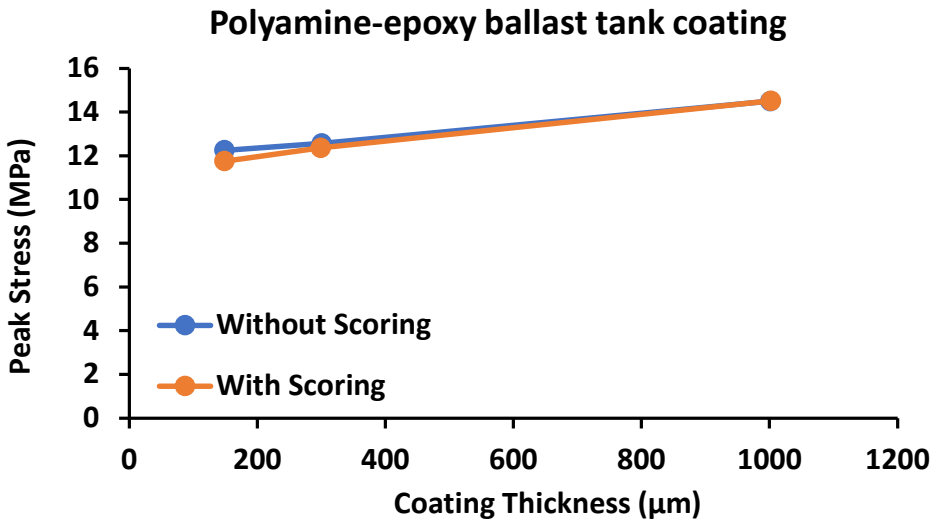

Figure 1.4 Pull-off stress of ballast tank coating on grit blasted steel

Peak stress increases with thickness in contrast to Figure 1.3. Applied by airless spray gun, T_g = 55 °C; E = 190 MPa. Replotted from Baek[32]

1.5 Rationale of research

The following chapters represent three studies in which the goal was to investigate and unravel the inconsistencies presented by practical coatings adhesion measurement and characterization methods. Each study challenges a different aspect of the current best practices, i.e., the status quo surrounding mechanical methods of coating adhesion measurement.

1.5.1 Overcoming bulk effects on adhesion measurement

To understanding coating performance variability in severe environments through mechanical methods of adhesion measurement, specifically adhesion as it relates to corrosion performance, there needs to be a way to account for the bulk properties effects on the test results. Ideally, it would be possible to delineate between bulk and interfacial properties with respect to time, hysteresis, and environmental conditions. One option for overcoming the interdependence of bulk and interfacial forces is to derive an exhaustive function that includes influencing variables from bulk and interfacial parameters, measure the bulk components in free films, and then back out the interfacial parameters. Such a numerical method is analogous to quantifying the work of adhesion from the internal stress-based predictive models in Figure 1.2 and Figure 1.3. As an alternative to the numerical method, an experimental method is proposed where testing parameters can be controlled to circumvent and minimize the bulk property effects on test results. In this scenario, bulk material properties remain unknown, but the differences in measured adhesion can be directly attributed to interfacial forces.

Measuring adhesion through the coating absorption of N-methyl-2-pyrrolidone (NMP) is an example of an interfacial characterization method that circumvents

mechanical properties. NMP is a good solvent for most polymers and induces a high degree of swelling. Bulk properties will dictate the maximum swelling ratio of the coating but knowing that value is not necessary to perform the experiment. Adhesion is quantified based on the extent of coating swelling required to induce delamination, which is not dependent on bulk properties. So long as the critical swelling ratio is less than the maximum achievable swelling, adhesion can be quantified. The problem with the NMP method is the criticality of capturing the extent of swelling at the point of delamination. As a result, this method is predominantly used qualitatively or semi-quantitatively based on the amount of time a coating can withstand immersion prior to delamination. [33,34]

In Chapter II, the quantification of interfacial strength through peel adhesion was approached by deliberately adjusting and effectively normalizing polymer mechanical properties. Polymers respond to temperature in similar and predictable ways. If the work of deformation is a substantial contributor to the force required to separate two surfaces, then the influence would be uneven between one polymer in a glassy state and another as a rubber, eliminating the possibility for determining a scientific basis for reliable adhesion attainment, retention, and loss. Adjusting the thermal frame of reference for the experiment narrows the source variables for peel forces down to interfacial factors.

1.5.2 Polymer mechanics approach to pull-off adhesion

Pull-off adhesion experimental results are influenced by seemingly infinite process variables where human error can interfere and generate data with high variation. Within the sample preparation and measurement procedures, alterations can be made to dolly geometry, dolly surface preparation, adhesive application, pull-off test fixture, and test execution. The available pull-off data published in the literature consists

overwhelmingly of collections of peak pull-off stresses. Chapter III argues that much of the noise can be reduced by capturing and analyzing the stress-strain and derivative of the stress-strain information generated from pull-off experiments run on mechanical testing systems. The curves can allow the detection of a variable outside of the main scope, like a defect-induced failure in the experiment, allowing for potentially otherwise unseen outliers to be eliminated.

Incorporating stress-strain analysis methods allowed conclusions to be made about which adhesive was most effective and how scoring should be performed to achieve the most accurate peak stress results. Of the four commercial adhesives and two adhesive masses investigated, a single adhesive and mass were identified for the application of test dollies to the coating topside. ScotchWeld DP460 (TM) applied at 30 mg was chosen because this adhesive resulted in consistent, high-quality pull results, in addition to having the highest peak stress among any adhesive evaluated. The method of scoring around each dolly was also evaluated, and a method was defined that resulted in higher data reliability and diminished data noise.

1.5.3 Understanding the unpredictability of coating adhesion

Coating failure is predominantly associated with coating-substrate de-adhesion, and the unpredictability of coating performance was shown to be directly rooted in the current unpredictability of adhesion. As a demonstration of the problems with predicting adhesion, the relationship between pull-off adhesion results and polymer film thickness was investigated. Methodologies developed in Chapter III were then employed to describe how adhesion prediction with respect to coating thickness could be better managed. Coating internal stress has been used as a starting point for predicting coating

adhesion with increasing thickness. It was shown that this relationship falls apart if the modulus is below a critical value and/or if there are solvents present.

The findings in Chapter II relating to interfacial polymer mobility are mirrored in Chapter IV. Where mobility and interfacial disruption are caused in Chapter II by thermal energy, in Chapter IV, they are caused by solvent plasticization. The anisotropic trapping of the solvent further complicates any attempt to fit pull-off data to pre-existing predictions. Chapter IV unearths the conditions that cause the model to collapse and makes suggestions for the underlying forces that caused the deviations from prediction.

CHAPTER II - DESIGN OF AN ADHESION MEASUREMENT FRAMEWORK TO NORMALIZE MECHANICAL DEFORMATION AND PROPERTIES WITH AN EMPHASIS ON THE IDENTIFICATION OF A UNIVERSAL ADHESION THRESHOLD OF CHAIN MOBILITY

2.1 Introduction

Surface coating performance depends on innumerable combinations of interrelated properties. Each performance property varies over time in a manner that can be described by three distinct phases of development, retention, and loss over a coating's service life. Among the different performance properties, the timeframes of each of the phases vary dramatically. Many dependent and independent processes overlap in terms of kinetic rates during each of the surface coating's service life phases. Analogous to human life, consisting of the macro-scale phases; birth, life, and death, these classifications do not adequately describe the varied events and life experiences that sum together to equal any of the three termed phases. Furthermore, the tendency towards oversimplification promotes characterization of average performance properties across the broad phases rather than the quantification of the quality or duration of performance properties on the timescale over which they change. Our research group has started to understand each of the dependent variables and the complicated relationships associated with surface coating processes of developing, retaining, and losing performance characteristics and measured properties in varied technology areas and perspectives. This dissertation was focused on quantifying and gaining an understanding of polymer-based coatings adhesion development and loss during each of the phases of a surface coating's service life.

Adhesion has been used as a generic term referring to a handful of different types of performance, rates, timelines, and characteristics. Any process or property under the umbrella of heterogeneous materials interface development has been considered generically as "adhesion," however, the range of size scales between molecular basis up to the macro-level size domain traverses an equally wide range of dependent variables. From a polymeric materials perspective, types of polymer adhesion sources have been commonly identified as chemical adhesion, mechanical adhesion, and practical adhesion. The necessary criteria for achieving a good, sufficient, or even a minimum threshold of adhesion have rarely been measured and continues to be poorly understood in simple or traditional coatings testing. Furthermore, the holistic and mechanistic basis of understanding of how coatings' adhesion is achieved, maintained, or ultimately fails at the coating-substrate interface continues to be unknown and rarely quantified. Adhesion has been established by many to be "all-important," and any given coating's longevity has been directly attributed to adhesion as a distinct and dependent variable towards the advancement of coating science.

Polymer-substrate interfacial failure has been shown to occur by several modes, physically by scratch or impact, or chemically by hydrolysis of interfacial interactions and/or corrosion of the substrate.[35] The intended use for a coating often determined which dominant failure mode was most likely and which design and performance properties are, therefore, more critical to develop and maintain over the course of the service life. Related polymeric material systems such as structural adhesives experience primarily physical loads, and joint durability relies heavily on polymer mechanical properties and the ability to transfer load stresses over greater contact surface area.[36] For

protective coatings, however, impact and scratch damage are less of a threat than environmental contamination, and in particular, protective coating failure is initiated by accumulation of corrosive species near the substrate that erode the interfacial contact area, disrupting the coating adhesion, as achieved by either mechanical anchor and/or chemical attraction where thereby diminish continued performance. How water, oxygen, and electrolytes interact with substrate surface atoms depends entirely on the polymer and substrate interfacial chemistry and morphology rather than the mechanical properties of the coating bulk directly. Within that context, the polymer-substrate interface does not form in isolation from the bulk polymeric material. The bulk of the coating affects the interface through interdependent variables, internal stress, residual solvent trapping, varying degree of cure, and film formation, which suggests that these variables need to be defined and quantified to further our understanding of these variables' influence on adhesion performance. Bulk mechanical properties have been shown to be dependent upon environmental conditions, e.g., contamination and hydroplasticization. Albeit well stated in the literature that adhesion is a very important factor in the coating performance lifetime, we suspected that the coatings specific adhesion testing methodologies and the acquired desirable information rarely overlap in concept as a result of the complicated nature of adhesion and the poorly understood basis for adhesion development and retention.[1–5]

We desired to measure and quantify the micro-scale interfacial information, such as interfacial interaction density, interaction strength, interfacial void volume, and chain orientation, that have been shown to most directly correlate with corrosion protection performance and found the process very challenging.[37] Straightforward, accurate

measurements of interfacial parameters require very limited/physically restricted sample types that deviate greatly from a commercially applicable coating-substrate system. Determining the density of interfacial interactions requires a technique that measures, in isolation, the interactions between substrate and coating atoms, distinct from all bulk secondary interactions. This requirement is met by vibrational modes detectable by infrared (IR) spectroscopy.[38] Quantification of the interactions is possible, but accessing the interface without perturbing the sample has continued to be a challenge for researchers and has not been practical or possible within production environments. Probing the interface via IR spectroscopy most often requires performing Fourier transform IR (FTIR) with a coated attenuated total reflection (ATR) crystal. Interactions are measurable at the coating-crystal interface, but the interface being analyzed is not that of a technologically relevant coating and substrate combination, and therefore, although this may teach about interactions, it is not currently possible to quantify interactions with a real substrate *in situ*. ATR crystals are frequently made of diamonds for their optical properties, but a diamond is not a substrate material that will ever be implemented, and the surface chemistry of diamond is very different from that of steel or aluminum. Aluminum can be chemically deposited onto the crystal to improve material similarities to that of common metallic substrates, but the aluminum film must be sufficiently thin for the FTIR beam to penetrate during normal acquisition parameters.[39] The effect of roughness on interface development and morphology is of great interest but is prohibited by the substrate restrictions imposed by ATR-FTIR spectroscopy.

The strength of the particular interacting molecular pairs found at the coating-substrate interface resists moisture accumulation by lowering thermodynamic preference

for hydrolysis and limiting void space for water accumulation. Interaction strength can be investigated by bringing atomic for microscope (AFM) tips, functionalized with a single molecule, into contact with a functionalized surface and separating them to measure the forces involved. The resulting data are valuable from a fundamental standpoint and can be used to estimate interfacial strength. Pauli et al. performed AFM approach-retract studies on asphalt films, finding a correlation between crude oil source and adhesion, with the implication that this will extrapolate to the fully formulated road surface or other final products.[40] Modeling coatings using small molecule studies creates an incomplete picture because the interface of a coating and substrate are traditionally formed from initial blends of liquids that transition by non-trivial pathways to a solid. Solidification is a result of crosslinking and solvent and carrier volatilization to varying degrees, and as a result, much of the chain conformation changes, and often the polymer chain morphology on an AFM probe surface will be different from those of the chain in an applied coating.

To compensate for sample geometry limitations of traditional interfacial characterization methods, macroscale mechanical measurements of adhesion have become the standard for facile interfacial testing of coatings (e.g., crosshatch, pull-off, peel, scratch, etc.).[41–44] These tests are practical in that they allow for much more relevant substrates, application methods, coatings, and geometries. Crosshatch is an easy and fast adhesion test that is accessible by anyone; the only tools necessary are a knife and tape. Most modifications to a formulation can be tested by crosshatch to check for any potential detrimental changes in adhesion. The only general requirement is that the samples are flat, and yet this is also often not strictly enforced during test utilization.[45]

There is no limit to the complexity, thickness, or mechanical properties of coatings in mechanical adhesion measurements. The substrate can be any chemistry or surface topography, making samples easier to produce and allowing results to be more directly applied industrially.

The downside of mechanical based adhesion tests for understanding interfacial strength is that results are strongly affected by bulk material properties. Broadly, the energy required to separate a coating from its substrate is a function of the work of deformation, the work of adhesion, and the internal stress in combination.[46] The work of deformation can be orders of magnitude larger than the work of adhesion as a result of the glassy nature of most polymeric materials for coatings. For 90° peel adhesion testing specifically, an equation thought to encompass all of the governing variables was described by Croll and is shown in Equation 2.1. The equation communicates that the work of adhesion (γ) has as strong an influence on the peel force as modulus (E) and Poisson's ratio (υ).[31]

$$\frac{F}{b} = \gamma - t_c \frac{E\varepsilon^2}{1-\upsilon} \qquad \text{Equation 2.1}$$

Mechanical methods of adhesion measurement can be misleading when trying to make decisions relating to interfacial strength, but in defense of the methods, such hurdles can be overcome. For instance, the mechanical properties like modulus that influence adhesion measurement results are relatively simple to measure or locate. Relationships like Equation 2.1 allow the measurable mechanical property and measured adhesion to be used to back-calculate the interfacial parameter, work of adhesion.

As an alternative to numerical methods of calculating the work of adhesion, the experimental method can be designed to circumvent the bulk properties entirely.

Numerous theoretical methods approach adhesion indirectly to eliminate interference.[47–50] Chapman suggested that adhesion could be quantified by the difference in thermal energy released upon dissolution of a substrate-bound film compared to a free film.[51] A capacitive method has been described where an electrode is applied to the uncoated side of a substrate and current of high and low frequency is passed through the sample, and the difference in capacitance relative to capacitance at high frequency is analogous to adhesion.[48] In these examples, the mechanical properties can be avoided because the coating is being compared to itself, but the methods have not experienced widespread use due to experimental limitations. Similarly, adhesion can be quantified based on the degree of swelling in a good solvent like N-methyl pyrrolidone (NMP) required to induce delamination, which is not dependent on mechanical properties. Unfortunately, capturing the degree of swelling is challenging, and the method is generally used qualitatively using the time to coating delamination in NMP.[33] The idea of quantifying adhesion information from macro-scale coating-substrate systems is not new but thus far has been largely unsuccessful.

To fully realize an experimental method that effectively quantifies interfacial strength independently from mechanical properties, the present study takes advantage of the almost universal nature of the glass transition temperature (T_g). The thermal response of polymer mechanical properties has been measured frequently and is understood to vary similarly about the T_g for a wide range of polymers, providing a solid foundation upon which to build mechanical-based adhesion measurements. Amorphous polymers regularly transition between a glassy phase at low temperatures defined by high modulus and more brittle failure to a rubbery phase at high temperatures defined by low modulus

and high elongation. The glass transition is defined as the temperature at which this transformation of mechanical response occurs. The specific temperature ranges these phases occupy are relative to the polymer's glass transition temperature, which can vary wildly in common polymeric materials (-100 – 300 °C).[52,53] Poly(dimethylsiloxane) (PDMS) and Kevlar in the glassy state have important fundamental morphological differences in addition to the temperature ranges the glassy states are accessible. PDMS will be completely amorphous, and the chains of poly(p-phenylene terephthalamide) that makeup Kevlar will be aligned and well-ordered with regions of crystalline and liquid crystalline phases.[54,55] It is important to note that modulus does not vary about T_g identically from polymer to polymer. The differences in structure and glassy modulus do not invalidate the use of a T_g-relative framework for understanding the adhesion of polymeric materials, for they are also what influence interfacial properties. Effects of chemistry and short-range polymer motion that influence interfacial strength are much easier to isolate when viewed in the same physical state, rather than simply at the same temperature where, for example, PDMS is rubbery, and Kevlar is glassy. It is hypothesized that a T_g-based framework of adhesion measurement for amorphous materials delineates and quantifies the chemical and interfacial effects on peel force from the mechanical contributions to improve interpretation of adhesion data.

The microscopic differences associated with polymer physical states also present a strong argument for normalization by glass transition. Changes in the extent of chain mobility seen macroscopically as different physical states contribute to the interfacial environment. Increasing temperature towards T_g increases local chain mobility and provides more functional groups to the interface. By comparing adhesion from a T_g-

based framework, the differences in peel force are a result of interaction strength and availability deriving from topography and network morphology, not available kinetic energy.

Charles Hofrichter and Douglas McLaren advanced the concept of interfacial fluidity in 1948 while investigating the effects of carbonyl group concentration and temperature on peel adhesion to cellulose.[56] Their coatings consisted of blends of PVC and polyvinyl acetate copolymers into which they incorporated increasing amounts of a maleic acid-containing polymer. Their results have been replotted in Figure 2.1 for review. They explained the temperature dependence of adhesion from a chain mobility and fluidity standpoint, suggesting that the concentration of adsorbing species increases (as Brownian motion increases) more rapidly than dipole sorption probability decreases with temperature. However, these were only hypothetical explanations, and the original paper had a very limited scope from looking at blends of the same polymer and lacked any depth of discussion specific to the measured thermal transition of adhesion at 50 °C.

TABLE I. EFFECT OF TEMPERATURE AND CARBOXYL CONCENTRATION ON PEEL STRENGTH

Weight ratio, VYHH/VMCH	99.5/0.5	99.0/1.0	98.5/1.5	98.0/2.0	97.0/3.0	94.0/6.0
Coating weight, g./sq. m.	4.44	3.89	4.23	5.53	4.77	4.06
Moles (COOH)/1000 g. polymer	0.00491	0.00983	0.01474	0.01975	0.02958	0.05916
Peel strength, g./1.5 inches						
−30° C.	...	85	88	105	105	165
−20° C.	...	78	85	123	...	...
−10° C.	58	93	88	127	153	245
0° C.	60	125	132	155	199	...
10° C.	70	119	190	200	243	303
20° C.	...	150	260	300	428	470
30° C.	...	352	535	570	685	990
40° C.	410	588	...	880	995	...
50° C.	570	853	960	1200	...	...
60° C.	507	695	855	1000	...	...

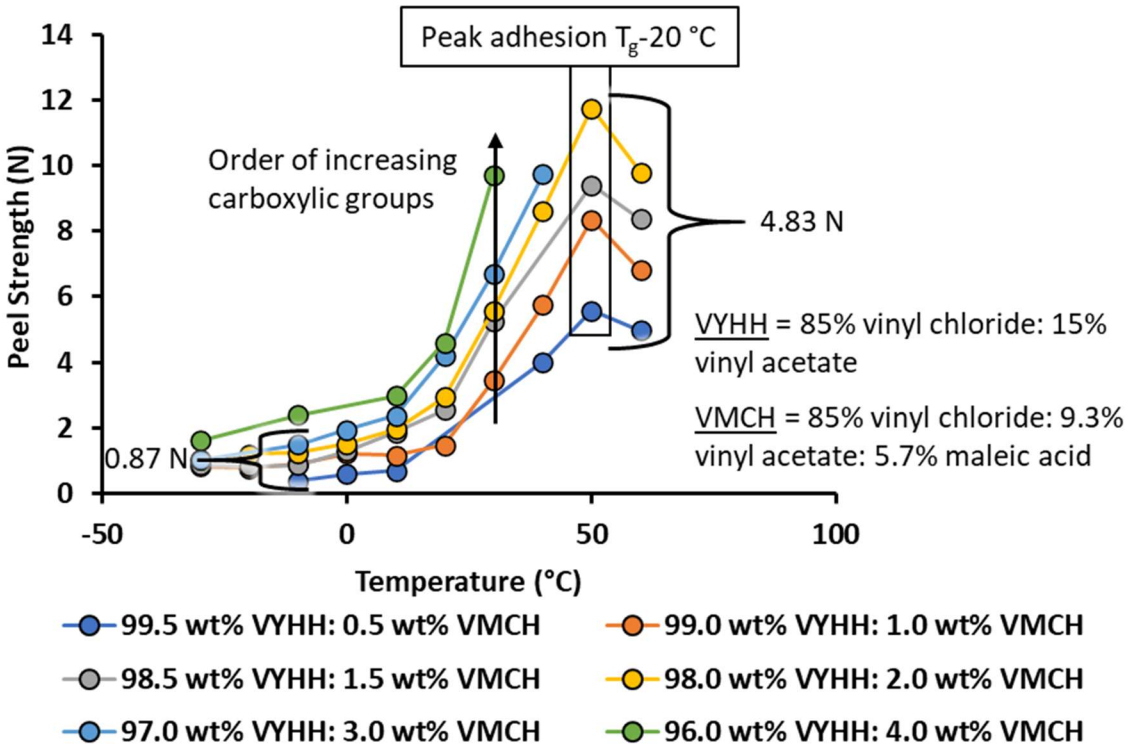

Figure 2.1 Replotted peel data from Hofrichter and McLaren[56]

Top) table captured directly from the publication; bottom) visualization of data from the table.

While Hofrichter and McLaren seemed to unintentionally discover one mechanism of the temperature dependence of adhesion, there are important dimensions that have been left unexplored for 70 years.[56] As temperature increases, the curves appear to diverge, and this would be a valuable property to investigate to better resolve interfacial variations between coatings with slight compositional differences. Results could further support the fluidity argument because the added benefit from the maleic acid groups is more prominent at higher mobility. The study was limited in scope by designing the polymer blends to have the same tack temperature (and by extension, T_g). T_g of the VYHH material used as the base resin was determined to be 70 °C, indicating peak peel force to be at T_g-20 °C for all blends; however, the gravity of the finding is minimal considering the chemical similarity among films.[57] Investigating only materials

with the same T_g led the peak adhesion temperatures overlapping relative to T_g be less impressive or noticeable. Finally, there was no explanation for the loss in adhesion above the peak temperature. It's hard to extrapolate whether their findings would persist across multiple thermal reference frames or with different materials.

In the present chapter, the findings of previous researchers were extended to thermoset coatings with differing T_gs and across different test temperature ranges. Importantly, the results replotted in Figure 2.1 demonstrate that within normal practices, where laboratories report drastic adhesion fluctuations could be a result of temperature changes and the effect of temperature is magnified within the real-world conditions of actual coating utilization, where a thermal fluctuation of 20-30 °C is expected on multiple time-scales with almost every practical example. The 99 VYHH: 1 VMCH formulation in Figure 2.1 experiences a quadrupling of peel force, a measured shift from 1.47 N to 5.76 N from 20°C to 40 °C. Rationally, the results, when plotted versus temperature, reveal that the common practice for testing of adhesion/coatings properties clarifies a potential source of noise in global results and the dramatic variance between labs solely based upon test temperature variability.

Our motivation was to advance the connection between accepted methodologies of coating science and molecular-level investigations. Efforts were made to better understand the relationships between mechanically measured adhesion and interfacial properties. Both our and previous studies found that adhesion is critically temperature-dependent and if that is overlooked when performing thermal cycling in the lab or naturally in the field, then the understanding of why, when, and how we achieve or lose adhesion will continue to be incomplete. Knowing the temperature dependence of

adhesion is beneficial both in how coatings will respond to mechanical stressors in thermally unregulated environments and also helps to isolate interfacial changes in practical systems by purposefully minimizing mechanical property effects while understanding what molecular building block parameters aid in attaining, retaining, and managing adhesion loss during material utilization.

2.2 Experimental

2.2.1 Materials

The epoxy-amine networks applied as model coatings were first described by Wand and composed of Epon 825 (diglycidyl ether of bisphenol A containing 0.05 repeat units) (Hexion), benzylamine (BA) (Acros 99%), 1,3-bis(aminomethyl)cyclohexane (BAC) (TCI, 98%) and Jeffamine ED-600 (Huntsman).[58] All chemicals were used as received. Monomers were formulated into one of three resins, designated based on their T_g, high T_g (HTg), mid-T_g (MTg), and low T_g (LTg). Weight ratios of monomers in the three resins and their respective T_gs are presented in Table 2.1. In addition to the reactive monomers, 0.1 wt% TegoWet 270 (Evonik), a polyether siloxane copolymer, was added to reduce defects and promote flow and leveling.

(a)

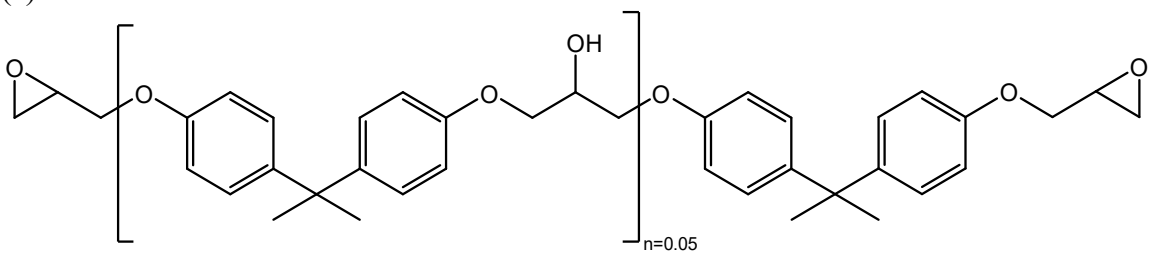

(b)

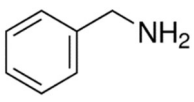

(c)

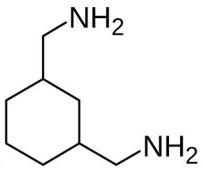

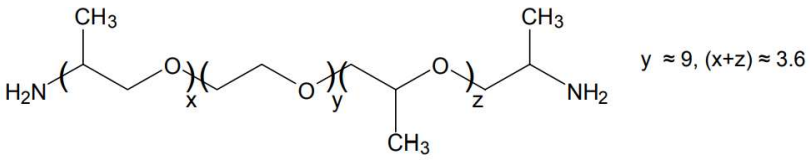

(d)

Figure 2.2 Building block material chemical structures for the thermoset research included herein

a) Epon 825; b) Benzylamine; c) Bis(aminomethyl) cyclohexane; d) Jeffamine ED-600

Table 2.1 Formulations used in 90° peel adhesion experiments for modular model coatings controlling T_g and maintaining crosslink density,

All coatings were applied to aluminum alloy 2024 by drawdown at 100% solids and cured at 60 °C for 2 hours followed by 80 °C for 1 hour, resulting in a dry film thickness of 40 µm. [a] T_g was quantified by dynamic mechanical analysis based on Tan δ maximum on poured bars of material kept at laboratory conditions.

Monomer	**High T_g (HTg) (wt%)**	**Mid T_g (MTg) (wt%)**	**Low T_g (LTg) (wt%)**
Epon 825	71	64.4	59.4
Benzylamine (BA)	1.9	0.9	0.2
1,3-Bis(aminomethyl) cyclohexane (BAC)	9.1	6.2	3.9
Jeffamine ED-600	18	28.5	36.5
T_g (°C)[a]	80	53	44

Peel samples consisted of coatings applied to Q-lab aluminum alloy 2024 panels cut to 1.5 x 5-inch shims. Aluminum substrates allowed shims to be easily cut to fit on the peel accessory sample table, which was compact to fit inside the oven attachment of the mechanical testing system shown in Figure 2.4. Black Leneta scrub charts were cut into 1 x 1.5-inch segments to be adhered to the peel tab end with a stoichiometric mixture of Epon 825 and BAC to prevent the peel tab from slipping out of the grips during the test. It was also important that the Epon 825-BAC adhesive achieved a T_g greater than the coatings being investigated to resist deformation between the Laneta chart and the peel tab at elevated temperatures.

2.2.2 Methods

2.2.2.1 Coating formulation and application

The coating formulation was accomplished in a 2-phase process. In the first phase, Epon 825 and BA were weighed out and combined by a Flaktek speed mixer for 1 minute at 1,800 RPM. The mixture was transferred to a roller, where it reacted for 30 minutes. This preliminary step served to partially chain extend the epoxy with BA in the absence of crosslinking amines.

High, medium, and low T_g networks were created by employing different ratios of a hard crosslinker (BAC) and a soft crosslinker (Jeffamine ED-600). However, these two crosslinkers have significantly different equivalent weights. To simultaneously maintain a constant crosslink density across all networks, increases in the BAC/Jeffamine ratio were offset by linear chain extension of the Epon 825 using BA. In this way, a constant MW between crosslinks of approximately 550 g/mol was maintained.

In the second phase, BAC and ED-600 were added to the chain extended epoxy, combined by speed mixer in a manner identical to phase one, and returned to the roller for another 3 hours for HTg, 4 hours for MTg, and 6 hours for LTg. Building the resin with a chain extension phase prevents amine blushing and renders the application of higher thickness films possible by increasing viscosity without decreasing workability. Without the pre-reaction, long chains form before branched network fragments leading to unmanageable levels of viscoelastic strands on coating application. After reaching a manageable viscosity, the sample was removed from the roller, and Tego Wet 270 was added and incorporated by speed mixer. Prior to the coating application, the resin was left to stand for 5 minutes to allow any accumulated bubbles to escape.

The viscous liquid coating was applied to aluminum substrate shims by manual drawdown. Substrate preparation included solvent cleaning with mineral spirits, drying under nitrogen, and wiping with a microfiber cloth. Liquid pre-polymer was dispensed by transfer pipet into the 1.5 inch^2 multiple-clearance square drawdown bar and draw using the 3 mils clearance side. Coated shims were placed immediately in a 50 °C oven and left overnight. The oven temperature was increased to 60 °C the following morning and held for two hours and finally increased again to 80 °C and held for one hour. Coating dry film thicknesses were an average of 40 μm.

2.2.2.2 Dynamic mechanical analysis

The glass transition temperature of each resin was quantified using dynamic mechanical analysis (DMA), where silicone molds with 60 × 5 × 1 mm wells were used to form sample bars. Liquid pre-polymer was poured into molds after the same processing steps as were performed to prepare coatings for application. Cure schedule for the bars was the same as for coated panels.

Thermal Analysis Q-500 DMA instrument was used with the film tension fixture. Oscillation amplitude was based on 0.1% strain at a rate of 1 Hz. The temperature ramp range scanned was different for each material based on its T_g, but the range was roughly T_g - 75 °C to T_g + 50. Material mechanical T_g was specified as the temperature at the peak of the Tan δ curve.

2.2.2.3 Peel sample preparation

After samples cooled to room temperature, a 1 cm wide lane was scored into the coating, as illustrated in Figure 2.3, using a Vision Engraving machine equipped with a burnishing tool. Peeling of the lane to form a tab to grip was initiated using a razor

blade; the shim was clamped to the benchtop to reduce movement of the sample during this process. The thickness of the resulting peel tab was increased by adhering pieces of a scrub chart to eliminate slipping of the peel tab from the test clamp. Scrub chart swatches were intentionally asymmetrical and wide to protrude from the front of the grip and could be used as a handle to more easily position the tab in the clamp parallel to the load before testing. Using a single central peel lane meant the clamps on the peel test table did not interfere with the sampling area.

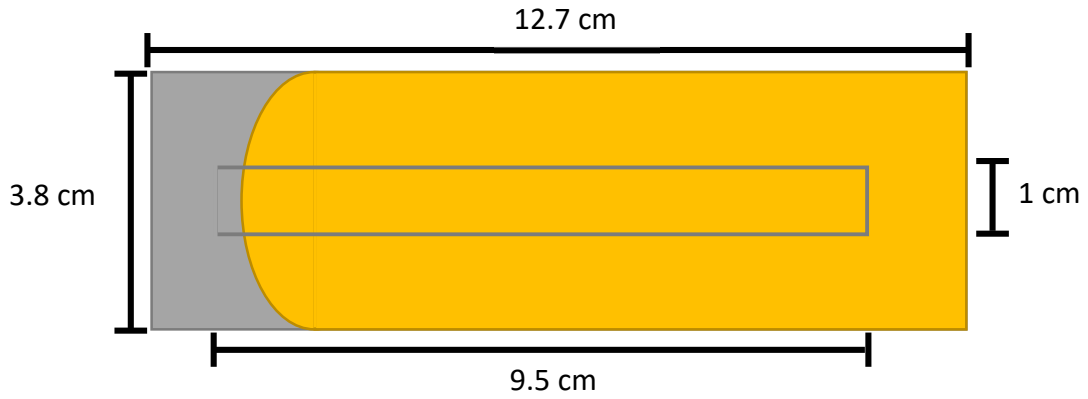

Figure 2.3 Top view Illustration of a peel sample

Indicates the path of the scribe tool from the metal (grey) at the top of the aluminum shim to the coating (yellow), forming a 1 cm wide and 9.5 cm long peel lane

2.2.2.4 Peel test table assembly and test execution

A custom peel test table was fabricated in-house due to the specific size and thermal requirements (see Figure 2.4). Maintaining a constant 90° angle between the peel tab and substrate was important for the validity of the test data. The constant angle was achieved from within the oven by drilling a hole through the roof to run a cable from an attachment point above the load cell to the mobile sample table, thereby keeping the distance the table moved equal to the extension of the crosshead on the MTS Insight load frame. The peeling rate was set to 10 mm/minute, and each run consisted of 1 cm of the

9.5 cm peel lane allowing multiple tests to be performed on the same lane. A thermocouple was fitted under the test panel (the blue wire in Figure 2.4) and the coating sample equilibrated in the oven for 5 minutes at the desired temperature before executing the experiment.

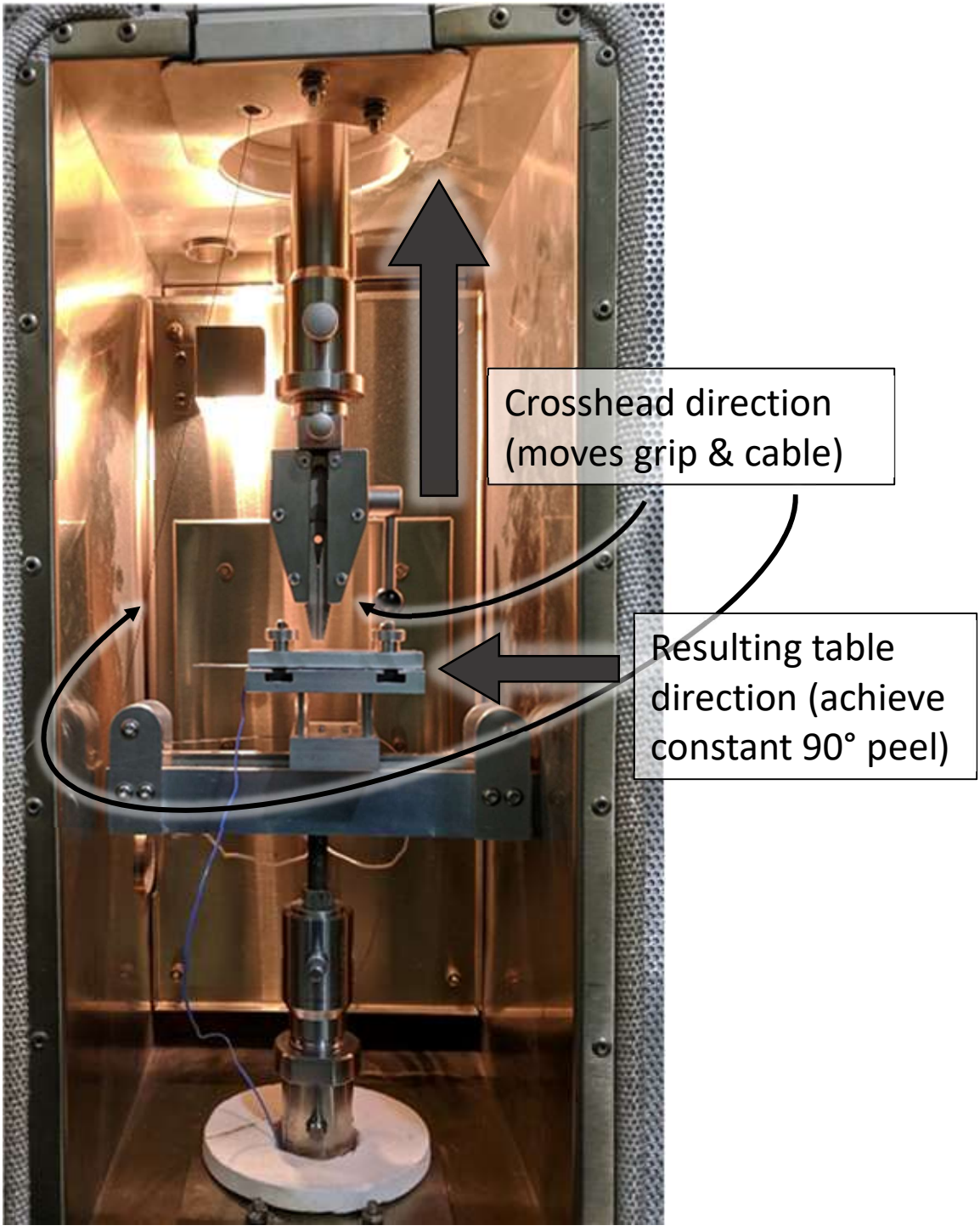

Figure 2.4 Peel adhesion accessory set-up inside the oven attached to the MTS Insight load frame.

A sample is clamped between the two metal beams closest to the grip

To compare the results of measuring adhesion at constant temperature versus constant thermal distance from T_g (T_g-T), two constant test temperatures and two T_g-T were investigated. The two constant environmental temperatures chosen were 20 °C and 40 °C because they provided a significant change in thermal energy without exceeding the T_g of any materials. The constant temperatures for each resin were T_g-5 °C and T_g - 20 °C. Absolute temperatures depended on the coating being studied. A summary of the environmental temperatures is presented in Table 2.2. Because 40 °C and T_g-5 °C for LTg were equivalent, T_g-10 °C was also investigated for LTg to maintain four test temperatures per resin.

Table 2.2 Environmental test temperature variables applied to each resin

[a] T_g – 10 °C only investigated for LTg because Tg – 5 °C ≈ 40 °C and that would result in only three temperatures

Resin	**HTg (°C)**	**MTg (°C)**	**LTg (°C)**
Constant 1	20	20	20
Constant 2	40	40	40
T_g – 5 °C	75	47	--
T_g – 10 °C[a]	--	--	34
T_g – 20 °C	60	32	24
Dry T_g by DMA (°C)	*80*	*52*	*44*

2.3 Results and Discussion

2.3.1 Dynamic Mechanical Analysis (DMA)

DMA was performed on poured sample bars of the three different thermoset networks both to describe their mechanical property dependence on temperature and to pinpoint each material's glass transition temperature (T_g). Thermomechanical responses were critical for establishing the rationale behind a T_g based peel adhesion measurement framework and thereby circumventing mechanical property influence on peel forces. In

Figure 2.5, the storage modulus, loss modus, and Tan δ are shown for HTg, MTg, and LTg. As expected for typical polymers, the three coating materials experience three physical states; glass, leather, and rubber. The temperature ranges occupied by each physical state is different for HTg, MTg, and LTg by design. Consequently, the storage modulus for each material viewed from a constant temperature frame of reference would be very different, unlike a constant number of degrees Celsius away from T_g (T_g-T).

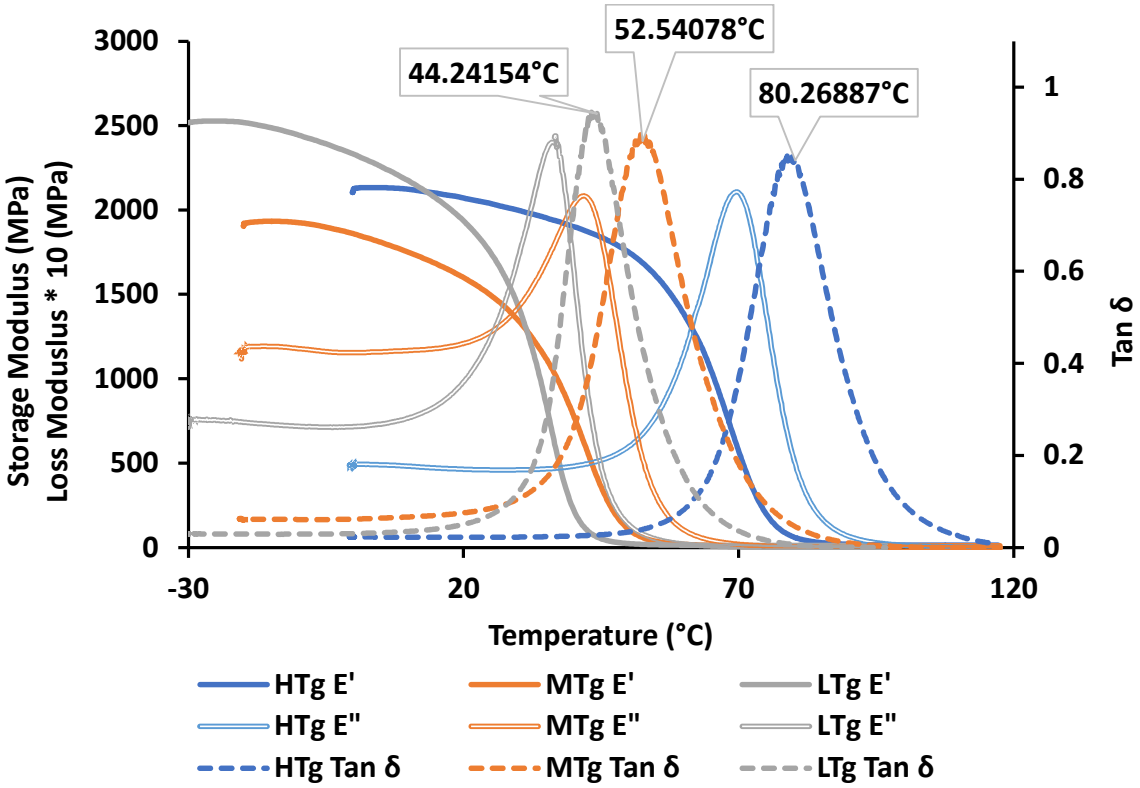

Figure 2.5 Dynamic mechanical analysis overlay of temperature ramp of model epoxy-amine networks

Storage modulus and loss modulus share one y-axis but material loss modulus values are 1/10 of what the figure indicates, so detail could be seen without adding a third axis. Experiments performed on poured bars cured for two hours at 60 °C and one hour at 80 °C. Film tension mode, oscillation amplitude = 0.1% strain; frequency = 1 Hz; ramp rate = 3 °C/min

Glass transition temperatures were quantified by DMA and used to establish T_g-T experimental temperatures. T_g was taken as the temperature where Tan δ reached a

maximum value. Figure 2.5 shows that T_g for HTg is 80 °C, for MTg is 52 °C, and for LTg is 44 °C. Multiple T_g-T temperatures were chosen to see how relationships between networks changed from one T_g-T to the next as compared with two constant absolute temperatures and to compare physical states. The glassy and leathery states could be compared by testing at T_g - 20 °C and T_g - 5 °C, respectively.

Initial validation of the constant T_g-T method can be made using storage modulus values extracted from DMA curves. Figure 2.6 compares isolated storage modulus points for HTg, MTg, and LTg at two constant temperatures and three T_g-T temperatures. An additional T_g-T of T_g-70 °C is included in Figure 2.6 that could not be measured by 90° peel due to the cooling function being unavailable on the load frame oven, but the comparison of multiple T_g-T in the same physical state is valuable even without the peel data. The magnitude and ranking order of storage moduli change dramatically when the temperature is increased from 20 °C to 40 °C. In the span of 20 °C, LTg modulus decreases by a factor of ten and changes rank to become the least stiff material, while HTg is the stiffest at both temperatures, and the storage modulus barely changes (an 8% reduction). These discrepancies are because in the 20 to 40 °C temperature range, MTg and LTg resins have transitioned from glass to leather, while HTg is a glass at both temperatures. By looking at a constant T_g-T instead, the resins are compared from the same physical state.

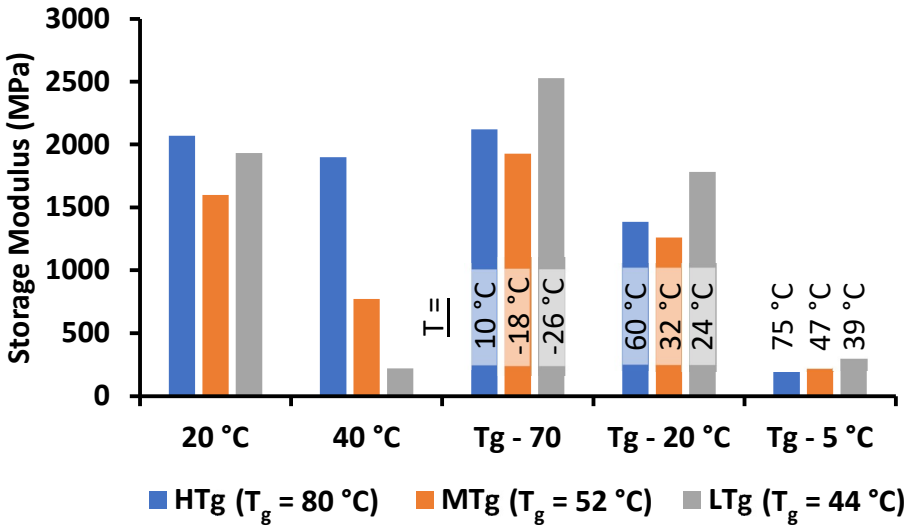

Figure 2.6 Direct and relative comparison of storage moduli at defined temperatures and temperatures below T_g as a visual to represent the contribution of mechanical resistance to deformation to overall mechanical adhesion measurement

Single values pulled from DMA curves at indicated temperatures

At temperatures corresponding to T_g - 20 °C and T_g - 70 °C, each material is in a glassy state, and while the magnitude of moduli changes, the order LTg > HTg > MTg persists. When the temperature is increased to T_g - 5 °C, all resins are in the leathery state, presenting a different order LTg > MTg > HTg but less variation between moduli. Differences between moduli at the same T_g-T give information about network fluctuations that have the potential to affect the interface as well. The resin with the highest T_g had the lowest storage modulus at T_g-5 °C, but not T_g-20 °C. The segmental motion required to transition into a rubber state in a crosslinked network involves the flexibility and cooperation of many neighboring network fragments, but there is significant local mobility in the leathery region just below T_g. Pistor describes three short-range motions and visualizations of the different types, and scales of network mobility are shown in Figure 2.7.[59] Bond wagging requires the least energy, followed by network linkage conformational changes, and then domain motion. At T_g-20 °C, bond

vibrations and conformational rearrangement are available, and some domain motion may also occur. Patil and coworkers quantified the cooperative segment length involved in the glass transition of epoxy amine networks and found the length needed for polyethylene oxide (PEO) containing polyether amines to be much lower than purely polypropylene oxide (PPO) polyether amines.[60] This suggests that at 24 °C (T_g-20 for LTg), the PEO blocks are mobile, and because of the high weight fraction of ED-600, that means little more energy is needed to achieve segmental mobility. With only the PEO blocks mobile, though, the storage modulus is very high. Adding thermal energy to reach 32 °C (T_g-20 for MTg) is enough to induce the same mobility in PPO. There are more Epon 825 trimer units in MTg than LTg, but the added aromatic rings do not contribute to stiffness more than the conformational freedom of ED-600 detracts from it.

A purely ED-600 driven interpretation of the storage moduli captured at T_g-20 °C cannot explain the increased modulus of HTg over MTg. The increased absolute temperature from 32 °C to 60 °C would initially suggest more energetic moving network units and a decrease in stiffness. However, the high concentration of 825-BA-825 trimers that grant HTg its high T_g also presents an additional possible route to elevated stiffness. Rigid 825 units resist segmental motion, but the higher available thermal energy provides aliphatic sections of the network like crosslink points with more mobility allowing for the organization of 825 units with some orientation supported by π-π secondary interactions. Orienting DGEBA units can explain the higher storage modulus of HTg over MTg.

At T_g-5 °C, all motions requiring less thermal energy than segmental motion have been accessed, and modulus is based on the stiffness of the domains. For HTg by the temperature segmental motion is induced, all network fragments are energetic to some

degree, and the domains are weak. For LTg, all the ED-600 has the thermal energy to move, which leads to domain motion, but the domains are composed of Epon 825 and Epon 825 trimers, which have not achieved conformational mobility and, therefore, the domains are stiff. Variations in chain mobility affect the interface more than the bulk stiffness despite the bulk properties having a greater effect on the measured value.

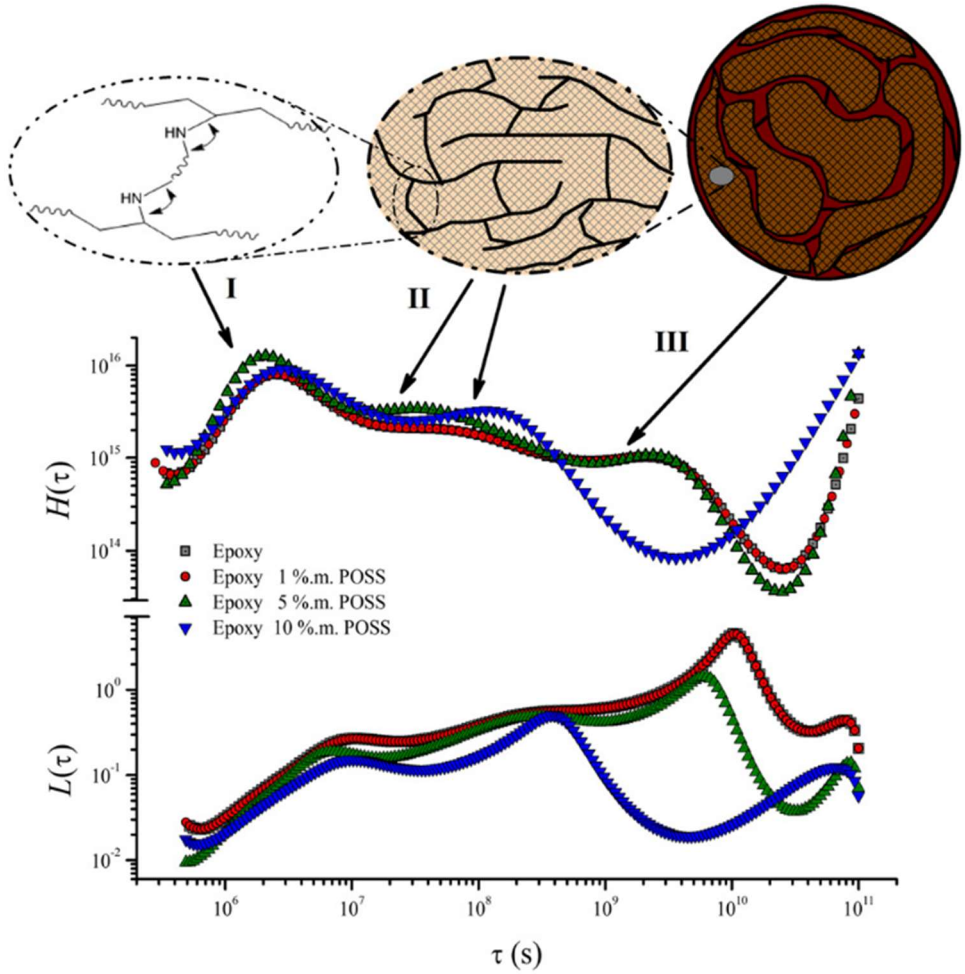

Figure 2.7 Calculated relaxation (H(s)) and retardation (L(s)) spectra from literature epoxy-amine and visualization of sub-T_g transitions with increasing loading of polyhedral oligomeric silsesquioxane (POSS)

Calculations performed by the nonlinear regularization (NLREG) method using DMA storage (E') and loss (E'') moduli obtained by the application of time-temperature superposition.[59]

2.3.2 Peel Adhesion Relative to Test Temperature

Adhesion was quantified by 90° peel at multiple temperatures to understand how the polymeric material's physical state can ultimately influence both measured peel force values and the interfacial structure. Temperature dependence of mechanical and interfacial properties combined to result in a fascinating temperature-dependent adhesion response for the three resins with high, mid, and low T_gs, shown in Figure 2.8. Two peel force measurement temperatures were constant for all three coating materials, 20 and 40 °C; the other two were based on material T_gs; T_g - 5 °C and T_g - 20 °C. Of the three resins, HTg had the weakest peel force and was the least affected by the change in temperature, with a peel force range of 1.64 N to 4.77 (ΔF = 3.13 N) over a 40 °C temperature range. The extent of temperature dependence was quantified as the slope approaching the peak, which for HTg was 78 mN/°C when approaching the peak from a lower temperature. The highest peak peel force, 6.56 N, was achieved by MTg, at T_g - 20 °C. Only one measurement was available at a lower temperature with which to calculate slope, and the resulting temperature dependence was 322 mN/°C, a value four times greater than for HTg. Finally, LTg was only measured at temperatures between the peak adhesion temperature and T_g, meaning there were no points to measure an approach slope with, and the range from T_g-20 °C to T_g-5 °C was used instead because it was probed for all resins. Temperature dependence of LTg was found to be 251 mN/°C in that range, and to compare the same region, slopes approaching the maximum peel force from higher temperatures for HTg and MTg were calculated to be 140 and 243 mN/°C, respectively. In addition to understanding the extent of adhesion variation within a temperature window, analyzing the rates of

adhesion growth and loss with temperature identifies differences between the sources of adhesion.

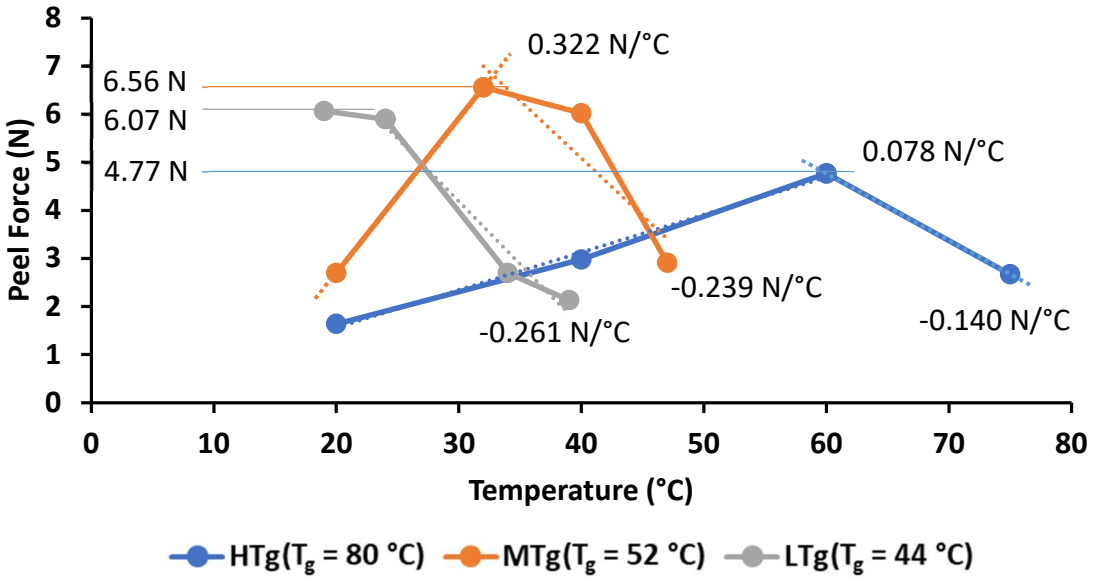

Figure 2.8 Peel force as a function of environmental test temperature for each of the three thermoset epoxy amine polymeric materials with varied T_gs.

Coatings were applied in bulk to AA 2024 and cured for two hours at 60 °C and one hour at 80 °C.

Increasing thermal energy induces chemical, structural, and mechanical changes in the network. On the bulk scale, the modulus is changing, but much more slowly approaching T_g-20 °C than T_g-5 °C; therefore, it is hypothesized that the increase in peel force is not mechanical property driven. Competing flow and sorption processes identified by Hofrichter and McLaren suggest rates of increase of adhesion with temperature correlate with endothermic heat of fluidity.[56] Increases in adhesion from the heat of fluidity are in competition with the exothermic sorption process. The small changes in molecular motion have a profound effect on the interface as the number of opportunities for polymer-substrate interaction increases with the added local chain mobility. Comparing the rates of adhesion increase corroborates this theory as MTg flows more easily than HTg and has a

faster rate of adhesion increase (Figure 2.8). Rates of adhesion loss are different from adhesion gain because it is driven by different processes discussed later.

At the molecular level, the thermally derived adhesion responses of HTg, MTg, and LTg can be explained. Jeffamine ED-600 is the most flexible component of the crosslinked network with an aliphatic linear chain length of 42 atoms. Epon 825 and its trimer provide the strongest interfacial interactions, comprised of aromatic rings, hydroxyl groups, and amine functional groups that bond most strongly to metal surfaces on a cohesive energy density basis. Solubility parameters (SP) calculated from group contribution theory are shown in Figure 2.9. Hansen and Wallstrom calculated solubility parameters for common substrates, including aluminum, which are reported in Table 2.3.[61] Compatibility of two materials based on solubility parameters is determined by their proximity to one another as opposed to a maximum or minimum value; therefore, the chemical compatibility of HTg over other resins is supported by the SP calculations. However, HTg does not achieve as high a peel force as MTg and LTg because even though there are more hydroxyl groups present, there is limited network flexibility to achieve high contact with the substrate functionality, even at high temperatures. The other extreme, LTg, has sacrificed too much of the functionality associated with Epon 825 to achieve a higher peel force than MTg, but because ether functional groups are effective for adhesion and ED-600 also provides mobility, LTg achieves a higher peel force maximum than HTg.

Table 2.3 Calculated solubility parameters for aluminum

From Hansen and Wallstrom.[61]

	Dispersion	Polar	Hydrogen bond	Total
Aluminum	7.6	-10.5	8.1	15.3

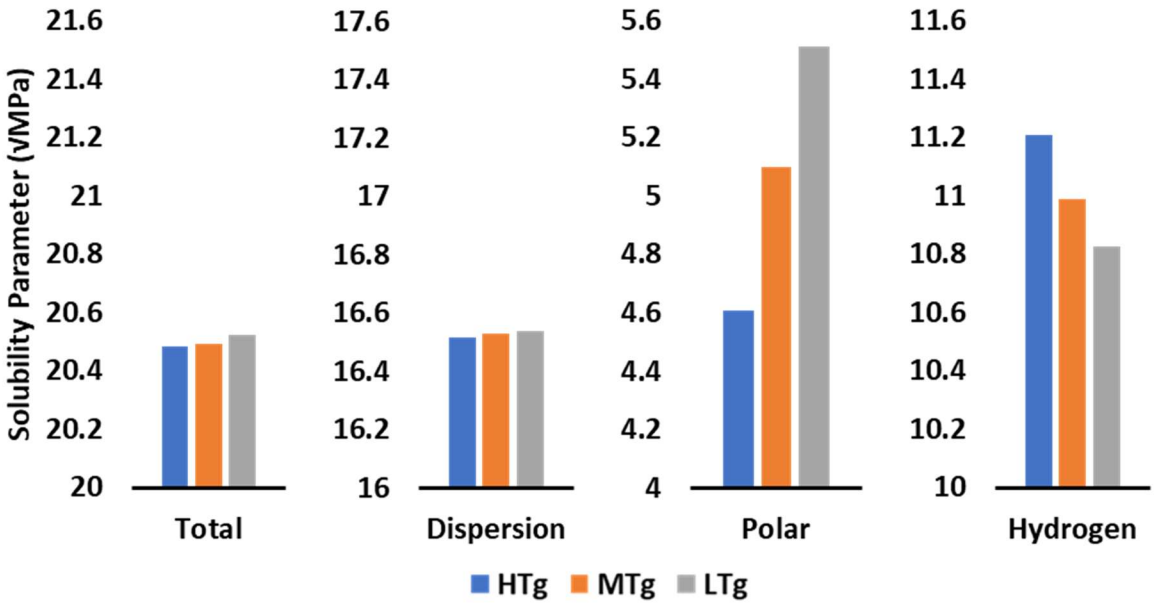

Figure 2.9 Calculated HSP solubility parameters for each of the three thermoset epoxy amine materials

Calculations based on group theory contributions of a network of 1:1 stoichiometry at 100% conversion.[62]

Another explanation for why HTg adhesion was so much lower than MTg and LTg was the magnitude of the contribution of sorption. Increasing temperature decreases interaction strength and extent of sorption due to the exothermic nature. Absolute temperatures were higher for HTg than MTg due to the 28 °C increase in T_g, which helps explain the peel force values. The higher T_g of HTg over LTg was driven by a higher 825 molar concentration, which related to higher concentrations of functional groups but limited mobility with the addition of higher free volume during cure.

Chain mobility can be quantified through the Tan δ curve produced from DMA. The ratio of integrals shown in Equation 2.2 compares the percentage of polymer chains that are mobile at a specific T_g-T temperature to all the chains as determined by the integration over the entire Tan δ peak.[63]

$$\%\ mobile\ chains(\Delta T_g) \approx \frac{\int_{Tg-60}^{Tg-T} Tan\delta}{\int_{Tg-6}^{Tg+37} Tan\delta} \qquad \text{Equation 2.2}$$

Figure 2.10 includes calculated fractional areas under the Tan δ curve that account for chain mobility at T_g-20 °C and T_g-5 °C. There is a positive linear correlation for both T_g-T temperatures. MTg shows the highest degree of mobility, which is consistent with having the lowest storage modulus at T_g – 20 °C. Many properties are involved in determining the peel force of a coating-substrate system, but which correlates with performance is still unknown.

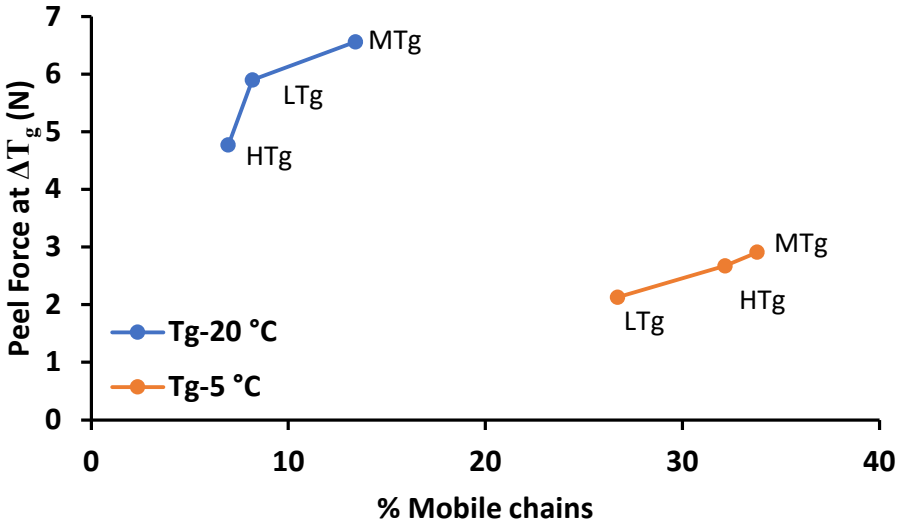

Figure 2.10 The fraction of mobile chains calculated using Equation 2.2 for all networks

Calculations of mobile chain fractions are based on the integration of DMA Tan δ. DMA was performed on 60 × 5 × 1 mm bars of material cured for 2 hours at 60 °C and one hour 80 °C.

The peak and downward trending loss of adhesion above T_g-20 °C has not yet been explained in the literature. Before investigating possible mechanistic pathways consistent with the peel force data that are occurring within the films and at the interface, it is imperative to make sure the same failure events are being compared at all temperatures. Peel force decreasing above T_g-20 °C because of a transition from adhesive to cohesive failure indicates a very different situation than peel force decreasing and maintaining the same failure mode. Failure surfaces were imaged by an optical

microscope for all coatings and test temperatures. Results from HTg for temperatures below, at, and above the peak peel force are shown in Figure 2.11. Images from room temperature and the remaining coating chemistries are now shown as they were similarly clean failure surfaces.

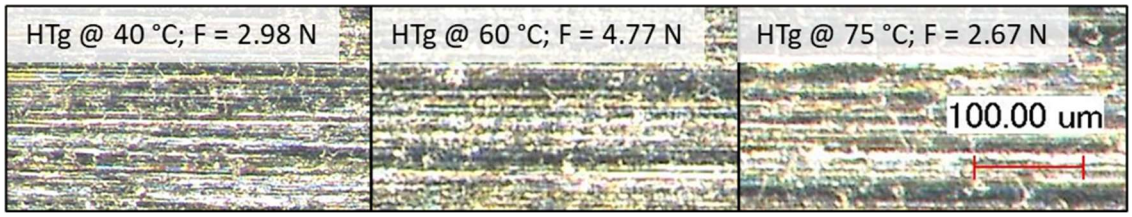

Figure 2.11 Fracture surfaces of HTg peeled at temperatures corresponding to peel forces left) below, middle) at, and right) above the peak peel force

Images were taken using a Keyence optical microscope at 200x magnification of an area exposed by peel experiments. No coating residue is visible on the substrates at any temperature for HTg or MTg and LTg (not shown).

Storage and Young's modulus correlate indirectly with peel force and can be considered the inverse of chain mobility. Peel force peaks at temperatures immediately preceding rapid changes in modulus where local chain bending and conformational motions give way to segmental motion. Thermodynamic processes such as relaxation benefit from segmental motion but are detrimental for interfaces as the heterogeneous interactions across the interface are less favorable than homogeneous cohesive interactions. Cohesive forces between network components are generally stronger than adhesive forces between dissimilar materials. This is supported by the similarities between cohesive energy densities of the three resins compared to the cohesive energy density of the substrate. Consequently, it is hypothesized that providing the thermal energy for network segmental motion allows more interfacial polymer functional groups to turn inwards, away from the interface, and form associations with bulk polymer functional groups. The orientation of chains in the original liquid film does not reflect

this preference because mobility decreased as available functional groups are changing, and intermolecular distance was decreasing, and because of the large degrees of freedom of the network building blocks, less thermodynamically favorable orientation was still statistically likely due to kinetics. If the solid forms were to be put in contact with the same substrate and heated, the same bonds would not form. Peel forces and associated storage moduli are plotted together in Figure 2.12 to support the assertion of a modulus-driven loss of adhesion. The rate of modulus loss changes at the same temperature as the adhesion begins to decrease.

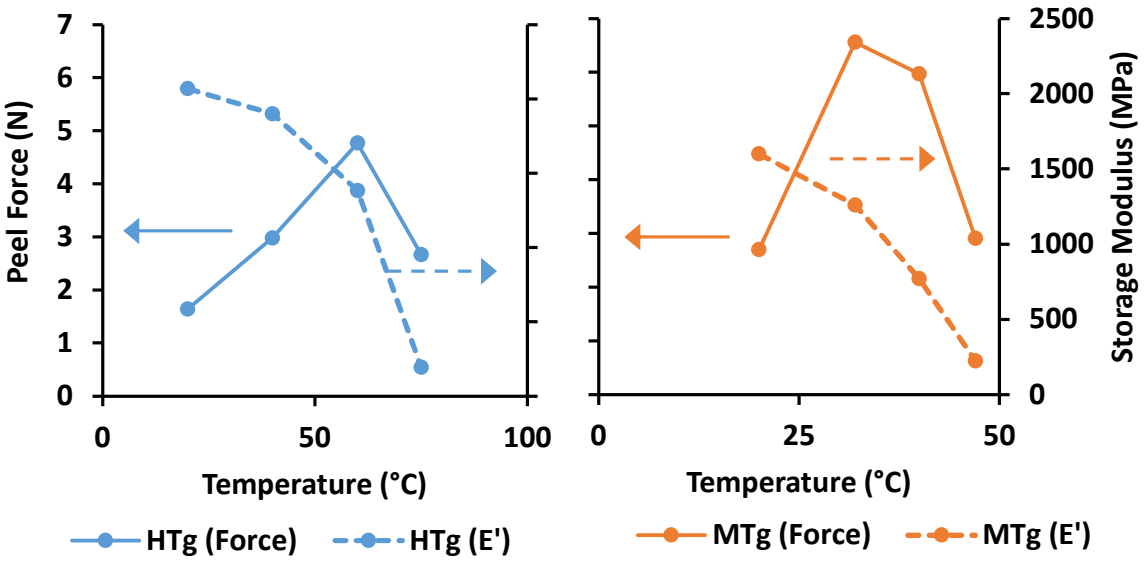

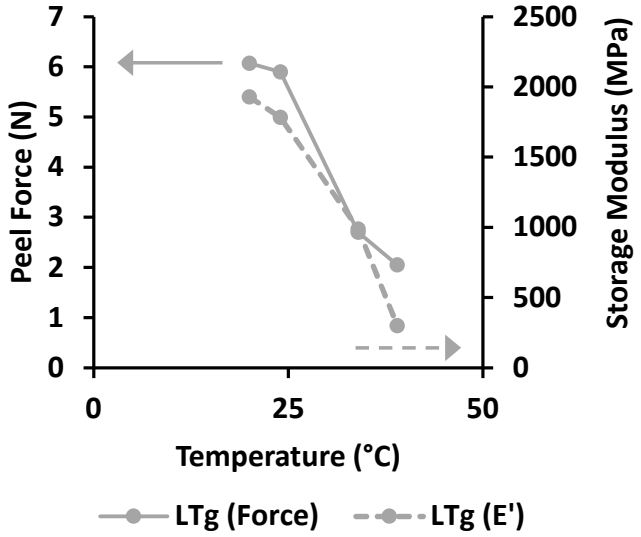

Figure 2.12 Relationship between peel force and storage modulus as measured by DMA

Peel force measured from 40 µm films on AA 2024, storage modulus measured on 1 mm thick bars

Visually it is difficult to discern any difference between the correlation of modulus and peel force at temperatures above and below peak adhesion. Correlation can be calculated as the closeness to a direct linear relationship between the two variables. Portraying peel force as a function of modulus, as shown in Figure 2.13, illuminates the effectiveness of a correlation calculation. The goal would be to compare the correlation coefficient of (modulus, peel force) data points at temperatures above and below the peak adhesion, but none of the data sets included more than one data point above and below the peak adhesion. Increasing the number of test temperatures and calculating both correlation coefficients would be an effective approach to validating the hypothesis.

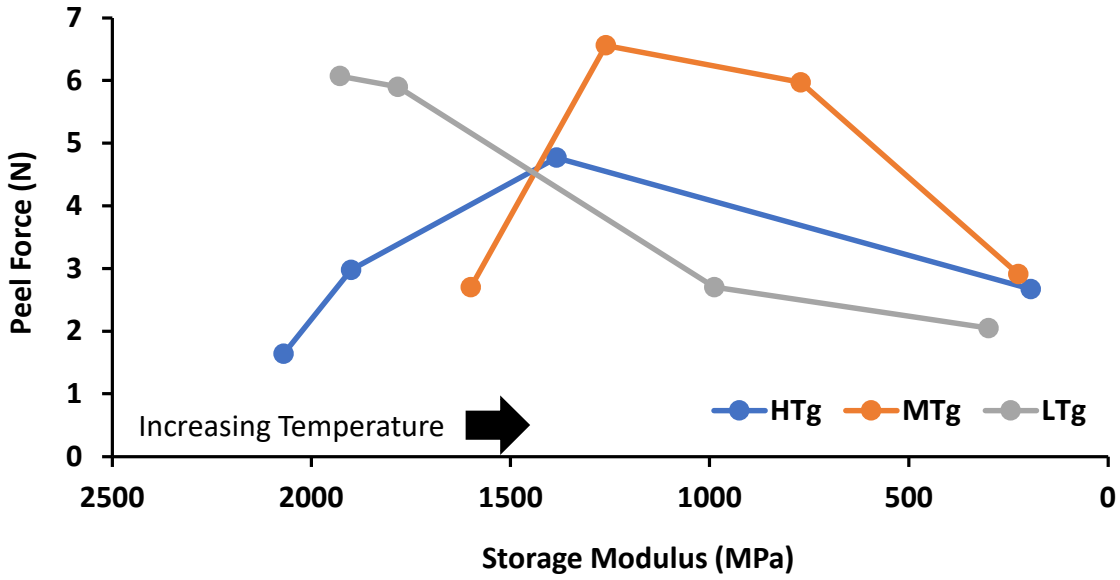

Figure 2.13 An illustration of the relationship between coating storage modulus and peel force

Correlation calculations above and below peak peel force are inconclusive

The increase in peel force with the test temperature towards T_g-20 °C was attributed to an increase in local chain mobility at the interface, but the heat of fluidity (the variable accounting for chain mobility by Hofreichter and McLaren) is not present in Equation 2.1. The absence of heat of fluidity suggests the dependent variables are themselves functions of other dependent variables. Each of the variables in Equation 2.1 was considered; the modulus is known to have an inverse relationship with the temperature at all temperatures; internal strain increases linearly with the coefficient of thermal expansion; film thickness increases with temperature. The remaining unknown that could account for the decrease in peel force is the work of adhesion (γ). In many cases, the work of adhesion is calculated from contact angle measurements or as a function of sorption strength and frequency, resulting in a quantity for thermodynamic work of adhesion. An example of thermodynamic work of adhesion as a function of temperature can be seen in Figure 2.14;

maxima are present, but the increase is linear towards the polymer glass transition. In the case of thermodynamic work of adhesion as with peel force, the increase in interfacial strength occurs despite decreases in individual interaction strength. Atomic interactions weaken with temperature because the formation of secondary interactions is an exothermic process, and the average distance between the participating atoms increases with kinetic energy. Decreases in interaction strength and sorption occur alongside decreases in modulus at all temperatures, which suggests practical work of adhesion calculated in Equation 2.1 is itself a function of multiple variables, including a variable that must be increasing (e.g., chain mobility), resulting in a non-linear response, accounting for a peak in peel force. Practical work of adhesion (WoA) includes the effects of roughness, mechanical adhesion, and the transition from side-chain motion to segmental motion.

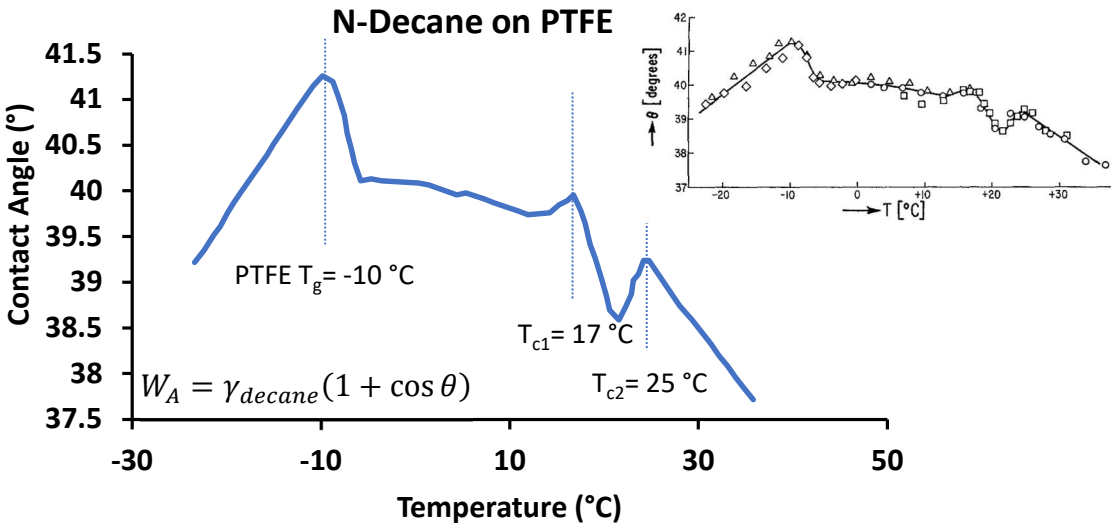

Figure 2.14 The contact angle of n-decane on PTFE to demonstrate the overall non-linear relationship with the temperature and the local linear increase in the region investigated by the present study

Replotted data from Neumann and Tanner[64]

There are no studies directly comparing practical work of adhesion of a coating to temperature, but Kendall makes a point to differentiate thermodynamic work of adhesion

from the practical work of adhesion or "adhesive energy".[65] Kisin, in their dissertation, likens the adhesive energy to fracture energy and equates it to the sum of thermodynamic work of adhesion and energy dissipated in plastic deformation at the peel front.[66] Zheng argues that adhesive energy is a component of the fracture energy but agrees the quantity is the sum of thermodynamic work of adhesion and dissipation energies. Venkataraman et al. calculated "practical work of adhesion" for a microscratch adhesion measurement method and included shear and normal stress, and shear and elastic modulus.[67] Practical work of adhesion was found to be non-linear with thickness, but never to decrease. Literature suggests practical work of adhesion can be modeled but that it also must be approached differently for each test geometry, and currently, no example of decreasing practical WoA with temperature has been presented. Identifying and taking advantage of the differences between thermodynamic and practical WoA could lead to important discoveries about the mobility and organization of chains at the interface and move adhesion science to a more systematic and purposeful study.

There is precedent to treat the adhesive energy in Equation 2.1 as a function, but no proposed functions can account for the peel force local maximum. Peel strength calculated with a positive linear work of adhesion is shown in Figure 2.15 and results in peel forces with linear temperature dependence. Hui et al. calculated thermodynamic and practical adhesion and asserted that practical WoA is much more influential than the thermodynamic WoA alone on the measured, practical adhesion.[68] The strong influence of practical WoA is consistent with Figure 2.15, where calculated practical WoA and calculated peel strength have a high correlation. The dependence of the final peel force on the adhesive energy is valuable supporting evidence for the hypothesis that the

adhesive energy value itself reaches a local maximum. Discovering that adhesive energy/practical work of adhesion achieves local maxima with respect to temperature is important for developing accurate models and understanding the interrelatedness of properties.

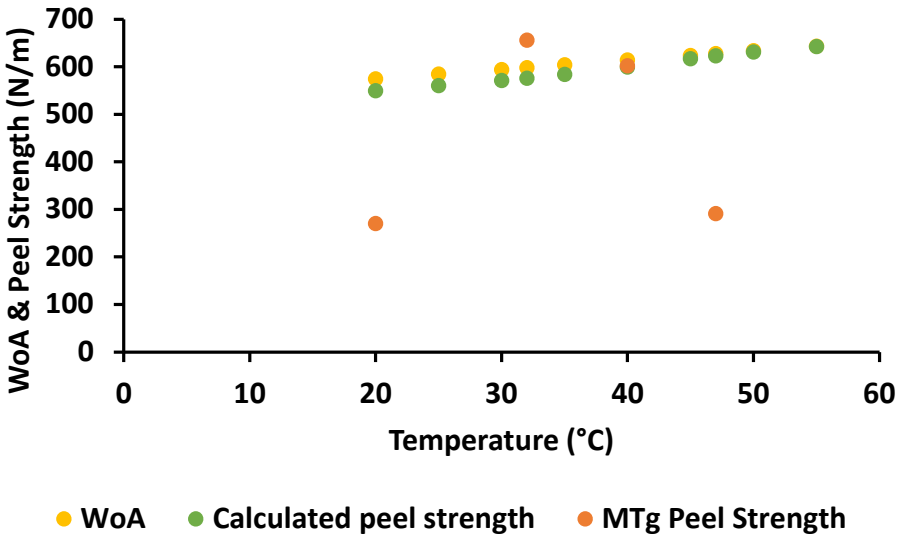

Figure 2.15 Modeling peel strength of MTg with a positive linear work of adhesion

Storage modulus was substituted for Young's modulus in Equation 2.1

Peel force has been shown to peak with respect to composition. Feldstein and Siegel formulated pressure-sensitive adhesives with poly(N-vinyl pyrrolidone) (PVP) and low molecular weight poly(ethylene glycol) (PEG).[69] Increasing the weight percent loading of PEG lead to a local maximum, which is shown in Figure 2.16. Composition in the case of PVP-PEG is analogous to test temperature because of the large disparity between PVP and PEG T_gs (130 and -63 °C, respectively); adding PEG has the effect of moving the material T_g closer to room temperature. Another important observation is how the peel force (P in Figure 2.16) correlates with the total work of viscoelastic deformation-at-break of the films (W_b) or area under the stress-strain curve. Tensile tests were never performed on LTg, MTg, and HTg at the peel test temperatures, but these

findings provide a path to pursue to identify the variables affecting practical work of adhesion in 90° peel adhesion measurements.

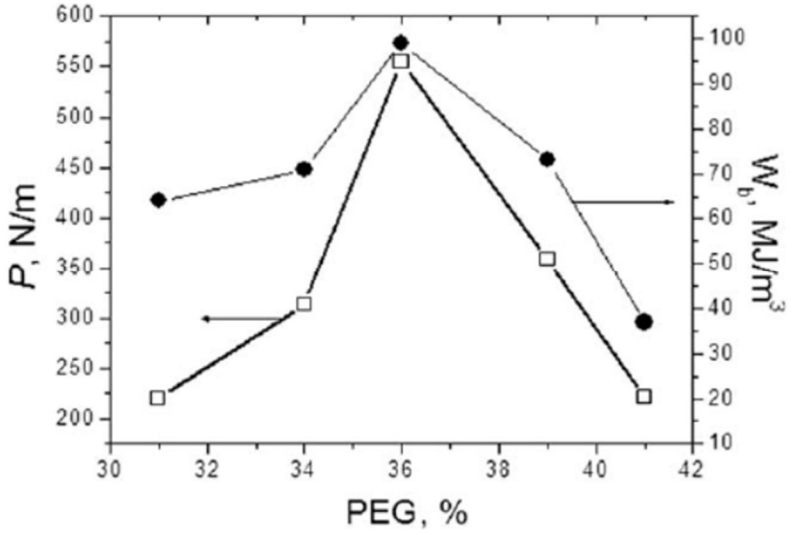

Figure 2.16 Local peel force (P) maximum with respect to poly(ethylene glycol) loading in poly(N-vinyl pyrrolidone) as a pressure-sensitive adhesive

Peel force correlates with the viscoelastic work of deformation at break. From Feldstein and Siegel.[69]

2.3.3 Peel Adhesion Relative to T_g

Adjusting the x-axis of Figure 2.8 to indicate the °C below T_g (T_g-T) of each measurement, instead of absolute temperature, aligns the curves together, as seen in Figure 2.17. Relative peak positions seen in this depiction are reminiscent of the alignment seen by Hofrichter and McLaren in Figure 2.1 on PVC-PVAc-maleic acid blends, which were designed to each have the same T_g.[56] The overlap indicates that between 20 and 25 °C below T_g, there was a critical level of network fragment mobility that increased polymer-substrate contact and the difficulty of delamination without compromising structural or interfacial stability. Aligning the curves makes the peel force magnitudes more easily comparable and reinforces that differences in peak peel force are dependent on more than

each material's degree of gassy or rubbery nature since those were essentially canceled out by adjusting to a T_g-T framework.

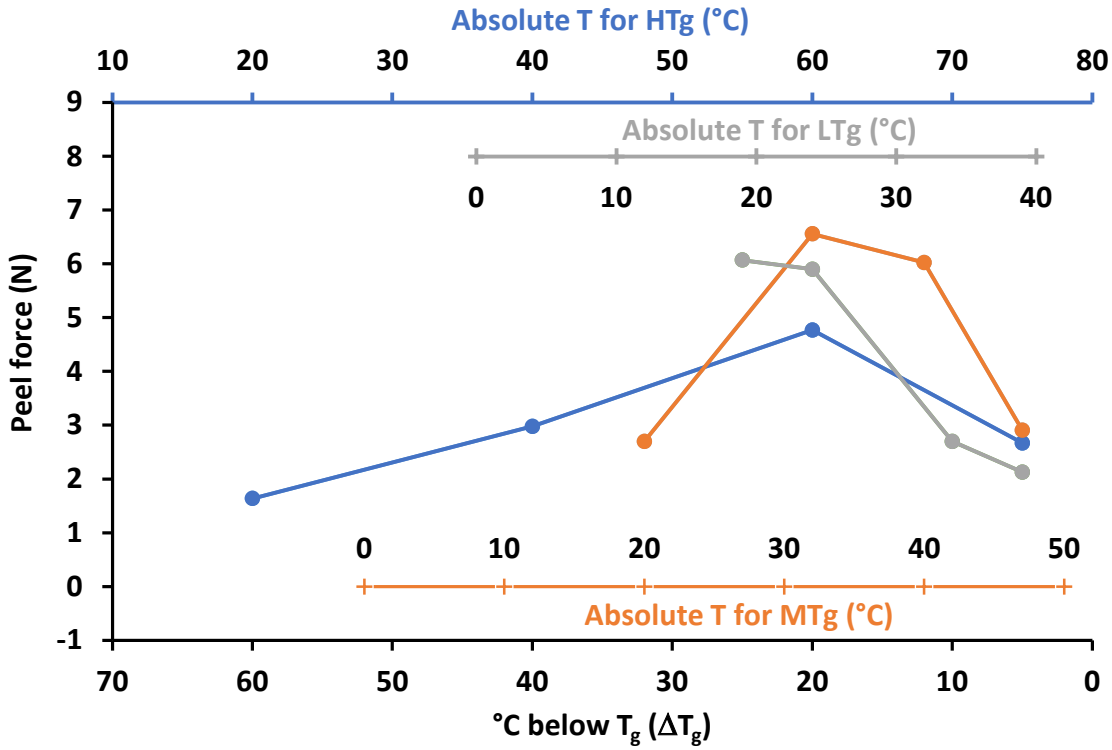

Figure 2.17 Material T_g temperature adjusted Peel force values for each of the three epoxy-amine thermoset polymeric materials, comparing test temperature and material T_g (T_g-T) with closely matched molecular weights between crosslinks.

Coatings were applied to AA 2024 and cured for 2 hours at 60 °C and 1 hour at 80 °C, resulting in 40 µm thick films. For clarity, test temperature is also displayed on additional x-axes for each coating.

Viewing the adhesion value as a sum of effects from sorption, viscosity, and energy dissipation suggests that there must be something universal that happens at T_g-20 °C to make all three epoxy-amine resins and vinyl blends experience the same peak position. As T_g is approached, the heat of fluidity increases, and an approximation of the heat of fluidity can be modeled using modulus as an analog for viscosity. Approximate heats of fluidity as a function of temperature for each coating chemistry are shown in Figure 2.18. There is a significant change in derivative at the temperature where

adhesion begins to decrease. An exaggerated increase in the heat of fluidity means the amount of energy required to achieve the same increase in flow becomes much greater; therefore, the diminishing return coupled with the transition to segmental motion is potentially responsible for the local maximum. Feldstein and Siegel attribute the peel force maximum to a transition from brittle interfacial failure to a fibrillar type of adhesive failure, which could be the macroscopic outcome of the heat of fluidity and modulus changes.

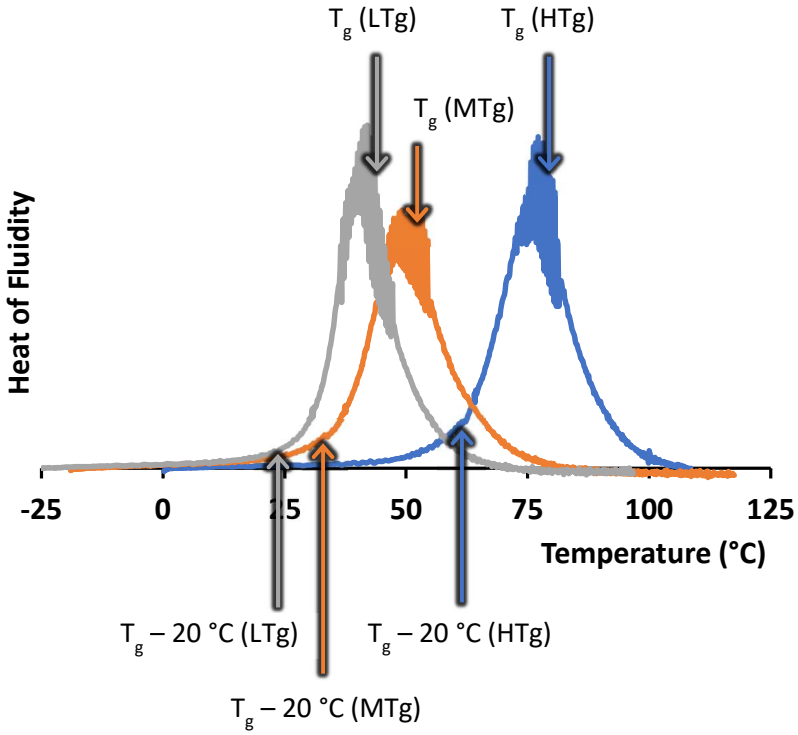

Figure 2.18 Calculation of hypothetical heat of fluidity based on equations from Hofrichter and McLaren.[56]

Modulus used as an analog for viscosity

One major goal of this work was to better isolate interfacial changes using mechanical based adhesion testing methods. Figure 2.19 compares peel adhesion measurements collected at constant temperature versus constant T_g-T. For constant

temperatures 20 and 40 °C, peel force comparisons between resins are inaccurate because of the differences in physical states between the coatings. At 20 °C LTg is at its highest adhesion; at 40 °C MTg has just passed the peak peel force temperature (T_g-20 °C = 32 °C), while HTg is still approaching the peak temperature (60 °C), which leads to LTg and MTg presenting exaggerated peel forces at 20 °C and 40 °C respectively. When all resins are compared at T_g - 20 °C, mechanical advantages associated with approaching T_g - 20 °C are removed, and the effects of the interface are more pronounced. The differences between peel forces at constant temperature relative to T_g are much smaller than at constant temperature, which is understandable considering the similarities in composition.

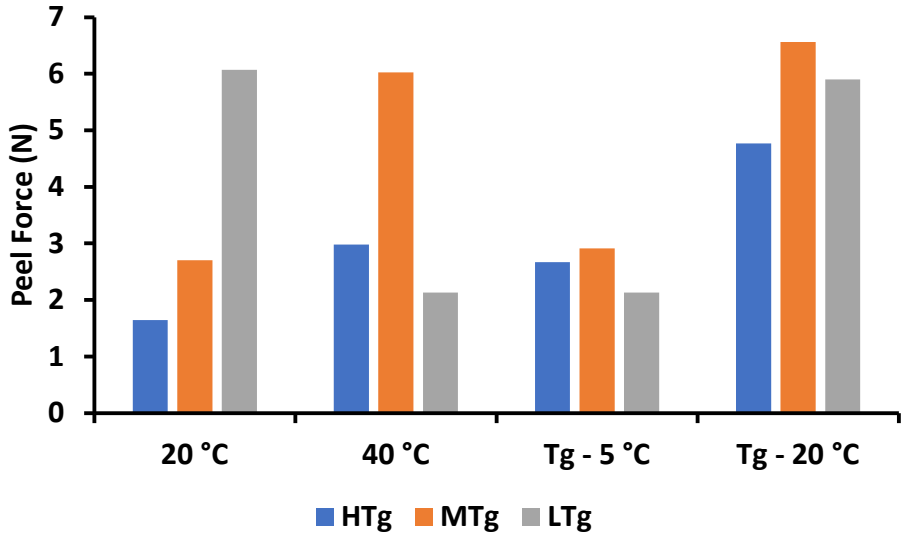

Figure 2.19 Comparison of peel forces collected at constant experimental temperature to constant thermal distance from T_g (T_g-T)

T_g of HTg = 80 °C; of MTg = 52 °C and LTg = 44 °C

In the absence of physical state effects, it was possible to discern that interfacial functionality is not solely responsible for interfacial strength. Calculated CED identified HTg as being the most chemically compatible, but MTg was observed to achieve the highest peel force. In both the leathery (T_g-5 °C) and glassy (T_g-20 °C) region, MTg

outperformed the other compositions, which was suggested to be a result of a large percentage of network mobility at the critical temperature, and a balance of domain stiffness and inter-domain flexibility as a leather. In the presentation style used in Figure 2.19, the effects of those mobile chains can be seen as the difference in peel force at constant temperatures relative to T_g.

In the transition from leather (T_g-5 °C) to glass (T_g-20 °C), the coating with the lowest peel force changes from LTg to HTg. How the peel force changes between the T_g-T temperatures illustrates how the phenomena introduced to explain storage moduli differences presented in Figure 2.6 relates to the changes in the interfacial environment. At T_g-20 °C, adhesion correlates well with percent network mobility. At T_g-5 °C, HTg benefits from the high concentration of hydroxyl groups, but the higher temperatures render the peel force lower than MTg. Whether T_g - 5 °C or T_g - 20 °C is more indicative of performance and under which conditions have yet to be explored, but this comparison sheds more light on interfacial variations than the constant test temperatures. Considering the thermally cyclic nature of the environment within which many coatings will be utilized, the full adhesion response over that temperature range may be more indicative of a coating potential for longevity than any single adhesion result, e.g., peel force at any single temperature.

Characterization of resins' mechanical and adhesive properties have identified similarities between different pairs of resins. Maximum peel forces for MTg and LTg were 0.5 N apart, which also reflected the proximity of their T_gs (only 8 °C difference). However, from a mechanical standpoint, HTg and MTg storage modulus responses correlate much better than LTg, which achieves much higher modulus values.

Considering the differences in T_g between HTg and MTg, the similarities are hard to see in Figure 2.5. By comparing the temperatures required to reach the critical modulus for each material, as shown in Figure 2.20, the similarities between moduli at the critical adhesion temperature of MTg and HTg are revealed. This suggests a morphological difference between LTg and the other resins. Achieving the highest modulus but having the lowest T_g points to there being something different about the domains involved in the thermal transitions while in HTg and MTg, they may just be different sizes or composition. LTg likely has different connections between domains; the connections could be made by epoxy units instead of ED-600 units, for example.

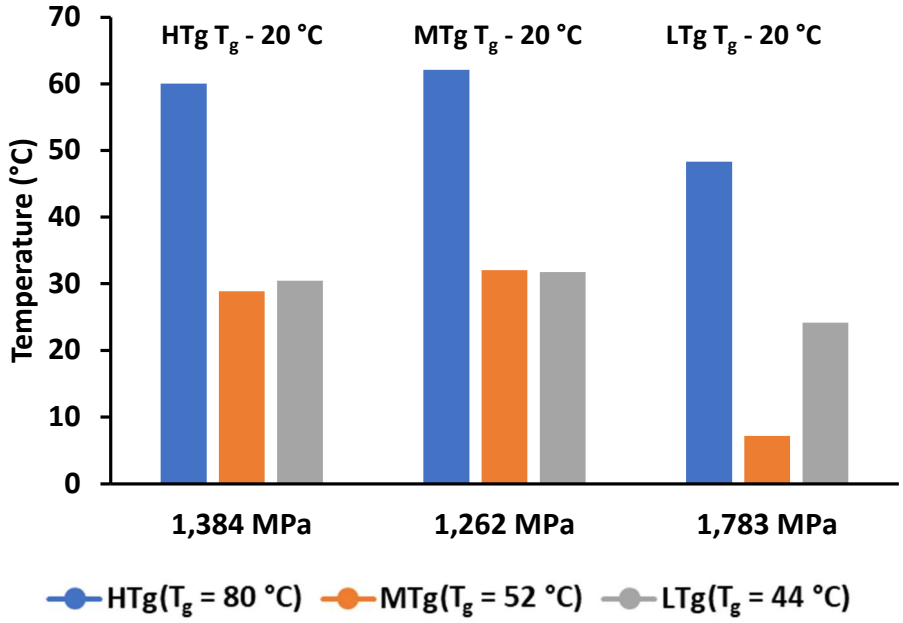

Figure 2.20 Storage modulus measured by DMA corresponding with T_g-20 °C for HTg, MTg, and LTg, alongside temperatures for remaining resin where the same storage modulus is achieved

For example, T_g – 20 °C for HTg is 60 °C, and according to DMA, storage modulus at 60 °C for HTg is 1384 MPa. MTg and LTg have a storage modulus of 1384 at 29 and 30 °C, respectively. Moduli obtained from DMA of poured bars in tension

Analysis of interfacial strength through mechanical methods of adhesion measurement is incomplete without consideration of material mechanical and interfacial

behavior. Peel adhesion measurement at constant temperature relative to T_g allows for normalization of polymer physical state but not the elimination of bulk property effects. Many phenomena like chain mobility that drive mechanical changes also affect the interface, so completely removing bulk effects from the interface would lead to unrealistic interfaces and results.

2.4 Conclusions

Experimentation in the present Chapter included measurement of the temperature dependence of mechanical properties by DMA and adhesion by 90° peel. From these data, it was possible to conclude,

1) peel adhesion varies significantly over temperature ranges near the glass transition temperature. Temperature ranges often experienced as environmental fluctuations within experimental testing,
2) the practical work of adhesion has a direct correlation with peel force. Practical work of adhesion is not an entirely interfacial variable but rather a function of an unknown number of variables, i.e., viscoelastic work, heat of fluidity, heat of sorption, degree of cure, solvent retention, etc.,
3) chain mobility and mechanical properties alone cannot explain peel force results and
4) network topology and heterogeneity influence bulk and interfacial properties through thermal relaxation.

By measuring peel adhesion at multiple temperatures, it was possible to map the temperature dependence of adhesion for high, moderate, and low T_g coatings.

Experiments revealed that each resin had significant temperature dependence of adhesion, and all systems exhibit higher peel force at T_g-20 °C. In the most extreme case, the peel adhesion of the model coating increased by a factor of 2.4 over a narrow range of 12 °C. At first glance, this appears to be a result of the 90° bend having less effect on the interface as modulus decreases, but in that case, the peel force should increase continuously with temperature as modulus continues to decrease through the peak peel force seen at T_g – 20 °C.

For each of the thermoset networks in the present study and the series of thermoplastic blends from the literature, the peak adhesion was achieved at T_g-20 °C indicated a unifying relationship between adhesion and the distance from a given material's glass transition temperature.[56] As temperature increases toward T_g-20 °C, peel force consistently increases as well, and this was attributed to local chain mobility. The interface benefits from active interfacial chains through the formation of a higher number of interfacial interactions despite the accompanying decrease in sorption favorability at higher temperatures.[56] Above T_g-20 °C, the local chain motion gives way to longer-range network flexibility. Local chain mobility increased the number of interfacial interactions, but homogeneous interactions within the polymer are energetically preferable, and those conformations can be achieved above T_g-20 °C.

The peel force transition did not occur at T_g exactly because of mechanical changes happening simultaneously. Peak peel force temperature corresponded to a shift from an elastic to a more viscoelastic material response where higher strains were accessible but much lower stresses. A high correlation between peel force and viscoelastic work, especially above T_g-20 °C, indicated the peel forces collected at

temperatures above critical adhesion is less dependent on the interface and more on mechanical properties. Finding correlations between peel force data and both heat of fluidity and viscoelastic work led to the conclusion that neither chemical nor mechanical properties alone can explain the results.

Previous literature modeled the peel force with respect to thickness by including material variables like modulus and work of adhesion. In the present study, the equation was used at multiple temperatures to understand the variable responsible for the local peel force maximum.[70] The commonly measured variables like modulus and internal stress vary monotonically with temperature, leaving the work of adhesion to best correlate with peel force. By modeling the response of each variable to temperature, it was determined that the equation uses a practical work of adhesion, it, in turn, being a function of bulk and interfacial properties, unlike the thermodynamic work of adhesion, which is purely a measure of the strength of interfacial forces and the hypothesized variable of interest for resisting interfacial chemical attack.

Relaxation experiments performed by Pistor and coworkers are relevant to the peel force responses of the epoxy-amine model coatings in both understanding their mechanical and adhesive responses.[59] The rotational, conformational, and domain motions that exist below the glass transition can explain how the lowest T_g material can result in the highest modulus in the glass phase. Additionally, for MTg and HTg, a modulus-based framework would lead to the same T_g-20 °C test temperatures but not for LTg, which has an equivalent modulus at T_g-13 °C instead. The difference suggests that the morphology of LTg may be considerably different from HTg and MTg to achieve the observed thermomechanical responses.

Solubility parameters and cohesive energy densities (CED) were calculated for each matrix material to further discern between the molecular basis for adhesion and temperature differences in material adhesion. Model coatings were composed of varying ratios of four common building block monomers, which led to similar CEDs. According to the calculations, the highest T_g material was found to be the closest to the CED of the substrate due to the hydrogen bonding component; however, HTg did not achieve the highest peel force. It was possible to quantify the fraction of mobile chains at peel measurement temperatures via an integration of the Tan δ curve collected from DMA up to the test temperature, compared to the total area under the curve. Comparing peel forces at T_g-20 °C to material moduli and fraction of mobile chains uncovered a much better correlation, and MTg achieved both the highest peel adhesion force and the largest modulus*mobile chain fraction result.

The predictable progression of physical states and the knowledge of the critical adhesion temperature can be used to design more meaningful adhesion experiments and prevent results from being skewed by mechanical transitions when interfacial information is desired. Viewing peel forces from a constant T_g-T framework, when polymer physical state is not a variable, the medium T_g resin has the highest adhesion. Measurement at room temperature would not lead to the same conclusions. Similar to the competition between sorption and flow, the adhesion strength of hydroxyl groups on Epon 825 is in competition with the mobility of Jeffamine ED-600. These data imply curious relationships among polymer physical state, morphology, chain mobility, and adhesion. The assertion of adhesion being lost to cohesion as segmental motion becomes available, and the relationship between practical work of adhesion and work of viscoelastic

deformation has not been experimentally proven, opening the door for important studies into aging, mechanical properties, and modeling.

CHAPTER III – EVALUATION OF STRESS-STRAIN AND DERIVATIVE-STRESS STRAIN RESPONSES FOR THE ADVANCEMENT OF PULL-OFF ADHESION DATA PROCESSING AND PROCEDURE OPTIMIZATION

3.1 Introduction

3.1.1 Pull-off adhesion testing

A variety of test methods are available for adhesion; while some are practical, none can be considered standard or capable of quantifying interfacial strength.[41,50,71] The macroscale and mechanical methods of measurement, like peel, pull-off, scratch, and indentation, which take full-scale coatings and apply a mechanical force to the interface in tensile or shear directions.[42,43] Macroscale chemical methods for early corrosion measurements like cathodic delamination or cyclic environmental exposure subject coated substrates to applied loads to the interface as challenge solutions of water and corrosive species. Methods have been developed, like microscale chemical methods, including Auger electron spectroscopy measures the energy required to remove layers of coating and can differentiate the cohesive bulk strength from the interface.[49,72] Finally, non-destructive methods are available like the capacitance and ultrasonic tests.[48] Unlike tensile modulus, which can almost always be measured by a tensile test, the appropriate adhesion measurement method to be used in a study depends substantially on the adhesion quantity of interest and the application space of the material.

The differences in treatment between bulk and adhesive properties arise from the numerous ways an interface can fail (chemical, physical, thermal) and the fact that the area of interest in the study of adhesion is obscured underneath a coating. Figuring out how to access the interface and interfacial information without compromising the

substrate or polymer sample is a crucial requirement. Mechanical tests are a logical choice for an interface in an application expected to experience large or frequent mechanical loads, but the methods are almost all destructive. To quantify adhesion over time, probing the same interface in a non-destructive method would be a requirement. Decisions on which test to perform can be based on ease or simplicity. Much coating adhesion testing is still performed by crosshatch and tape methods despite having no way to account for human error or collect quantitative data. Accuracy or depth of information are sacrificed in order to avoid dealing with an obtuse instrument like in ultrasonic or x-ray tomography methods.[73]

Literature indicates a complacency of researchers to accept the uncertainties that come with an already available method rather than modifying the approach to lessen shortcomings. For example, adhesion measurements collected from mechanical testing methods have notoriously high standard deviations but are employed regularly anyway because the test is easily accessible from a theoretical understanding and practical execution standpoint. Opportunities are available to address the variation that is being ignored. The processes an instrument and sample go through in the duration of an adhesion measurement is often treated as a black box. The sample was made with care, but after being put in the load frame or environmental chamber, forces are applied, the system fails, and a number is produced, but what happens during the experiment can be equally valuable for understanding how the material functions. Intermingling between science and practice within the coatings field provides novel opportunities and pressure to pursue a balance of simplicity in characterization methods but depth in the results.

Pull-off adhesion measurement provided a perfect example of a widely used mechanical method with overlooked potential additional data. The measurement technique quantifies adhesion as the tensile force required to separate two surfaces, and in the process, generates stress versus strain force measurements that provide more quantified values than the single force measurements resulting from the peel test used in Chapter II. The sample geometry and test method execution for pull-off and tensile-butt tests are depicted in Figure 3.1. Tensile methods are often chosen for their balance of straightforward concept and procedure while providing numerical results. Measurements can be performed on-site using a portable tester (as is described in ASTM D4541), granting the method attractive versatility and the ability to compare field and laboratory data. Significance and depth of information can be added to the measurements if the portability is sacrificed to be performed on laboratory load frames.

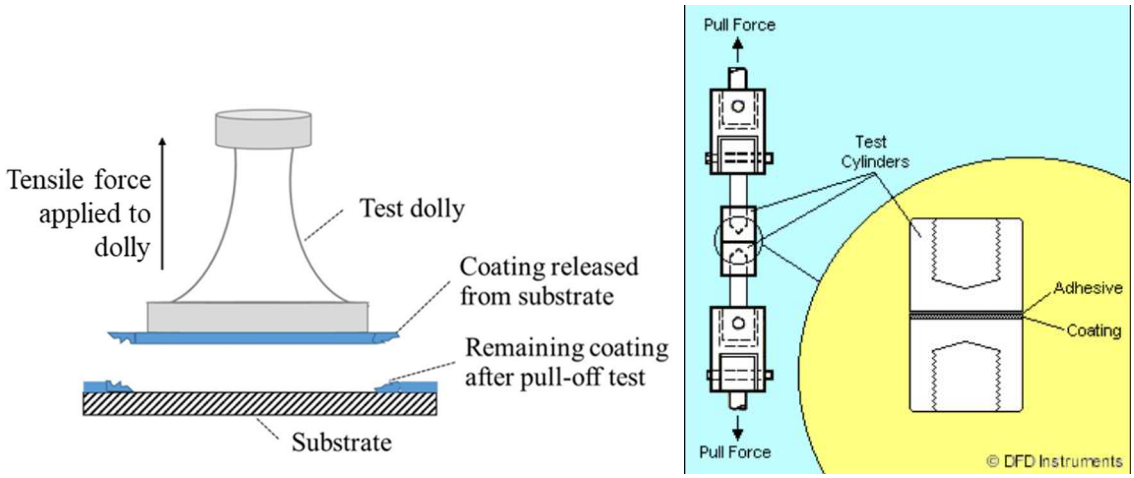

Figure 3.1 Illustration of pull-off sample geometry and testing procedure. ASTM D4541 on left and ASTM C633 on right

From Meng et al.[74] and Maxwell[21]

As a mechanical method of testing adhesion, pull-off suffers from high variability, which is partially a result of the seemingly infinite number of dependent variables in the testing process. From the geometry of the dolly to methods of preparing

the test surface and how the dolly is applied, they will all change the peak pull-off stress measured for a coating. Some variables have been previously explored in the literature and technical reports. Fletcher and Barnes investigated the effects of adhesive mixing ratio, the brand of adhesive, dolly and coating surface preparation method, dolly geometry, adhesive cure procedure, and testing instruments and found that all sample preparation variable affected the peak stress outcome.[19] Unfortunately, their treatment of the results were statistically questionable. Each sample set consisted of n = 5 pulls, where they only averaged the middle three values, even when none of the values could be considered outliers. Maxwell compared the two ASTM geometries shown in Figure 3.1, where D4541 incorporates a coated flat substrate as the sample and requires the attachment of a dolly and C633 sandwiches the coating and adhesive between two identical platens and found the orientations to give comparable results.[21] Like Fletcher and Barnes, however, the sample sizes Maxwell used were suspiciously small. Roche et al. described the predictable way pull-off force and peak stress of an epoxy coating changed with dolly diameter but fell short of extending the finding to general rules for how to compare peak stresses between studies using different dolly surface areas.[75]

The present study addresses both the adhesive amount and adhesive brand. Finding the optimal adhesive configuration is critical for success in pull-off adhesion testing to ensure failure at the desired interface. When force is applied to a dolly in a pull-off experiment, the coating-substrate, coating-adhesive, and adhesive-dolly interfaces are all being stressed, but only failure at the coating-substrate interface yields usable information. The two other interfaces must be stronger than the interface of interest to quantify coating adhesion. Having an effective method for determining the

right adhesive is an important foundation, and numerical support for minimizing adhesive mass per dolly eliminates another variable from the optimization process.

Scoring around the dolly and segregating the test area from the surrounding coating is a sample preparation parameter that every researcher who is working to improve the pull-off adhesion methodology has tried to understand. The competing philosophies are that the act of scoring initiates failure at the interface prior to the execution of the test, leading to results that are lower in peak stress and with a higher variation. The counterargument is that without scoring, the applied stress extends beyond the area under the dolly, and part of the fracture surface includes cohesive failure through the coating thickness. Roche et al. performed pull-off on epoxy paint with and without scoring around the dollies over a range of thicknesses and found that the scored peak stress was reduced at all thicknesses studied. They identified this as evidence of interfacial failure initiation during the scoring process. Baek et al. found a similar trend, but also that the difference in peak stress caused by scoring decreases with thickness. Fletcher and Barnes found that scoring reduced the peak pull-off stress but concluded, based on failure surfaces, that scoring was damaging the adhesive coating interface more than the coating substrate interface. These data are not wrong, but the authors assume that the higher value is the correct value. Without scoring, the interfacial strength is artificially inflated. Turunen et al. modeled the stress distribution in a pull-off sample geometry with and without isolation of the area under the dolly and found that when scoring is avoided, stress concentrates at the adhesive-dolly interface, and stress is distributed outside the volume under the dolly. The goal of the pull-off test is to initiate delamination between the coating and substrate; however, looking at the stress

distributions in Figure 3.2 from Turunen, the failure is more likely to occur at the adhesive coating interface if no scoring is performed. This confirms that the peak stress will be higher when scoring is avoided, but the value is not representative of the interfacial strength.[30]

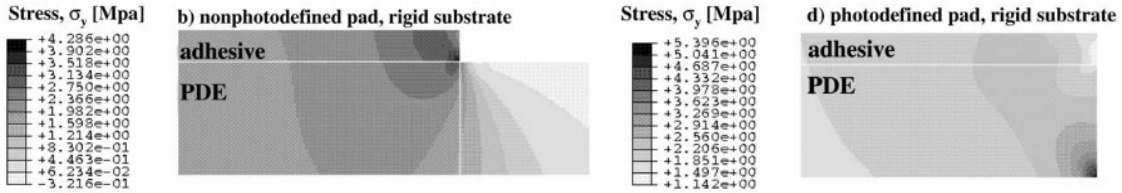

Figure 3.2 Model of stress distribution within coating during pull-off testing with and without scoring

From Turunen et al.[30]

Deciding on a scoring method is not trivial because of the damage it can cause to the coating system. The scoring method should isolate the exact area under the dolly while disturbing the sample as little as possible otherwise. In addition to the illustrations of stress distribution, Turunen also developed a remarkable scoring technique. By selectively photocuring test areas, it was possible to remove the uncured regions without damaging the testing areas. A procedure like this is the theoretical ideal, but not all coatings can be photocured and treated this way. The holy grail is to develop a procedure that can be performed on any applied coating that performs at the level of the development of individual test pads. Inserting something like a knife around the dolly will induce transverse pressure and potentially induce delamination. Carving the coating away can potentially initiate cracking. There is no easy answer to isolating the test area.

3.1.2 Stress-strain mechanics

At its core, the pull-off adhesion test is a specialized tensile test, which means in addition to the peak stress, there are numerous conclusions that can be made from the

stress-strain curve. As a consequence of tensile forces being applied to interfaces instead of material bulk, the resulting stress-strain curves look considerably different. Bulk tensile tests of polymers generally display easily recognizable elastic and plastic regions (Figure 3.3), while pull-off responses appear to only be the elastic region. In the elastic region, chains align, and volume is redistributed, making the material strain reversible. In the plastic region, chains start to slide past each other, and when the sample is released from straining, new local thermodynamic orientations are found, leaving permanent deformation. There is not enough material between the substrate and the dolly to allow for plastic deformation in most cases. As a result, differences between experiments are better seen in the derivative of the stress-strain curve.

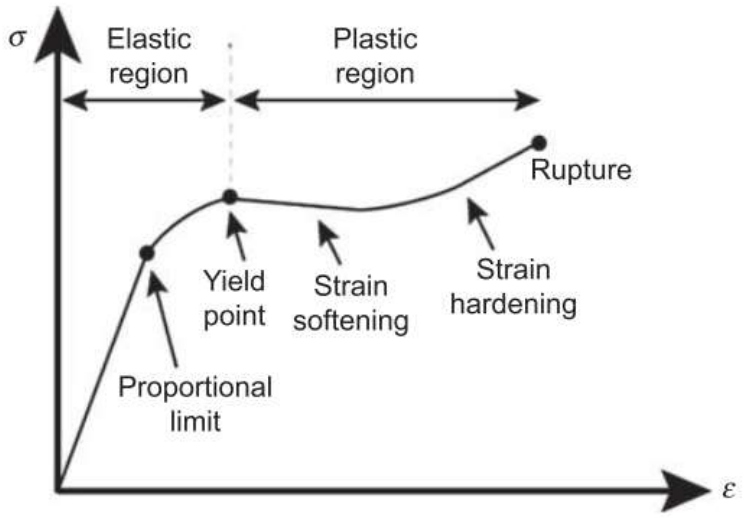

Figure 3.3 Example stress-strain curve of a bulk material with major differences in deformation and resistance to deformation identified along the stress-strain curve

From Arrospide et al.[76]

In this study, a novel data analysis method is described to increase the depth of study possible with pull-off adhesion testing. The method is demonstrated through distinguishing between and choosing an adhesive and scoring method. By analyzing the stress-strain and derivative stress-strain curves associated with pull-off adhesion

experiments in addition to the pull-off peak stresses, it is easier to identify a successful test from an outlier and an accurate measurement of the interface from a flawed one. The adhesives and scoring methods that worked best on the epoxy-amine networks of this study do not automatically translate to all systems, but the features of a reliable experiment are expected to be universal.

Scoring the coating prior to testing is still highly controversial, but the use of the derivative stress analysis method can help with the determination of an effective method. How the substrate-coating-adhesive-dolly stack-up responds to tensile forces can be seen in the derivative curves. An ideal experiment increases in stress linearly with strain and fails uniformly and simultaneously across the test area. Any deviation from the constant derivative stress is investigated from a mechanics perspective.

3.2 Experimental

3.2.1 General materials

All parts of this study used aluminum Elcometer 20 mm diameter dollies and Q-lab cold rolled steel QD panel substrates.

3.2.1.1 Adhesives

Commercial adhesives evaluated were Araldite, Scotchweld DP 460 (3M), JB Weld, JB Clear Weld, and Hysol 9340 (Loctite). Araldite, JB Weld, and Hysol were prepared by weighing and mixing manually. JB Clear Weld components are provided in a fused tube and automatically dispensed in intended quantities, and were mixed manually. Scotchweld DP 460 was dispensed and mixed automatically using a static mixing nozzle.

3.2.1.2 Coating

A coating was only applied to the steel substrates in the scoring method evaluation section of the study. The coating used was an epoxy amine with the chemical composition presented in Table 3.1. All monomers were used as received.

Table 3.1 Model coating raw material composition and weight percent

Monomer	**Loading (wt%)**
Epon 825	73.4
Benzylamine (BA)	10.9
1,3-Bis(aminomethyl) cyclohexane (BAC)	5.3
Jeffamine ED-600	10.4
T_g	80 °C
MW Between Crosslinks	950 g/mol
Young's Modulus	2,835 MPa

3.2.2 Methods

Dolly preparation and application remain consistent across all parts of this study. Adhesion between adhesive and dollies was improved by increasing surface roughness. Clean dollies were abraded with 60 grit sandpaper, followed by a Scotch Brite pad. Debris was removed by rinsing dollies in wash ethanol and wiping on paper towels. The adhesive was applied with an applicator stick and spread across the surface. The quantity of adhesive was limited to approximately 30 mg per dolly except for when comparing adhesive quantity where 60 mg amounts were also studied. The adhesive coated dolly was pressed firmly into the panel and then weighed down with a vial containing 170 g of lead shot. Finally, the adhesive was allowed to cure for 24 hours under ambient conditions.

In all cases, substrates were prepared by cleaning with mineral spirits, dried under flowing nitrogen, and wiped with a microfiber cloth. For adhesive comparison studies, four panels were prepared, each with two dollies, resulting in a total of 8 pull-offs per adhesive.

3.2.2.1 Coating preparation and application

The crosslinked epoxy-amine network model coating was prepared incrementally. Chain extended epoxy trimers were formed first by combining Epon 825 and BA in a speed mixer at 1800 RPM for one minute and letting the monomers react for 30 minutes on a roller. Once Epon 825 and BA were reacted, the BAC and Jeffamine were added and incorporated by speed mixer. The mixture was rolled for three hours. A final 0.1 wt% Tego 270 was added to help eliminate defects, and the mixture was run through the speed mixer one last time.

The importance of scoring was demonstrated on a set of three panels with a total of eight applied studs. Coatings for scoring validation were applied at 35 mils. Serrated tube saw, diamond tube saw, and 90° pick scoring methods were tested on coatings with a range of thicknesses. The coatings were applied by manual drawdown at 3, 5, 7, 9, 11, and 13 mils.

A different distribution of samples was used for panels prepared with the Dremel rotary cutting tool. Three sample sets of 10 panels each were prepared at 1, 3, and 6 mils, each with three dollies for a total of 30 dollies per thickness. An additional set of high thickness panels was also prepared, one panel at 10, 20, and 30 mils. Within the 30 dollies associated with the 6 mil data set, nine were scored with a laser etching instrument instead of the rotary tool to compare the scoring methods.

3.2.2.2 Scoring techniques

In addition to an unscored control sample set, the scoring methods used were a serrated tube saw, a 90° pick, a diamond-studded tube saw, a laser engraver, and a handheld Dremel rotary tool. Images of the handheld scoring tools are shown in Figure 3.4. The serrated hole saw came with a handle and was provided by Defelsko to accompany their Positester portable adhesion tester. A diamond-studded hole saw with a 22 mm internal diameter was purchased from McMaster-Carr, and the handle from the serrated saw was applied to this tube saw as well. The pick used was a Pittsburgh 90° pick. The rotary tool was a Dremel 395 corded handheld tool fitted with a tapered point carbide tip. All scoring methods were used to carve out a trough of coating immediately outside the diameter of the stud all the way through the thickness to the metal substrate.

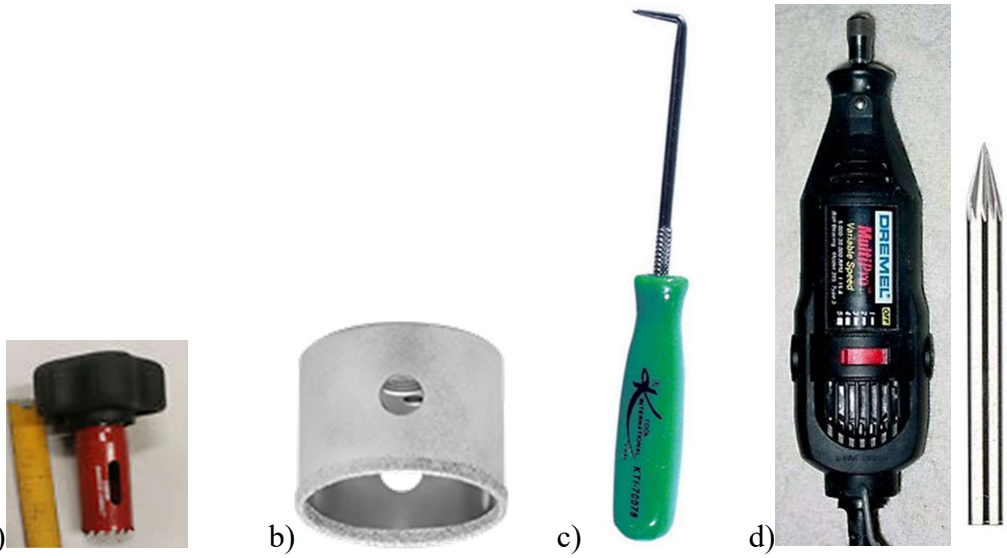

Figure 3.4 Handheld scoring tools

a) Serrated hole saw; b) diamond hole saw; c) 90° pick; d) Dremel rotary tool with carbide steel tapered tip

The laser engraver was the only automated scoring technique explored. The instrument was a Boss Laser metal laser marker with a ytterbium 20W fiber laser. Pulses were shot at 20 kHz at a wavelength of 1064 nm and a spot size of 50 µm.

3.2.3 Pull-off test procedure

Pull-off adhesion experiments were performed on a 10 kN Mechanical Testing Systems Insight load frame equipped with a 10 kN load cell at a strain rate of 2 mm/min to achieve failure in under 100 seconds as described by ASTM.[77] The load frame accessories were custom made and shown in Figure 3.5. A coated panel is held in the lower accessory underneath a cross-plate with a hole to fit the dolly through. The upper accessory was a grip to slide over the exposed dolly connected to the adapter head by a steel cable. A foam block was placed underneath the panel, which pushed the panel up against the cross plate to eliminate any noise caused by gravitational forces, keeping the panel level and making it easier to start each run without any pre-existing stress.

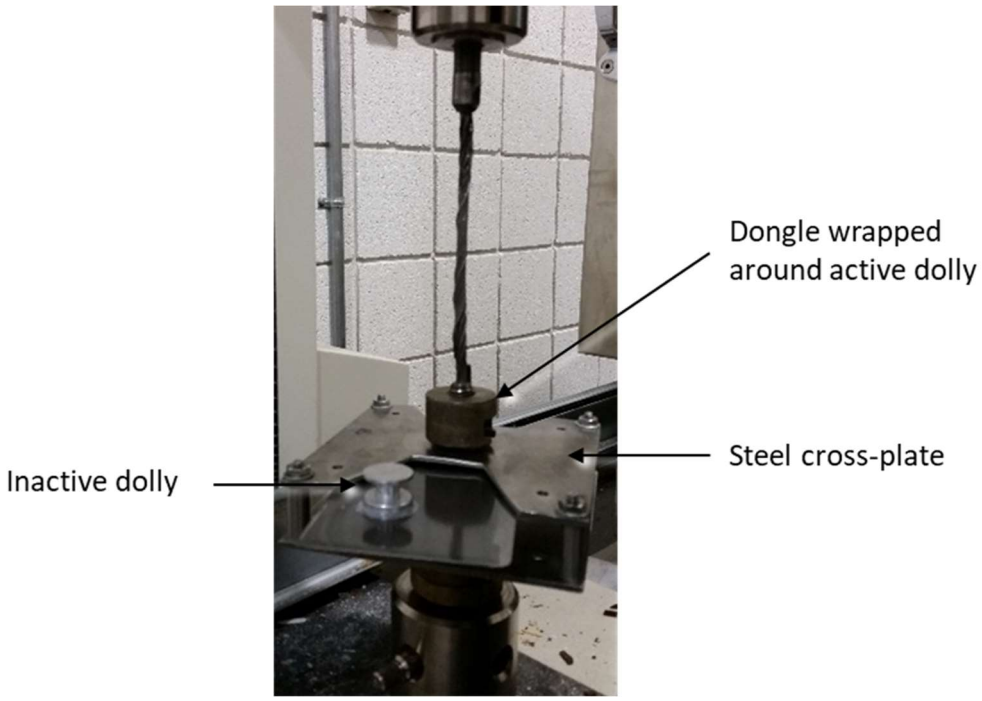

Figure 3.5 Image of custom pull-off adhesion accessories for MTS Insight designed to maintain constant pull angle and optimize z-axis force

Also shown: QD panel with 20 mm aluminum studs adhered with ScotchWeld DP460. Sample variations minimized by maximizing dollies per panel and processing all panels from a data set together from the same resin batch

3.2.4 Calculations

Internal stress and work of adhesion were determined by finding the best fit of Equation 3.1 to the experimental data. The process of finding the best fit is explained in detail in APPENDIX B.

$$\sigma_z = \sqrt{\frac{4.286E\gamma}{t_c} - 2.572\sigma^2} \qquad \text{Equation 3.1}$$

In Equation 3.1, σ_z is peak stress and is a function of t_c for coating thickness, Young's modulus (E), work of adhesion (γ), and internal stress (σ).

3.3 Results and Discussion

3.3.1 Adhesive quantity and data analysis methodology

The upward motion of the load-frame crosshead transfers loads to the coating through the adhered dolly and adhesive. Tensile loads applied to induce adhesive failure in pull-off are analogous to the load applied to a dogbone to induce cohesive failure; in both cases, a stress-strain curve of the process is generated and can be analyzed. Different coating deformation modes in response to a pull-off test can be visualized using the derivative of the stress-strain output with respect to stress. By visualizing the data in this manner, small changes in slope become more apparent, more clearly indicating the strain regimes for linear elastic and yielding processes. Understanding the various mechanical processes occurring during the pull-off test can help identify why peak stresses are higher or lower than anticipated. Increasing strain in the elastic deformation region of a material would produce an increasing slope in the stress-strain curve as the resistance to further deformation increased. In turn, if the slope is not increasing, that indicates a transition to plastic deformation, yielding, or a stress relaxation mode such as

cracking or peeling. The pull-off test is designed to measure the force required to separate the surfaces of interest, and only the coating deformation is valid in that context. The plastic deformation of the cross-plate or the substrate indicates the test is not measuring the strength of the coating-substrate interface as intended. How the slope changes over the course of a pull-off adhesion measurement is utilized to help indicate the measurement accuracy and detect any other deformation processes.

Validation of the use of stress-strain and derivative stress-strain curves for assessing pull-off results is first demonstrated using data collected on Hysol 9340 applied at 30 and 60 mg per dolly. This comparison allows for the analysis of data sets with a minimal number of changing variables. Findings from the comparison also quantitatively support the claim that the adhesive layer should be as thin as possible. Hysol adhesive (30 mg) was applied to 8 aluminum dollies, pressed directly onto four steel panels, and subsequently pulled off to produce stress-extension and derivative stress-extension curves. Sample extension is reported instead of strain because the calculation of strain requires the input of an initial sample length between the clamps, which is too difficult to accurately measure for pull-off geometry.

It is not uncommon for failure under a dolly to occur in stages, albeit often within limited amounts of strain. This type of failure event is undesirable and is one of the ways stress-extension curves can be used to methodically eliminate erroneous results. Incomplete failure events have distinct characteristics that appear in the stress-extension curve and are highlighted in Figure 3.6. Irregularities in pull-off samples are not always apparent in the stress-extension curves, but incomplete failures are better identified in the stress-extension than derivative. Shoulders generated in the stress-extension curve

appear as negative values in the derivative curves, which cloud other details related to the material emphasis in testing. By truncating the derivative traces to only include positive values, more details are discernable. No information is sacrificed in processing the derivatives because such mechanical events are easily visible in the stress-extension curves. Before presenting a full data set, it is important to establish the rationale for removing negative derivative stress values from subsequent curves.

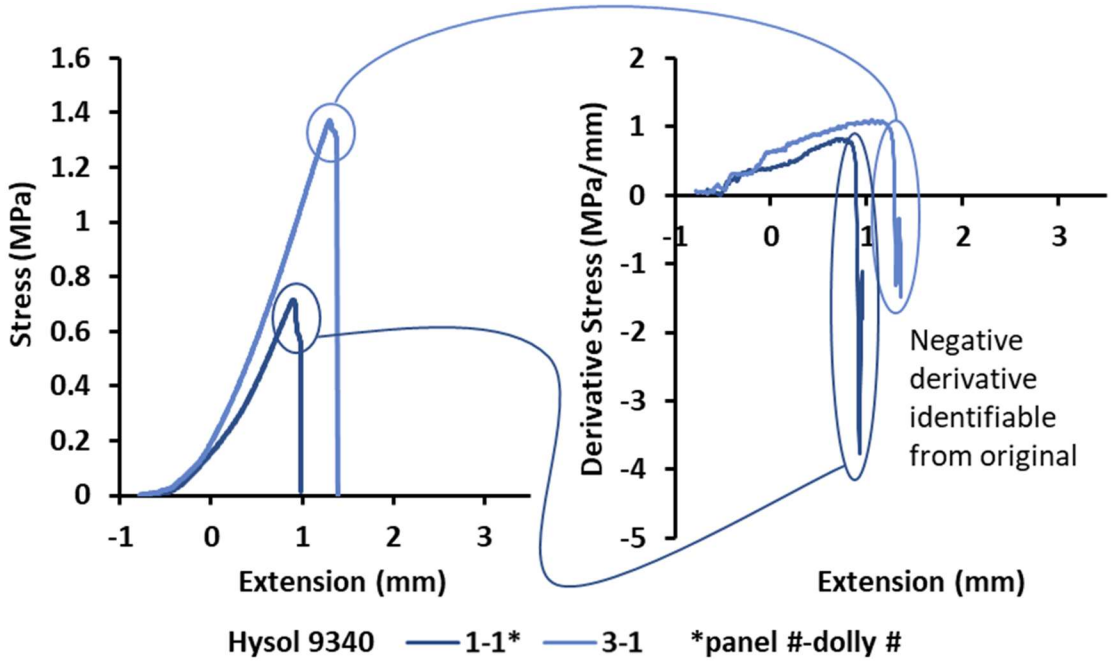

Figure 3.6 Example of how fragmented failure presents itself in pull-off stress-extension (left) and derivative stress-extension (right) of two dollies applied with Hysol 9340 and processed with the same cure and pull-off test.

Comparison between stress-extension and derivative stress-extension failure regions to demonstrate the importance of truncating negative derivative values and how to identify incomplete failures in the stress-extension curve.

Dollies coated with 30 mg of adhesive were applied to uncoated cold-rolled steel QD panels and cured at ambient for 24 hours. Pull-off performed at 20 °C (T_g=22.5 °C) and a rate of 2 mm/min

Eight dollies were applied with 30 mg Hysol 9340 adhesive, cured, and then pulled off from cold-rolled steel QD panels as a control experiment to reveal the associated stress-extension and derivative stress-extension curves that were presented in

Figure 3.7. Of the eight experiments, dolly 1-1 and 3-1 possessed shoulders at the peak stress, as seen in Figure 3.6, which indicated that the test area experienced a partial crack prior to catastrophic failure instead of failing across the entire area simultaneously. The subset of curves that indicated uniform failure across the entirety of the test area is shown in Figure 3.8.

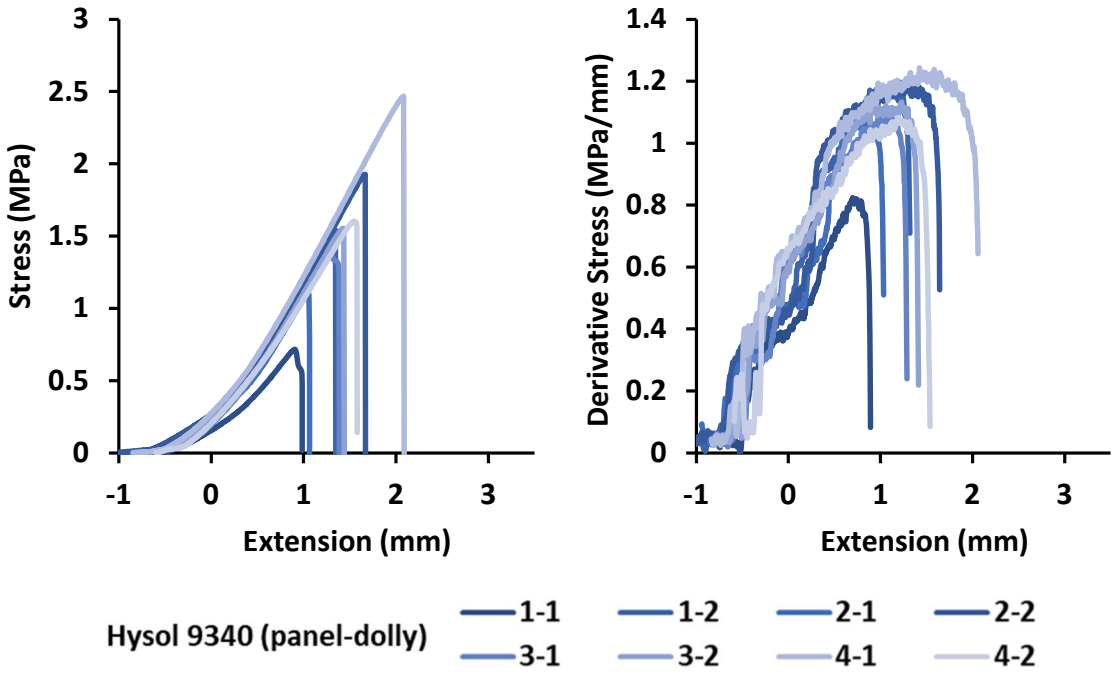

Figure 3.7 Truncated pull-off stress-extension and derivative stress-extension for eight dollies applied to cold rolled steel with Hysol 9340 and processed with identical cure and pull-off test revealing variability associated with destructive testing of this type

All negative derivative stress values were removed, as described in Figure 3.6. Dollies coated with 30 mg of adhesive were applied to uncoated QD panels and cured at ambient for 24 hours. Pull-off performed at 20 °C (T_g=22.5 °C) and a rate of 2 mm/min.

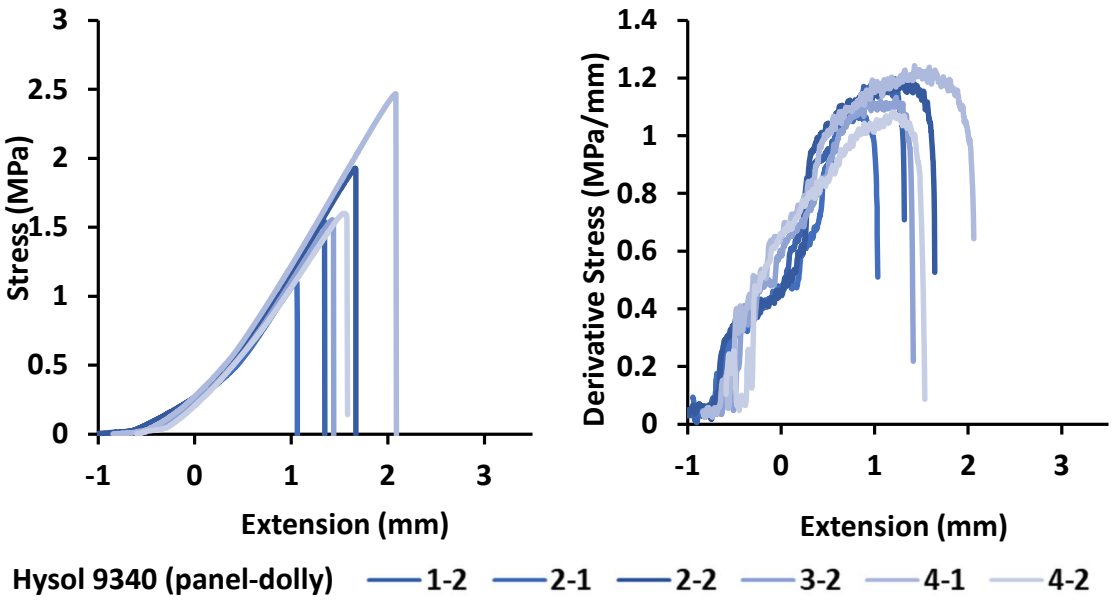

Figure 3.8 The pull-off stress-strain (left) and derivative stress-strain (right) of the subset of dollies applied with Hysol 9340 from Figure 3.7 depicting complete and brittle interfacial failures

Pulls experiencing fragmented failures (Figure 3.6) were removed. Dollies coated with 30 mg of adhesive were applied to uncoated QD panels and cured at ambient for 24 hours. Pull-off performed at 20 °C (T_g=22.5 °C) and a rate of 2 mm/min

In addition to the two tests with jagged peaks, dollies can be eliminated using numerical methods. Outlier identification was performed based on 1.5*interquartile range calculation for peak stress, slope, and derivative at failure. Testing for outliers by multiple means accounts for multiple ways the pull-off test could have deviated from normal. Peak stress outliers indicate something went wrong, but the origin of the deviation is difficult to pinpoint. The high number of variables leads to high data variation; therefore, few pulls can be identified as outliers by this method. Variation in the slope of the stress-strain curve indicates something is abnormal about one of the materials in the stack-up. The material was stressed more or less in response to the strain than other instances due to substrate bending or poor adhesive mixing. Finally, variation in the derivative at failure infers information about the failure event; if failure did not

occur simultaneously across the area under the dolly, then the derivative at failure was reduced.

Narrowing down the Hysol adhesive data set involved multiple outlier calculations. Of the six remaining dollies in Figure 3.8, only 4-2 was determined to be an outlier based on slope. The resulting validated runs are presented in Figure 3.9 and present a few common features without the misleading nature of different slopes and varying failure modes. In addition to the sharp failure event, the derivative stress curves all overlap and have similar shapes, reaching 1 MPa/mm in steps and then increasing linearly until a short downward curve. Each feature represents a mechanical event occurring in the pull-off experiment. These five runs can be considered representative of the performance of the average dolly applied with Hysol 9340 at 30 mg. The peak stresses achieved vary from 1.104 to 2.468 MPa, which is a large range compared to other adhesives investigated in this chapter but is an accurate representation of the inconsistency to be expected of the bond formed between the Hysol adhesives and the metal surface and should be considered when comparing and deciding on an adhesive.

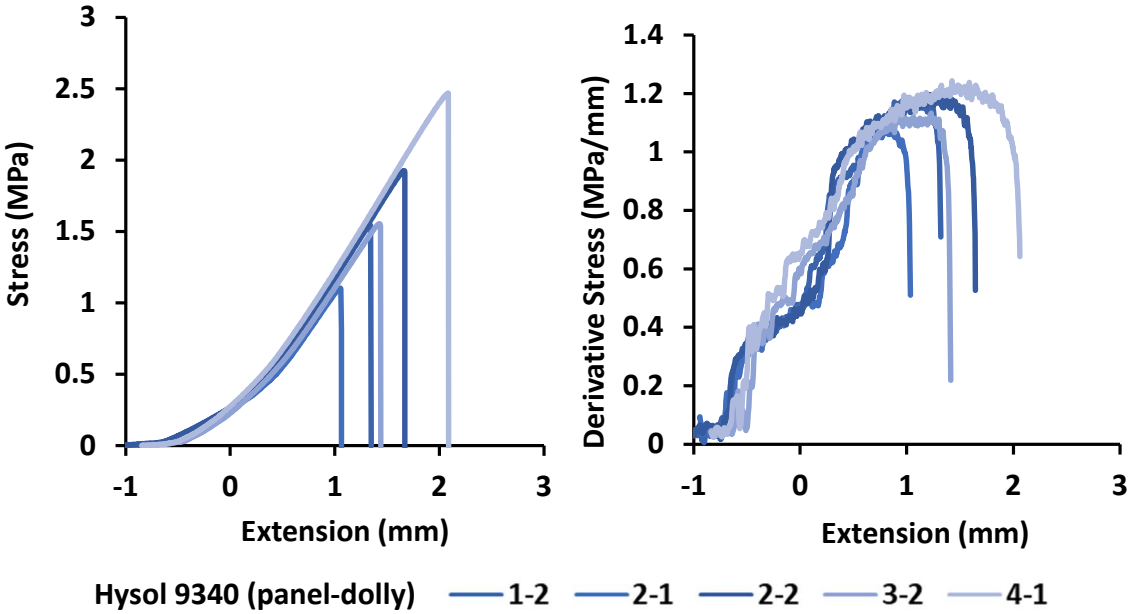

Figure 3.9 Representative pulls of Hysol 9340 applied at 30 mg.

The validated subset of tests from Figure 3.7 and Figure 3.8 that failed cleanly and were not outliers, outliers were removed based on peak stress, slope, and derivative value at failure. Dollies were applied to uncoated QD panels and cured at ambient for 24 hours. Pull-off performed at 20 °C (T_g=22.5 °C) and a rate of 2 mm/min.

As an example of how derivative stress can be applied as an analysis tool and to verify that 30 mg is the appropriate quantity of adhesive to apply to dollies, stress-extension and derivative stress-extension curves of Hysol 9340 applied at 60 mg were analyzed. The overlay of all eight dollies tested with 60 mg adhesive is displayed in Figure 3.10 with negative derivative stress values removed. From this data set, dollies 1-1, 1-2, and 2-2 are removed. Dolly 1-2 experienced fragmented failure, as indicated by the multiple shoulders. Both dollies 1-1 and 2-2 are outliers when calculations are performed without including dolly 1-2. Test 1-1 is an outlier with respect to peak stress value, and 2-2 is an outlier with respect to the derivative value. With those traces removed, the successful samples are displayed in Figure 3.11. From the remaining data, the true character of Hysol applied at 60 mg could be discerned.

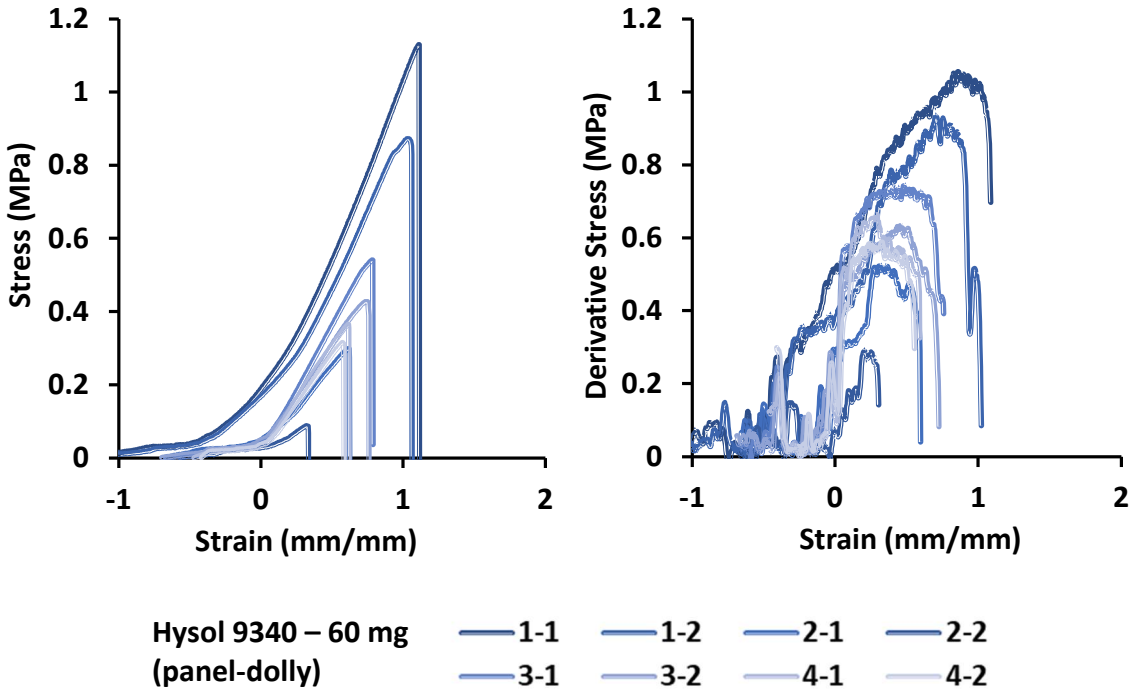

Figure 3.10 Pull-off stress-extension and derivative stress-extension curves of Hysol 9340 applied in 60 mg quantity

All negative points associated with failure in derivative stress-extension traces are removed. Dollies coated with adhesive were applied to uncoated QD panels and cured at ambient for 24 hours. Pull-off performed at 20 °C (T_g=22.5 °C) and a rate of 2 mm/min.

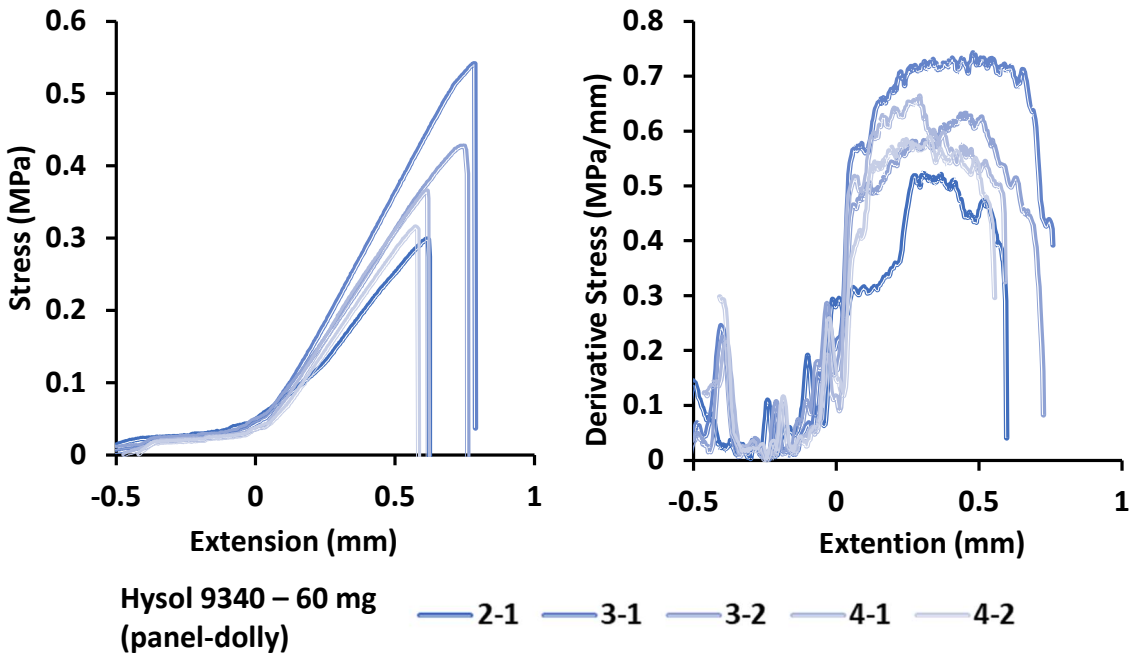

Figure 3.11 Representative pulls of Hysol 9340 applied at 60 mg

The subset of samples shown in Figure 3.10. Dollies coated with adhesive were applied to uncoated QD panels and cured at ambient for 24 hours. Pull-off performed at 20 °C (T_g=22.5 °C) and a rate of 2 mm/min.

The effect of doubling the amount of adhesive used can be seen in Figure 3.12. Between the two different adhesive masses, the number of successful and valid experiments remains constant. Additional adhesive material significantly decreased peak stress to approximately 25% of the value at 30 mg. The highest peak stress considered from 60 mg is lower in peak stress than all the valid dollies from the 30 mg set. The standard deviation of peak stresses is reduced for 60 mg but would not be successful at pulling most coatings from the substrate. Therefore, 30 mg of adhesive was chosen as the standard amount, and subsequent pull-off data will be analyzed using similar logic.

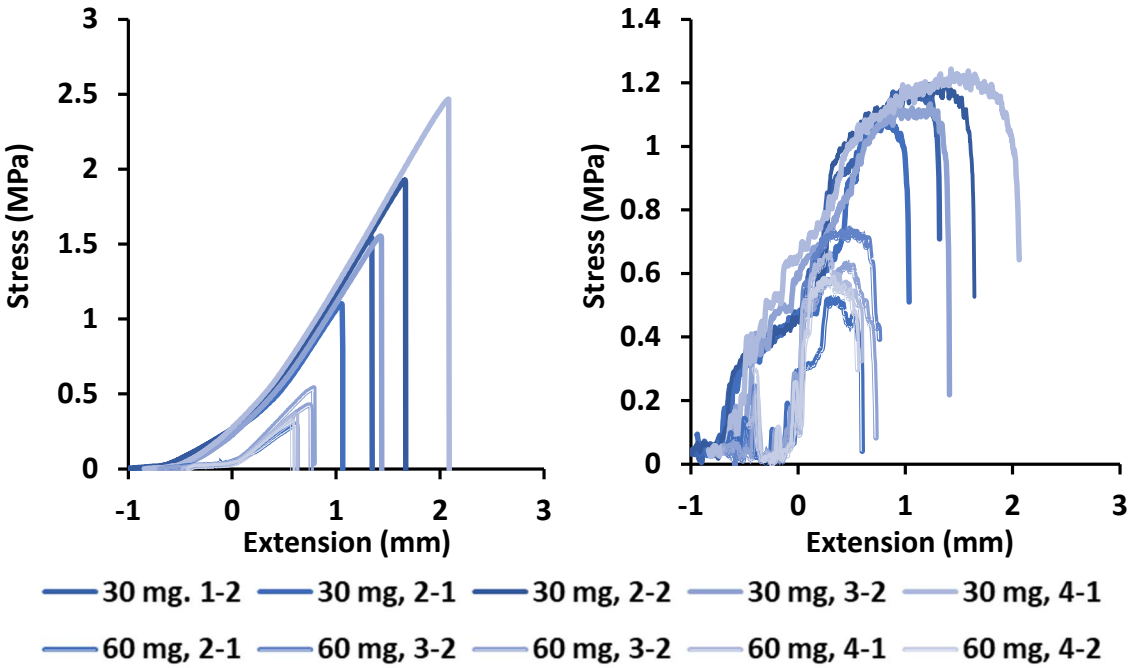

Figure 3.12 Comparison of representative curves of Hysol 9340 (filled 2K epoxy) applied at 30 and 60 mg

All 30 mg samples achieved greater peak stress than 60 mg samples. Dollies coated with adhesive were applied to uncoated QD panels and cured at ambient for 24 hours. Pull-off performed at 20 °C (T_g=22.5 °C) and a rate of 2 mm/min.

3.3.2 Choice of adhesive

Four adhesives were screened by adhering eight dollies to four bare cold rolled steel substrates and performing pull-off tests after adhesives cured for 24 hours. All adhesives are two-part epoxies, Hysol and JB Weld contain fillers, Araldite, and DP 460 are unpigmented. Stress-extension and derivative stress-extension are presented for each adhesive; Hysol 9340 (as shown previously in Figure 3.6 through Figure 3.9), ScotchWeld DP 460 (Figure 3.13), Araldite (Figure 3.14), and JB weld (Figure 3.15). The number of representative samples was consistently between four or five dollies out of the initial eight. The major differences between sets of stress-extension curves are the values of peak stress and the standard deviation. A summary of the means and standard deviations of all adhesives is presented in Table 3.2. Of the tests reported, Scotch-Weld

DP460 had the highest average peak stress of 4 MPa and the lowest standard deviation of 4% of the peak stress value.

Table 3.2 Summary of adhesive sample set statistics

Calculations were performed only on tests previously deemed successful

Adhesive	Hysol 9340	Scotch-Weld DP 460	Araldite	JB Weld	Hysol 9340 (60 mg)
Average (MPa)	1.76	4.01	0.92	2.09	0.39
Standard Deviation	0.58	0.18	0.09	0.11	0.1
Standard deviation %	32.9	4.5	10.2	5.4	25.2

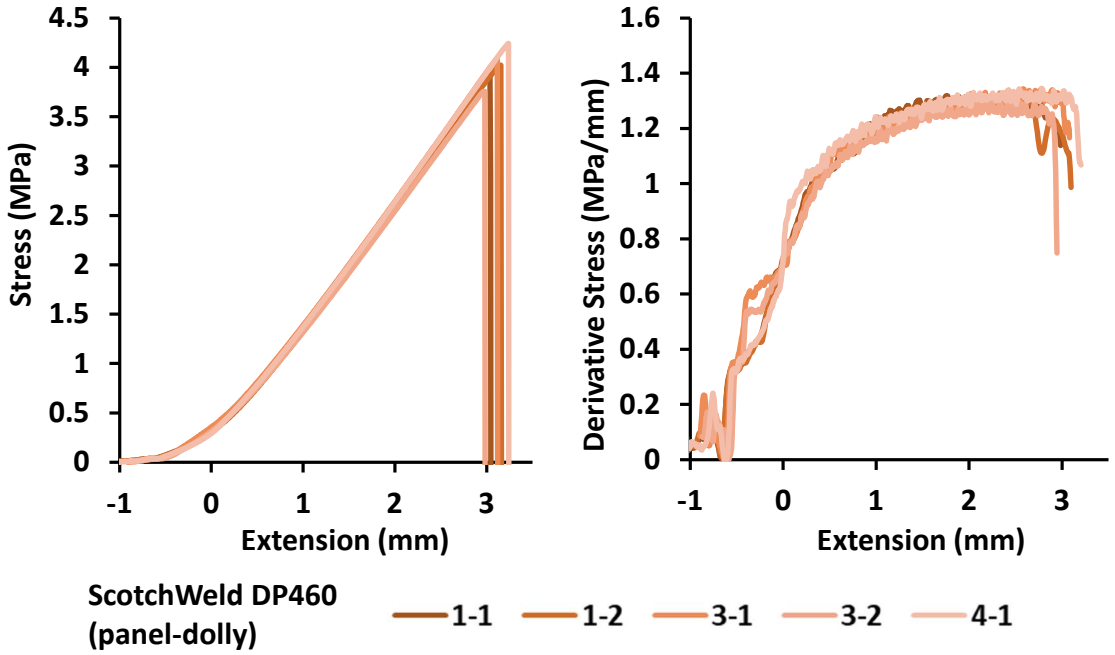

Figure 3.13 Representative pulls of ScotchWeld DP 460 (clear 2K epoxy)

Adhesive applied in 30 mg quantities to aluminum dollies, adhered directly to cold rolled steel substrates, and cured for 24 hours at ambient. Pull-off performed at 20 °C (T_g=66.8 °C) and a rate of 2 mm/min.

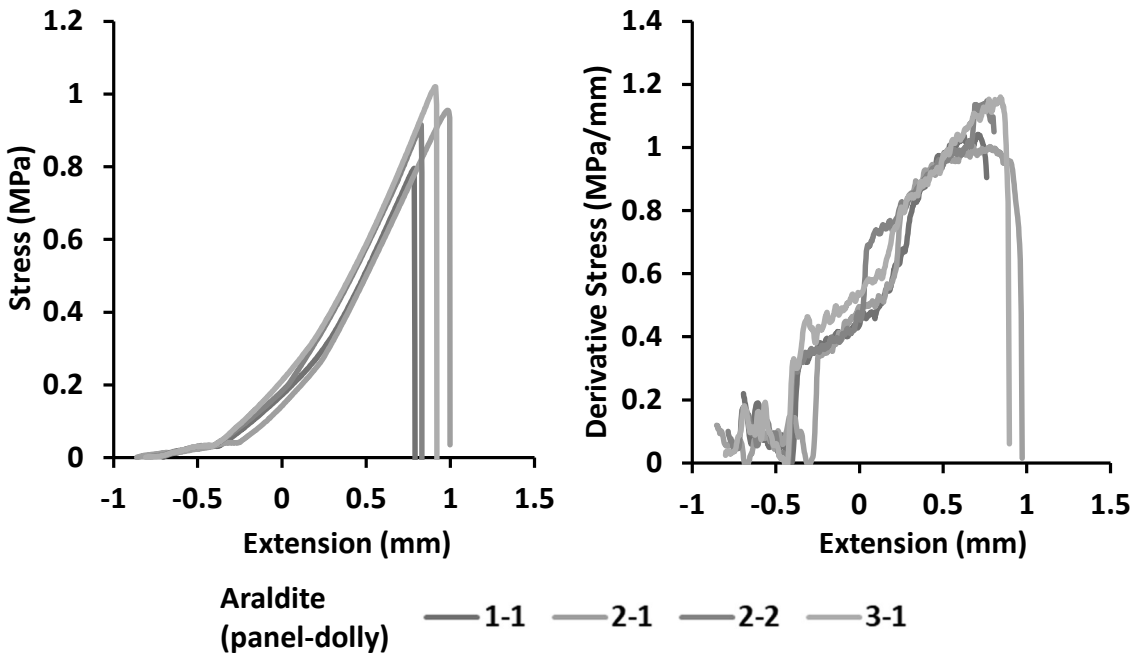

Figure 3.14 Representative pulls of Araldite adhesive (clear 2K epoxy)

Adhesive applied in 30 mg quantities to aluminum dollies, adhered directly to cold rolled steel substrates, and cured for 24 hours at ambient. Pull-off performed at 20 °C (T_g=61.4 °C) and a rate of 2 mm/min.

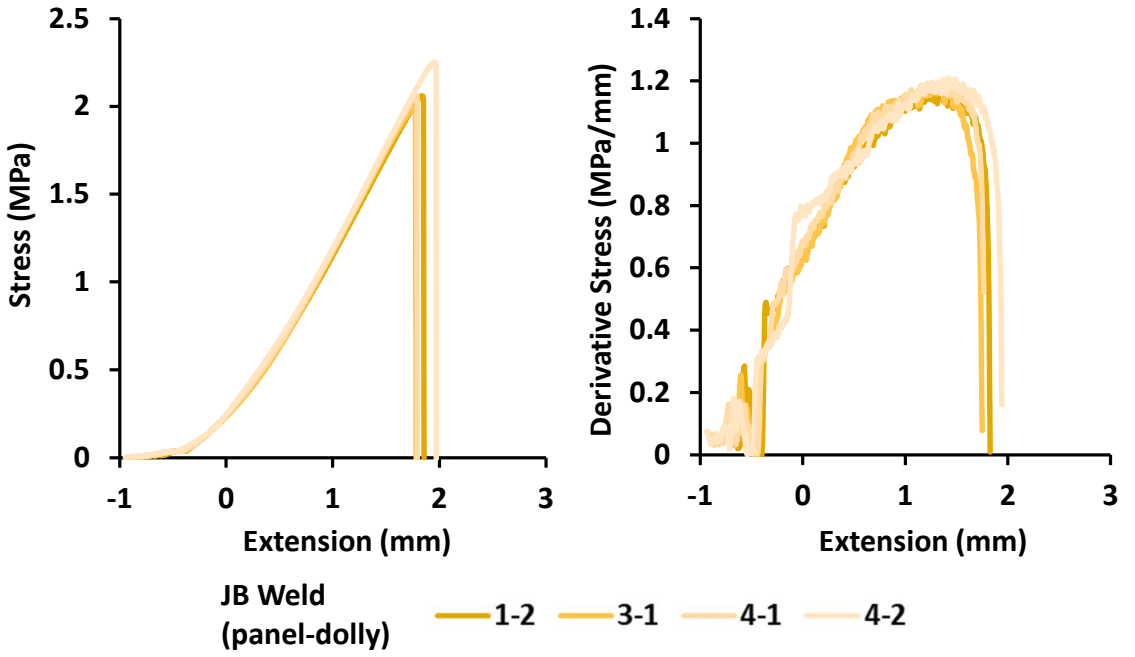

Figure 3.15 Representative pulls of JB Weld (filled 2K epoxy)

Adhesive applied in 30 mg quantities to aluminum dollies, adhered directly to cold rolled steel substrates, and cured for 24 hours at ambient. Pull-off performed at 20 °C (T_g=41.1 °C) and a rate of 2 mm/min.

Similar conclusions can be drawn from the derivative stress plots. A side-by-side comparison of one representative sample from each adhesive set is shown in Figure 3.16). The criteria for grading adhesives by derivative stress curves are less quantifiable than the average peak stress and standard deviation as were used in the stress-extension evaluation. Grading derivative stress is more based on shape. Araldite demonstrated inferiority through the derivative stress-extension curves being consistently noisy throughout and never reach a steady response. Similarly, the Hysol peak stresses are so varied that only one run achieves a linear region in the derivative curve. Finally, Scotch-Weld DP460 was chosen over JB Weld because of how sharp the failure peaks were; the derivative curves of DP 460 didn't decrease in value all the way to y=0 as JB Weld did. The clustered and leveled derivative stress curves of DP 460 can be used as an example of successful and valid pull-off experiments

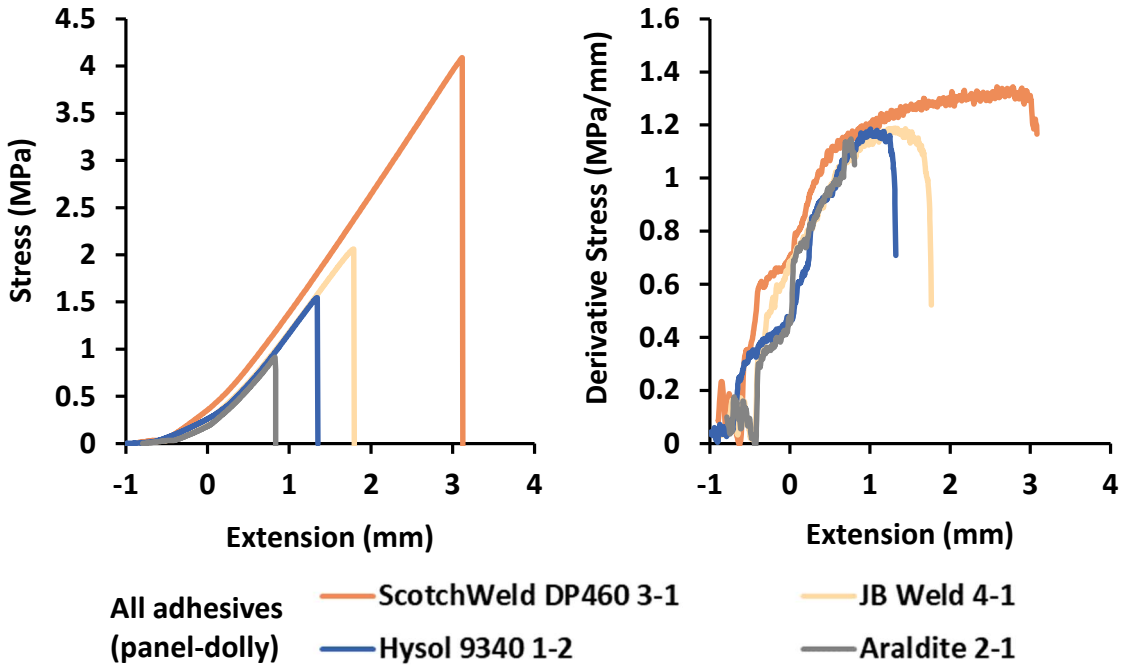

Figure 3.16 Comparison of single representative samples from each adhesive set

Adhesive applied in 30 mg quantities to aluminum dollies, adhered directly to cold rolled steel substrates, and cured for 24 hours at ambient. Pull-off performed at 20 °C and a rate of 2 mm/min.

In most cases, the adhesive that results in the highest peak stresses is the right choice, but this analysis of adhesives was mostly intended to walk through the process of derivative stress data analysis, which can be used on more complicated analyses. In Chapter IV, the method was used to understand changes occurring due to solvent trapping, which could not be explained by just the peak stresses. Adhesive pull-off stress-strain and derivative curve analysis developed a simple model system to demonstrate the process and practical uses of the analysis method.

3.3.3 Scoring and Scoring Method

Turunen published stress distribution models of the coating in a pull-off test with and without scoring. The distribution images are shown in Figure 3.2 and presented a reason to believe that separating the testing area below the dolly was necessary, but the

importance relative to potential damage to the system during scoring was uncertain.[30] Five scoring methods were investigated. The process of rating the scoring methods included analysis of stress-extension and derivative stress-extension curves, as seen for the adhesive decision in the previous section. Additionally, peak stress accuracy was tested against a literature model for peak-stress vs. thickness.[31] The model (which will be discussed more in Chapter 4) predicts that in high modulus coatings, increasing thickness should decrease peak stress due to added internal stress.

The importance of scoring was made quantifiable in a series of panels coated with a constant 35 mil thickness. Peak stresses from the resulting eight pull-offs in Figure 3.17 do not demonstrate the expected negative relationship between peak stress and thickness. A broad range of peak stresses from 0.9 to 3.4 MPa was achieved, indicating another variable was influencing peak stress values. Despite scoring having been attempted using a diamond tube saw, cohesive failure through the coating thickness persisted. Embedding the diamonds into the tube saw required a mass of material at the end of the saw, making the "blade" end wider than the rest of the internal diameter. As a consequence, the internal diameter of the tube saw had to be greater than would be required for a serrated tube saw in order to fit over the applied dolly, and the trough created in the coating by the saw wasn't directly adjacent to the dolly.

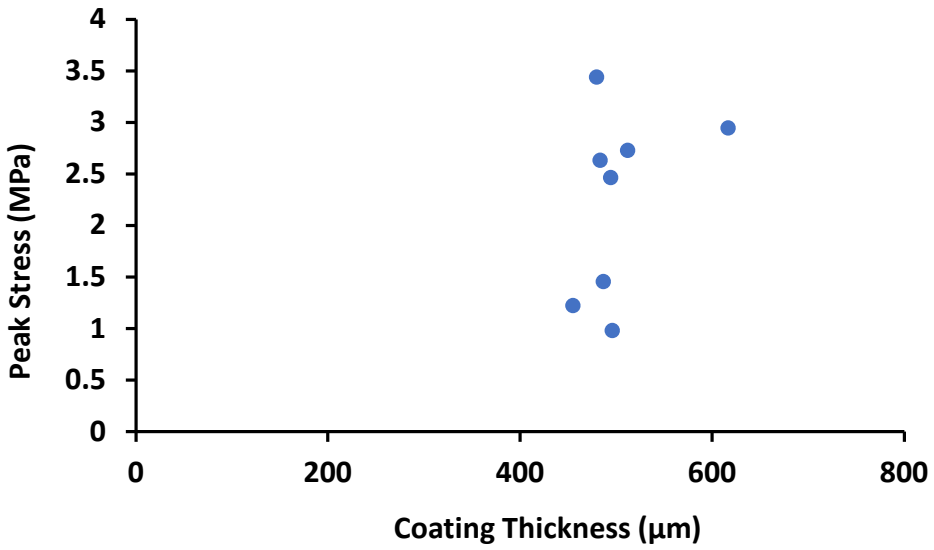

Figure 3.17 Pull-off peak stress for single model coating applied in bulk at 35 mils to QD panels. Showing no relationship with thickness

Panels cured for two hours at 60 °C and one hour at 80 °C. All dollies applied with ScotchWeld DP 460 and cured for 24 hours at ambient. Dollies scored with a diamond-studded tube saw. Pull-off performed at 20 °C and a rate of 2 mm/min.

Analysis of the failure surfaces revealed that cohesive failure through the coating around the perimeter was occurring at least partially in every dolly. Scans of the failure surfaces are shown in Figure 3.18, where significant coating and adhesive material can be seen within the scoring area. The extent of cohesive perimeter failure was measured through image analysis, and higher peak stress dollies corresponded to a greater percentage of cohesive failure around the perimeter. The relationship between the extent of cohesive failure along the perimeter and peak stress is linear and presented in Figure 3.19. It makes sense that the more the failure surface contained cohesive failure through the coating thickness, the greater the resulting peak stress, and the response would be more apparent on thick coatings. A positive relationship between perimeter failure and peak stress suggested that high peak stress values were the most inaccurate rather than representing an improvement of adhesion. It follows then that the low peak stress pulls

with the low perimeter failure are most accurate. The goal of a successful scoring technique is to separate the volume immediately under the dolly from the remainder of the coating without damaging the interface within the test area and minimize cohesive perimeter failure.

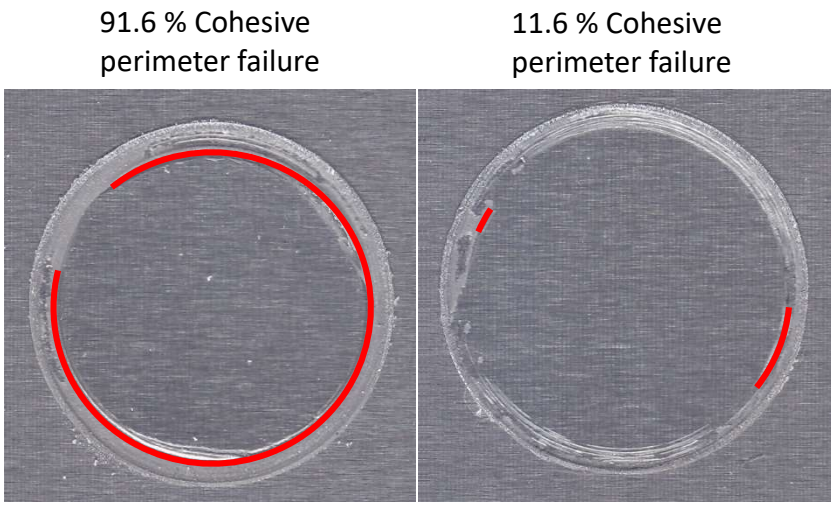

Figure 3.18 Pull-off failure surfaces from sample set in Figure 3.17 exhibiting highest and lowest percentage cohesive perimeter failure

The % cohesive perimeter failure was determined by the number of degrees around the dolly's perimeter that failed through the coating thickness

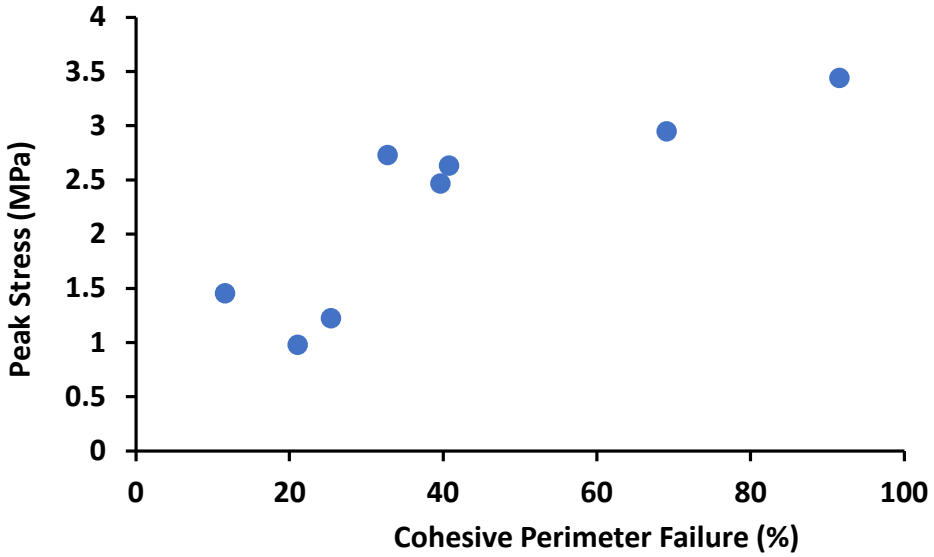

Figure 3.19 Pull-off peak stresses of coating from Figure 3.17 re-plotted against the extent of cohesive perimeter failure to illustrate the numerical effect that avoiding scoring can have on adhesion results

Cohesive perimeter failure values were determined by the method shown in Figure 3.18. Coating applied in bulk at 35 mil to QD panels and cured for two hours at 60 °C and one hour at 80 °C. All dollies applied with ScotchWeld DP 460 and cured for 24 hours at ambient. Scored with diamond-studded tube saw. Pull-off performed at 20 °C and a rate of 2 mm/min

After demonstrating the importance of scoring for achieving accurate adhesion values, possible scoring methods were investigated. The tools studied were a serrated tube saw, diamond tube saw, Dremel tool, laser etching instrument, and a dental pick. Additional methods were theorized where the test region would be isolated via hole punch after the coating was cured enough to avoid flow into the cut but not enough to accumulate stress, but those methods resulted in picture-framing of the film within the test area or incomplete separation. A control sample set was also prepared without any scoring.

The two saws and dental pic were validated using coated panels representing a range of thicknesses with the goal of determining the degree of success based on the degree of correlation between experimental data and model prediction. Six panels, each

having a different applied thickness (3, 5, 7, 9, 11, and 13 mils), were prepared with three dollies per panel, leading to a total of 18 pulls per scoring method. Unfortunately, this complicated the comparison of derivative stress within a scoring method data set because differences in features could be a result of the different thicknesses, not abnormalities necessarily. The derivative methodology was applied to bolster the conclusions made from the peak stress versus thickness data.

Stress-extension and derivative stress-extension curves associated with the control panels for which pull-off was performed without scoring are plotted in Figure 3.20. The degree of overlap and consistency of these curves is remarkable; nothing like it was seen for any of the sample sets in the adhesive screening tests. Consistency between pulls is attributed to a well-formed and consistent interface. The decrease in derivative value with increasing extension was unexpected but likely due to a transition from elastic deformation parallel to the tensile force to elastic deformation due to shear because of the connected coating outside the test area.

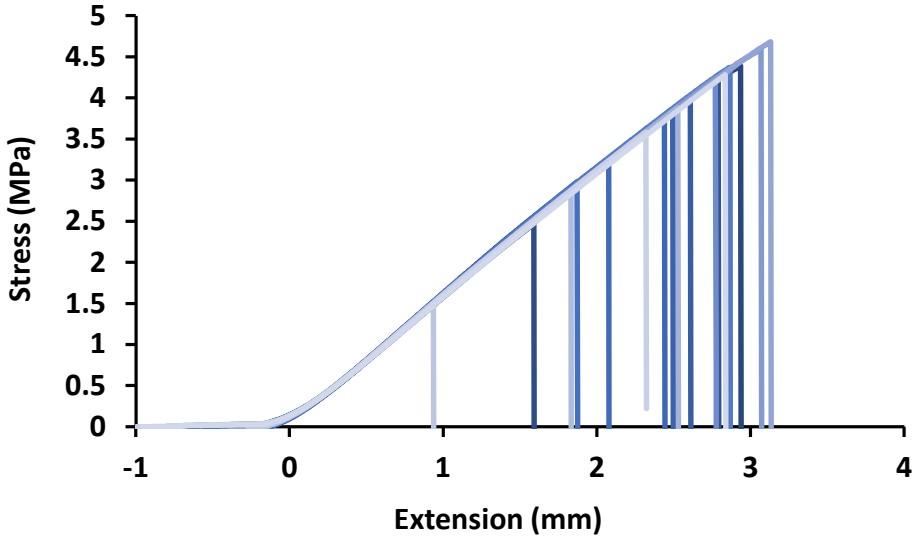

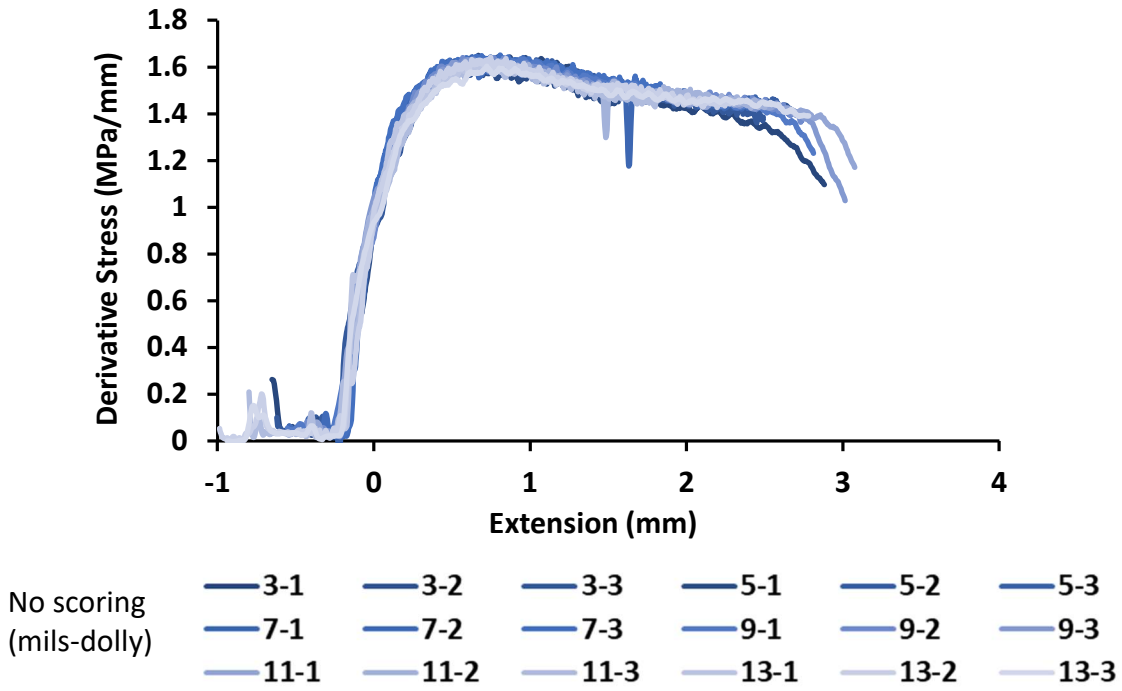

Figure 3.20 Stress-extension (top) and derivative stress-extension (bottom) from pull-off experiments performed on the model coating without scoring

Model coating applied in bulk to QD panel, one panel per applied thickness (3, 5, 7, 9, 11, and 13 mils). Panels cured for two hours at 60 °C and one hour at 80 °C. All dollies applied with ScotchWeld DP 460 and cured for 24 hours at ambient. Pull-off performed at 20 °C and a rate of 2 mm/min.

The liquid coating was applied at multiple thicknesses to take advantage of the relationship between peak stress and thickness. Described by Croll and presented in Equation 3.1, it predicts how peak stress (σ_z) decreases with the thickness (t_c) as a function of Young's modulus (E), work of adhesion (γ), and internal stress (σ).[31] No calibration curve exists for pull-off peak stress; therefore, another method was developed to gauge the scoring methods. How closely peak stresses of increasing thickness fit with Equation 3.1 sheds light on the accuracy of the results without requiring the correct peak stress to be known.

While the uniformity and overlap of stress-extension curves in Figure 3.20 are uncharacteristically high for pull-off results, the fit to Equation 3.1 gives reason to doubt

the accuracy of the experimental data. Figure 3.21 presents the peak stresses and thicknesses for the 18 samples pulled without scoring alongside a best-fit prediction. Peak stress appears to be independent of thickness when no scoring is performed, and there is no internal stress that can be plugged in to fit the peak stresses at high thicknesses. At low thickness, there is a moderate correlation between experiment and theory because the additional force required to fail cohesively around the perimeter of the dolly is low. As thickness increases, that added work required for failure increases, and the experimental data deviates further from theory.

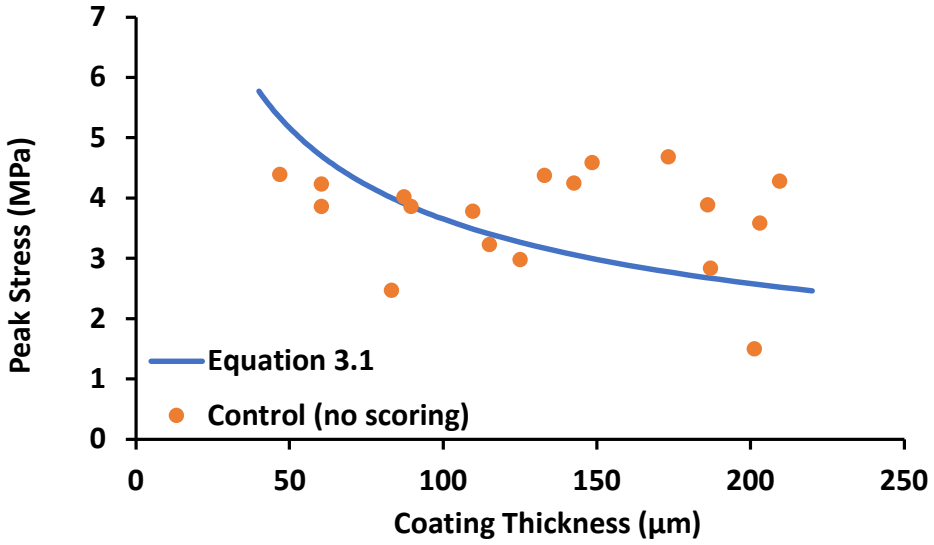

Figure 3.21 Pull-off peak stresses from coated panels tested without scoring and fit to Equation 3.1.

Fitting was employed as a tool to grade scoring methods. Peak stresses from model coating experiments originally presented in Figure 3.20. Quantities used in fit: E=2500 MPa; σ=0 MPa; γ=0.12 N/m. Model coating applied in bulk to QD panel, one panel per applied thickness (3, 5, 7, 9, 11, and 13 mils). Panels cured for two hours at 60 °C and one hour at 80 °C. All dollies applied with ScotchWeld DP 460 and cured for 24 hours at ambient. Pull-off performed at 20 °C and a rate of 2 mm/min.

The apparent thickness independence of peak stress in Figure 3.21 is potentially due to the competition between the reduction in interfacial strength with thickness due to internal stress and the increase in resistance to pull-off failure due to the added

requirement of failing cohesively through more material. In the epoxy-amine coating used in this study, the competing forces appear to exactly counteract each other leading to peak stress that is essentially thickness independent. Two dollies, 5-1 and 13-1, fail at relatively low stresses compared to the predictive curve, possibly indicating a defect around the perimeter of the dolly that initiated the crack and fracture surface. From this study, it can be said that the ideal scoring method would be akin to a localized defect, leaving the interface unharmed but significantly decreasing the added force required for failure.

Most portable adhesion testers are sold with a serrated tube saw for the purpose of scoring around dollies. Considering how prevalent the tool is in the field, it was important to demonstrate the effects that serrated tube saws were having on the coating numerically. While the tube saw as a scoring tool benefits from being easy to use, not requiring electricity, and quickly cutting through the thickness of a coating, the tearing action of the saw teeth is believed to do more harm than good. The way force is applied by the user to the saw, and by extension, the coating, is also violent and inconsistent; dollies often separate from the substrate during the scoring process when using a serrated tube saw.

Stress-extension curves for the subset of successful tests from six panels scored using the serrated tube saw are presented in Figure 3.22. Differences between the serrated saw and the control are readily apparent without looking at the distribution of peak stresses. Out of the 18 dollies applied, only 14 could be tested because four dollies were detached during the scoring process. Of the remaining 14 dollies, only 11 are were considered successful. Two were eliminated based on their deviation from the best fit.

Outlier calculations were performed on residuals instead of peak stress values because the peak stress values are expected to change and wouldn't be an accurate measure of accuracy. Both samples eliminated based on the magnitude of the residual between experimental and prediction achieved much larger peak stresses than would be predicted by the model. Experimental data exceeding the model suggested incomplete scoring or cohesive perimeter failure. The derivative curves of the removed samples support the incomplete failure theory because the curve shape matched those of the control. One more was eliminated based on being an outlier with respect to derivative stress values. Findings from the control suggested that if the interface is constant, the (derivative) stress-extension curves overlap. Curves resulting from coatings of various thicknesses deviate in the peak stress achieved, not the mechanical path to get there, concluding that derivative stress value should be constant at any single extension. Greatly reduced derivative values suggest extensive interfacial damage.

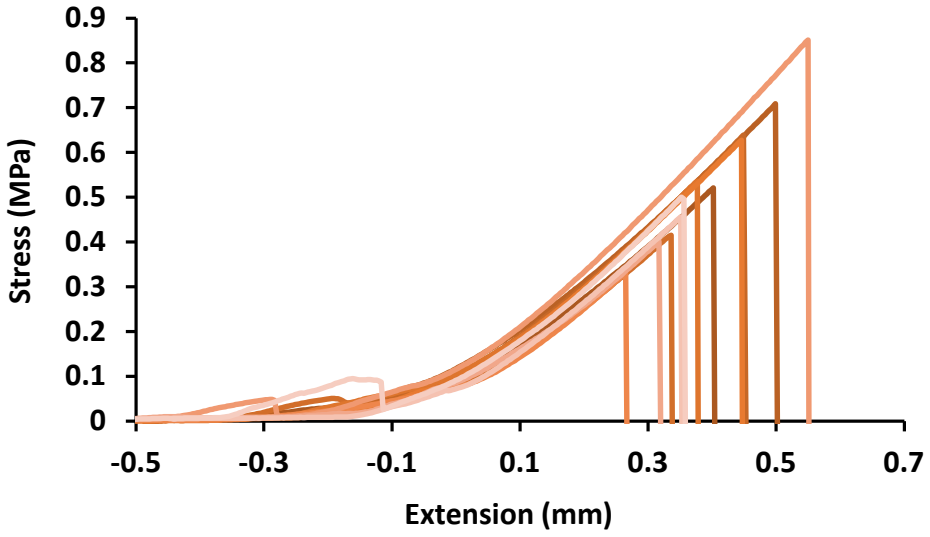

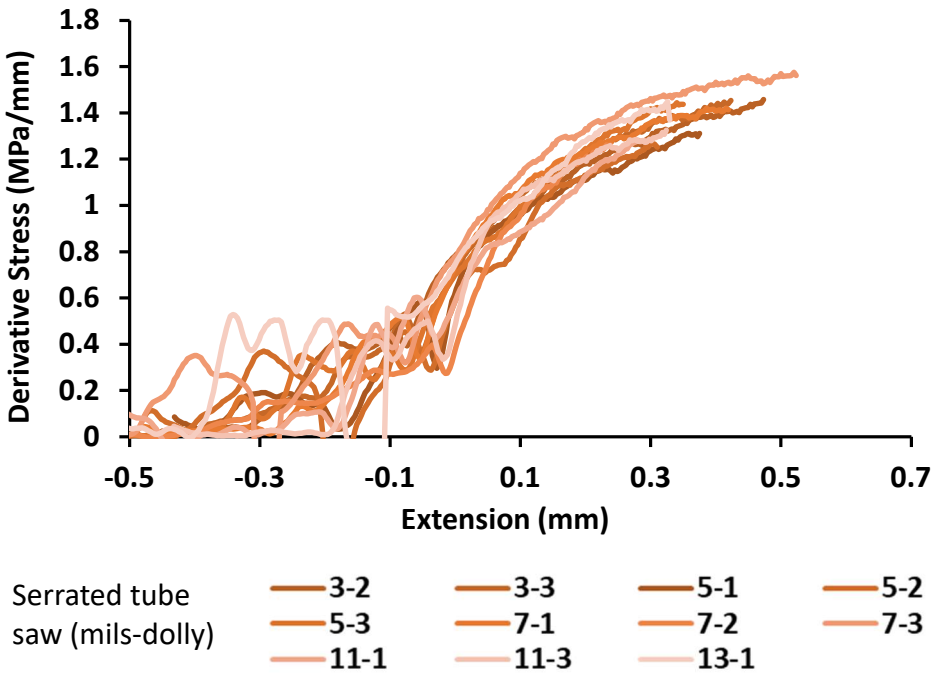

Figure 3.22 Stress-extension (top) and derivative stress-extension (bottom) from pull-off experiments performed on the model coating and scored with serrated tube saw

Serrated tube saw reveals a consistently large variation in peak stress and resistance to deformation. Data set pruned to eliminate outliers. Model coating applied in bulk to QD panel, one panel per applied thickness (3, 5, 7, 9, 11, and 13 mils). Panels cured for two hours at 60 °C and one hour at 80 °C. All dollies applied with ScotchWeld DP 460 and cured for 24 hours at ambient. Pull-off performed at 20 °C and a rate of 2 mm/min.

The primary differences between stress-extension curves of tube saw dollies, and those of the control are 1) the distribution of slopes, 2) the reduction in average peak stress from 3 MPa to 0.5 MPa, and 3) peculiar features that appear in tube saw curves below 0 mm of extension. All three distinguishing features point to damage at the interface. The large variation in slopes indicates a variety of interfaces implying interfacial defects; those defects then lead to lower peak stresses. The local maxima in the negative extension region are likely from cracks that lead to a partial separation of the interface early in the test, which is a good explanation for the differences in slope since the cracking would lead to different areas of applied force.

For further comparison between the serrated tube saw and control samples, the representative derivative stress curves are also shown in Figure 3.22. There is variation between all samples at every point of extension, in contrast with the uniformity seen among control experiments. In the control specimen, the derivative curves came to a peak and slowly decreased in stages, but the serrated tube saw data appear to never reach the peak derivative value before failing.

The industry standard of scoring by tube saw is partially vindicated through the thickness relationship. Figure 3.23 presents the peak stresses and thicknesses of the eleven valid tests performed on serrated tube saw scored dollies. The fit of the data to theory is much better than for that of the control. Peak stress values are potentially lower than the true value due to interfacial damage, but the goodness of fit suggested that all interfaces have been affected equally by the tube saw such that the relative differences between experiments remain valid. The precision of the pull-off test as a whole was increased by the addition of scoring with a serrated tube saw but at the cost of accuracy and efficiency.

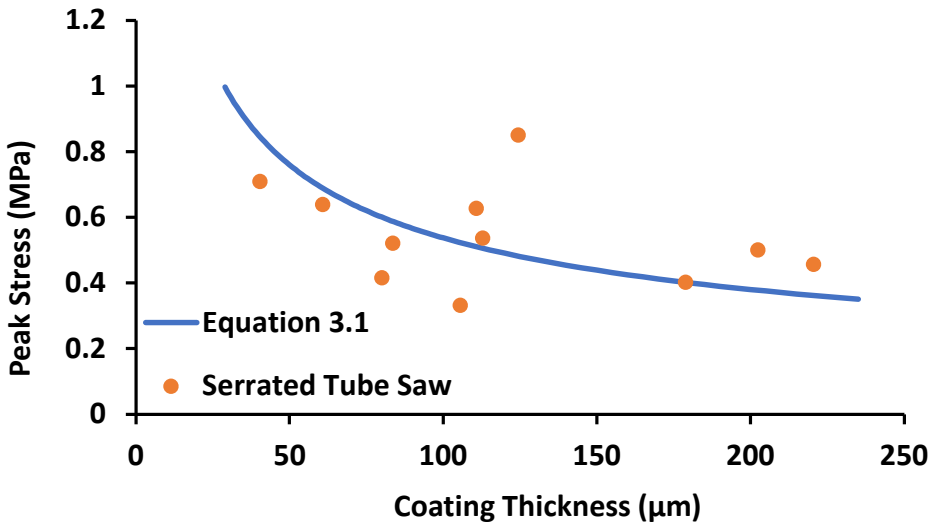

Figure 3.23 Pull-off peak stresses of coated panels; scored with serrated tube saw and fit to Equation 3.1.

Peak stresses from model coating experiments that were originally presented in Figure 3.22. Quantities used in fit: E=2500 MPa; σ=0 MPa; γ=0.0027 N/m. Model coating applied in bulk to QD panel, one panel per applied thickness (3, 5, 7, 9, 11, and 13 mils). Panels cured for two hours at 60 °C and one hour at 80 °C. All dollies applied with ScotchWeld DP 460 and cured for 24 hours at ambient. Pull-off performed at 20 °C and a rate of 2 mm/min.

After the damaging nature of the serrated tube saw was revealed, a less aggressive tube saw was attempted. The intention was to keep the procedure as similar as possible to that of the serrated tube saw while reducing the extent of interfacial fractures caused by the scoring process. Instead of teeth to cut into the coating, the diamond-studded tube saw ground through the coating. Stress-extension curves in Figure 3.24 demonstrate an improvement over the serrated saw. Three tests were considered invalid, two had premature and incomplete failures, and one due to having an outlier slope. No dollies were separated during the scoring process. The maximum peak stress reached (4.05 MPa) is 87% of the maximum peak stress achieved in the control set (4.68 MPa) and slope variation is much lower than was seen for the serrated saw. There were still

samples with uncharacteristically low stress like 5-1, bringing the gentleness of the diamond saw into question.

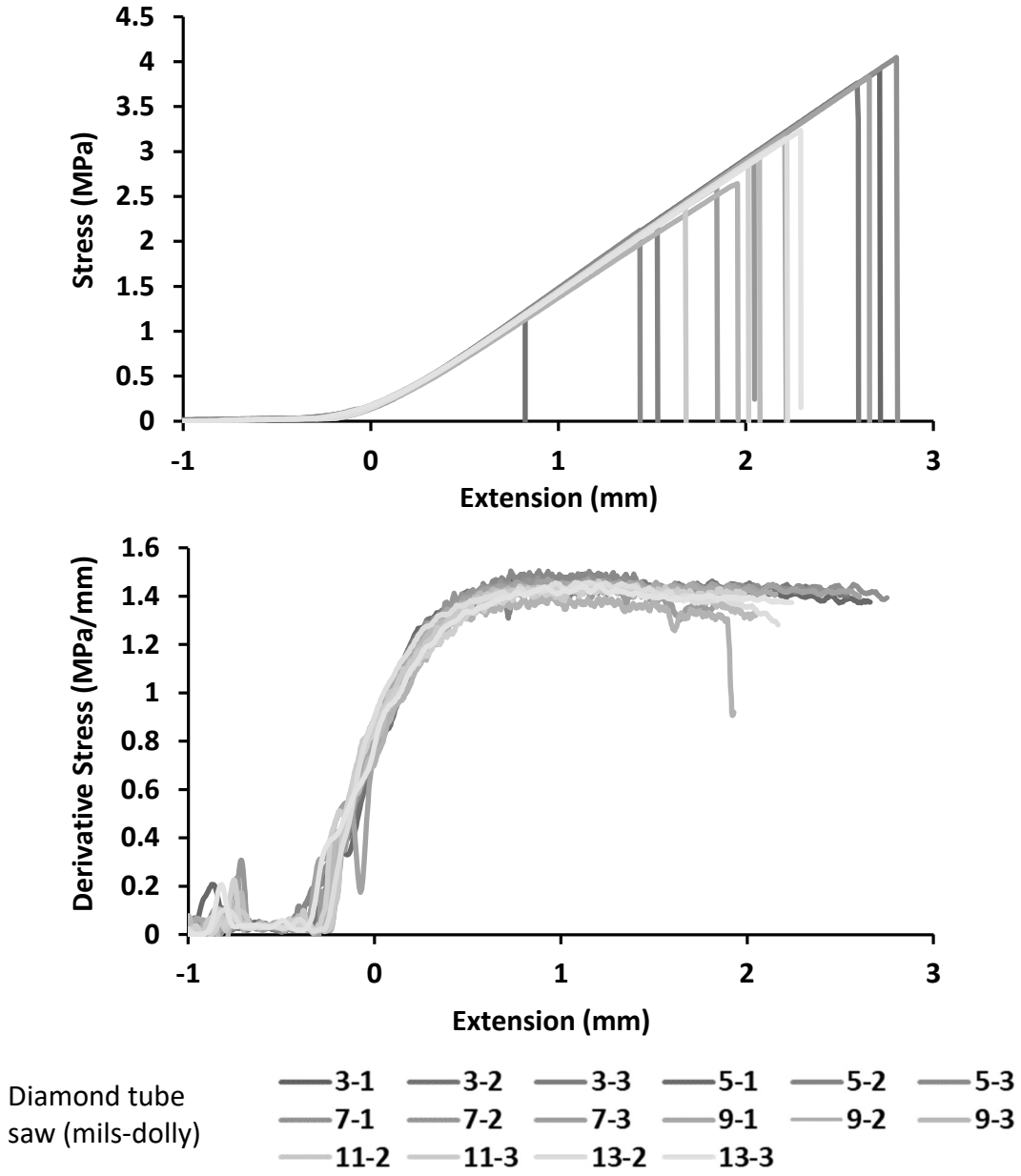

Figure 3.24 Stress-extension (top) and derivative stress-extension (bottom) from pull-off experiments performed on the model coating and scored with diamond tube saw

Data set pruned to eliminate outliers. Model coating applied in bulk to QD panel, one panel per applied thickness (3, 5, 7, 9, 11, and 13 mils). Panels cured for two hours at 60 °C and one hour at 80 °C. All dollies applied with ScotchWeld DP 460 and cured for 24 hours at ambient. Pull-off performed at 20 °C and a rate of 2 mm/min

Further comparisons and conclusions can be drawn about the diamond tube saw from derivative stress curves and model fitting in Figure 3.24 (bottom) and Figure 3.25, respectively. The derivative curve shape in Figure 3.24 more closely resembles that of the control, reaching a peak derivative value and maintaining a constant slope, indicating less interfacial damage. In the control curves, each sample began to decrease in derivative stress value after reaching a peak at approximately 0.7 mm of extension. The peak is less pronounced in the diamond saw samples indicating less yielding, and relaxation modes were made possible in the transverse direction by limitation of stress distribution outside the test area. Similarly, the fit of the peak stresses to the model is better with the diamond saw than the control, but not as good as with the serrated saw. The greater similarity to the control can be attributed to the width of the saw edge, as described earlier in this section, in association with Figure 3.19. Having the point of contact between the saw and the coating further away from the dolly than with the serrated saw overestimated the peak stresses. In some cases, the whole increased area generated by the diamond tube saw was pulled away without any cohesive perimeter failure, which may explain low-stress samples like 5-1.

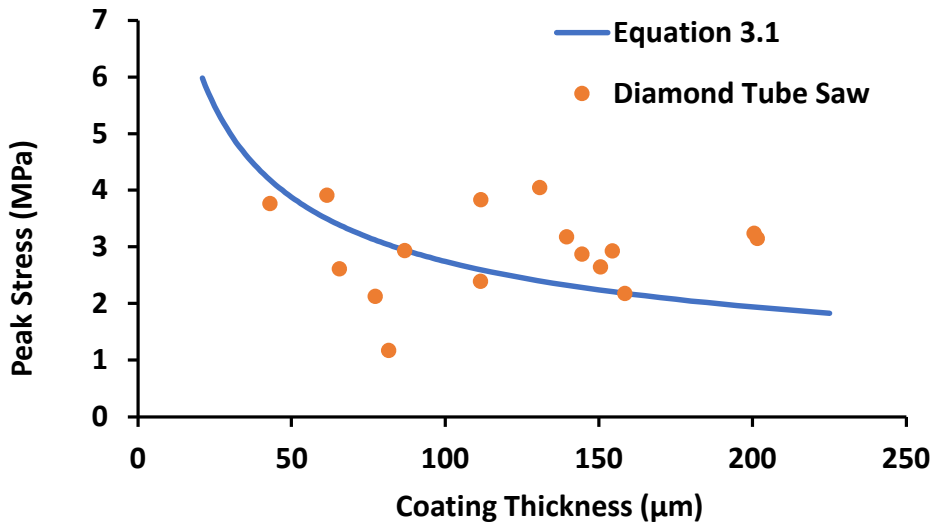

Figure 3.25 Pull-off peak stresses of coated panels scored by diamond tube saw and compared to a model defined by Equation 3.1

Peak stresses from model coating experiments that were originally presented in Figure 3.24. Quantities used in fit: E=2500 MPa; σ=0 MPa; γ=0.070 N/m. Model coating applied in bulk to QD panel, one panel per applied thickness (3, 5, 7, 9, 11, and 13 mils). Panels cured for two hours at 60 °C and one hour at 80 °C. All dollies applied with ScotchWeld DP 460 and cured for 24 hours at ambient. Pull-off performed at 20 °C and a rate of 2 mm/min

Another scoring tool option explored was a 90° pick; the initial assessment was that it allowed for more control than the serrated tube saw, which was hypothesized to be less damaging to the coating. The fineness of the tip also ensured the scoring pathway was immediately adjacent to the dolly, unlike what was seen in the diamond-studded tube saw. Stress extension curves for the 90° pick are presented in Figure 3.26, where four tests were removed. Two tests were removed due to fragmented failure. Two more were removed for having unrealistically high peak stresses that were determined to be outliers based on residual values from the model fit. Peak stresses of the successful dollies averaged to 1.1 MPa, which was much closer to the average found with the serrated saw (0.54 MPa) than for the diamond saw and control.

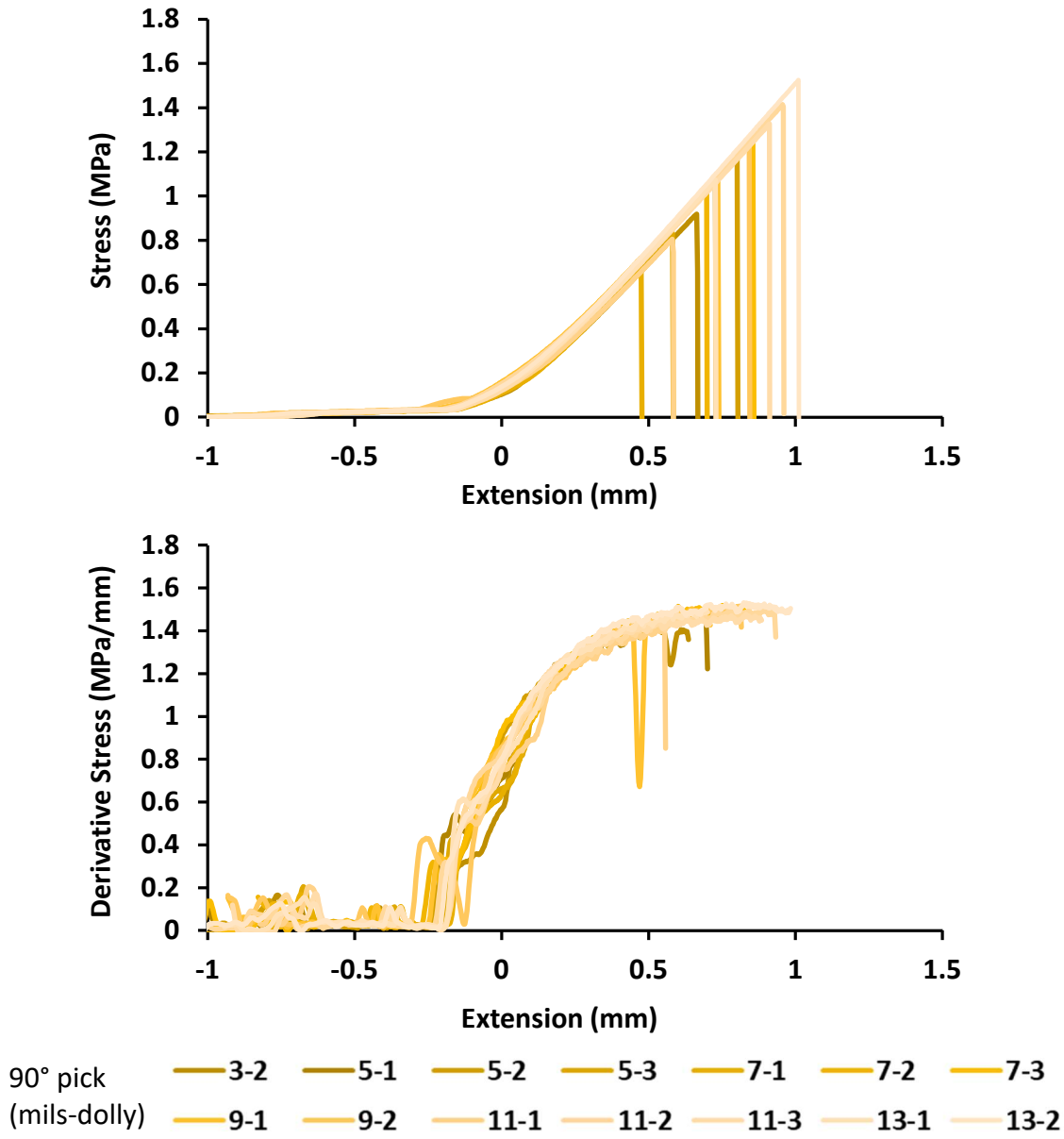

Figure 3.26 Stress-extension (top) and derivative stress-extension (bottom) from pull-off experiments performed on the model coating and scored with 90° pick

Data set pruned to eliminate outliers. Model coating applied in bulk to QD panel, one panel per applied thickness (3, 5, 7, 9, 11, and 13 mils). Panels cured for two hours at 60 °C and one hour at 80 °C. All dollies applied with ScotchWeld DP 460 and cured for 24 hours at ambient. Pull-off performed at 20 °C and a rate of 2 mm/min

Similarities between the dental pic and serrated saw can also be seen in the derivative curves (Figure 3.26, bottom). Both tools resulted in undulations in the derivative curves that persisted at all extensions. The damage to the interface is clearly

reduced when the dental pick is used compared to the tube saw based on the higher stresses that were achieved. Another commonality between the pick and the tube saw is there is no plateau in the derivative curves, some pick samples seem to reach a peak, unlike in the saw, but failure occurs shortly after. There is a general deviation between prediction and reality with increasing thickness shown in Figure 3.27; the data suggest that the manual nature of the process makes it inherently difficult to eliminate all material from around the dolly and cohesive perimeter failure occurred as a result. However, the correlation between experiment and prediction for the pick is still better than the fit for the control or the diamond-studded saw.

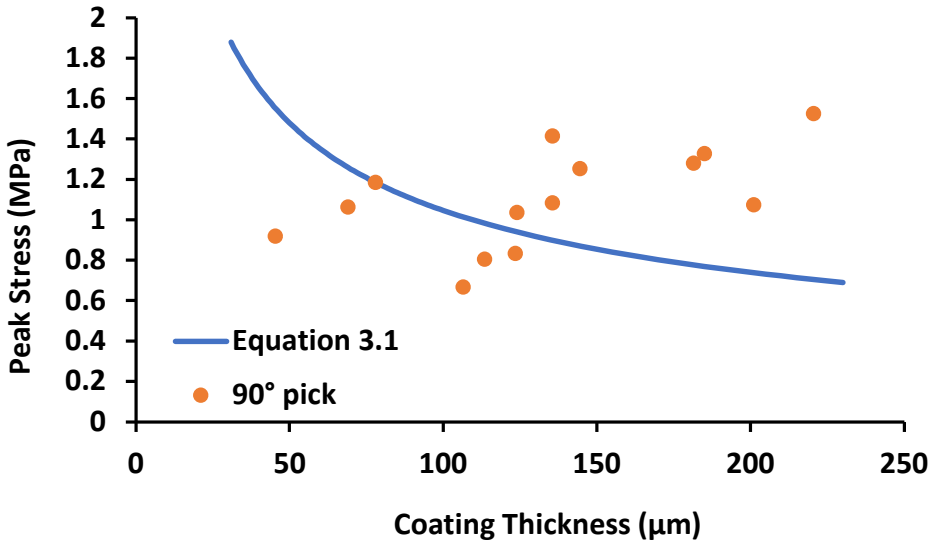

Figure 3.27 Pull-off peak stresses of coated panels scored by 90° pick, fit to Equation 3.1

Peak stresses from model coating experiments that were originally presented in Figure 3.26. Quantities used in fit: E=2500 MPa; σ=0 MPa; γ=0.010 N/m. Model coating applied in bulk to QD panel, one panel per applied thickness (3, 5, 7, 9, 11, and 13 mils). Panels cured for two hours at 60 °C and one hour at 80 °C. All dollies applied with ScotchWeld DP 460 and cured for 24 hours at ambient. Pull-off performed at 20 °C and a rate of 2 mm/min

With these findings in mind, it was decided that the ideal scoring tool was something with the accuracy of the dental pick, in terms of isolating the action immediately adjacent to the dolly but with some moving parts to ensure complete

segregation between the test area and the surroundings. A Dremel rotary tool was identified as the best option for meeting the scoring tool criteria. The use of a pointed tungsten carbide tip allowed for the energy of the Dremel to be focused neatly around the dolly. Scoring every dolly was still time-consuming, but it was easy to ensure complete separation of the two areas. However, the extent of damage done by the Dremel process was hard to quantify.

The use of a Dremel tool was decided on without an equivalent thickness range test; however, many pull-off experiments were run on the coating at multiple thicknesses. The sample sizes were increased to 30 dollies in order to increase confidence in the results. A representative set of 18 dollies was chosen from applied thicknesses equivalent to those explored by the previous scoring methods to make the results more comparable among scoring methods. Stress-extension and derivative stress-extension curves for three batches of coating material applied at 1) 3 mil, 2) 6 mil, and 3) 10 and 20 mil are shown in Figure 3.28. The degree of variation in slope and shape is broad, but these data also represent variation between coating batches, which was not the case for previous methods. While the spread of the data casts doubt, the fitting with model equations supports the use of the Dremel tool. Figure 3.29 shows all the peak stresses associated with the pull-off tests from Figure 3.28 and how they fit the predictive model. Aside from some high peak stress outliers in the 3 mil data set, the model is followed closely, and the Dremel was considered an acceptable scoring method.

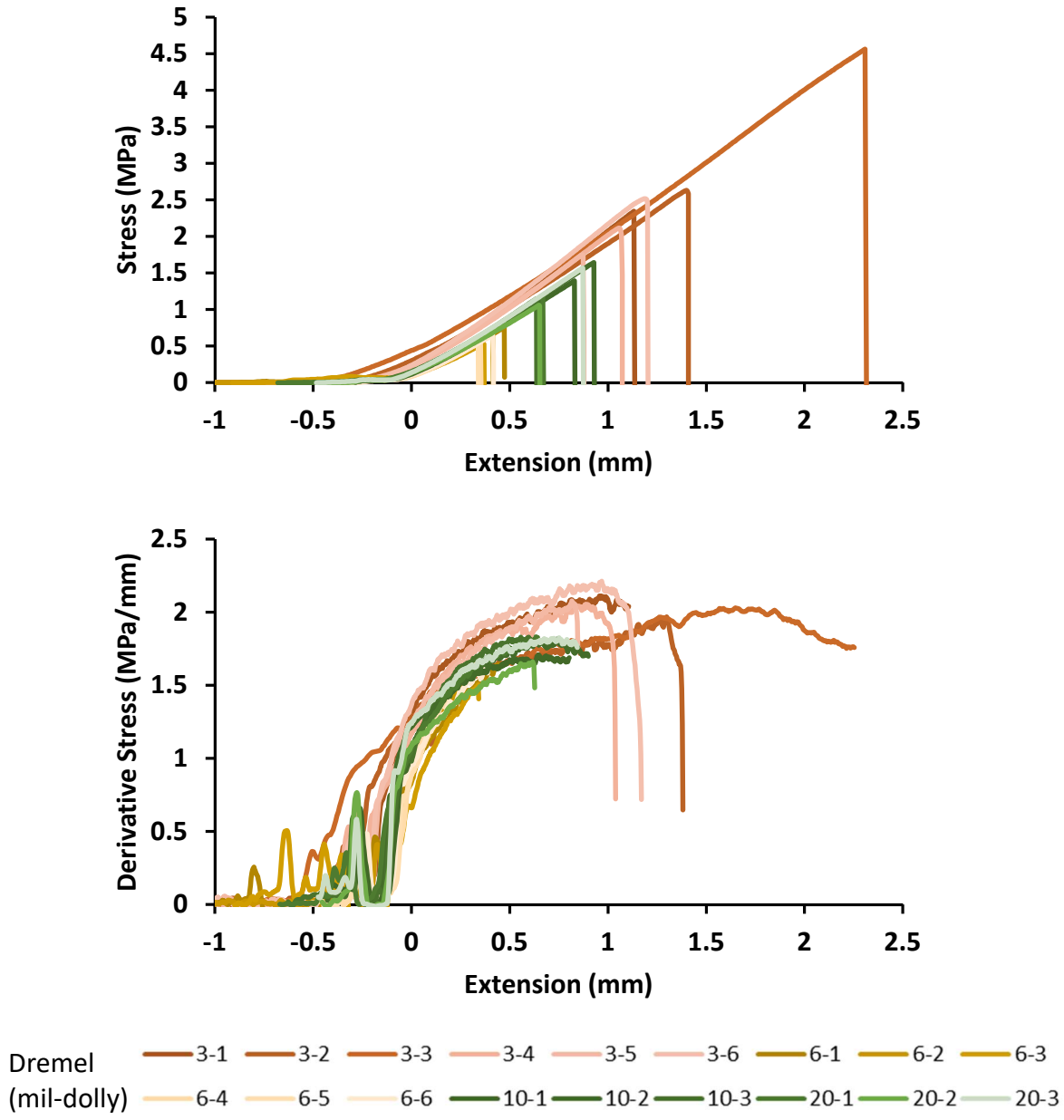

Figure 3.28 Stress-extension (top) and derivative stress-extension (bottom) from pull-off experiments performed on the model coating and scored with Dremel rotary tool

Model coating applied in bulk to R panel, ten panels per applied thickness; 3 and 6, and one panel per thickness 10, 20, and 30 mil. A subset of 18 dollies was chosen from the original pool to make results more directly comparable to previous scoring methods. Panels cured for two hours at 60 °C and one hour at 120 °C. All dollies applied with ScotchWeld DP 460 and cured for 24 hours at ambient. Pull-off performed at 20 °C and a rate of 2 mm/min

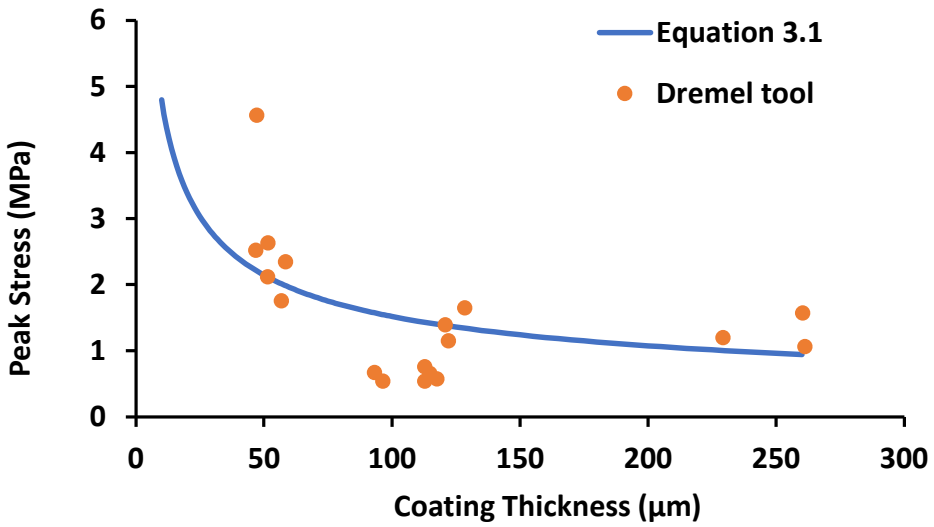

Figure 3.29 Pull-off peak stresses of coated panels scored by Dremel rotary tool, fit to Equation 3.1

Peak stresses from model coating experiments were originally presented in Figure 3.28. Quantities used in fit: E=2500 MPa; σ=0 MPa; γ=0.021 N/m. Model coating applied in bulk to R panel, ten panels per applied thickness; 3 and 6, and one panel per thickness 10, 20, and 30 mil. A subset of 18 dollies was chosen from the original pool to make results more directly comparable to previous scoring methods. Panels cured for two hours at 60 °C and one hour at 120 °C. All dollies applied with ScotchWeld DP 460 and cured for 24 hours at ambient. Pull-off performed at 20 °C and a rate of 2 mm/min.

The time-consuming nature of the Dremel tooling process prompted the investigation of one more scoring method; laser etching. A simple graphical program file told the etching instrument to direct the laser in a wide-rimmed circle pattern with an inner diameter of 20 mm. The laser essentially charred the polymer in its path and appeared to render the external coating disconnected from the coating underneath the dolly. One of the failure surfaces of a laser-etched dolly is depicted in Figure 3.30, showing no evidence of cohesive perimeter failure but instead of incomplete separation. The coating material closest to the substrate was degraded, but the top layer persisted, causing both interfacial damage and peeling failure. A test run of the laser was performed on the 6 mil applied thickness panels, alongside the Dremel dollies originally introduced in yellow in Figure 3.28. Dremel results alongside the small subset of laser

samples are shown in Figure 3.31. The stress-extension curves tell the whole story; while the derivative stress curves of the laser are equally unusual looking, they're not necessary to see what went wrong. All of the dollies prepared using the laser demonstrate segmental failure and/or slow peel, indicating there was significant damage to the interface.

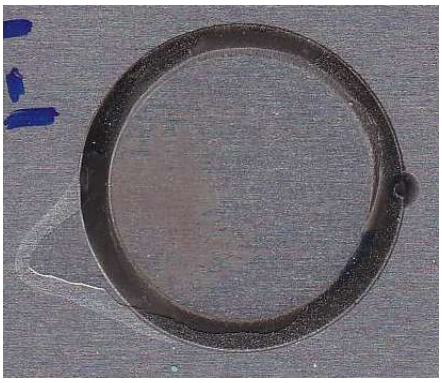

Figure 3.30 A representative failure surface of a laser-etched dolly

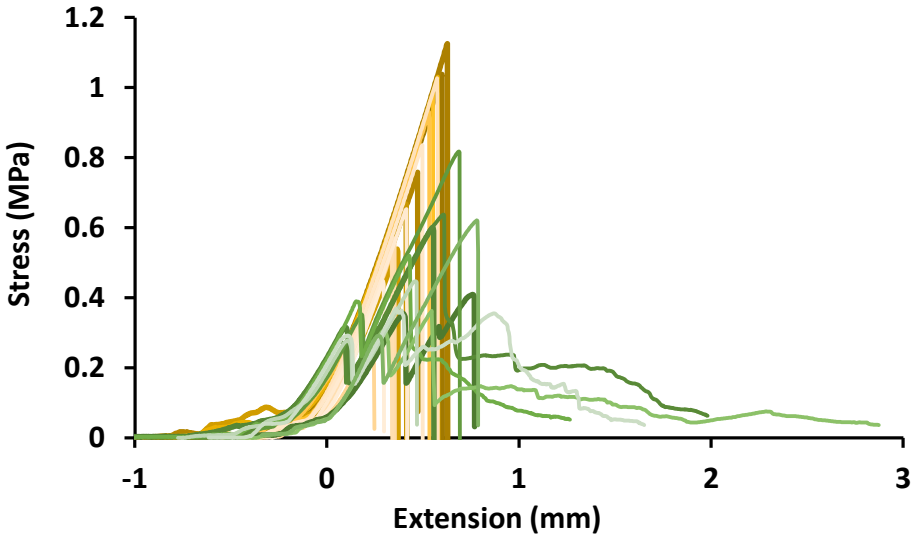

Figure 3.31 Pull-off test load-frame output for coatings scored with Dremel (yellow) and laser etching instrument (green)

Model coating applied in bulk to R panels, at 6 mils. Panels cured for two hours at 60 °C and one hour at 120 °C. All dollies applied with ScotchWeld DP 460 and cured for 24 hours at ambient. Pull-off performed at 20 °C and a rate of 2 mm

The appropriate way to score around a dolly prior to testing is not straightforward, and the method for determining a scoring method is not trivial. Scoring was determined to be a necessary step by correlating peak stress with the amount of the perimeter around a dolly that failed cohesively through the thickness in a pull-off test. Identifying an acceptable scoring method was demonstrated using a serrated tube saw, diamond-studded tube saw, 90° pick, Dremel rotary tool, and laser engraver. The serrated tube-saw, dental pick, and laser damaged the interface significantly, and the diamond-studded tube saw didn't score close enough to the dolly to be effective. The Dremel tool was decided on as the best scoring practice for its minimal damage and level of scoring completeness.

3.4 Conclusions

Pull-off adhesion testing has a lot of potential as a method to advance the understanding of coating substrate interfaces. Past uses of the pull-off test have been limited to rough in-field checks and flimsy method development supporting data. The present work improves the validity and versatility of pull-off adhesion studies by analyzing the stress-extension and derivative stress-extension curves associated with pull-off tests.

Stress-extension and derivative stress-extension analysis was employed to mathematically identify outliers and ultimately make adhesive and scoring method choices for an epoxy-amine coating. Refining the sample preparation and testing method in this way helps eliminate misleading results and improves confidence in the method. Successful tests show sharp failure peaks in the stress-extension curve and overlapping curves with an extended plateau in the derivative stress-extension. This process was used to compare adhesive amounts, four adhesive, and five scoring methods. The use of

additional mechanical information could differentiate between outliers and legitimate data much more easily than using only the peak pull-off stresses.

Conclusions by this method were that adhesive content needs to be minimized, Scotch-Weld DP460 was the preferred adhesive for this system, and scoring by the Dremel rotary tool ensured complete separation of the test area from surrounding coating while minimizing cohesive perimeter failure. Findings were supported both by (derivative) stress-extension curves and fitting to a predictive model. Statistical analysis was able to be performed on data sets with no true mean by comparing the difference between prediction and experimental instead of the experimental values themselves.

The importance of scoring was also demonstrated by correlating peak stress with cohesive failure around the perimeter of the dolly. These findings add practical support for stress distribution models found in the literature.

CHAPTER IV – IMPROVING ACCURACY OF ADHESION PREDICTIONS WITH RESPECT TO THICKNESS

4.1 Introduction

A pervasive problem in coating science is the predictability of coating performance from pristine coating properties. Performance parameters, including adhesion, hardness, and permeability, are altered by prolonged exposure to elevated temperatures, cyclic relative humidity, and other chemical and physical stimuli during use. Researchers are working towards being able to fully describe how each performance parameter will change over time-based on characterizing the coating material and the environment of the location the coating is intended to function in. Consistently, however, field testing and in-use performance deviate from predictions from laboratory characterization, implying there are relationships missing from the coating performance predictive models. Being able to reduce extended field testing of coatings but retain predictive insights will accelerate the field and the market in innumerable ways.

4.1.1 Thickness and adhesion

Thickness is reported whenever coatings are applied, but its influence on properties and performance is very rarely studied. The parameter is considered from the standpoint of a minimum requirement, i.e., the film needs to be thick enough to cover filler particles and eliminate defects. Changing thickness is considered trivial as it is viewed as a quantity independent of coating properties. Not only does the geometry of coatings lead to property variations from bulk due to confinement effects, but there are other processes thickness plays a role in.[78,79] As will be discussed further in this chapter, increasing thickness magnifies internal stress and the extent of solvent trapping. Organic

coatings most often can be found in use with thicknesses ranging anywhere from 20 to 1,000 μm in a variety of end-use applications such as architectural cladding and aerospace vessels.[80,81,90–92,82–89] In addition to the wide range of applied thicknesses, thickness will fluctuate in a non-uniform fashion across the surface over time during use.[80,90] Erosion, degradation, and swelling processes naturally occurring during use translate to a variation in thickness that can trend in either direction. The ramifications of a working thickness range spanning three orders of magnitude and the unpredictable loss of thickness over time are largely unknown, and making predictions of performance, including response to differences in thickness as a critical factor, has not been attempted.

One predictive model in the literature identifying thickness as a primary variable was found by Croll, and it describes how thickness influences adhesion strength.[31] The relationship is described in Equation 4.1, where σ_z is the tensile stress required to separate a coating and substrate in a pull-off adhesion test, E is the coating's Young's modulus, γ is work of adhesion, t_c is the coating thickness, and σ is the internal stress.

$$\sigma_z = \sqrt{\frac{4.286E\gamma}{t_c} - 2.572\sigma^2} \qquad \text{Equation 4.1}$$

This chapter makes regular references to both "internal stress" and "peak stress," which warrants a direct comparison for clarification. Internal stress is a result of coating shrinkage being resisted by attractive forces acting between surface atoms of the substrate and adjacent coating molecules. If a mass of liquid coating material could be cured in suspension without touching any surfaces like a substrate, shrinkage due to solvent evaporation, polymerization, and thermal expansion would be isotropic.[93] However, the interfacial interactions that develop with a substrate present prevent contraction from occurring uniformly at all points within the coating volume. Not all asymmetrical

contraction leads directly to internal stress. Anisotropy becomes permanent stress when relaxation times are slower than the volume change, which occurs when T_g increases above the environmental temperature.[94] Peak stress is the maximum stress withstood by the coating before cohesive or adhesive failure and is a pull-off adhesion testing specific value intended to quantify interfacial strength.

How the relationship looks in practice can be seen using the original literature data replotted in Figure 4.1. Croll modified the energy balance model described by Kendall for the purpose of developing a direct method to quantify adhesion using thickness and internal stress.[31,95] Stress from coating contraction applies tensile forces on the interface lowering the external force required to separate the surfaces. Increasing thickness increased total internal stress, and therefore adhesion could be quantified by the maximum thickness achievable before spontaneous delamination.

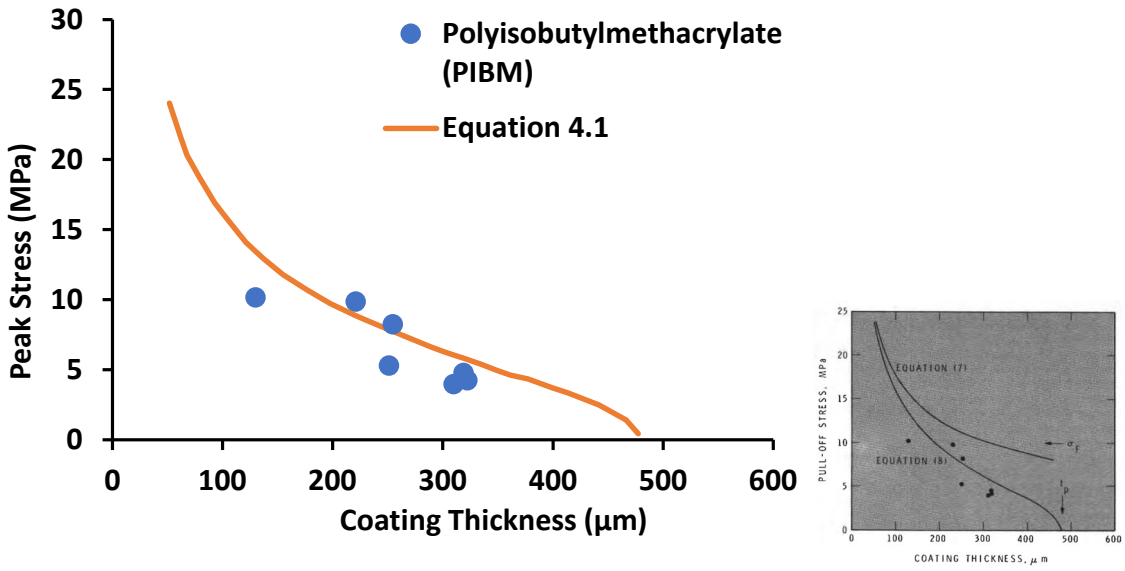

Figure 4.1 Pull-off peak stresses of PIBM applied to steel feeler gauge and plotted against a best-fit of Equation 4.1

Data replotted from Croll.[31] PIBM applied in toluene, dried at ambient for 9 months. Resulting film properties: E = 1980 MPa, T_g = 47 °C; MW = 193 kg/mol. Pull-off rate 1 mm/min

To demonstrate the accuracy of Equation 4.1 outside of the original paper, Figure 4.2 presents two examples where pull-off adhesion decreases with thickness. In the first example, an adhesive was investigated by Reedy and Guess instead of a coating.[96] For an adhesive, the tensile butt geometry of the test method was more appropriate than a standard pull-off with a dolly, but the mechanics were the same. The second example is from Singer et al., where model barnacles were removed from an anti-fouling coating. For both systems, the data could be fit after digitization to Equation 4.1 with good agreement. The method of finding the internal stress and work of adhesion from literature results is described in the experimental section and employed on data collected in the present study.

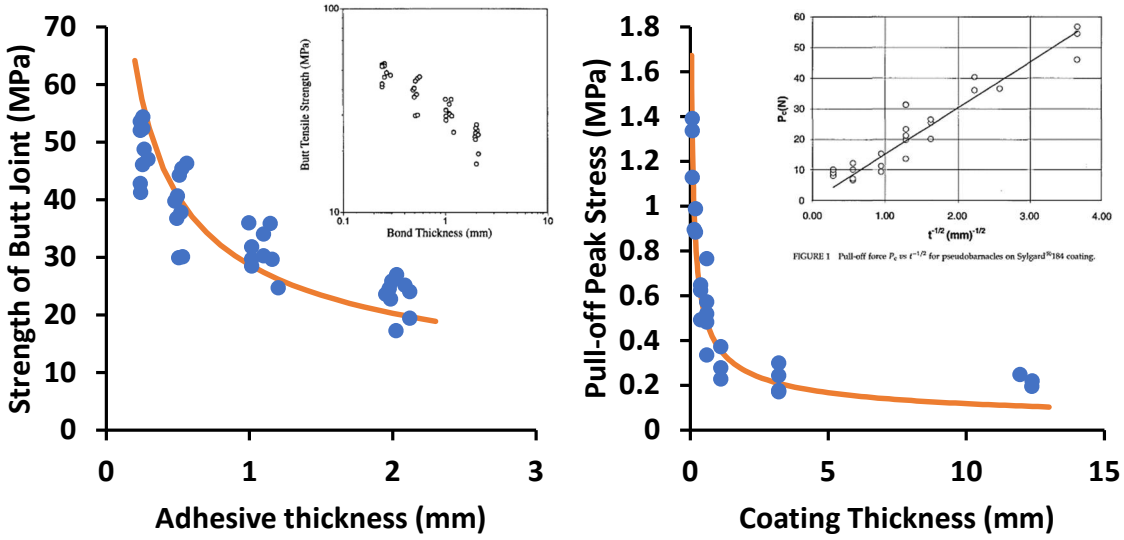

Figure 4.2 Example literature peak stress data that can be fit to Equation 4.1

Left) An adhesive of Epon 828 and T-403 in tensile butt geometry,[96] right) removal of pseudo-barnacle material from silicone coating.[97]

Despite the apparent predicting potential of Equation 4.1, it is not being employed in the design of new coatings or predictive models of current coatings. Other literature sources present the opposite relationship, giving a reason to believe the model is

incomplete. Baek et al. report pull-off peak stress values that *increase* with coating thickness, which are described in more detail in the Results and Discussion section. The authors asserted the increase in peak stress with thickness was a result of yielding by both the substrate and the coating.[32] Yielding behavior is not addressed by Equation 4.1 but clearly needs to be addressed for an effective model. Roche et al. were able to induce both positive and negative relationships between adhesion and thickness with the same epoxy coating depending on if scoring was performed around the dollies or not (Figure 4.3). The explanation offered was that increasing peak stress with thickness correlates with energy dissipation.[75] The uncertainties of coating thickness coupled with the extreme thickness dependence of adhesion means wildly varying coating adhesion spatially and temporally for environmentally exposed coatings, making any aspect of performance impossible to predict.

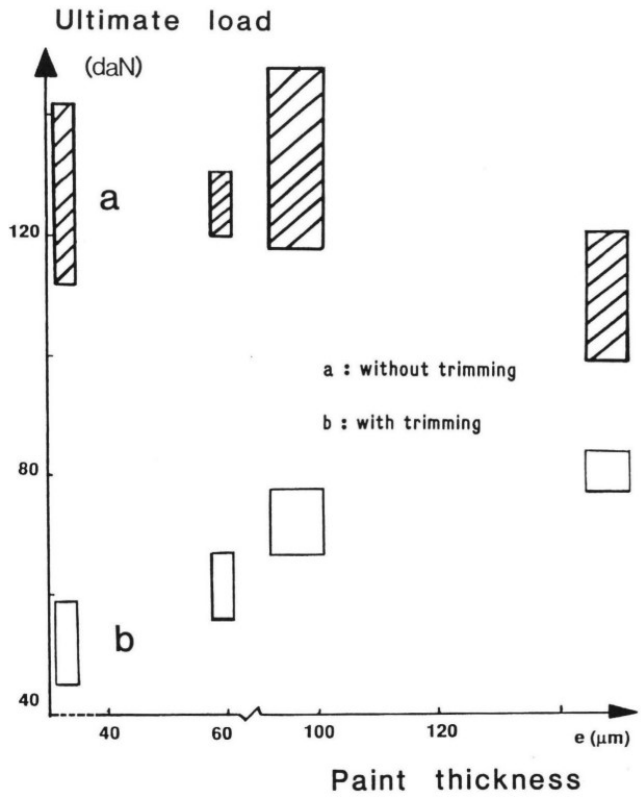

Figure 4.3 Pull-off peak stress results from literature that cannot be fit to Equation 4.1 and comparing data with and without trimming (scoring)

Results from an epoxy paint performed by Roche et al.[75]

Keeping consistent with the literature references, adhesion measurements in this chapter are acquired using pull-off testing. In general, the advantages of using pull-off over peel testing are that 1) data is more physically relatable, 2) the standard requirements are easier to meet (a 90° bend in the peel tab is hard to ensure), and 3) the method is more relevant to in-field coating testing. The reason it was chosen in this study, however, is due to the lower limit of testable thickness. Due to the handling of the peel tab required in peel testing, the thickness minimum is dependent on the ability to create a tab that withstands formation and testing, resulting in a lower limit of ~30 µm. Testing via pull-off also granted the added benefit of applying the findings of Chapter III to the data analysis of the current chapter.

Analysis of the stress-strain curves resulting from pull-off tests can be performed similarly to that of a standard tensile test, identifying an elastic region and potentially a plastic region. The differences between elastic and plastic responses in pull-off adhesion stress-strain curves are more subtle than a tensile test performed on bulk polymer. Identifying the mechanical mechanistic differences between pull-off tests is made easier by including the derivative of the stress where small changes in the stress-strain curve become more pronounced. Any decrease in the derivative stress value implies yielding or the initiation of an additional elastic mode. Stress-strain and derivative stress-strain data were used to help validate the accuracy of peak stress numbers and explain mechanical phenomena occurring in the film preceding failure.

Literature examples of the proposed derivative stress-strain analysis can be found in other application spaces. Zhao and coworkers analyzed the derivative stress curve for a polymeric stent in tension (Figure 4.4, left), identifying three zones where the derivative stress response changes, 1) an initialization zone of decreasing derivative, 2) a reinforcing zone where derivative increases, and 3) a yielding zone.[98] Similarly, Chen and coworkers performed tensile tests on wheat straw farmed from three different locations (Figure 4.4, right) and found the first derivative response decreased irregularly with strain, indicating a simple elastic model would be inaccurate in fitting the data.[99] A similar approach is used in this chapter to help identify elastic and yielding regions in the mechanical response.

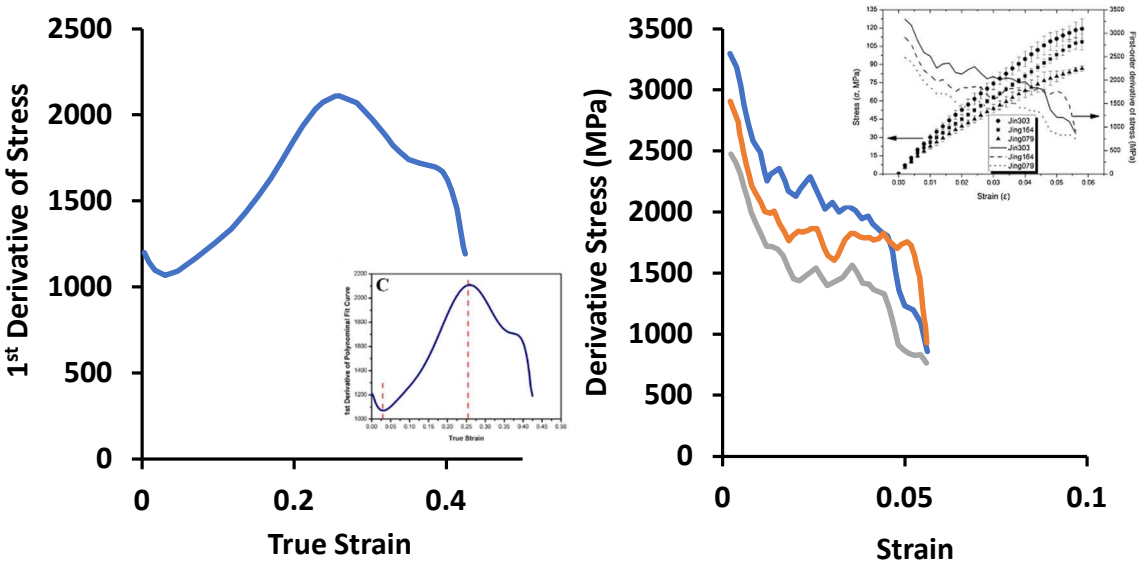

Figure 4.4 Literature examples of derivative stress analysis to expose yielding mechanisms

Left) Polymeric braided stent from Zhao et al.[98] Right) Wheat straw filaments from Chen et al.[99]

4.1.2 Solvent Trapping

Solvents are an invaluable part of coating formulations, providing reduced viscosities to simplify the application process and aiding in film formation.[100] Addition of solvent increases system complexity in both time and space. Not only must the polymerization reactions and interactions between binder and fillers be accounted for when attempting to predict coating properties, morphology, and topology but now how all species within the forming coating interact with the solvent. The transient nature of solvents means the polymerization reaction is happening in parallel with solvent loss during cure. Rates of the two processes are interdependent, requiring a detailed timeline of both processes if film properties are going to be predicted but accurately monitoring and quantifying all the aspects of solvent loss is not trivial.

Quantifying the total residual solvent at all times during a reaction pathway is not enough to describe the system at any particular moment. Solvents are not retained

uniformly within a coating, which affects both how properties develop and the properties of the final film. One of the more permanent ways solvent affects a coating is through residual solvent and solvent trapping. The presence of an impenetrable substrate on one side of a solvent containing coating and the formation of a vitrified skin on the air interface can lead to trapping of solvent near the substrate. The rate of solvent loss in a film relative to the rate of vitrification dictates the extent of solvent trapping.[101] The implications of trapped solvent are more than just uncertainty of coating composition; trapped solvent causes anisotropic plasticization, correlating with a reduction in T_g, reduced mechanical properties, and higher permeability to corrosive species.

Until now, the literature model predicting adhesion from thickness was unchallenged because modulus, internal stress, and work of adhesion remained constant with thickness.[31,96,97,102] When solvents are introduced, anisotropic solvent loss results in solvent trapping that increases linearly with dry film thickness. When solvent trapping occurs, and every thickness is a different coating composition, the modulus, work of adhesion, and stress constants become functions of thickness. The present study shows residual solvent inverts the relationship between pull-off peak stress and thickness at a critical thickness above which the relationship is positive. It is hypothesized that the inversion point corresponds to the thickness where stress relaxation due to solvent plasticization is greater than stress increase due to thickness.

Results presented in Chapter II indicate that thermal plasticization increases adhesion up to a maximum peel force, which occurs at a test temperature of T_g - 20 °C. The change in chain mobility at the interface that occurs with thermal plasticization is equivalent to the plasticization caused by the trapped residual solvent. The weight

percent of residual solvent in the cured film increases with thickness because of the added distance solvent must travel from the substrate through the coating. Increased levels of trapped solvent mean a greater extent of plasticization and a decrease in T_g with thickness. Plasticization of a coating resulting in a T_g of ambient + 20 °C will experience the highest possible measured adhesion for that material. Consequently, the relationship between thickness and adhesion in solvent-borne coatings is more complicated than in bulk. Knowing the total residual solvent in a coating is not enough to predict performance either because the trapped solvent is heterogeneously distributed in the coating. Measurements of residual solvent and modulus are an average of the total film thickness, but adhesion only experiences the inner surface of the coating, where the highest concentration of solvent is present. Adhesion measurements describe the effect of solvent trapping on properties and provide a window into the conditions in the interfacial environment.

4.2 Experimental

4.2.1 Materials

Model coatings evaluated in this work were epoxy-amine networks composed of one of two ratios of Epon 825 (diglycidyl ether of bisphenol A containing 0.05 repeat units), benzylamine (BA) (Acros 99%), 1,3-bis(aminomethyl)cyclohexane (BAC) (TCI, 98%) and Jeffamine ED-600 (Huntsman). In addition to the reactive monomers, 0.1 wt% TegoWet 270 (Evonik) was added to eliminate defects and promote flow and leveling. Coatings applied with solvent included a blend of 1:1 by weight of dipropylene glycol n-propyl ether and reagent grade ethanol, both procured from Aldrich. All chemicals were used as received. Monomer ratios formulated to generate high modulus (HMo) and low

modulus (LMo) model coatings are presented in Table 4.1. Substrates used were cold rolled steel panels purchased from Q-Lab with the composition presented in Table 4.2. Cold rolled steel panels are available from Q-Lab with different surface topographies; in this study, coatings were applied to two finish styles, smooth QD and rough R.

Table 4.1 Coating formulations

LMo coatings were applied to QD panel substrates and cured at 60 °C for two hours and 80 °C for one hour. HMo coatings were prepared either on QD and cured at 80 °C or on R panels and cured at 120 °C (all coatings were first cured at 60 °C for two hours). Not included in the table is 0.1 wt% of Tego Wet 270.

Monomer	**High Modulus (HMo) (wt%)**	**Low Modulus (LMo) (wt%)**
Epon 825	73.4	59.4
Benzylamine	10.9	0.2
1,3-Bis(aminomethyl) cyclohexane	5.3	3.9
Jeffamine ED-600	10.4	36.5
T_g (°C)	80	44

Table 4.2 Composition of Q-Lab cold rolled steel panels

The same material is used for QD and R panels; only the surface topography is different

Element	**Composition (at%)**
Iron	99.185
Manganese	0.6
Carbon	0.15
Phosphorus	0.03
Sulfur	0.035

4.2.2 Methods

4.2.2.1 Coating formulation and application

Epoxy-amine coating network formation was accomplished via a 2-stage process. In the first stage, Epon 825 and BA were combined by a Flaktek speed mixer for 1

minute at 1800 RPM. The mixture then reacted on a roller for 30 minutes to extend Epon 825 linearly with BA in the absence of the multifunctional amines (BAC and ED-600). Adding a pre-reaction step minimizes competition with crosslinking reactions and ensures a high yield of trimer formation. The second stage was the addition of BAC and ED-600 to the chain-extended epoxy, combined by speed mixer for the same duration and RPMs as the trimer stage, and returned to the roller for another 3 hours. Roller speed was not monitored or controlled but needed to be low enough to produce a tumbling motion of the resin instead of centrifugally pinning the mixture to the wall of the cup.

Building the resin in this manner makes the application of higher thickness films possible by increasing viscosity without decreasing workability and prevents amine blushing by increasing molecular weight to avoid phase separation and evaporation during cure. Tego Wet 270 was added after the partially formed network was removed from the roller and combined again by speed mixer. The procedure for solvent-borne coatings deviates from 100% solid films at this step, where solvents were added at the same time as Tego Wet. After the addition of the solvents, the mixture was blended by speed mixer at 1,800 rpm in one-minute increments until a smooth blend was formed. Prior to applying the coating, the resin was left for 5 minutes to let any accumulated bubbles dissipate.

Substrate preparation included cleaning with mineral spirits, drying under nitrogen, and wiping with a microfiber cloth. The liquid coating was applied to steel substrates manually by drawdown using a 3 in^2 drawdown bar. A wide range of applied thicknesses was used to achieve a dried film thickness range from 20 to 500 μm. Coated panels were placed immediately in a 50 °C oven and left overnight. The following

morning, the oven temperature was increased to 60 °C and held for two hours and finally increased again to either 80 or 120 °C and held for one hour. The oven was then turned off, and the coated panels cooled with the oven for another two hours.

4.2.2.2 Pull-off adhesion sample preparation

Cured coatings were prepared for pull-off testing by marking test locations and measuring thickness. Highly localized thickness measurements were made due to the importance of coating thickness to the study. Locations of dollies were identified in advance of their application and marked with a sharpie so thickness could be measured in the exact location the dolly would go. Thickness was measured by a DeFelsko Positector 6000 thickness gauge.

Aluminum dollies (diameter = 20 mm) were applied to the coating surface to act as handles in the pull-off test. Surface preparation steps were performed on the dolly faces to improve adhesion between the dolly and adhesive. First large deep grooves were formed using 60 grit sandpaper, and then the faces of those grooves were textured by abrasion with Scotch-Brite™ pads. Any debris accumulated on the surface during sanding was removed by immersion and agitation in ethanol and wiping dry.

Once dry, the dollies were ready to be applied to the coating surface. Dollies were applied to the coating surface with 3M Scotch-Weld™ DP460 2K epoxy adhesive based on findings described in Chapter 3. After spreading the adhesive onto the prepared dolly surface, it was pressed firmly onto the marked area, and a 160 g weight was then placed on top of the dolly to hold it down and ensure a minimal adhesive film thickness. The adhesive was cured at ambient conditions for at least 24 hours before testing.

4.2.2.3 Pull-off adhesion test procedure

Pull-off adhesion experiments were performed using a 10 kN MTS Insight load frame and a 10 kN load cell at a strain rate of 2 mm/min to achieve failure in under 100 seconds as described by ASTM.[77] The load frame accessories used in pull-off testing were the same as in chapter 3. Prior to testing, the area of coating underneath the dolly was separated from the surrounding coating by scoring through the coating with a Dremel tool. This procedure is often controversial,[19,32,45,75] but models of stress distribution and data from the previous chapter have clearly identified scoring as an important step for achieving precision and accuracy.[30]

4.2.2.4 Young's Modulus determination by mechanical tensile test

Literature models for predicting pull-off adhesion with respect to thickness require the inclusion of the coating's Young's modulus. Films of each resin, prepared at 70 and 400 μm thickness and with 0 and 20% solvent content, were drawn on polypropylene boards and cured the same as coatings on steel. After curing, free films were removed from the board, and 13mm wide strips were punched from the film. Tensile testing was performed on the same load frame and at the same 2 mm/min extension rate as pull-off tests.

4.2.2.5 Residual solvent quantification by thermal gravimetric analysis

Understanding of how the coating system was changing with increasing thickness was a critical step in correlating differences in adhesion with the coating composition. Volatile content was quantified by thermal gravimetric analysis (TGA) of 8 mm diameter punches of free films of various thickness prepared on and removed from polypropylene boards. TGA experiments were run from 30 - 600 °C at a ramp rate of 20 °C/min. The

boiling points of the solvents were 78 °C (ethanol) and 212 °C (DPnP), and to ensure mass loss from both species were accounted for, the residual solvent content was regarded as the mass loss occurring between test onset and 250 °C.

4.2.3 Calculations

Internal stress and work of adhesion were determined by finding the best fit of Equation 4.1 to the experimental data. The process of finding the best fit is explained in detail in APPENDIX B.

4.3 Results and Discussion

4.3.1 High modulus coating – effect of cure temperature

Adhesion response to thickness was quantified for two cure profiles; two hours at 60 °C followed by one hour at 80 °C or one hour at 120 °C. The reason for examining two cure temperatures was to have multiple sample systems with the same composition to investigate the robustness of the thickness relationships. The effects of increasing the cure temperature were an increase in internal stress in bulk and a decrease in weight percent of residual solvent in the final solvent-borne films. Solvents used in this study were ethanol and DPnP, with boiling points of 78 and 212 °C, respectively. Increasing the maximum cure temperature from 80 °C to 120 °C decreases the total residual solvent content and was predicted to decrease the ratio of residual ethanol to DPnP.

Curve shapes in peak-stress versus thickness figures will be the focus of discussion when comparing cure temperatures because, in this section, the cure temperatures *and* the substrates were varied. The decision to change substrates was made based on the observation that the QD-panel substrates would begin to deform at a certain stress level during testing, but the data collected has proven to still be valuable. Warping

of the substrate was addressed by changing to a thicker substrate. Increasing substrate thickness from 0.5 mm for QD-panels to 0.8 mm for R-panels was enough to eliminate the deformation mode; unfortunately, the panels also had different surface topography. SEM images of the substrate surfaces are shown in Figure 4.5. With this in mind, conclusions relating to the effect of cure temperature will be made after eliminating interference by substrate effects.

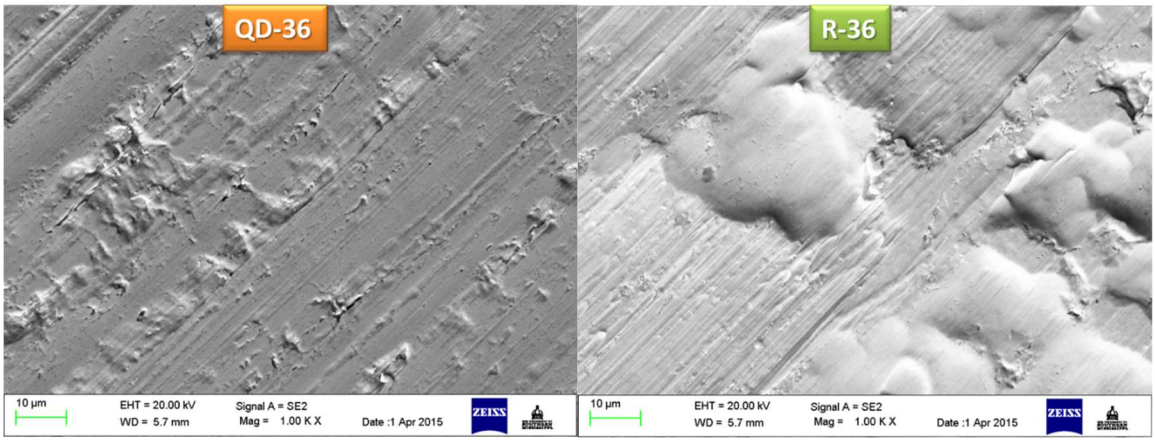

Figure 4.5 SEM images of surfaces of QD and R panel substrates taken at 1,000x magnification

Illustrate the difference in topography between the two substrates used in section 4.3.1 comparing cure temperature

4.3.1.2 Bulk

Pull-off peak stress as a function of thickness for HMo applied in bulk and cured at 80 °C is compared to the same coating heated to 120 °C in Figure 4.6. Peak stress decreased with thickness in a manner predictable by Equation 4.1 for both cure temperatures. Best fit curves of Equation 4.1 for each cure profile are included in Figure 4.6 and indicate pull-off peak stress to be greater at all thicknesses for the lower cure temperature films on QD, despite having lower roughness. Average roughness (R_a) is higher on R panels, 0.42 µm versus 0.32 µm for QD, which can be seen from the larger range in the z-direction in Figure 4.7. In most cases, an increase in roughness

corresponds to an increase in adhesion, but the QD panels had more frequent sharp v-like surface features, which led to an overall increase in peak stress. Changes in topographic elevation for both QD and R are gradual, and the abrupt features seen primarily in QD are likely to contribute more to adhesion. Such a conclusion is consistent with the findings of Kim et al., who demonstrated mechanical adhesion depends on the frequency of surface features much more feature than their depth.[103]

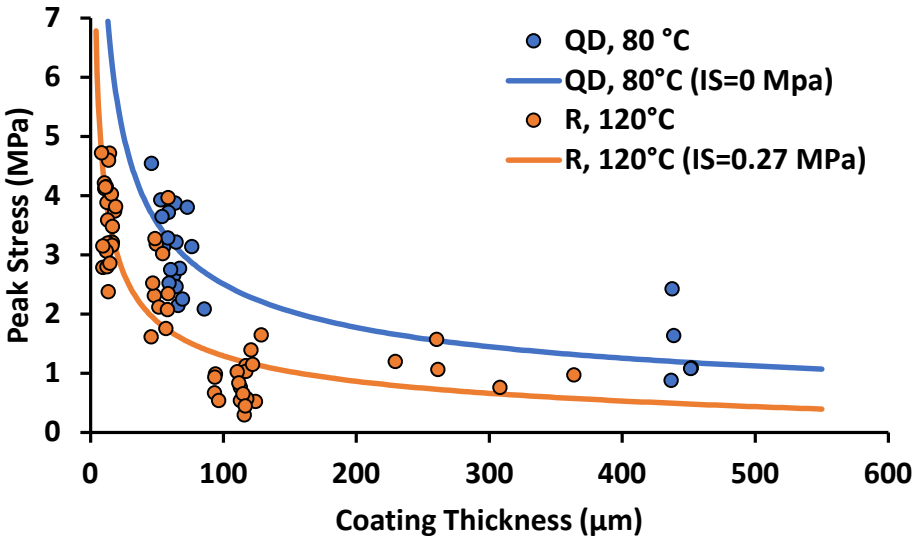

Figure 4.6 HMo coating applied in bulk to QD and R panels

Films on QD cured at 80 °C and films on R cured at 120 °C for one hour after curing for two hours at 60 °C. Lines represent best fits of data according to Equation 4.1.[6]

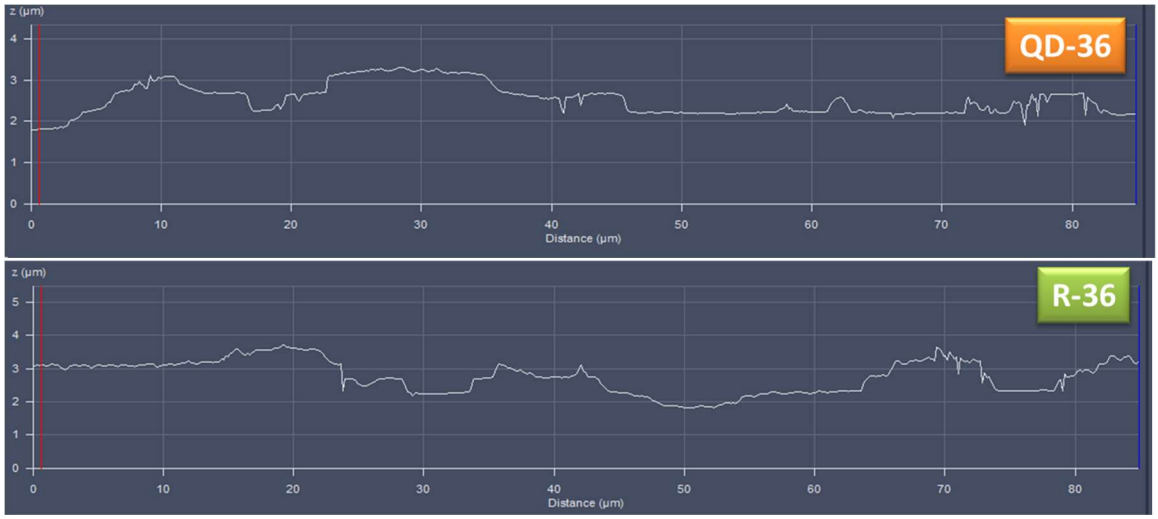

Figure 4.7 Confocal microscope topographical measurement of substrates employed in cure temperature comparison

For reference, when comparing peak stress between cure temperatures that were also applied to different substrates

Comparing the model fit to Equation 4.1 of the two cure temperatures indicated a change in internal stress. The 120 °C cure temperature imparted a calculated internal stress value of 0.27 MPa, and the best fit for the 80 °C cured coating required the internal stress be equal to 0 MPa. Reduced internal stress in 80 °C cured coatings could be attributed to incomplete conversion, but the degree of conversion was determined to be the same for both systems, according to FTIR. Even though T_g remains the same when cured at 80 or 120 °C, the difference in internal stress is ascribed to thermal shrinkage. Internal stress accumulates when changes in volume are not matched by relaxation, and after cure, cooling and contraction are expected to occur faster than relaxation. While higher thermal expansion leading to greater internal stress is in accordance with expectation, an internal stress result of 0 MPa is peculiar.

The absence of internal stress or the reduction in adhesion with increasing coating thickness could be easily explained on their own, but if the reduction in adhesion depends on internal stress, what is driving the reduction in peak stress without internal stress.

Mathematically, Equation 4.1 reduces to Equation 4.2 in the absence of internal stress, which clearly indicates that peak stress decreases with thickness. It is harder to visualize the physical explanation for why adhesion would decrease with thickness in the absence of internal stress. Thickness has no effect on the material itself, but the availability of more material enhances the effect of other properties. A material's modulus indicates the difficulty of deformation, but no matter how stiff the material is, some strain will accompany the stress. When thickness increases and deformation becomes considerable, a transverse force is generated as the coating attempts to contract under the tensile load of a pull-off test. An output of 0 MPa for internal stress is not uncommon; fitting the pseudo-barnacle data in Figure 4.2 also indicated there was no internal stress.

$$\sigma_z = \sqrt{\frac{4.286E\gamma}{t_c}} \qquad \text{Equation 4.2}$$

Understanding how a coating could form with no stress is also important for building confidence in the results. The sources of internal stress of formation are predominantly reaction shrinkage and thermal shrinkage. Reaction shrinkage is minimal because of the reaction chemistry of the thermoset network. Epoxy-amine chemistry is widely used in primer coatings in part because the polymerization reaction has low shrinkage. As the distance between amine and epoxy monomers decreases, the epoxy monomer lengthens as the epoxide ring opens. Ramos et al. calculate the shrinkage for an epoxy-amine with T_g = 175 °C to be ~4% at all cure temperatures. The shrinkage percent experienced on the substrate will be less than that because some of the reaction and volume change occurs in a reaction vessel on the roller. Thermal shrinkage is minimal because the coefficient of thermal expansion increases above T_g and cure

temperature never exceeded the T_g of HMo.[104] Relaxation of the shrinkage stress is also much more prevalent at temperatures above T_g, but relaxation slows faster than cooling and therefore curing above the ultimate T_g still results in more shrinkage.

Differences between calculated internal stresses are not a result of substrate variations. Surface roughness will affect the work of adhesion, but internal stress is a bulk phenomenon acting on the interface. As described in the discussion of Figure 4.7, the topography of QD panels is more conducive to polymer adhesion, and the calculated work of adhesion values reflect that. The work of adhesion for HMo on QD is 0.058 N/m and 0.024 N/m for R. Reduced work of adhesion contributes to the spontaneous delamination thickness but not the value of internal stress. How rapidly peak stress is reduced with thickness dictates calculated internal stress, not the magnitudes of peak stress. Substrate topography will influence stress distribution in the film, but the magnitude depends on the extent of volume restriction during cure.

The biggest direct effect substrate seems to have on pull-off results is seen in the stress-extension and derivative stress-extension curves. Chapter III describes a method of analyzing pull-off adhesion experimental data through the stress- and derivative stress-extension responses, the application of which will be extended here. Figure 4.8 presents stress-extension and derivative stress-extension curves for high and low thickness examples of HMo cured at 80 °C and 120 °C. This figure sets a precedent for how the mechanical response is affected by different thicknesses. Equation 4.1 describes the effect thickness should have on pull-off peak stress but not the mechanical response. Figure 4.8 demonstrates that films of the same material will follow the same mechanical response pathway and fail at different points along that pathway depending on thickness

and imposed internal stress. In addition, Figure 4.8 shows the effect substrate has on the mechanical response. Both high and low thickness films on QD experience a much higher slope than the polymer networks applied to R panels. The difference in cure temperature affects internal stress, but if that was the source of the change in slope, then R should resist further strain more than films on QD. Instead, it is proposed that the interphase in coatings applied to QD is more resistant to deformation because of the orientation of the surface features. Roughness on R is isotropic, but mill lines on QD run parallel to the draw direction, which promotes network fragment alignment in the surface features, generating a stiffer interphase region.

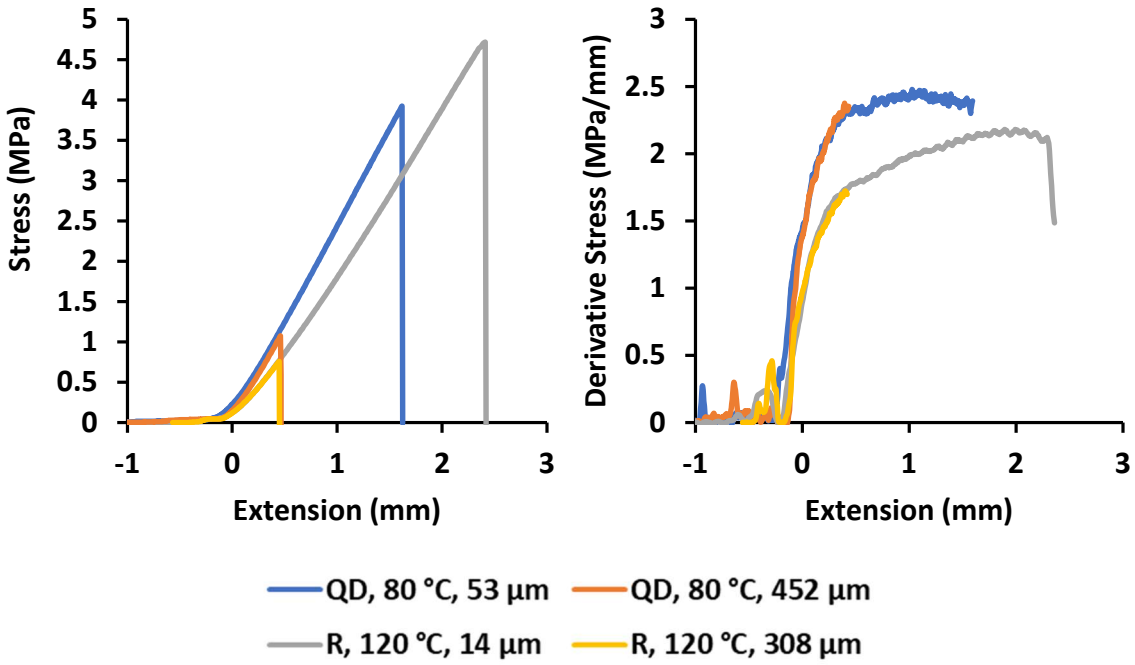

Figure 4.8 Representative stress-extension (left) and derivative stress-extension (right) curves

HMo applied in bulk, cured at different temperatures and with varying dry film thicknesses

The use of derivative stress-extension curves also reveals the effect substrate thickness has on the mechanical response. In Figure 4.8, the low thickness QD curve

peaks in derivative value around 1 mm, indicating the 2.5 MPa of stress achieved at that extension was enough to induce yielding of the substrate. Yielding represents an additional relaxation mode, and stress no longer increases as rapidly with strain. This curve shape is characteristic of pull-offs performed on QD panels.

4.3.1.3 Solvent-borne (80% solids)

Solvent effects on HMo resins prepared by differing cure schedules are seen in Figure 4.9. Both 80 and 120 °C cured polymer networks decrease in peak stress with thickness up to a critical thickness and then begin to increase in peak stress above the critical thickness. Variables used to define the model fit curve in Figure 4.6 (modulus, work of adhesion, and internal stress) were assumed to be constant over the investigated thickness range for coatings applied in bulk, but that changes in the presence of a solvent. A thickness response like this has not been described anywhere previously and suggests neither coating has a traditional spontaneous delamination thickness. Another aspect the two cure temperatures have in common is the trajectory of the positive relationship above the critical thickness; it appears to decrease in slope with further increasing thickness.

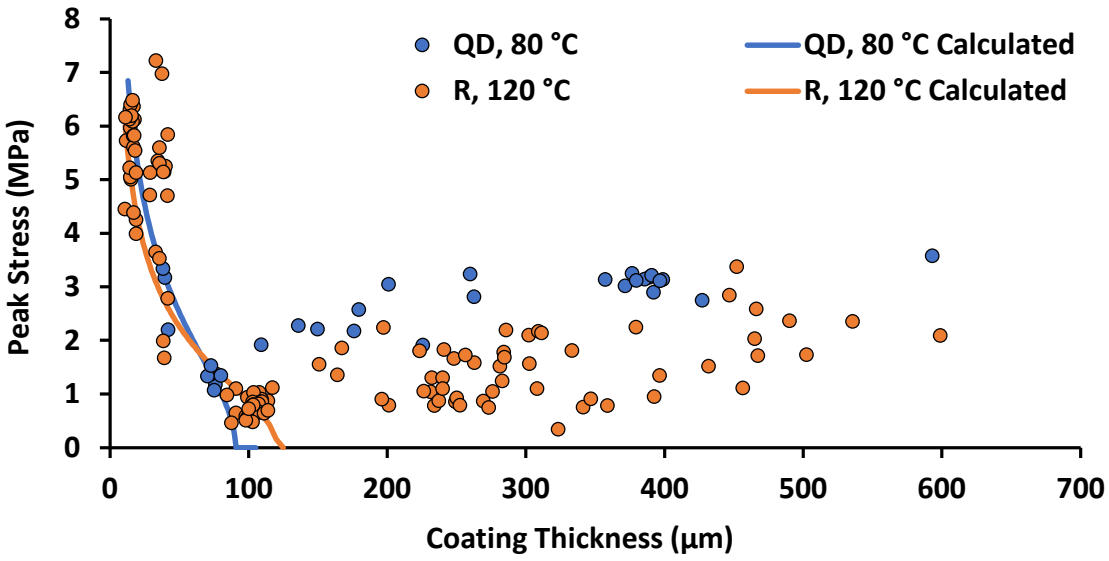

Figure 4.9 HMo applied at 80% solids to QD and R panels, cured at 80 and 120 °C, respectively

The solvent blend is a 50:50 by weight solvent mixture of ethanol and DPnP.

The critical thickness value varies from one cure temperature to the other. Increasing the maximum cure temperature from 80 °C to 120 °C increases the critical thickness from 75 µm to 100 µm. Curing at higher temperatures results in a reduction of residual solvent, which was quantified by TGA, and the results are summarized in Figure 4.10. All coatings applied with solvent experience increasing residual solvent content in the final film with thickness. The residual solvent can be calculated through the equations describing the linear trendlines fit to the mass loss data for the critical thicknesses. Table 4.3 shows that HMo cured at 80 °C at 75 µm has approximately twice as much residual solvent as coatings cured at 120 °C do at 100 µm. Some of the inconsistency was attributed to the different substrates, forming different interphases and the asymmetry of solvent distribution to be centered around the substrate interface means it likely plays a role.

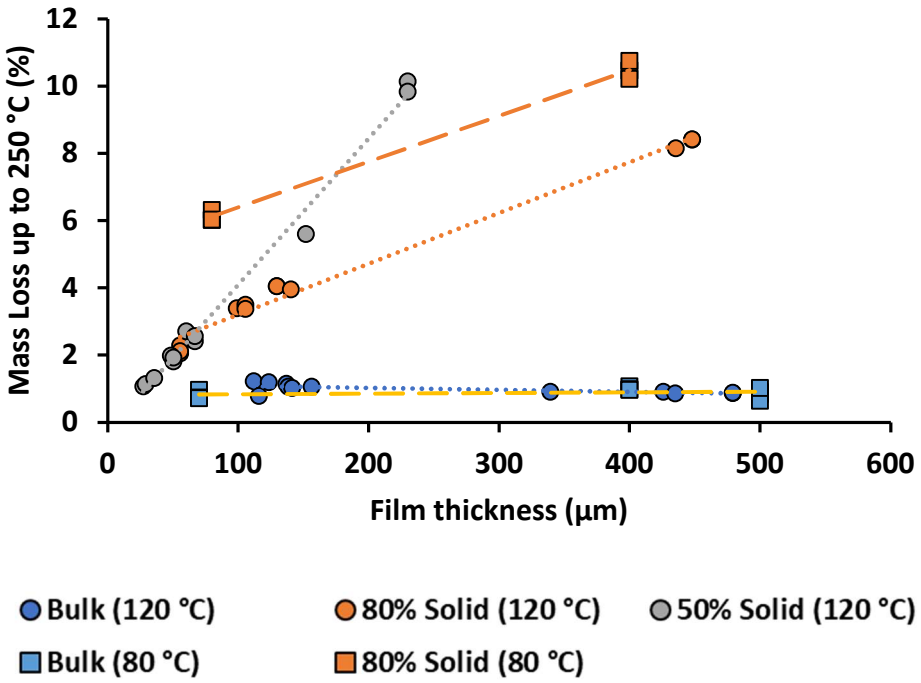

Figure 4.10 Residual solvent in HMo free films as a function of thickness and initial solvent loading

Films were obtained by peeling coatings from polypropylene sheets, and residual solvent was quantified by mass loss up to 250 °C as measured via TGA.

Table 4.3 Residual solvent content at critical thicknesses seen in Figure 4.9, calculated from trendlines in Figure 4.10

Total residual solvent content is not sufficient to explain the critical thicknesses.

Thickness (µm)	Wt% solvent 80 °C	Wt % solvent 120 °C
75	6.06	2.83
100	6.40	3.21

Another contribution to the low critical thickness of networks cured at 120 °C relative to residual solvent is the selectivity of solvent retention and swelling versus solvent absorption. Critical thickness indicates when the initiation of yielding takes less force than interfacial failure. Tensile tests indicate the effect of solvent trapping on modulus and yielding deformation. High and low thickness film examples of stress-

strain curves of HMo applied in bulk, and 80% solid, cured at 80 °C are shown in Figure 4.11 and demonstrate that solvent-borne films show a thickness dependence of mechanical response. Increasing cure temperature drives off disproportionately more ethanol than DPnP due to the difference in boiling points, 78 °C and 212 °C, respectively. As a smaller molecule, ethanol is expected to fill voids in the network without disrupting intra-network interactions. Plasticization is likely dependent primarily on DPnP, which is assumed to be the only solvent remaining in 120 °C cured coatings. At 75 μm, coatings cured at 80 °C are predicted to have the same loading of DPnP as 100 μm thick coatings cured at 120 °C. The distinction between solvent content and the extent of network disruption is consistent with hydration and swelling models described by Mao *et al.,* where a film can be completely hydrated but not swollen.[105] Network disruption is considered a requirement for swelling. The deformation aspect of pull-off testing reveals an important truth about the method; it measures the difficulty of separating surfaces, not interfacial strength. In environments where mechanical forces are the primary drivers towards coating failure, the difficulty of separating the surfaces may correlate well with performance, but the distinctions have never been addressed, and pull-off has been used to justify corrosion resistance.

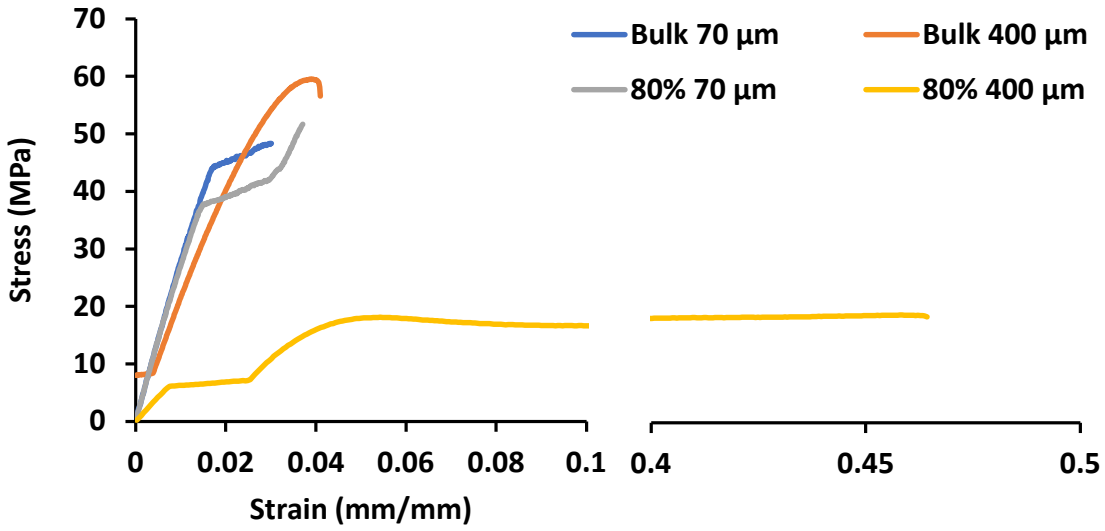

Figure 4.11 Tensile experiment on free films of HMo at high and low thickness comparing bulk applied and 80% solids applied model coatings.

Free films were formed from coatings applied to polypropylene boards. Note how thin films release solvent and thick films applied from solution trap solvent and provide a new toughened response to the tensile stress.

As an additional tool for analyzing the two data sets, Equation 4.1 was fit to the peak stresses below the critical thickness. Decreasing peak stress with thickness below the critical thickness implied internal stress was increasing in the film as would be predicted by the equation, allowing for effective internal stresses to be calculated in the sub-critical thickness region. Effective internal stress was calculated to be 1.75 MPa for coatings cured at 80 °C on QD panels and 1.18 MPa for coatings cured at 120 °C on R panels. It is possible for internal stress to increase from 0 and 0.27 MPa in bulk to 1.75 and 1.18 MPa respectively in solvent-containing systems despite plasticization because solvent loss adds another dimension to film shrinkage. Shrinkage of the film during cure in the presence of solvent is now the sum of 1) the difference between monomer and polymer volume, 2) thermal shrinkage, and 3) the loss of solvent volume. There is also a gradient to the solvent loss. Contraction at the air interface where all solvent is removed

is much greater than at the substrate interface where some solvent remains. The extent of contraction at the air and substrate interfaces are more closely related in bulk. The detrimental effects of added shrinkage on internal stress lessen as the contracting volume (air interface) moves away from the substrate and is dampened by a low modulus layer caused by trapped solvent, allowing for the increase of adhesion with additional thickness. The critical thickness where adhesion begins to increase with increased thickness indicates where enough solvent is trapped within the film to provide overall stress relaxation despite larger differences in shrinkage. Increasing adhesion slows with thickness above 75 μm because the properties of HMo applied at 80% solids continue to change with thickness, and the added mobility becomes less beneficial.

In bulk, the elevated cure temperature led to additional internal stress, but in the presence of solvents, the effective internal stress is greater for 80 °C cured coatings in the thickness region below the critical thickness. The rearranging of internal stress relationships is also due to the asymmetric solvent loss of substrate-bound films. The lower effective internal stress of 120 °C cured networks relative to 80 °C is possible because the total volume of trapped solvent is lower than in the 80 °C cured films. If air interface residual solvent concentration is predicted to be zero for both cure temperatures, the difference in shrinkage between the air and substrate interfaces is reduced when less total residual solvent is present.

How the addition of solvent changes the polymer networks from a mechanical perspective can be visualized and quantified using graphs of the derivative stress versus extension. Figure 4.12 compares the effect of solvent on coatings cured at 80 °C on QD with those cured at 120 °C on R. At thicknesses equal to or below the critical thickness,

solvent-containing films respond to tension in much the same way as coatings of an equivalent thickness applied in bulk. Above the critical thickness, there is a significant reduction in modulus, and yielding is present in films on both substrates. This suggests the critical thickness corresponds to a critical solvent loading where the extent of plasticization allows yielding, and stress is distributed throughout the coating instead of being transferred entirely to the substrate interface. As thickness increases above the critical thickness, more plasticizer is added in the form of residual solvent, and more elongation is possible before catastrophic adhesive failure, resulting in further increases in peak stress.

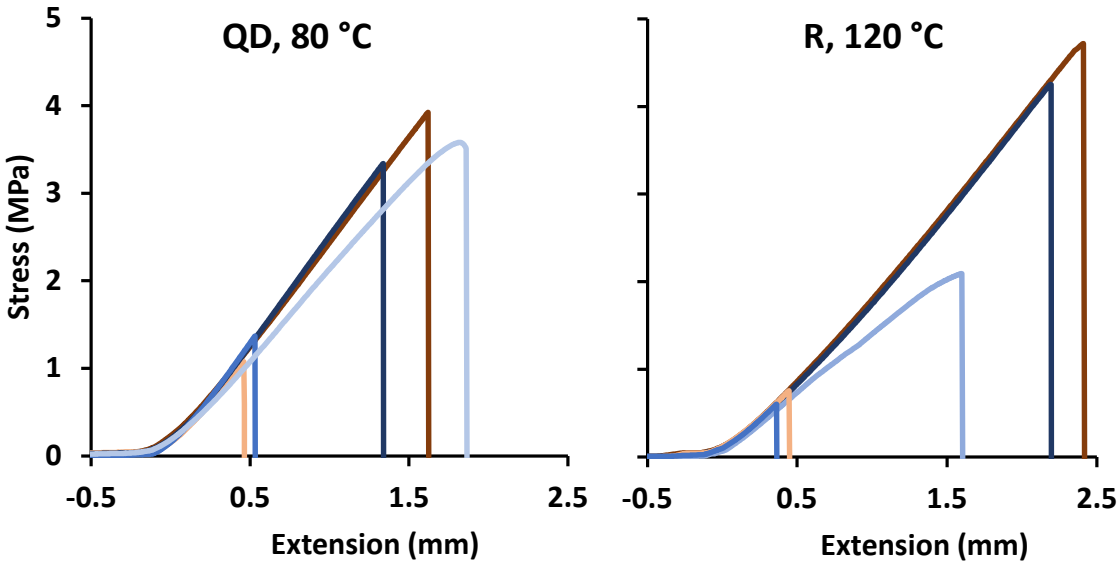

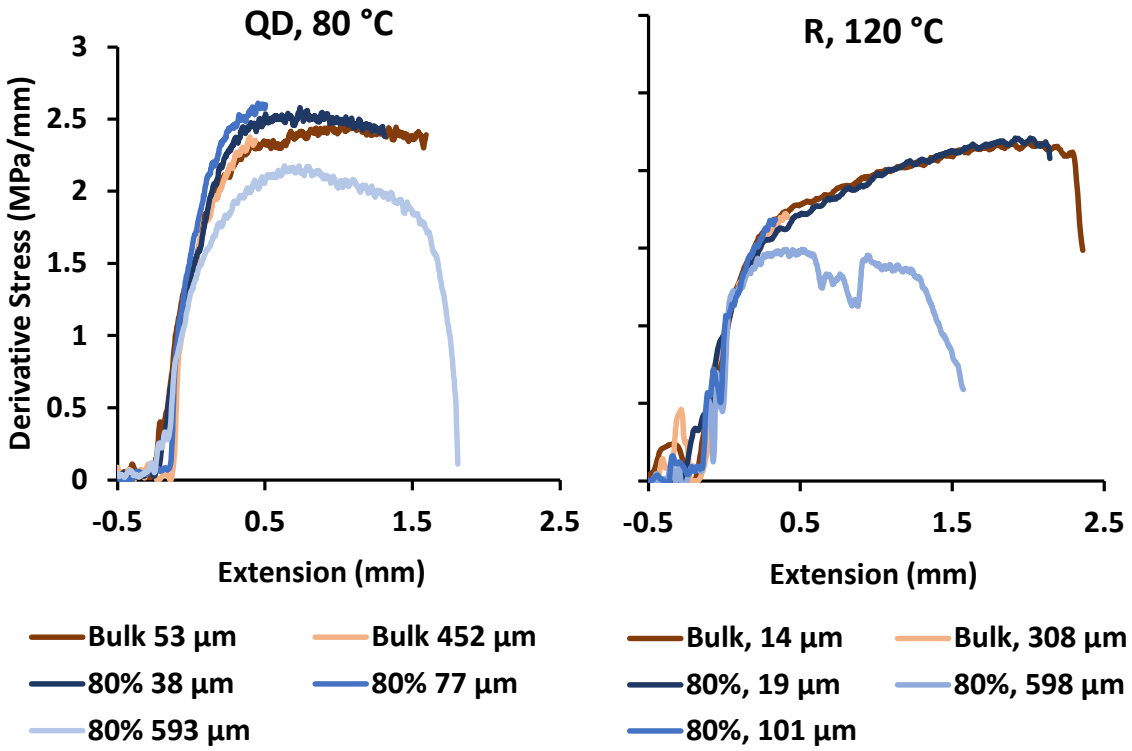

Figure 4.12 Effect of solvent on the mechanical responses of HMo coatings applied on QD or R panels and cured at 80 °C or 120 °C, respectively

Presented thicknesses represent the high and low extremes, and an additional point in solvent-borne coatings for the critical thickness

Adjusting the cure temperature of HMo coatings demonstrated the repeatability of 1) fitting Equation 4.1 to high modulus coatings in bulk and 2) the relationship inversion with the addition of solvent. Increasing the cure temperature caused changes in other features of the adhesion-thickness relationship. In bulk, the increased cure temperature increased the calculated internal stress from 0 to 0.27 MPa. For solvent containing HMo coatings, both cure temperatures experienced a critical thickness above which adhesion increased with thickness. The critical thickness was higher for coatings cured at 120 °C because there is less trapped solvent per unit thickness. Internal stresses predicted for the thicknesses below the critical thickness resulted in internal stress equaling 1.75 MPa for

80 °C films and 1.18 MPa for 120 °C cured films, which is accounted for by lowering the shrinkage gradient due to solvent trapping in the through-thickness direction.

4.3.2 Effect of applied solids content on the relationship between film thickness and pull-off peak stress

Identifying the effects that solvents have on the adhesion-thickness relationship prompted further investigation into how the relationship changes as a function of solvent loading. This portion of the study was performed using HMo networks, applied on R-type Q-panels, cured at 120 °C, with varying solvent loadings of 0, 20, and 50 wt%. Figure 4.13 presents an overlay of the peak stresses resulting from the three different solvent loadings along with their fits of the energy balance model to the exponential loss region.

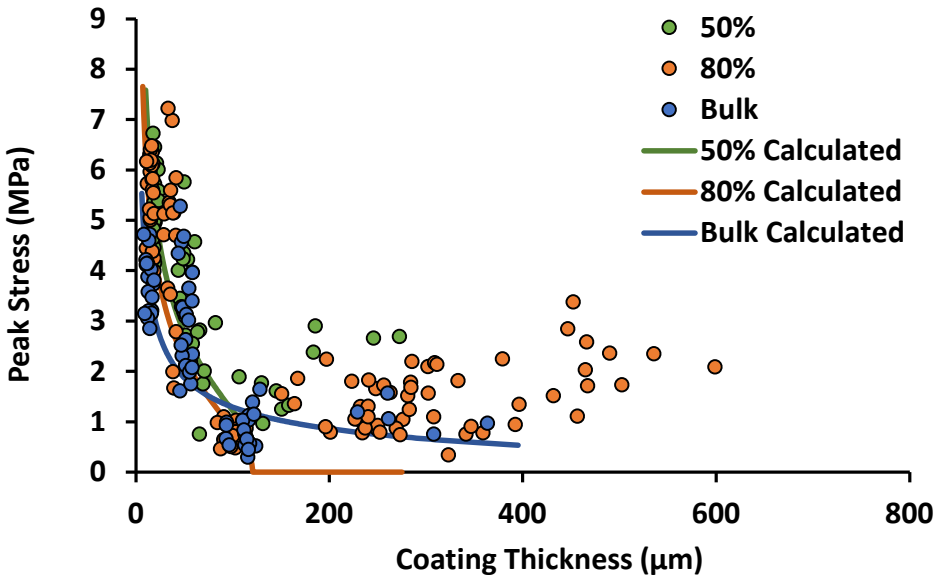

Figure 4.13 Comparison of the relationship between pull-off peak stress and thickness for coatings applied at 80% solids, 50% solids, and bulk with the same binder formulation

The solvent package was 1:1 by weight ethanol and DPnP. Coatings were applied to R panels and cured for 2 hours at 60 °C and 1 hour at 120 °C.

Investigation of additional solvent loaded allowed for further investigation into the variation in critical thickness and effective internal stress. As expected, based on the peak stress response to the thickness of the coatings applied at 80 wt% solids, the 50 wt% coating possessed a critical thickness in place of a spontaneous delamination thickness. From the available data set, the critical thickness for the 50 wt% solids system (65 μm) is lower than 80 wt% solids (100 μm), which is consistent with the findings from the cure temperature comparison. The diffuse spread of the 50 wt% solids peak stresses makes it hard to definitively say what the transition thickness is, but calculating the residual solvent for 65 μm 50% solids HMo and 100 μm 80% solid predicts 3 wt% loading for both coatings.

Effective internal stress calculated from the thickness region below the critical thickness (t_{cr}) was shown to increase compared to internal stress calculations in bulk for the two cure temperatures and was expected to increase further with more solvent. This trend continues with internal stress increasing from 0.27 MPa in bulk to 1.18 MPa in 80 wt% solids, and finally to 1.36 MPa for the 50 wt% solids coatings.

4.3.2.2 Understanding the adhesion pathway

In bulk and 20 wt% solvent examples, four sample sets were produced and tested; a low thickness set, a medium thickness set, a set around the critical thickness, and a set way above the critical thickness (t_{cr}). Only three were reported for 50 wt% solids in Figure 4.13 because the set applied at 16 mils, intended to account for the t_{cr} region, was applied at very low viscosity (η) and responded very differently in pull-off experiments. The desire to maintain constant network fragment size on coating application led to the same reaction times being used for all solvent loadings and, therefore, very different

viscosities. A comparison between peak stresses from the low η sample set and all other coating systems is presented in Figure 4.14. A broad range of thicknesses was achieved, and at all thicknesses, dollies from this data set achieved higher peak stress than any other sample.

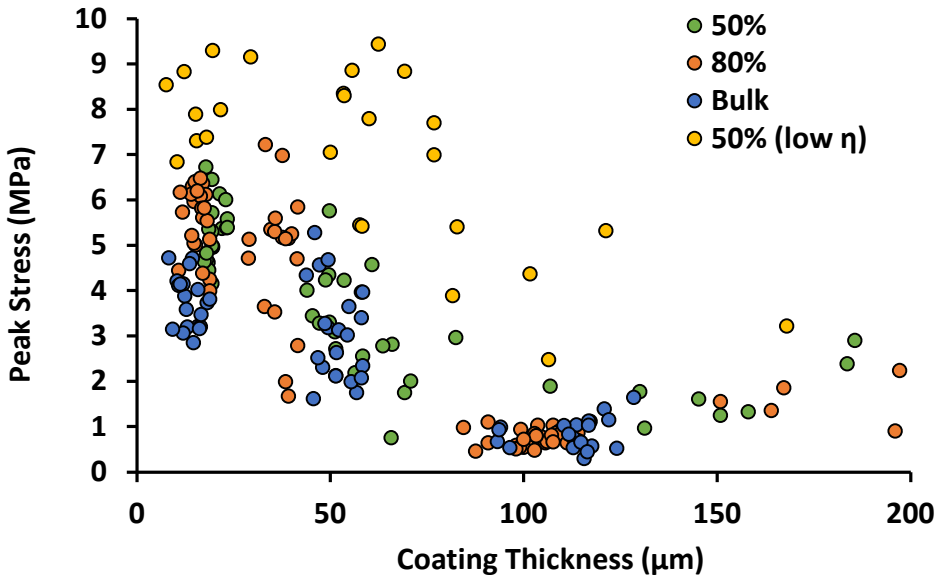

Figure 4.14 Comparison of 50 wt% solid applied at low viscosity (η) to bulk, 80 wt% and 50 wt% solids applied at high η

The solvent package was 1:1 by weight ethanol and DPnP. Coatings were applied to R panels and cured for 2 hours at 60 °C and 1 hour at 120 °C.

It was expected that at low thicknesses, below $t_{cr,}$ when there was minimal residual solvent for films of all applied solvent loadings, the pull-off peak stresses would overlap. To a certain extent, this was found to be true. Looking at the low thickness sample set for each of the standard coatings in Figure 4.15, they all occupy similar ranges of thickness and peak stress. The low η applied coating, however, deviates from both peak stresses at the intended thickness and the unintentional low thickness. Increased peak stress at low applied η supports the idea of more numerous accessible interphase morphologies and interfacial segregation of monomers that preferentially bind to the

substrate. These hypotheses suggest that the process of forming the interface benefits from the presence of solvents even if the final residual solvent content is low.

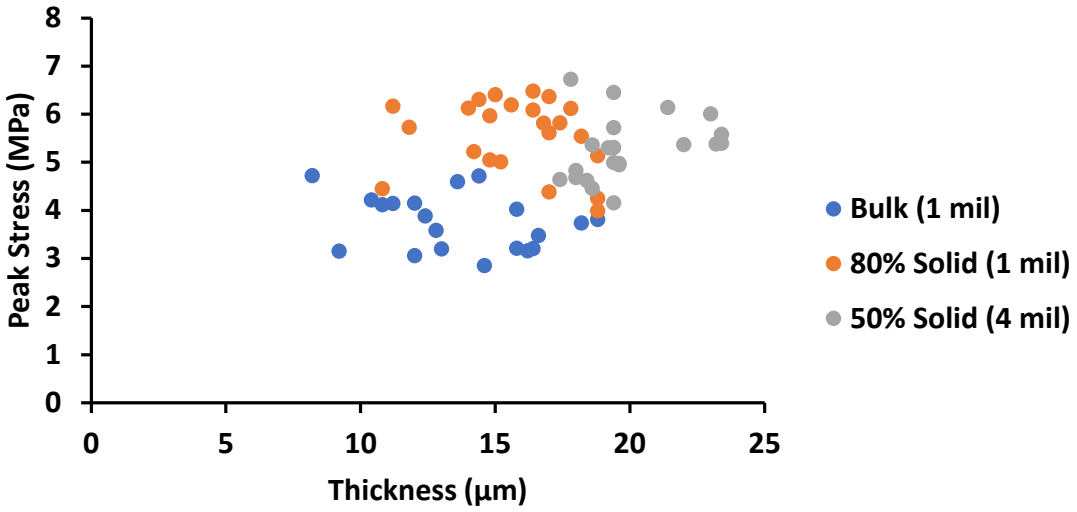

Figure 4.15 Peak stress distribution of pull-offs from thin coatings

Associated derivative stress-strain curves are shown in Figure 4.16, Figure 4.17, and Figure 4.18 for bulk, 80% solid, and 50% solid, respectively

Stress-extension and derivative extension curves were analyzed for every pull-off experiment to determine which were representative of the sample films and should be included in Figure 4.13. Processing of the mechanical responses uncovered how the low η coatings responded differently from other sample sets throughout the pull-off test. The derivative curves can take on several shapes, but the films of similar thickness had derivative stress-extension curves with similar attributes across solvent loadings.

Low thickness films result in high pull-off stresses, but there are many mechanical pathways of achieving high peak stress, as demonstrated in the comparison of cure temperatures with and without solvent (Figure 4.12). Derivative value with respect to the extension can increase rapidly to the point of failure, or reach a maximum derivative value, and decline before failure or reach an extended plateau or linear

trajectory. For bulk, 80 wt%, and 50 wt% solids at low thickness, all solvent loadings demonstrate a gradual linear change in the derivative. Figure 4.16, Figure 4.17, and Figure 4.18 are the derivative-stress response for pull-offs of low thickness films for bulk, 80% solid, and 50% solids, respectively. Each figure shows an initial rapid increase in derivative stress value up to 0.1 mm of extension, followed by a steady linear increase until the failure region where the derivative value rapidly decreases and ends. The average derivative stress value of 2 MPa/mm is the same for each solvent loading level.

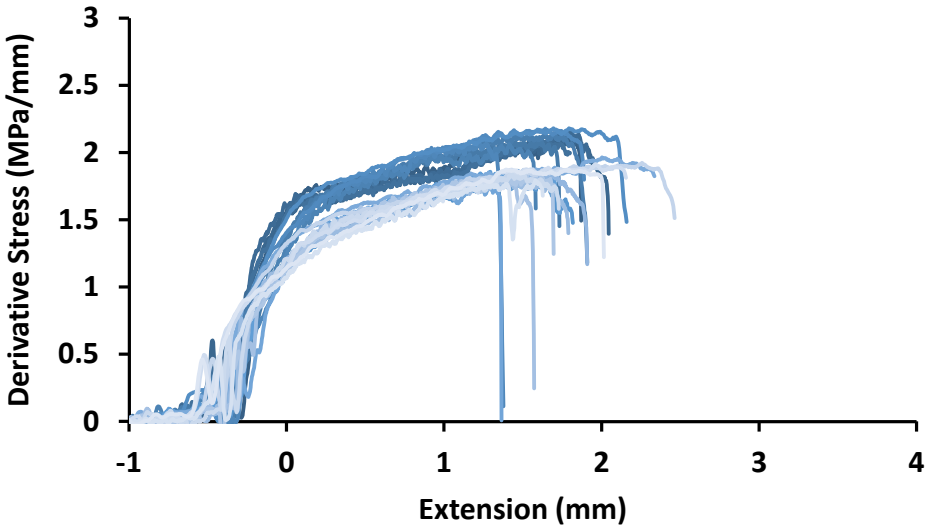

Figure 4.16 Derivative stress of pull-off adhesion experiments for bulk coating applied at 1 mil

HMo model coating applied to R panels, cured for two hours at 60 °C and one hour at 120 °C

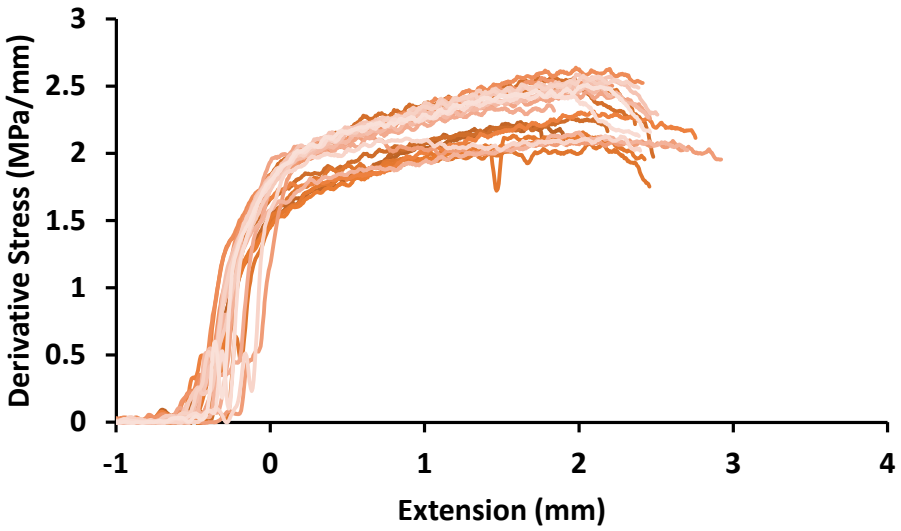

Figure 4.17 Derivative stress of pull-off adhesion experiments for 80% solid coating applied at 1 mil

Epoxy-amine applied to R panels, cured for two hours at 60 °C and one hour at 120 °C

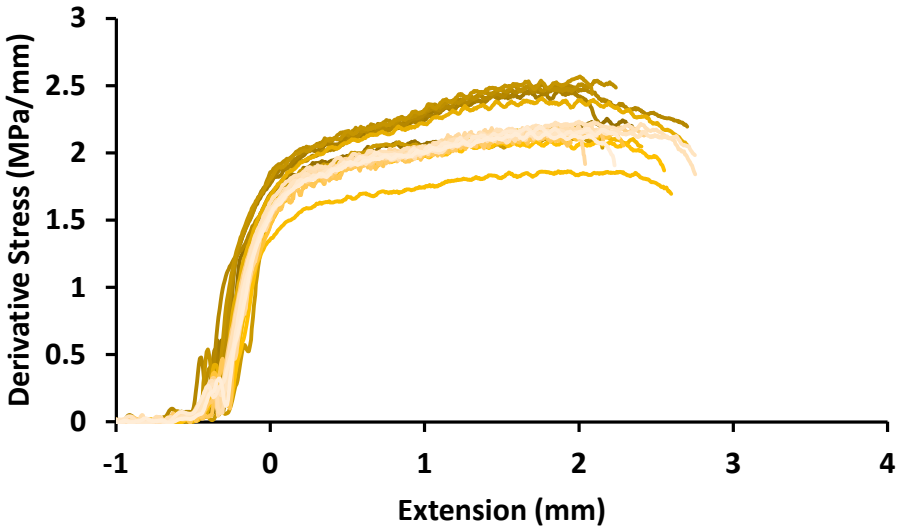

Figure 4.18 Derivative stress of pull-off adhesion experiments for 50% solids coating applied at 4 mil

HMo model coating applied to R panels, cured for two hours at 60 °C and one hour at 120 °C

In the 50% solid system specifically, applying 16 mil at low viscosity lead to a broad range of thicknesses within one data set, as shown in Figure 4.14, even though 80 µm was being targeted. Derivative stress-extension curves from the 16 mil applied

(shown in Figure 4.19) look nothing like low applied film thickness in Figure 4.16 - Figure 4.18 or the other high applied film thickness coatings (see Figure 4.20 and Figure 4.21 for bulk and 80% solids, respectively). The traces for 50% solid applied at 16 mil are rounded and curve downward and achieved much higher derivative values, around 9 MPa/mm. Bulk and 80% solid films applied at 6, and 8 mils respectively resulted in very brittle and low elongation pulls, which 50% solids was able to achieve, as seen in Figure 4.22, at much higher applied thicknesses (20 – 45 mils) but also reaching much greater derivative values (~5 MPa/mm)

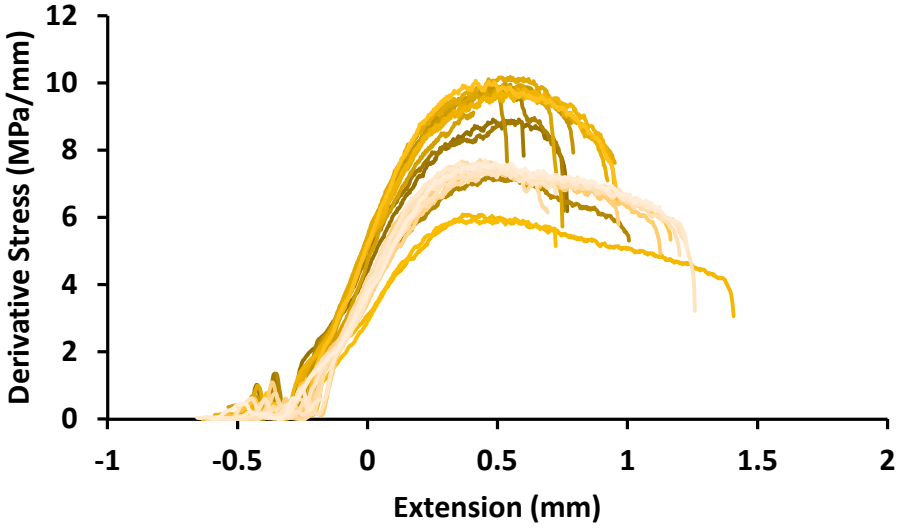

Figure 4.19 Derivative stress of pull-off adhesion experiments for 50% solids coating applied at 16 mil

Associated peak-stress versus thickness distribution in **Error! Reference source not found.**

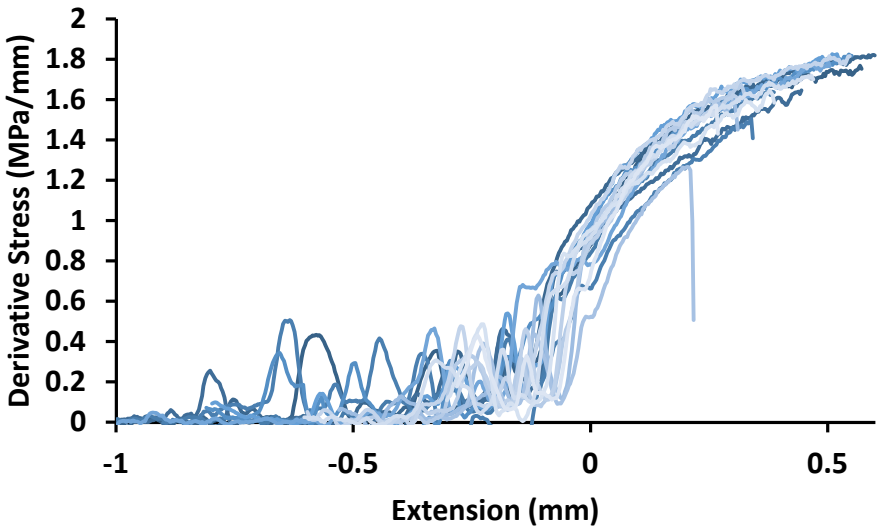

Figure 4.20 Derivative stress of pull-off adhesion experiments for bulk coating applied at 6 mil

HMo model coating applied to R panels, cured for two hours at 60 °C and one hour at 120 °C

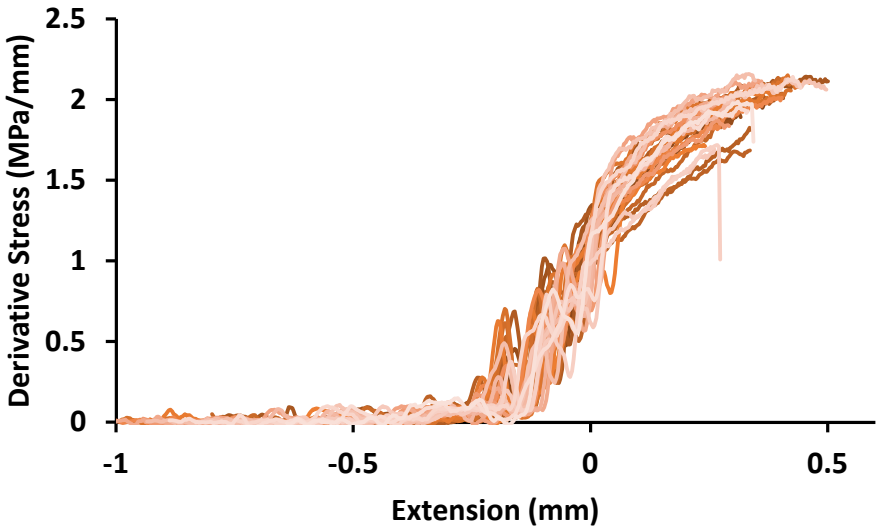

Figure 4.21 Derivative stress of pull-off adhesion experiments for 80% coating applied at 8 mil

HMo model coating applied to R panels, cured for two hours at 60 °C and one hour at 120 °C

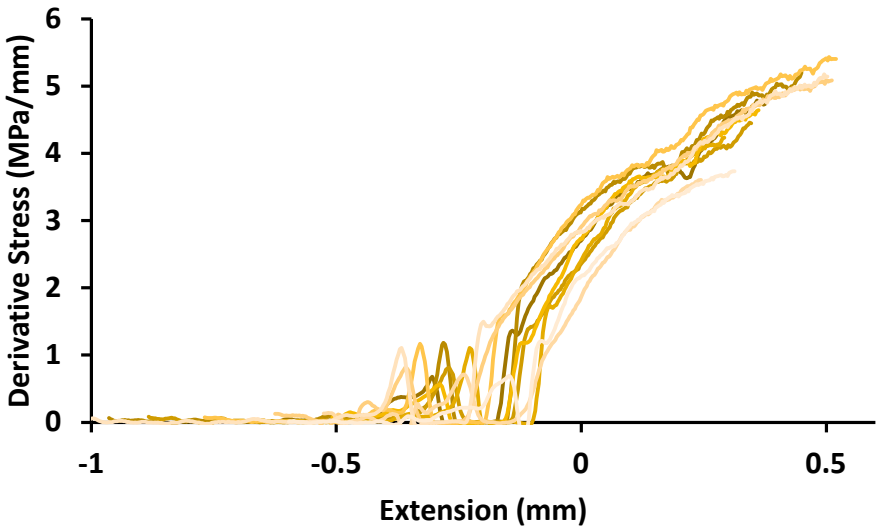

Figure 4.22 Derivative stress of pull-off adhesion experiments for 50% solid coating applied at 20, 25, 35, and 45 mil

HMo model coating applied to R panels, cured for two hours at 60 °C and one hour at 120 °C

The absolute thickness dictates the derivative shape more than the thickness in relation to the critical thickness. In coatings applied in bulk, there is no critical thickness, but the mechanical responses of the films are equivalent until yielding deformation modes are made readily available above the critical thickness, and therefore the short derivative curves seen in bulk at 100 µm in Figure 4.20 are mirrored by 80% solid in Figure 4.21 and 50% solid (Figure 4.22) from 100 to 300 µm even though the predicted critical thickness was around 65 µm.

4.3.3 Effect of coating material modulus on the relationship between film thickness and pull-off peak stress

Literature results presented in the introduction, including Figure 4.3, demonstrated the series of inconsistencies in the relationship between adhesion and thickness for different coating chemistries. Such contradictions are different from those presented in previous sections that required the addition of solvent to be realized.

Researchers who found a positive relationship between adhesion and thickness in bulk identify yielding as an explanation for the trend have yet to explore the phenomenon further. Until the present study, no attempts have been made to reconcile the differences between the systems and propose a material property-based explanation for the opposing responses. By performing pull-off adhesion testing on two coatings with vastly different moduli, the criteria for positive and negative relationships were established.

As seen in solvent-containing networks above the critical thickness, if yielding is induced prior to interfacial failure, then the thickness-peak stress relationship will be positive. Those criteria place requirements on both the bulk material and the interface. A negative relationship can result from a low modulus material if the interface is weak. The pull-off adhesion of a high modulus resin (HMo) with E = 2500 MPa and a low modulus resin (LMo) with E = 900 MPa were investigated over a wide range of thicknesses to understand the extent to which the adhesion relationship with thickness depends on modulus.

4.3.3.1 Bulk

Peak stress is predicted by Equation 4.1 to decrease with thickness as total internal stress increases. Figure 4.23 summarizes pull-off peak stress data of HMo and LMo networks applied in bulk onto QD panels and cured to a maximum temperature of 80 °C. Both HMo and LMo exhibited peak stress values that were thickness dependent, but the two resins have opposing relationships with thickness. Peak stress for HMo coatings decreased with thickness in a manner consistent with Equation 4.1, while LMo peak stress tripled from 2 to 6 MPa in the range between 40 to 450 μm.

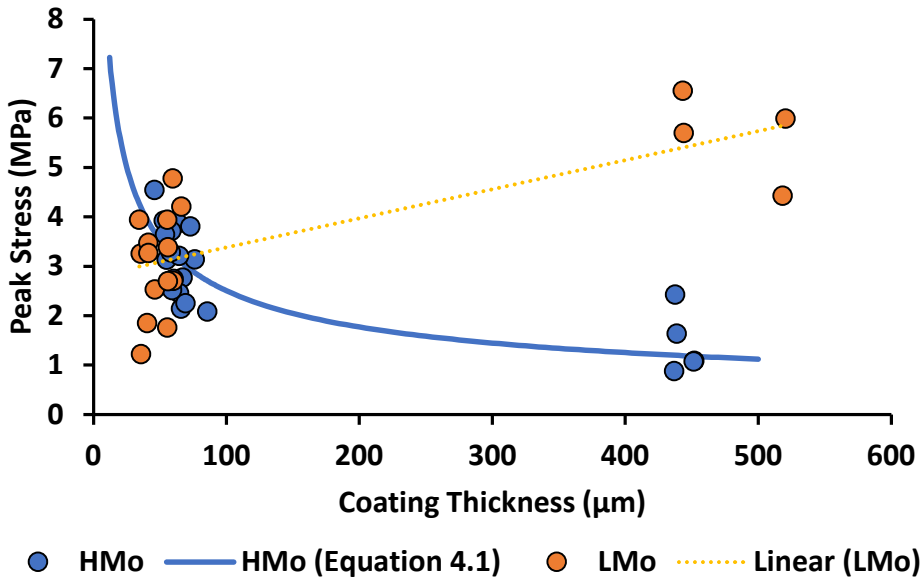

Figure 4.23 Pull-off adhesion peak stresses for high and low modulus epoxy networks.

Quantities used in fit: E=2500 MPa; σ=0 MPa; γ=0.059 N/m. HMo applied at 2, 3, and 30 mil, and LMo applied at 3 and 30 mil in bulk to QD panels. Coated panels cured for two hours at 60 °C and one hour at 80 °C. All dollies applied with ScotchWeld DP 460 and cured for 24 hours at ambient. Pull-off performed at 20 °C and a rate of 2 mm/min.

The model fit curve in Figure 4.23 represents the best fit of the peak stress values to Equation 4.1 and is the same data and fit as is reported in Figure 4.6. No attempts were made to fit peak stresses from LMo films because the relationships associated with the model are not applicable if adhesion increases with thickness. Examples of peak stress increasing with thickness have been reported in the literature,[32,75] but an exponential decrease of peak stress with thickness is the only response that has been described, explained, and modeled.[31]

Adhesion increases with thickness for LMo, which can be explained in the context of a critical plasticization threshold. There is a modulus threshold crossed between HMo and LMo that is analogous to the critical thickness in solvent-borne networks to make the adhesion-thickness relationship change. Unlike in previous sections, nothing needs to be added to LMo for yielding to be favored over adhesive

failure. The modulus of HMo at room temperature is high enough that in response to applied external forces, the load transfers through the material without deformation. Conversely, when forces are applied to LMo, it deforms easily. Literature can help support the theory of modulus being the critical parameter. Baek et al. and Roche et al. published examples of coatings that increase in pull-off peak stress with thickness and cite yielding as the reason.[32,75]

Peak pull-off stresses compiled from the literature for materials with moduli above and below that of LMo are compared in Figure 4.24. Modulus and T_g values of the materials plotted are in Table 4.4. Croll predicted the adhesion decay of poly(isobutyl methacrylate) (DuPont Elvacite 2045) coatings using Equation 4.1 over a thickness range of 100 - 300 µm. Polyisobutyl methacrylate has a T_g of 50 °C,[31] and while there are no reports of the modulus of Elvacite 2045 specifically, a PIBM sample with T_g = 47 °C showed a modulus of 1980 MPa, much greater than the modulus of LMo.[106] A literature example of a coating with a positive relationship between thickness and pull-off stress similar to LMo was shown by Baek and coworkers.[32] No information was reported about the ballast tank coating used in their study, but other sources list ballast tank coatings as having a T_g of 55 °C,[107] and Young's modulus of 190 MPa, much lower than LMo.[108,109]

Table 4.4 Comparison of HMo and LMo properties with literature coatings that exemplify positive and negative relationships with the thickness

[a]Pull off data for ballast tank coating from Baek.[2] [b]Ballast tank coating T_g was measured by Paik and Thayamballi.[7] [c]Ballast tank Young's modulus determined by Ringberg.[8,9] [d]Pull-off data collected for PIBM is reported by Croll using Elvacite 2045, which has a T_g reported in its technical data sheet.[6] [e]Modulus of PIBM measured by Torres and coworkers.[10]

Material	T_g (°C)	Young's Modulus (MPa)
Ballast Tank Coating[a]	55[b]	190[c]
LMo	44	900
PIBM[d]	50	1980[e]
HMo	80	2500

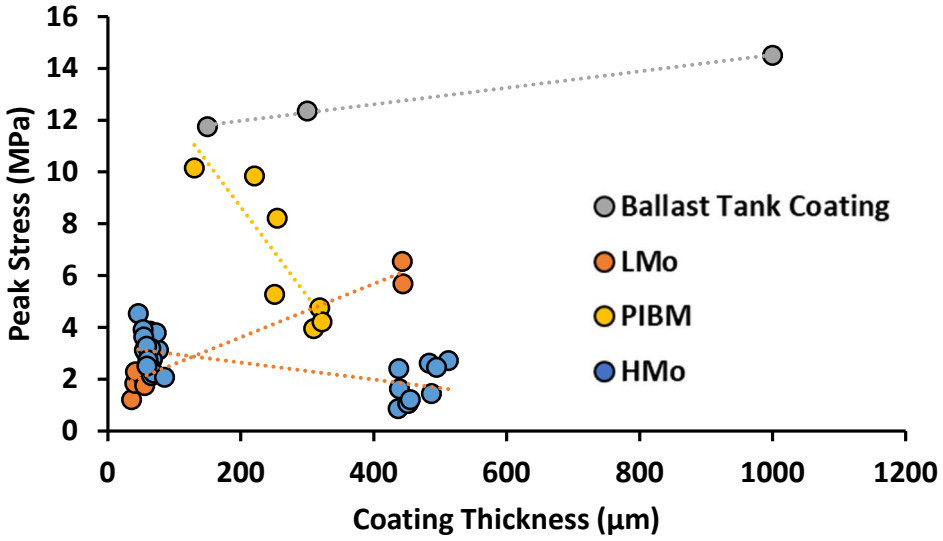

Figure 4.24 Comparison of pull-off stress as a function of thickness

Ballast tank coating data extracted from Baek and coworkers[2] and PIBM data replotted from Croll[6]

A correlation between modulus and thickness response can be made from the literature and present experimental data. The thickness response of the ballast tank coating with a modulus of 190 MPa is positive, with high peak stress values at all thicknesses. Increasing to a modulus value of 900 MPa for LMo maintains the positive response to thickness, the peak stress values are lower for LMo than the ballast tank

coating, but I don't think this can necessarily be attributed entirely to the modulus change. The next highest modulus material is PIBM with twice the stiffness of LMo (1980 MPa), and the predicted decrease in peak stress with thickness is achieved. Finally, HMo with 2500 MPa Young's modulus also decreases in peak stress with thickness.

Identifying modulus as the driving force of the adhesion-thickness relationship inversion can be supported with stress-strain and derivative stress-strain curves corresponding to the pull-offs. Literature suggests yielding is a key factor, but it has yet to be isolated and proven. Four representative pull-off experiments have been isolated for comparison to understand what mechanical mechanistic differences there are between coatings of high and low moduli in response to external stress at high and low thickness. Figure 4.25 includes the stress-strain and derivative stress-strain responses of HMo and LMo at high and low thicknesses. Derivative stress-strain of HMo at both thicknesses show a predominantly linear elastic response, a high derivative value is reached, and before yielding can take place, failure occurs. There is a slight increase in the derivative value with increased thickness, and that is consistent between HMo and LMo. Low thickness HMo and LMo are very similar in their peak derivative stress, but the peak stress is closer to that of the high thickness HMo.

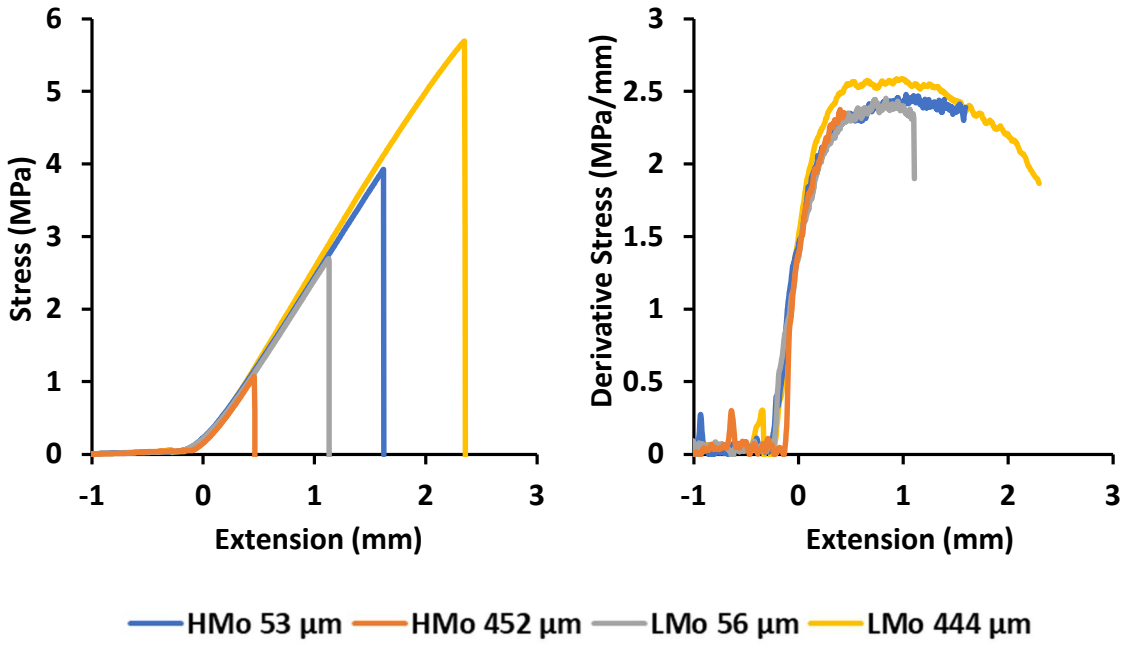

Figure 4.25 Comparison of the mechanical responses of HMo and LMo systems applied in bulk at high and low thickness

Model coatings applied to QD panels. Coated panels cured for two hours at 60 °C and one hour at 80 °C. All dollies applied with ScotchWeld DP 460 and cured for 24 hours at ambient. Pull-off performed at 20 °C and a rate of 2 mm/min.

In low thickness samples, the yielding of LMo films is already apparent. At high and low thickness, LMo decreases in slope prior to failure. Curves of LMo derivative stress-strain can be analyzed in three regions 1) elastic, where slope increases to a maximum 2) yielding, indicated by a gradual decrease in slope, and 3) peeling, where the derivative values decrease more rapidly. The process of yielding involves molecules sliding past each other, keeping stress from increasing as quickly. Differences between LMo and HMo in crosslink density and cohesive forces result in plastic deformation at lower stresses in LMo.

A new relaxation mechanism in LMo is indicated by a change in the direction of derivative curves at extension = 1.04 mm for low thickness and 2.2 for high thickness. Based on the dependence of the onset strain on thickness, the new relaxation mode is

ascribed to partial peeling of the coating prior to the catastrophic failure. The force acting in the x-y plane due to material contraction as the coating extends in the z increases more rapidly in thin films, causing the peeling in thick films to happen at higher strain.

Pull-off peak stress data of materials with high and low modulus demonstrate opposing relationships with thickness. The high modulus coating experienced a decrease in peak stress with thickness as predicted in the literature despite having no calculable internal stress. When coating modulus is low, there is an increase in peak stress with thickness as yielding and contraction in the transverse direction is made more available with thickness. The decrease in peak stress with thickness for high modulus materials is exponential, while the increase for low modulus materials is linear.

4.3.3.2 Solvent-borne (80% solids)

Solvent-borne coatings respond to increasing thickness differently than those applied in bulk. Experimental results for HMo and LMo coatings applied at 80% solids along with a fit of a subset of HMo to Equation 4.1 are shown in Figure 4.26. Both materials' responses are different from what is seen in bulk. In the presence of solvents, neither the peak stress of HMo nor LMo decrease consistently with thickness. In bulk, the best fit curve of HMo indicated peak stress decayed rapidly at low thicknesses and then decreased unperceptively with thickness in the plateau region until a theoretical spontaneous delamination thickness. The solvent-based films of HMo resulted in decreasing peak stress in the thickness range below 75 μm, which can be fit by a model curve. Above 75 μm, however, all thickness increases are accompanied by an increase in pull-off stress.

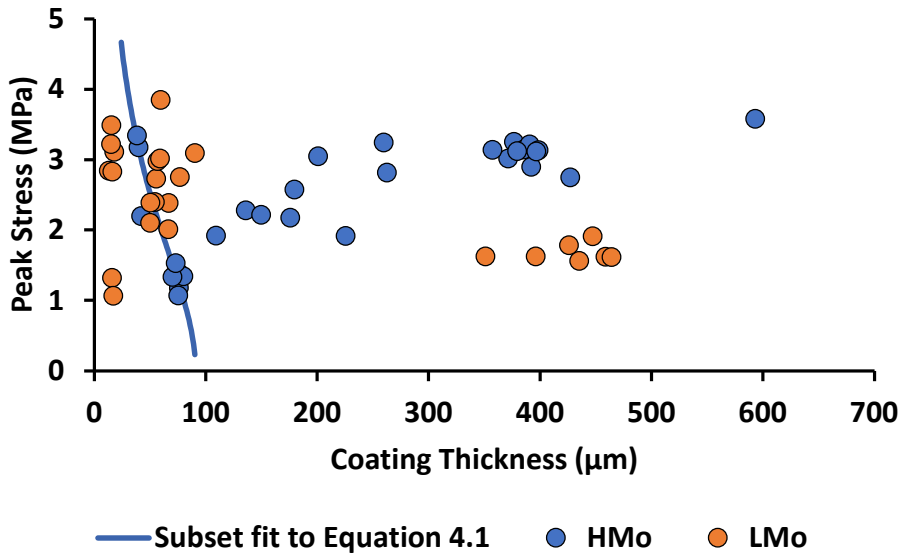

Figure 4.26 Comparison of pull-off adhesion peak stresses as a function of thickness for HMo and LMo applied at 80% solids

Equation 4.1 fitted to HMo samples below critical thickness. Solvent blend: 1:1 by weight ethanol to DPnP. Model coatings applied to QD-panels and subsequently cured for two hours at 60 °C and one hour at 80 °C. All dollies applied with ScotchWeld DP 460 and cured for 24 hours at ambient. Pull-off performed at 20 °C and a rate of 2 mm/min

Fitting the model to peak stresses below 75 µm and calculating internal stress makes several assumptions but retains validity. Solvent trapping is seen to occur at all thicknesses in Figure 4.10, indicating the modulus is changing in the sub-75 µm range. The residual solvent content is found to be 5.55 and 6.05 wt% the minimum and maximum thickness within this range (38 and 75 µm respectively) extrapolating the trendline associated with 80 wt% solid films cured at 80 °C to Assuming in the low thickness range that the only remaining solvent is DPnP then T_g can be estimated by the Fox relationship (Equation 4.3). Glass transition temperature of the solvent is estimated using the equation found by Fedors and rearranged in Equation 4.4.[110] Applying the equations in tandem results in a film T_g of 39 °C at 38 µm and 36 °C at 75 µm. Predicted T_gs are at least 40 °C lower than the bulk resin, which, based on findings in Chapter II,

would assume a decrease in adhesion as T_g continues to approach room temperature. Internal stress appeared to dominate in the region below the critical thickness and was calculated to be 1.75 MPa, much larger than the 0 predicted in bulk.

$$\frac{1}{T_g} = \frac{w_{polymer}}{T_{g,polymer}} + \frac{w_{solvent}}{T_{g,solvent}} \quad \text{Equation 4.3}$$

$$T_{g,solvent} = \left(\frac{T_m + T_b}{rT}\right) - T_b \quad \text{Equation 4.4}$$

Calculated T_gs are not necessarily representative of the modulus response of HMo films containing trapped solvent. Residual solvent contents for HMo over a range of thicknesses with maximum cure temperatures of either 80 °C or 120 °C are reported in Figure 4.10. In the control system without solvent, the volatile content remained constant over all thicknesses and for both cure temperatures. Weight percent residual solvent increases linearly throughout the experimental thickness range for 80 and 50% solids. Similar to the LMo response to thickness changes in bulk shown in Figure 4.23 and literature data in Figure 4.24, decreasing modulus correlates with inverting the adhesion-thickness relationship. Unlike previous figures, in Figure 4.26, the modulus is also a function of thickness, and the inversion happens at a critical thickness.

To further understand the HMo adhesion response to the thickness in the presence of solvents, the derivative stress of 80% solid HMo, below, at, and above the critical thickness is plotted alongside the derivative stress of bulk LMo, in Figure 4.27. Derivative stress curves were used to establish a mechanical explanation for the residual solvent effects on adhesion response to thickness. Both LMo in bulk and HMo in 80% solid achieve high peak stresses at a high thickness that would not be predicted by the model. Derivative stress traces of 80% solid HMo at 38 and 77 μm in Figure 4.27 are

consistent with those found for bulk HMo in Figure 4.25. At low thickness, a maximum derivative value is reached and held (or slowly decreased due to flexing of the substrate and/or cross-plate), and higher thickness films follow the same path but end at lower strains. In 80% solids, the added thickness sees a transition of HMo derivative traces to be more reminiscent of LTg in bulk at high thicknesses, a prominent peak derivative value, a more rapid decline in derivative value, followed by slow peeling failure. High strains were achieved at high thicknesses by yielding after reaching the maximum derivative stress. The maximum derivative stress value achieved for high thickness coatings of 80% solid HMo is much lower than the rest in Figure 4.27, which is consistent with the level of residual solvent at that thickness.

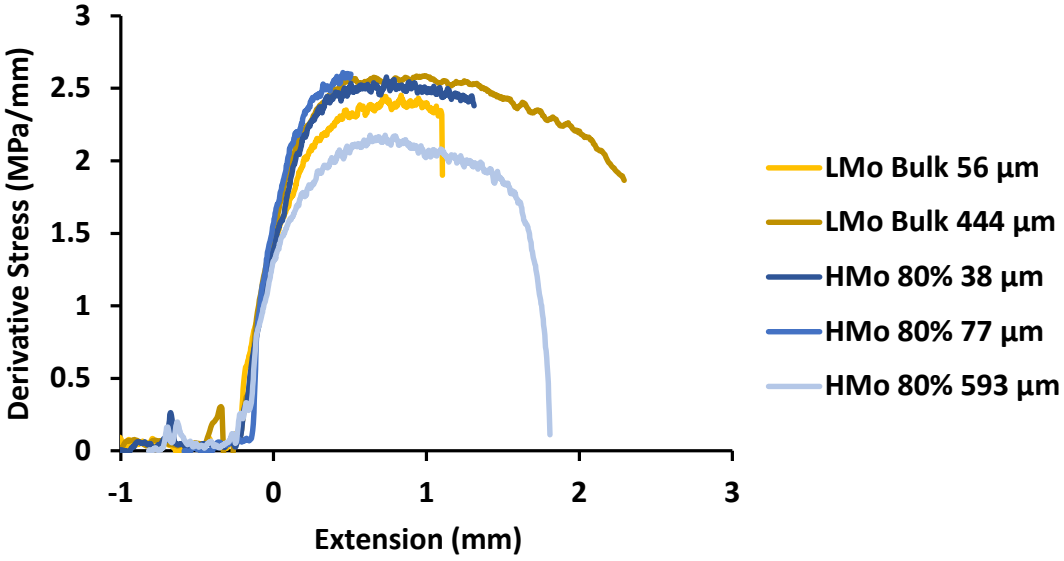

Figure 4.27 Derivative stress responses of HMo applied at 80% solids, and LMo applied in bulk to compare two systems that increase in pull-off peak stress with the thickness

Model coatings applied to QD panels and cured for two hours at 60 °C and one hour at 80 °C.

The addition of solvents causes LMo to lose its positive relationship with thickness. Considering the relationship between modulus and the adhesion-thickness relationship found in literature and the present study, further decreasing the modulus with

solvent was expected to maintain a positive relationship. If lower modulus means a stronger positive relationship with thickness, then the effect should have been stronger. Adding solvent lowers the modulus unambiguously and allows for more yielding modes, but in this case, now the interface suffers. Results from Chapter II suggest added interfacial mobility only increases adhesion to a point. The addition of solvent and further increasing segmental motion at the interface meant adhesion would no longer increase with thickness.

Solvent damage to the interface can be seen in Figure 4.28. Examining the derivative stress of high thickness bulk and high thickness films of 80% solid LMo may explain why plasticization leads to decreased adhesion. The addition of solvents led to reduced derivative value from 2.4 to 1.6 MPa/mm, and drastically different curve shapes at the point of failure. Reduction in the maximum achieved derivative value happened to HMo at high thicknesses in the presence of solvent (Figure 4.27), but the resulting peak stress was greater than achieved for the higher derivative value experiment, and therefore a reduced slope cannot account for reduced adhesion. Stress-extension is presented alongside the derivative curves in Figure 4.28 for better visualization of the failure process. The two thicknesses of 80% solid LMo overlap well until a very gradual failure occurs in the high thickness system. In this case, the locally rubbery material lacked the cohesion to induce failure all at once. Stress is concentrated on the edges (as modeled by Turunen[30]), where it failed first, and due to the high flexibility, the edges failed separately from the rest of the area, which slowly peeled toward the center. Peeling failure indicates both the pliability of the film but also the weakness of the interface supporting the segmental mobility claim from Chapter II. Short-range mobility that was advantageous

for assuming a thermodynamically favored position became detrimental as chains gain the mobility to turn around and associate cohesively instead.

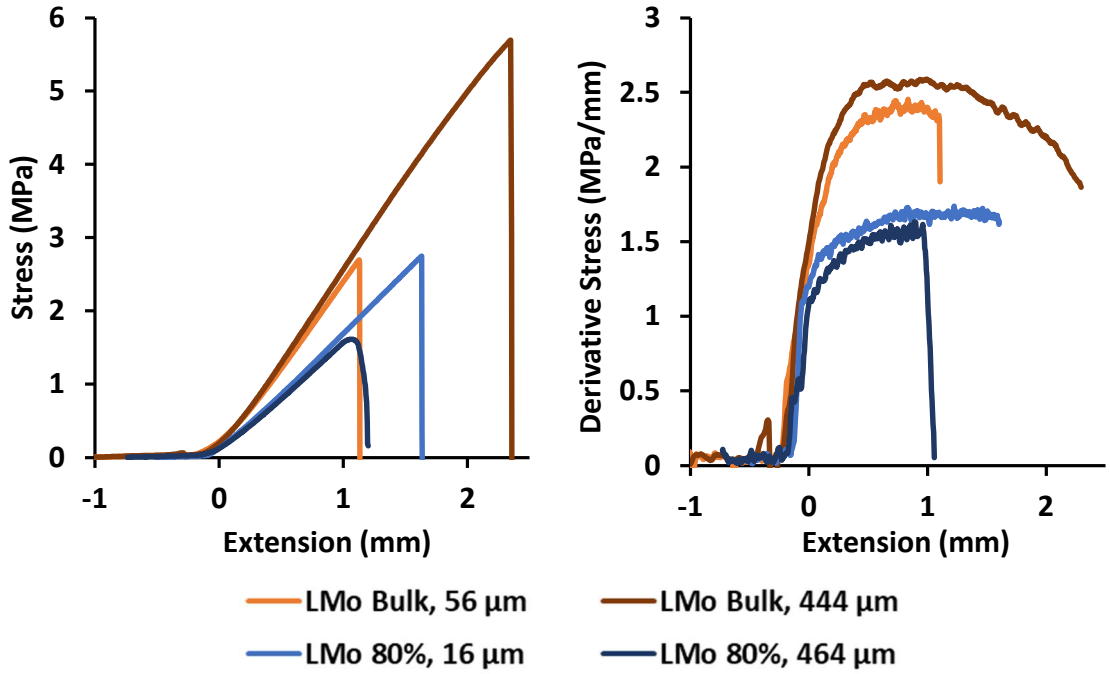

Figure 4.28 Stress response of LMo in bulk and 80% solvent at high and low thickness

Differences in mechanical response to understand the effects that solvent trapping has on LMo. Model coatings applied to QD panels and cured for two hours at 60 °C and one hour at 80 °C.

Another parallel between thermal and solvent plasticization and reduction in adhesion is how solvent disrupts interactions between polymer chains and substrate functionality. Additional thermal energy increases mobility and makes the secondary interactions required for adhesion less favorable, reducing the extent of sorption.[111] Solvent distribution through the film was anisotropic as a result of the directionality of solvent loss. If a solvent can only leave the coating through the air interface and that region vitrified first, then the highest solvent concentration will be at the substrate interface, lowering the work of adhesion. By the same mechanism that solvent induces

plasticization in bulk coatings, it causes solvolysis at the interface.[112] The extent that residual solvent interferes with interfacial interactions affecting pull-off adhesion is likely to be a function of the chemistry of the solvent, the coating, and the mobility of the chains at the substrate interface. The peak stress of HMo above the critical thickness was shown to decrease in slope with increasing thickness in a logarithmic fashion, supporting either solvent accumulation at the substrate-interface and the detrimental levels of interfacial chain mobility.

Pull-off adhesion results establish a modulus dependence of the relationship between adhesion and thickness. No prior attempts had been made to understand the scenarios where adhesion increased with the thickness or how they compared to the energy balance based models for the adhesion thickness relationship established by Kendall and Croll.[31,95] When modulus is low, there are multiple yielding mechanisms available, allowing the film to withstand higher strains. How this increased resistance to separation transfers to coating longevity and performance is unknown. Molecular events and stimuli that initiate interfacial cracks are expected to correlate with adhesion measured by this method, but corrosion protection could not be predicted by pull-off alone. Solvent plasticization induced the chain mobility-based events described in chapter 2. As interfacial solvent plasticization occurred, HMo gained short-range motion inverting the typically negative adhesion thickness relationship to positive above a critical thickness. Conversely, LTg, which had a low enough modulus to have a positive relationship with thickness in bulk, did not benefit from solvent plasticization. Long-range mobility and solvolysis in high thickness LTg coatings with solvent greatly lowered work of adhesion. Stress-strain curves produced during the pull-off adhesion

experiments and their derivatives were used in the method described in Chapter 3 to better understand the mechanics behind the response of each film. A possible use for the increase in adhesion with thickness in HMo that is a result of plasticization by the residual solvent is eliminating the spontaneous delamination thickness.

4.4 Conclusions

The goal of this work was to 1) understand how the relationship between adhesion and modulus supersedes the thickness-adhesion relationship dictated by coating internal stress, 2) explore how solvent affects these relationships, and 3) to describe the use of pull-off adhesion stress-strain and derivative stress-strain curves to identify mechanical processes occurring during testing. Pull-off peak stress data on coatings with high and low T_gs (HMo and LMo) ultimately showed that a high modulus is a requirement for a negative relationship between pull-off peak stress with coating thickness that is described in the literature. Low modulus coatings experience multiple yielding mechanisms during a pull-off test allowing high peak stresses to be achieved at high thicknesses, in contradiction to prediction.

The addition of solvents caused a change in the thickness response for high and low modulus coatings. HMo transitioned from showing a predictable decrease in peak stress with respect to film thickness in bulk to exhibiting a relationship inversion at a critical thickness in solvent-borne coatings. Above the critical thickness, peak-stress increases with thickness, eliminating the spontaneous delamination thickness. TGA revealed a linear increase in concentrations of trapped solvent with film thickness. The solvent reduces film modulus, suggesting the critical thickness indicates the thickness where enough solvent is trapped to achieve the critical modulus required to change the

adhesion-thickness relationship. Furthermore, derivative pull-off stress-strain curves support the increase in adhesion, clearly showing yielding regions as trapped solvent increases.

Increasing the cure temperature of HMo had significant impacts on the adhesion thickness response with and without solvent. Bulk HMo cured at 120 °C demonstrated increased internal stress compared to bulk HMo cured at 80 °C. At 80% solid HMo cured at 120 °C had higher critical thickness, increasing to 100 μm from 75 μm when cured at a maximum temperature of 80 °C. Fits to the data below the critical thickness resulted in internal stresses much greater than either system in bulk, potentially due to the volume loss gradient that forms between the interfaces from anisotropic solvent loss and vitrification of the surface. Internal stress is lower and critical thickness is higher for 120 °C cured films because of the reduction in trapped solvent per unit thickness.

Another important finding was the consistency between results found in thermal and solvent plasticization with respect to adhesion. Elevated test temperatures in chapter 2 revealed that peak adhesion is achieved at T_g-20 °C. In pull-off adhesion experiments, HMo increases in peak stress with the addition of solvent above the critical temperature, indicating advantageous increases to local chain motion. For LMo, the addition of solvent causes both solvolysis and long-range mobility driving functional groups away from the substrate surface. Therefore, a positive relationship with thickness was seen in bulk, but not in 80% solid coatings. This finding is not only important to consider alongside a coating's desired application but also explains how as a coatings scientist adjusts formulation variables to match end application requirements, those variables that

impact the system's T_g often exhibit dramatic variability in adhesion results and continue to be difficult to compare or understand on a molecular or system basis.

CHAPTER V – SUMMARY AND FUTURE WORK

This dissertation was organized to gain an understanding of how adhesion of polymer-based coating was attained, retained, and eventually lost during material utilization. Our research was motivated by the need to understand useful relationships between polymer building block molecular design, polymer properties, and results gathered from mechanical methods of measuring coating adhesion. The conventional adhesion measurement method was one of the greatest challenges with current coating science use, design, and future materials utilization. Mechanical adhesion testing methods were most appealing as *in situ* testing on full-scale coating-substrate systems and the series of quantitative results generated by the methods. Often, the scope of such methods has been limited by the end user's capabilities, shallow experimental design methodologies, and data analysis practices. Novel approaches to mechanical testing of adhesion investigated herein provide and establish the basis for logical connections between coating adhesion testing and interfacial investigations of material properties and adhesion versus practical variables that were shown to be critical with qualitative measurements.

A specific, established limitation of mechanical methods of testing adhesion was that the applied coating's mechanical properties grossly affected numerical adhesion results. Applying mechanical force to the coating inherently engages mechanical responses dictated by bulk coating mechanical properties, such as stiffness, which then defines test results. Mechanical adhesion results are a function of a combination of polymer-substrate interfacial properties and bulk polymer properties. Chapter II summarized the results collected from 90° peel tests with an emphasis on discerning

between the influence of polymer/coating interfacial and bulk phenomena dictating measured peel adhesion performance. Results were obtained using model coatings characterized by a novel technique designed to mitigate the influence of polymer physical state on the adhesion data collected. The method entailed using an adjusted temperature profile test range with reference to each polymer network's glass transition temperature. Peel forces measured at constant temperature relative to T_g were compared with testing performed at consistent ambient temperatures to add practical context and reference for each materials' adhesion.

The model amorphous glassy thermoset polymeric materials were as similar as possible with respect to molecular building blocks and yet designed to vary in final bulk, dry glass transition temperature. The T_g was originally thought to be the primary factor influencing modulus and thereby peel force of the materials at any given temperature. By performing 90° peel adhesion tests at T_g normalized test conditions (i.e., a constant temperature below each polymer network's T_g), T_g-20 °C, for example, the thermal conditions were adjusted so that each polymeric material possessed the closest possible and most comparable bulk physical state. Therefore, the peel force differences were more directly a measure of the polymer-substrate interactions and chemically driven relative modulus differences.

In addition to our glass transition temperature centered testing framework, a common trend was observed. A local peel force maximum arising at T_g-20 °C was observed in the present study on three amorphous crosslinked epoxy-amine polymer networks with fully cured T_gs ranging from 44 to 80 °C, and literature results from thermoplastic vinyl polymer blends, suggesting a possibly universal phenomenon. The

previous literature study could not explain the local maximum, only the increase approaching the critical temperature. While the relative temperatures remained constant, the absolute values of peel adhesion varied from 4.77 N/cm to 6.56 N/cm in the current dissertation work.

Our research efforts combined with scant literature supported that an increase in adhesion culminates in a local peak adhesion as each coating system approaches their respective temperature of T_g-20 °C, and these consistent results were attributed to a balance between short-range chain mobility in the glassy state and leathery mobilized and sticky polymer chains. The data suggests that the population of mobile network fragments is different for each resin system at the critical temperature even though 'segmental motion' is the same criteria for the glass transition in all cases. Our hypothesis was that peak adhesion, measured as the resistance to 90° peel from the substrate, occurs for each polymer-substrate combination at a mechano-interfacial transition between elastic failure and ductile failure. The magnitude of peel force at the peak temperature correlated with calculated percent mobile chains. Calculations of the percentage of polymer chains in the higher mobility physical state were performed by integrating the area under the DMA Tan δ curve. The middle T_g resin achieved the highest peel force with an estimated 13.4% of chains in the leathery state and provided the highest resistance to deformation, while the lowest peak peel force resulted from the high T_g material with 6.9% calculated mobile chain fraction. We expect that the phenomenon of an average number of polymer chains, albeit not the same polymer, are mobilized at any given moment, and therefore the balance between immobilized and

mobilized polymer chains shifts in spatial and temporal terms to facilitate the greatest combination of mechanical resistance of removal from the substrate.

Considering the subtle differences in resin chemistry can explain the differences in peak peel force. The high concentration of epoxy trimer in the high T_g system requires that these fragments be participating in some of the local conformational motion prior to the glass transition. However, in the lowest T_g network, there is enough polyether amine that segmental motion is induced without requiring that the epoxy trimers become flexible. Variations in the mobile population are the underlying cause of differences in modulus, energy dissipation, and mechanical responses before failure at the same temperature relative to T_g. Network topology and composition also dictate the percentage of mobile chains required for segmental motion. The model coating, which achieved the greatest peel force, possessed the largest percentage of mobile chains at the critical temperature.

These results have broad implications as materials performance for all systems was shown to be directly dependent upon an identical thermally adjusted balance of ratios between glassy and leathery physical states, regardless of the absolute adhesion. The added degrees of freedom for polymer building blocks and higher polarity functional groups increases the total number of polymer-substrate interfacial interactions and thereby increased the measured resistance to peel. Increases in peel force with temperature were despite the reduced favorability of polymer sorption as temperature rises for any given system.

Analyzing mechanically measured adhesion through a mechanical property lens also identified a morphology transition between the resins. How the networks form and

ultimately soften is key to understanding the mechanical and, by extension, the adhesion results. Epoxy-amine networks cure into a heterogeneous system of interconnected domains. Within the domains, crosslinking is high, and the domains are more loosely connected. The sequential modifications to the network composition ultimately lead to a difference in morphology. The difference in morphology was identified as a break in the trend between modulus at peak adhesion temperature. For a theoretical example, between the concentrations of ED-600 used in the moderate T_g material to the low T_g material, there is a transition, and the domains switch from being connected by ED-600 to Epon 825 trimer, which makes the inter-domain connections much stronger and can explain the high modulus of the low T_g material compared to the other two which seem to respond similarly but at different temperatures. Another effect of the network topology is the level of flexibility of the mobile fraction of the network. The high concentration of Epon 825 trimers in the high T_g material is what drives the T_g but therefore required a high absolute temperature to reach T_g-20 °C and suggested the ED-600 network fragments are highly energetic and the domains are loose, lowering modulus and peel force.

The relationships between mobility, sorption, and temperature remain true above T_g-20 °C; however, as the percentage of higher mobility polymer chains increases, the results facilitated more facile removal from a given substrate. In the high modulus glassy state, short-range motions of network fragments are possible. Increasing temperature promotes local network regions to the rubbery state, and because the cohesive interactions within a polymer seem to be consistently more thermodynamically favorable, temperatures above T_g-20 °C allowed interfacial groups the mobility to abandon

heterogeneous interactions with the substrate in favor of homogeneous interactions with more compatible organic functional groups. When the thermal energy is available to provide mobility and reorganization of the functional groups (defined as those groups interacting most energetically with the substrate and, therefore, more important for a given system's overall resistance to loss of adhesion) to fold the functional groups inward and adhesion is lost. Peak adhesion temperature is also accompanied by a mechanical change. In practice for 90° peel adhesion measurements the, practical work of adhesion value dictates the peel strength, but the work of adhesion employed in predictive equations is not simply a difference in surface energies. Practical work of adhesion or adhesive energy is known to be a function of many other variables; modulus, heat of fluidity, heat of sorption, and, most importantly, viscoelastic work at break. Data present in the literature indicated a similar peak in peel adhesion upon a critical concentration of plasticizing polymer, which is analogous to the temperature increase, and it corresponded to viscoelastic work and a transition between brittle interfacial failure during peel and a fibrillar type failure. The molecular changes between local and segmental motions are hypothesized to be the underlying cause of the transition. The practical work of adhesion is a function of modulus and the previously mentioned sorption and chain fluidity. Increasing temperature up to T_g-20 °C sees an increase in adhesion despite modulus loss, interfacial gains are greater than bulk losses, but above T_g-20 °C, bulk forces dominate as modulus decreases much more rapidly. It is imperative to place the results in the context of the most common testing results. If we view the results shown in Figure 5.1, it is clear that most polymeric materials are tested by labs, quality control during production with large variations in temperature. The reality is that most materials will continue to be

utilized across a wide variety of temperatures. Our results and the reality of polymeric materials use requires, at a minimum, that every adhesion testing protocol have a specified temperature range of testing to mimic material utilization. Then adhesion results become more of a performance map that defines the high and low limits for each application. In reality, processes will most likely not be adapted. Albeit important to understanding the adhesion for each material combination the 1.8x to 2.8x differential in peel force adhesion results across 15 °C, it was clarifying to see how even a small variation in thermal conditions for measuring adhesion result in dramatic peel values. Glass transition temperatures are not normally direct design criteria; however, material performance balancing is usually a driver for each formulation variable, and it is critical to account for the differences in adhesion over even small ranges of temperature. Adding variables like the degree of cure, amount of trapped residual solvent, and the environmental conditions (e.g., differences in material performance with low, medium, and high relative humidity as a result of hydroplasticization) to the scientific approach enhances the power of performance predictions.

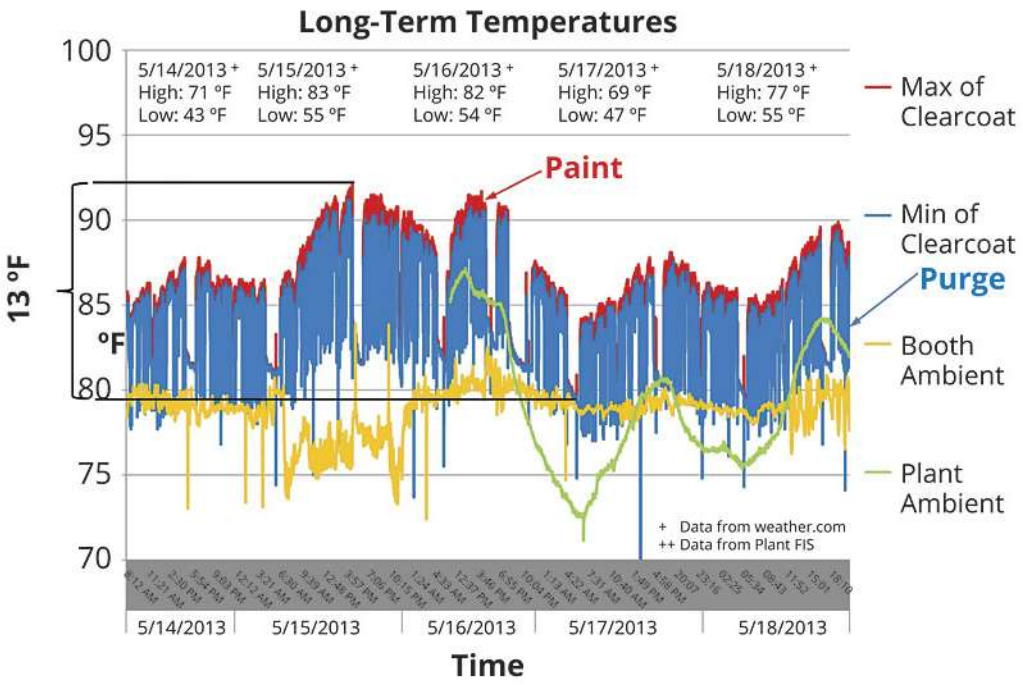

Figure 5.1 Temperatures experienced by a paint film in a plant and during spraying in a spray booth

Temperature controlled booth. Figure from Bonner.[113]

Furthermore, in Chapter III and Chapter IV, we utilized the pull-off adhesion mechanical method and the results confirmed numerical and statistical pathways to reduce inherent adhesion characterization noise and gain an understanding of material results. The characterization and analysis methods we developed allowed us to explore a wider set of adhesion-dependent performance variables, thickness, plasticization, and solvent trapping, and an interdependent internal stress result. Measured adhesion confidence was established by systematically evaluating pull-off adhesion testing variables such as the adhesive and the scoring method. Incorporation of the modifications into pull-off practice allowed for relationships to be visualized and conclusions to be developed. Chapter III presents a method of analyzing pull-off adhesion stress-strain curves to validate individual results as meaningful and diagnose

problems created during sample preparation or in the pull-off testing process. For example, when the slope of the stress-strain curve shifted versus sample replicates, the different slopes (different from samples without scoring or damage) consistently represented coating damage occurring during sample preparation. Also woven into the results were the detection of different yielding mechanisms with some possibility for physical state dependence as shown in Chapter II, however, with testing rate relative to relaxation rate implications and yet the detection of differences in material internal stress as well. Each of these variables is relevant and provided greater insight and lower noise than the common single values as most often measured as only peak pull-off stress. Using the new method of data analysis, the ideal coating topside adhesive for pull-off applications was definable. The implications and optimization for each possible scoring method were determined and resulted from noise minimization through the repeated testing results.

Albeit a common practice, the poorly defined literature and testing protocol for scoring around dollies used for pull-off adhesion were more controversial than understood at the onset of the research. We established that each scoring method resulted in different degrees of interfacial damage often caused by the different scoring processes. In addition to demonstrating the important effects that different techniques/methods of scoring had on the samples through the derivative stress-extension curves, the definitive importance of scoring was quantified in Chapter III. Optical microscopy observations included analyzing the failure surfaces from pull-off experiments on a high thickness coating presented a direct relationship between pull-off peak stress and cohesive perimeter failure. By driving the propagating crack to go through the coating thickness

with incomplete scoring, the peak stress value was consistently overestimated and considered misleading. The absolute stress requirements for crack propagation are much lower than crack initiation, and the scoring process, when properly applied, was shown to be a method that cleanly separates the test area from the surrounding coating without producing any initiating cracks in the test area. A Dremel rotary tool with a tapered carbide tip (Figure 5.2) was chosen for its precision in isolating the exact area underneath the dolly and consistently achieving complete separation of the area from the remainder of the coating.

Figure 5.2 Dremel rotary tool model 395 and tapered point carbide tip

Analysis of derivative stress-strain curves and determination of a scoring method was aided by fitting peak stress data to a predictive model. Historical literature communicated that pull-off peak stress should decrease in a predictable manner with increasing coating film thickness without any other influential variables. The model accuracy at predicting adhesion values based upon physics principles (a balance between substrate and polymer bulk modulus, interfacial adhesion, and internal stress) also further supported the effectiveness of the scoring method. This approach was also used in Chapter IV to back-calculate internal stress (σ) and work of adhesion (γ) of coatings by

fitting peak stress to Equation 5.1. Finding the parameter values that, when applied in the model, lead to the closest fit based on the smallest sum of residuals (Equation 5.2) was an effective method for calculating material properties that were cumbersome or difficult to measure.

$$\sigma_z = \sqrt{\frac{4.286E\gamma}{t_c} - 2.572\sigma^2} \qquad \text{Equation 5.1}$$

$$\text{Residual} = \sqrt{\left(t_{c.exp} - t_{c.cal}\right)^2 + \left(\sigma_{z.exp} - \sigma_{z.cal}\right)^2} \qquad \text{Equation 5.2}$$

Chapter IV focused on testing and describing the validity and limitations of the internal stress-driven relationship between pull-off peak stress and thickness shown in Equation 5.1. Tools for coating adhesion prediction are rare, and therefore, it was surprising that Equation 5.1 was not being applied to lifetime prediction methods more often. Unfortunately, as was found in Chapter IV, the scope of Equation 5.1 is limited, and rules for when and how to apply the predictive equation had never been established. The predictive capabilities of Equation 5.1 for determining peak stress at a given thickness hinge on internal stress driving pull-off peak stress to exponentially lower values with increasing thickness. Unfortunately, several other literature sources demonstrate the opposite relationship. A comparison of the effect of changing thickness on two different coatings established another important relationship between thickness response and coating modulus.

High modulus polymeric materials were shown to be a requirement to achieve pull-off peak stress that consistently decreases with thickness in a manner that can be modeled by Equation 5.1. The critical modulus for this relationship inversion from

negative to positive depends on the coating adhesion as well, and therefore several important and interdependent variables were shifting and often in different ways and magnitudes. Mechanical properties were shown to be important, and we have already established that mechanical properties are thermally dependent. If coating mechanical yielding occurred during pull-off testing in advance of catastrophic interfacial failure, then the measured peak stress was proven to increase with respect to thickness. Mechanical yielding represents molecular shifts in energy dissipation and increases the modes of available dissipation mechanisms and, in turn, increases the difficulty of separating the polymer-substrate surfaces and these values, albeit real, can be misleading depending upon the modes of damage and the rates of deformation but these values do not necessarily correlate with the interfacial strength.

During the course of our research, we also established that solvent trapping, a common phenomenon whereby solvent persists permanently at different concentrations within coatings and dependent upon many other overlooked variables. Variables that affect trapped solvent concentration and location include the degree of conversion at application, application method, the relative rate of evaporation versus degree of cure up to the point of vitrification (very complex and dependent upon the physical state, gelation, and environmental conditions, see the dissertation work of Mark Early for greater depth).[114] Solvent trapping in our research led to the asymmetrical plasticization of coatings, further changing the adhesion-thickness relationship. Unlike any previous attempt at quantifying adhesion with respect to thickness, when solvents were introduced, each system's material properties each become dependent upon thickness. Increasing thickness was found to increase the weight percent of trapped solvent linearly, and that

subsequently affected the modulus, the momentary measured average glass transition temperature, and the work of adhesion. When a high modulus coating was applied with solvent, two distinctly different thickness ranges emerged. A critical thickness delineated the regions of negative and positive relationships for internal stress versus thickness. Below the critical thickness, experimental peak stresses could still be predicted using the energy balance model shown in Equation 5.1. As thickness increased beyond the critical thickness-threshold, the measured adhesion steadily increased instead of the predicted and often cited consistent decrease with respect to thickness, as was the case for the solvent-free high modulus materials. The critical thickness was shown to be complex, and the coatings that exhibit critical thicknesses and relationship inversions appear to not possess a spontaneous delamination thickness that would have been predicted by the energy balance model, but performance at higher film thickness values (beyond practical for most coatings) could provide greater insight and understanding on the millimeter thickness range as to how the interfacial chains behave.

Adjusting the trapped residual solvent content using cure temperature variables was found to influence the critical thickness position. Increasing the maximum temperature of cure resulted in greater solvent evaporation/emission and resulted in films with reduced weight percent solvent at all thicknesses. As a consequence, the thickness needed to accumulate enough solvent to initiate yielding prior to catastrophic failure during a pull-off experiment constantly increased. Calculated internal stress was affected by and was shown to be interdependent on the change in cure temperature as a result of varying degrees of relaxation, differentials in the coefficient of thermal expansion, and differential in free volume. In bulk applied polymeric materials, the added thermal

shrinkage from cooling after cure increased the calculated internal stress values with respect to cure temperature. Conversely, when fitting peak stress data from films with thicknesses below the critical thickness in the solvent containing films, increasing cure temperature resulted in decreased calculated internal stress. We hypothesized that lowering the total residual solvent volume resulted in less variation in solvent concentration gradients between the air and the substrate interface for equivalent films cured at higher temperatures.

Bulk applied low modulus coatings that experienced a positive relationship between thickness and adhesion exhibited thickness independence once solvents were used during application. Incorporating solvents into the low modulus coating seems to be analogous to the decrease in adhesion with increasing temperature exhibited in Chapter II when T_g normalized temperature testing was utilized. Low modulus coatings with added residual solvent have the capacity for mechanical yielding during pull-off testing, just as was the case in bulk systems, but with the added solvent, the interface in our examples exhibited reduced pull-off adhesion values. The concept was also connected to Chapter II in that the percent of interfacial bonding sites for polymer was reduced by the presence of solvent (i.e., substrate surface sites were occupied by interacting with solvent instead of polymer). A combination of solvolysis of interfacial secondary interactions and increased chain mobility lead to the same weakened interface as test temperatures above T_g-20 °C, where all of our data exhibited drastically reduced adhesion. Trapped solvent reduced polymer T_g towards room temperature, inducing the same effect of moving T_g relative to the temperature test conditions, which was shown to be critically important. It

was envisioned that solvents could drive higher or lower adhesion values, depending on other variables.

- A high modulus material applied in bulk at a specified low thickness has few modes of mechanical energy dissipation and therefore resists mechanical stresses to maintain good adhesion purely through a lack of internal stress and good load transfer
- Plasticization of the high modulus material through solvent trapping or thermal energy changes the bulk and interfacial properties simultaneously.
- At low loadings of solvent or thermal energy, the interface is affected more than the bulk, and the added chain mobility increases mechanically measured adhesion, which also allows for mechanical yielding prior to interfacial failure, further increasing force required to separate the surfaces
- Further plasticization to a leathery material sees a reduction in adhesion as interfacial functional groups are free to associate with the bulk or solvent, and mechanically measured adhesion value is dominated by the rapidly decreasing modulus value
- At greater coating thickness in bulk, internal stress is significant, and the act of straining results in significant transverse shrinkage due to Poisson's ratio leading to a much lower mechanically measured adhesion
- Reductions in adhesion due to internal stress can be eliminated with plasticization as well such that adhesion increases at higher thicknesses and mechanical yielding takes place before an interfacial failure

- A low modulus material applied in bulk does not require external plasticization to experience mechanical yielding prior to interfacial failure. Adhesion is at its peak in bulk at room temperature.
- Plasticization through solvent or temperature leads directly to the leathery modulus driven loss of adhesion.

Finally, the effects of solvent on the adhesion-thickness relationship were explored through varying solids content. Increasing solvent loading in the high modulus coating maintained the bimodal result, i.e., a two-phase relationship between adhesion and thickness. For a constant cure temperature, the critical thickness of adhesion relationship inversion decreases as %solids decreased, which was predicted with the increased levels of solvent trapping. The consistent higher concentration of solvent detected at the substrate interface in high thickness films led to the gradual decline of the positive relationship between pull-off peak stress and thickness above the critical thickness. An unexpected outcome of the additional solvent is the increase of noise in the adhesion results, and this is problematic but also the reality of changing solvent/polymer/substrate interfacial dynamics. The average value of pull-off peak stress decreased with respect to the thickness in the low thickness region demarcated by the critical thickness, but the data results exhibited a higher standard deviation at any single thickness was greater with respect to peak stress. A sizable portion of the peak stress noise comes from the variation in dry film thickness, and these are real but problematic issues when applying, curing, and testing polymer-based coatings. Because of the low viscosity at application, a wide range of thicknesses were achieved for the same applied thickness. This demonstrated that the highest peak stresses came from those coatings

applied at high thicknesses and lower solids and, as a result, achieved low thickness; these data demonstrated the path function nature of adhesion development. The implication is that two films of the same thickness and residual solvent content formed using the same cure profile could possess different adhesions depending on how that final film was reached. These data suggest that applying coatings at low viscosities allows for improved orientational freedom such that a low viscosity solution applied at a high wet film thickness and allowed to spread will produce a stronger interface over a higher viscosity solution applied at a wet film thickness more closely resembling the dry film thickness.

This dissertation has established that achieving good adhesion involves a very complex interplay between materials and environmental conditions; many interdependent variables impact the ability to even measure good adhesion, much less achieve higher adhesion values. Adhesion results were shown to be dependent upon thickness, material composition and type, temperature, internal stress, solids content at application, solids content once applied, and solids content after vitrification or cessation of flow. Furthermore, each of these variables is also codependent or at least interdependent. Since most coatings scientists consider the loss of a coating's adhesion to the substrate to be a point of major failure, it was critically important to know that reliably measured adhesion performance was varying in advance of catastrophic failure and when the environmental conditions and the threshold minimum interfacial adhesion coexist then catastrophic failure will occur, however smaller subsets of failure or potential failure are also occurring in intermittent or prolonged periods of time based upon many complex variables. Therefore it is recommended at a minimum that coatings scientists measure

adhesion much like a performance parameter variable; adhesion performance maps could potentially drive new variables to be used to reduce the likeliness of crossing any critical performance threshold and allowing the polymer to be released from the substrate in an easy and facile manner. With low noise, reliable, and carefully interpreted adhesion data, it is possible to use those data in service life prediction models and in remaining service life prediction models for slow processes of coating failure, e.g., corrosion initiation and prolonged but steadily decreased polymer-substrate interfacial connectivity.

Future work includes supporting the present findings and hypotheses, along with pushing coating performance prediction accuracy. Relationships between thickness and temperature will be explored for other coating chemistries. The focus will be placed on more accurately defining the modulus requirement suggested by this work. Identifying peak adhesion with thermal plasticization on thermoplastic and thermoset coatings with and without fillers is of interest in order to potentially find limits to the relationship. Afterward, chain mobility could be purposefully engineered and modified to determine the role interfacial flexibility plays in the gain and loss of adhesion with plasticization.

The thermal plasticization method of adhesion analysis will be probed on coating systems with significantly different interfaces, and the results will be correlated with performance. Silane and additive adhesion promoters will be employed to quantify their adhesion at a constant thermal distance from $T_{g,}$ and then interfacial failure will be investigated in a variety of conditions. When considering the mechanical nature of the tests, the most probable correlation will be with resistance to mechanical stimuli like steps and bumps, so fatigue testing will be used. The intention of the constant T_g-T testing protocol is to make distinctions between interfacial strength, which influences

coating performance against chemical and environmental stimuli. Salt fog, Prohesion, and field testing outcomes are expected to correlate more directly with adhesion measurements at constant T_g-T than constant test temperature.

Pull-off adhesion testing specifically has significant potential but needs attention to standardize the procedure. Parameters of the testing procedure, such as accessory geometry and sample orientation, have the potential to influence the stress-strain response but have yet to be investigated. There's a certain level of understanding about how to improve the dolly-adhesive interface, but it has never been optimized. Scoring with the Dremel tool is also not ideal, and future work would include designing improved scoring techniques. Finding and resolving sources of variation in pull-off adhesion testing is an important cornerstone to support all subsequent research efforts with the method.

In the broad scope, this research provides a foundation and direction for approaching coating performance prediction from both the standpoint of advancing the understanding of coating adhesion and the methods of analyzing it. By demonstrating how mechanical methods of adhesion measurement can be used to advance the scientific study of full-scale coating systems, the underlying relationships can be more readily established.

APPENDIX A – Peel adhesion data processing for Chapter II

A.1.1 Peel Force Instrument Output - Interpretation and Processing

Processing the raw force versus extension output by the MTS to a single representative peel force is not trivial. Conclusions can be skewed depending on how the output is interpreted. An example of peel force data as it is exported from the instrument is presented in Figure A.1 for LTg at 39 °C. There was a plateau indicating the adhesion strength but defining where the plateau starts, and the range of extension to average peel force values over was not straightforward. The default way the TestWorks software outputs and report the data is as "peak load," but considering the data/instrument noise, peak load was not considered accurate. One option for determining the extension where the plateau initiates is to take the derivative of the load. Ideally, the plateau is demarcated by the extension region where derivative load equals zero and peel force can be taken as an average of forces corresponding to extension in the plateau region, but noise in the force values is enough that derivative force crossed zero well before the average was zero (Figure A.2). This poses the same problem as in the force-extension output of figuring out where the derivative was truly zero.

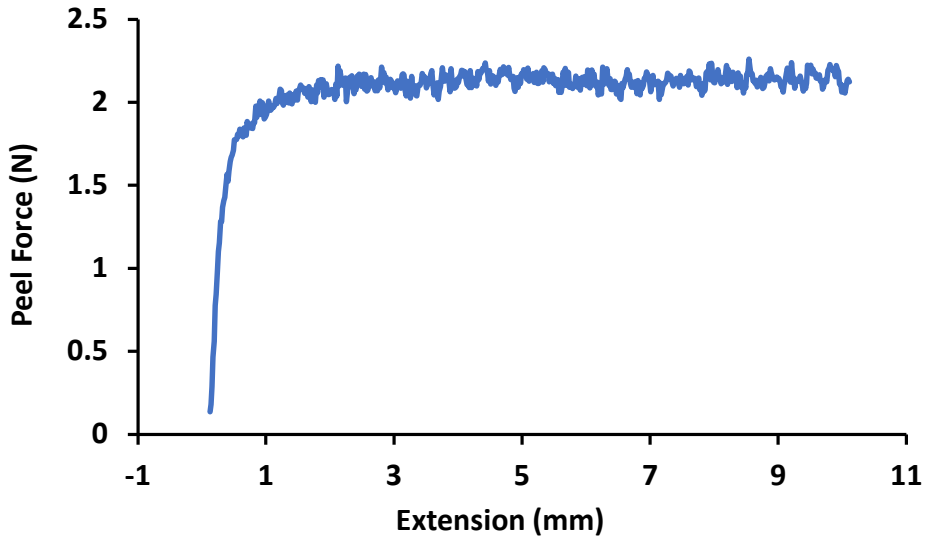

Figure A.1 Example Load cell output from a 1 cm long peel adhesion test from the

Sample shown is LTg tested at 39 °C prepared on AA 2024 and cured for two hours at 60 °C and one hour at 80 °C

The method used here to determine the start of the plateau was to calculate the sum of all derivative values over incrementally smaller distances starting from extension = 0 mm. The extension value that corresponds to the sum of all subsequent derivative values equaling zero is then used as the critical extension point, and all peel forces with extensions greater than that critical extension are averaged together to give the representative peel force. Figure A.2 presents the derivative of LTg peel force data, alongside the sum of all derivative values from extension = x to the endpoint of 10 mm. When the sum of subsequent derivatives becomes, zero is the point where the derivative is effectively zero. The extension where the average of derivative values first becomes negative would also work, and in this example sample, both numerical methods indicate the same critical extension value (1.842 mm). With that critical extension, the average peel force from 1.842 mm extension to 10 mm is 2.13 N, and that value will be used to indicate the adhesion of LTg at 39 °C in the following figures.

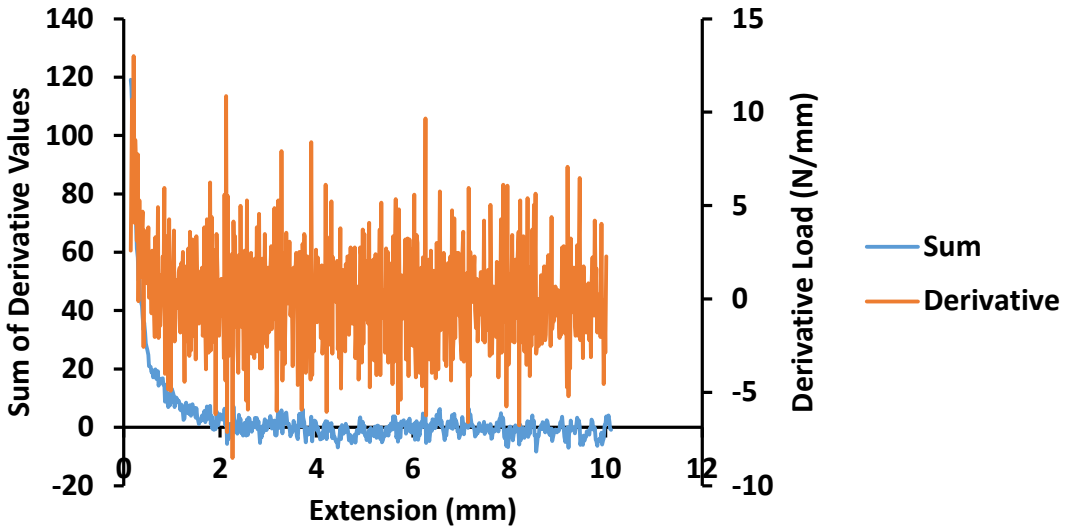

Figure A.2 Derivative of peel force output compared with a plot of points of the form (extension, the summation of derivative values of greater extension)

To demonstrate the large amount of noise in the derivative and the inaccuracy of using when derivative first equals zero versus the sum of subsequent derivative values.

APPENDIX B Iterative Calculation Process for Finding Fitting Parameters

In Chapters III and IV, pull-off peak stress results were fit to an empirical model equation (Equation B.1). Variables in the equation include pull-off peak stress (σ_z), work of adhesion (γ), coating thickness (t_c), Young's modulus (E), and internal stress (σ). Of these variables, only E, t_c, and σ_z were measured, σ and γ were estimated by an iterative fitting method.

$$\sigma_z = \sqrt{\frac{4.286E\gamma}{t_c} - 2.572\sigma^2} \qquad \text{Equation B.1}$$

After narrowing down data sets through outlier calculations to their representative points, the subsets of pull-off data were used to calculate a best-fit curve. The work of adhesion was calculated first using one experimental data point (thickness and peak stress) as a seed value in a rearrangement of Equation B.1 shown in Equation B.2. In this initial calculation, a guess value is used for the internal stress, usually 0.1 MPa. The resulting work of adhesion, Young's modulus measured in tensile tests, and the guess internal stress are the basis for the first model for predicting pull-off peak stress from coating thickness.

$$\gamma = \frac{t_c}{4.286E}(\sigma_z{}^2 + 2.572\sigma^2) \qquad \text{Equation B.2}$$

No matter what internal stress guess value was used, the predictive curve includes the seed value. At this point, the accuracy of the model is quantified by calculating the residuals between the experimental points and calculated points. Considering that both the thickness and the peak stress could be incorrect, the distance between the experimental data point and a point on the curve is calculated by the point distance formula (Equation B.3) between a data point and the closest point on the predictive curve.

An example data set with the closest points along the curve highlighted is shown in Figure B.1. A solving tool was then used to find the internal stress that results in the lowest sum of residuals. After finding the best internal stress for the first seed value and the associated sum of residuals, another experimental data point is used as a seed value. The process is repeated until a global minimum of residuals is found. Reported internal stresses are the value that minimizes the residual of the curve based on the seed value that leads to the lowest total residual.

$$\text{Residual} = \sqrt{\left(t_{c.exp} - t_{c.cal}\right)^2 + \left(\sigma_{z.exp} - \sigma_{z.cal}\right)^2} \qquad \text{Equation B.3}$$

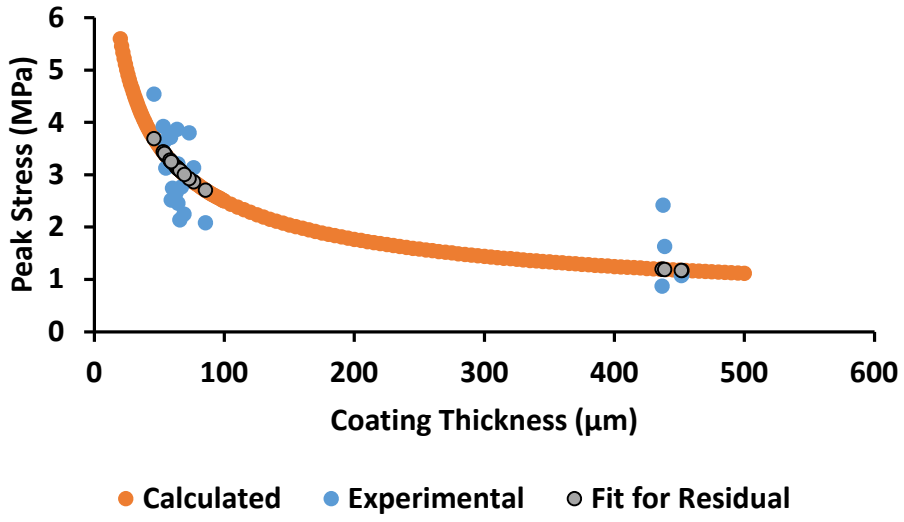

Figure B.1 Example peak stress data (blue) and the best fit curve (orange) including the points along the curve that residuals were measured from (grey)

REFERENCES

(1) Kittel, J.; Celati, N.; Keddam, M.; Takenouti, H. Influence of the Coating-Substrate Interactions on the Corrosion Protection: Characterisation by Impedance Spectroscopy of the Inner and Outer Parts of a Coating. *Prog. Org. Coatings* **2003**, *46* (2), 135–147. https://doi.org/10.1016/S0300-9440(02)00221-7.

(2) Wan, K.; Li, J.; Xu, W.; Yu, L.; Hou, B.; Liu, M. Enhanced Interphase Adhesion and Anticorrosion Properties in Epoxy Coating Modified via Acrylic Resin. *Int. J. Electrochem. Sci.* **2016**, *11* (11), 8914–8926. https://doi.org/10.20964/2016.11.06.

(3) Funke, W.; Haagen, H. Empirical or Scientific Approach to Evaluate the Corrosion Protective Performance of Organic Coatings. *Ind. Eng. Chem. Prod. Res. Dev.* **1978**, *17* (1), 50–53. https://doi.org/10.1021/i360065a014.

(4) Al-Khaldi, T. A.; Lyon, S. B. The Effect of Interfacial Chemistry on Coating Adhesion and Performance: A Mechanistic Study Using Aminobutylphosphonic Acid. *Prog. Org. Coatings* **2012**, *75* (4), 449–455. https://doi.org/10.1016/j.porgcoat.2012.06.011.

(5) Funke, W. How Organic Coating Systems Protect Against Corrosion. *ACS Symp. Ser.* **1986**, 222–228.

(6) Bouchet, J.; Roche, A.-A. The Formation of Epoxy/Metal Interphases: Mechanisms and Their Role in Practical Adhesion. *J. Adhes.* **2002**, *78* (9), 799–830. https://doi.org/10.1080/00218460213836.

(7) Tape Adhesion Test for Paint Finishes. General Motors: Warren, MI 2002, pp 1–6.

(8) Sims, M. K.; Juda, W. J.; Haltom, B. C. Impact of Silanes on the Solution Stability of Latex and Ultimate Paint Film Properties. *Waterborne Symp.* **2020**.

(9) Schuman, T.; Thames, S. F. Coating Solvent Effects Producing Adhesion to Molded Plastic Parts. *J. Adhes. Sci. Technol.* **2005**, *19* (13–14), 1207–1235. https://doi.org/10.1163/156856105774429109.

(10) Subramanian, V.; Van Ooij, W. J. Silane Based Metal Pretreatments as Alternatives to Chromating. *Surf. Eng.* **1999**, *15* (2), 168–172. https://doi.org/10.1179/026708499101516407.

(11) Jaehne, E.; Oberoi, S.; Adler, H.-J. P. Ultra Thin Layers as New Concepts for Corrosion Inhibition and Adhesion Promotion. *Prog. Org. Coatings* **2008**, *61* (2–4), 211–223. https://doi.org/10.1016/j.porgcoat.2007.09.044.

(12) Palanivel, V.; Huang, Y.; Van Ooij, W. J. Effects of Addition of Corrosion Inhibitors to Silane Films on the Performance of AA2024-T3 in a 0.5 M NaCl Solution. *Prog. Org. Coatings* **2005**, *53* (2), 153–168. https://doi.org/10.1016/j.porgcoat.2003.07.008.

(13) Palanivel, V.; Van Ooij, W. J. Modified Silane Coating as an Alternative to Chromates for Corrosion Protection of Aluminum Alloys. *Silanes and Other Coupling Agents* **2004**, *3* (9), 135–159. https://doi.org/10.1017/CBO9781107415324.004.

(14) Mirabedini, S. M.; Scantlebury, J. D.; Thompson, G. E.; Moradian, S. Adhesive Strength of Powder Coated Aluminium Substrates. *Int. J. Adhes. Adhes.* **2005**, *25* (6), 484–494. https://doi.org/10.1016/j.ijadhadh.2005.01.005.

(15) ASTM. Standard Test Methods for Measuring Adhesion by Tape Test. ASTM International: West Conshohocken, PA 2009.

(16) Tsaur, A.T.; Tsaur, T. Peel Adhesion as a Function of Peel Angle, Peel Rate, and

Peel Temperature.

(17) Kinloch, A. J.; Lau, C. C.; Williams, J. G. The Peeling of Flexible Laminates. *Int. J. Fract.* **1994**, *66* (1), 45–70. https://doi.org/10.1007/BF00012635.

(18) Hu, D.-C.; Chen, H.-C. Humidity Effect on Polyimide Film Adhesion. *J. Mater. Sci.* **1992**, *27* (19), 5262–5268. https://doi.org/10.1007/bf00553402.

(19) Fletcher, J. F.; Barnes, D. J. *Pull-off Adhesion Testing of Coatings - Improve Your Technique*; 2015.

(20) Harries, K. A.; Sweriduk, M. E. Factors Affecting Direct Tension Pull-Off Test Results of Materials Bonded to Concrete. *Adv. Civ. Eng. Mater.* **2016**, *5* (1), 20160046. https://doi.org/10.1520/acem20160046.

(21) Maxwell, A. S. *Comparison of Coating Adhesion Values Obtained from ASTM D4541 and ASTM C633 Pull-off Tests*; 2004.

(22) Yu, C.; Ju, P.; Wan, H.; Chen, L.; Li, H.; Zhou, H.; Chen, J. Designing a PAI/PTFE Coating with Enhanced High-Temperature Tribological Properties by S8-POSS: Solid-Liquid Dual Lubrication. *Prog. Org. Coatings* **2020**, *145* (January), 105667. https://doi.org/10.1016/j.porgcoat.2020.105667.

(23) Wang, Y.; Chen, C.; Wu, X.; Wang, Z.; Wen, S.; Yu, J.; Yan, C.; Cong, W. Improved Antibiofouling Properties of Photobioreactor with Amphiphilic Sulfobetaine Copolymer Coatings. *Prog. Org. Coatings* **2020**, *144* (February), 105666. https://doi.org/10.1016/j.porgcoat.2020.105666.

(24) Haramagatti, C. R.; Nikam, P.; Bhavsar, R.; Kamath, V.; Sawant, V. S. Stability Assessment of Iron Oxide Yellow Pigment Dispersions and Temperature Dependent Implications of Rheological Measurements. *Prog. Org. Coatings* **2020**,

144 (February), 105669. https://doi.org/10.1016/j.porgcoat.2020.105669.

(25) Ollendorf, H.; Schneider, D. A Comparative Study of Adhesion Test Methods for Hard Coatings. *Surf. Coatings Technol.* **1999**, *113* (1–2), 86–102. https://doi.org/10.1016/S0257-8972(98)00827-5.

(26) Marsh, J.; Scantlebury, J. D.; Lyon, S. B. The Effect of Surface/Primer Treatments on the Performance of Alkyd Coated Steel. *Corros. Sci.* **2001**, *43* (5), 829–852. https://doi.org/10.1016/S0010-938X(00)00070-6.

(27) Cros, B.; Vallat, M. F.; Augereau, F. Characterization of Aluminium Coated Poly(Ethylene Terephtalate) Films by Acoustic Microscopy. *J. Mater. Sci.* **1997**, *32* (10), 2655–2660. https://doi.org/10.1023/A:1018671005485.

(28) Rats, D.; Hajek, V.; Martinu, L. Micro-Scratch Analysis and Mechanical Properties of Plasma-Deposited Silicon-Based Coatings on Polymer Substrates. *Thin Solid Films* **1999**, *340* (1), 33–39. https://doi.org/10.1016/S0040-6090(98)01338-8.

(29) Kawai, J.; Adachi, H.; Kitajima, Y.; Maeda, K.; Hayakawa, S.; Gohshi, Y. Inelastic Mean Free Path of Photoelectrons in Ag Determined by Total Reflection X-Ray Photoelectron Spectroscopy. *Anal. Sci.* **1997**, *13* (5), 797–801. https://doi.org/10.2116/analsci.13.797.

(30) Turunen, M. P. K.; Marjamäki, P.; Paajanen, M.; Lahtinen, J.; Kivilahti, J. K. Pull-off Test in the Assessment of Adhesion at Printed Wiring Board Metallisation/Epoxy Interface. *Microelectron. Reliab.* **2004**, *44* (6), 993–1007. https://doi.org/10.1016/j.microrel.2004.01.001.

(31) Croll, S. G. Adhesion Loss Due to Internal Strain. *J. Coatings Technol.* **1980**, *52*

(665), 35–43.

(32) Baek, Y. H.; Chung, M. K.; Son, S. M.; Song, E. H.; Shin, C. S.; Baek, K. K. Reliability on Coating Pull-off Adhesion Strength Test. *NACE - Int. Corros. Conf. Ser.* **2009**, No. 09007, 1–10.

(33) Bajat, J. B.; Dedić, O. Adhesion and Corrosion Resistance of Epoxy Primers Used in the Automotive Industry. *J. Adhes. Sci. Technol.* **2007**, *21* (9), 819–831. https://doi.org/10.1163/156856107781061512.

(34) Van Ooij, W. J.; Edwards, R. A.; Sabata, A.; Zappia, J. Testing the Adhesion of Paint Films to Metals by Swelling in N-Methyl Pyrrolidone. *J. Adhes. Sci. Technol.* **1993**, *7* (8), 897–918. https://doi.org/10.1163/156856193X00510.

(35) Engenharia, D. De; Paulo, U. D. S.; Paulo, S. Failure of Diamond-like Carbon (Dlc) Coatings in Automobile Engines -a Review. **2019**, No. June.

(36) Ebnesajjad, S.; Landrock, A. H. *Adhesives Technology Handbook*, 2nd ed.; Ebnesajjad, S., Ed.; William Andrew: Norwich, NY, 2008.

(37) Lee, I.; Wool, R. P. Thermodynamic Analysis of Polymer-Solid Adhesion: Sticker and Receptor Group Effects. *J. Polym. Sci. Part B Polym. Phys.* **2002**, *40* (20), 2343–2353. https://doi.org/10.1002/polb.10286.

(38) Guo, Z. C.; Wang, R. M.; Wang, Y. F. Application of Bilayer Silanisation Treatment to Improve Corrosion Resistance and Bond Durability of Aluminium Alloy. *Trans. Inst. Met. Finish.* **2008**, *86* (1), 55–61. https://doi.org/10.1179/174591908X264347.

(39) Öhman, M.; Persson, D.; Leygraf, C. In Situ ATR-FTIR Studies of the Aluminium/Polymer Interface upon Exposure to Water and Electrolyte. *Prog. Org.*

Coatings **2006**, *57* (1), 78–88. https://doi.org/10.1016/j.porgcoat.2006.07.002.

(40) Pauli, A. T.; Grimes, W.; Huang, S. C.; Robertson, R. E. Surface Energy Studies of SHRP Asphalts by AFM SURFACE ENERGY STUDIES OF SHRP. **2019**, No. August.

(41) Mittal, K. L.; Kern, W. Selected Bibliography on Adhesion Measurement of Films and Coatings. *J. Adhes. Sci. Technol.* **1987**, *1* (1), 247–262. https://doi.org/10.1163/156856187x00265.

(42) Awaja, F.; Gilbert, M.; Kelly, G.; Fox, B.; Pigram, P. J. Adhesion of Polymers. *Prog. Polym. Sci.* **2009**, *34* (9), 948–968. https://doi.org/10.1016/j.progpolymsci.2009.04.007.

(43) Chen, J.; Bull, S. J. Approaches to Investigate Delamination and Interfacial Toughness in Coated Systems: An Overview. *J. Phys. D. Appl. Phys.* **2011**, *44* (3). https://doi.org/10.1088/0022-3727/44/3/034001.

(44) Briscoe, B. J. *Adhesion Measurements of Films and Coatings*; 1995; Vol. 28. https://doi.org/10.1016/0301-679x(95)90002-a.

(45) Croll, S. G.; Vetter, C. A.; Keil, B. D. Variability of Pipe Coating Pull-off Adhesion Measurements on Cylindrical Steel Pipelines. In *Pipelines 2012: Innovations in Design, Construction, Operations, and Maintenance - Doing more with Less*; 2012; pp 231–241.

(46) Perera, D. Y. On Adhesion and Stress in Organic Coatings. *Prog. Org. Coatings* **1996**, *28* (1), 21–23. https://doi.org/10.1016/0300-9440(95)00585-4.

(47) Chopra, K. L. *Thin Film Phenomenon*; 1969.

(48) Bullett, T. R.; Prosser, J. L. The Measurement of Adhesion. *Prog. Org. Coatings*

1972, *1* (1), 45–71. https://doi.org/10.1016/0300-9440(72)85003-3.

(49) Frey, H.; Khan, H. R. *Handbook of Thin-Film Technology*; 2015.

(50) Mittal, K. L. Adhesion Measurement of Thin Films. *Electrocompon. Sci. Technol.* **1976**, *3* (1), 21–42. https://doi.org/10.1155/APEC.3.21.

(51) Chapman, B. N. Thin-Film Adhesion. *J. Vac. Sci. Technol.* **1974**, *11* (1), 106–113. https://doi.org/10.1116/1.1318537.

(52) Laredo, E.; Suarez, N.; Bello, A.; Marquez, L. The Glass Transition in Linear Low Density Polyethylene Determined by Thermally Stimulated Depolarization Currents. *J. Polym. Sci. Part B Polym. Phys.* **1996**, *34* (4), 641–648. https://doi.org/10.1002/(SICI)1099-0488(199603)34:4<641::AID-POLB4>3.0.CO;2-T.

(53) Hsiao, S. H.; Yang, C. P.; Lin, W. L. Synthesis and Characterization of New Diphenylfluorene-Based Aromatic Polyamides Derived from 9,9-Bis[4-(4-Carboxyphenoxy)Phenyl]Fluorene. *Macromol. Chem. Phys.* **1999**, *200* (6), 1428–1433. https://doi.org/10.1002/(SICI)1521-3935(19990601)200:6<1428::AID-MACP1428>3.0.CO;2-J.

(54) Chatzi, E. G.; Koenig, J. L. Morphology and Structure of Kevlar Fibers: A Review. *Polym. Plast. Technol. Eng.* **1987**, *26* (3–4), 229–270. https://doi.org/10.1080/03602558708071938.

(55) Fragiadakis, D.; Pissis, P.; Bokobza, L. Glass Transition and Molecular Dynamics in Poly(Dimethylsiloxane)/Silica Nanocomposites. *Polymer (Guildf).* **2005**, *46* (16), 6001–6008. https://doi.org/10.1016/j.polymer.2005.05.080.

(56) Hofrichter, C. H.; McLaren, A. D. Temperature Dependence of the Adhesion of

High Polymers to Cellulose. *Ind. Eng. Chem.* **1948**, *40* (2), 329–331. https://doi.org/10.1021/ie50458a030.

(57) Das, G.; Banerjee, A. N. Tensile Modulus-Structure Relationship of Poly(Styrene-Co-Acrylonitrile) and Poly(Vinyl Chloride-Co-Vinyl Acetate) Blends. *J. Appl. Polym. Sci.* **1995**, *58*, 2127–2130.

(58) Wand, S. Modifying Inhibited Primer Performance via Control of Epoxy-Amine Matrix Structure and Composition. *Dissertations* **2019**, *1612*.

(59) Pistor, V.; Barbosa, L. G.; Soares, B. G.; Mauler, R. S. Relaxation Phenomena in the Glass Transition of Epoxy/N-Phenylaminopropyl - POSS Nanocomposites. *Polymer (Guildf).* **2012**, *53* (25), 5798–5805. https://doi.org/10.1016/j.polymer.2012.10.018.

(60) Patil, P. N.; Rath, S. K.; Sharma, S. K.; Sudarshan, K. Soft Matter Ether of Bisphenol-A Based Epoxy – Polyether Amine. **2013**, 3589–3599. https://doi.org/10.1039/c3sm27525f.

(61) Hansen, C. M.; Wallström, E. On the Use of Cohesion Parameters to Characterize Surfaces. *J. Adhes.* **1983**, *15* (3–4), 275–286. https://doi.org/10.1080/00218468308073232.

(62) Hansen, C. M. *Hansen Solubility Parameters: A User's Handbook*; 2013; Vol. 53. https://doi.org/10.1017/CBO9781107415324.004.

(63) Iyer, K. A. Chain Mobility , Secondary Relaxation , and Oxygen Transport in Terephthalate Copolyesters with Rigid and Fl Exible Cyclic Diols. *Polymer (Guildf).* **2017**, *129*, 117–126. https://doi.org/10.1016/j.polymer.2017.09.049.

(64) Neumann, A. W.; Tanner, W. The Temperature Dependence of Contact Angles n

Polytetrafluoroethylene / n-Decane. *J. Colloid Interface Sci.* **1970**, *34* (1), 1–8.

(65) Kendall, K. Thin-Film Peeling-the Elastic Term. *J. Phys. D. Appl. Phys.* **1975**, *8* (13), 1449–1452. https://doi.org/10.1088/0022-3727/8/13/005.

(66) Kisin, S. Adhesion Changes at Metal–Polymer Interfaces: Study of the Copper–(Acrylonitrile–Butadiene–Styrene) System, 2007, Vol. Philosophy. https://doi.org/10.6100/IR617210.

(67) Venkataraman, S. Continuous Microscratch Measurements of the Practical and True Works of Adhesion for Metal / Ceramic Systems. **1996**, 3133–3145.

(68) Hui, C.; Glassmaker, N. J.; Tang, T.; Jagota, A. Design of Biomimetic Fibrillar Interfaces : 2 . Mechanics of Enhanced Adhesion. **2004**, No. July, 35–48. https://doi.org/10.1098/rsif.2004.0005.

(69) Feldstein, M. M.; Siegel, R. A. Molecular and Nanoscale Factors Governing Pressure-Sensitive Adhesion Strength of Viscoelastic Polymers. *J. Polym. Sci. Part B Polym. Phys.* **2012**, *50* (11), 739–772. https://doi.org/10.1002/polb.23065.

(70) Croll, S. G. ADHESION LOSS DUE T O INTERNAL STRAIN. *J. Coatings Technol.* **1980**, *52* (665), 35–43.

(71) Tran, P.; Kandula, S. S.; Geubelle, P. H.; Sottos, N. R. Comparison of Dynamic and Quasi-Static Measurements of Thin Film Adhesion. *J. Phys. D. Appl. Phys.* **2011**, *44* (3). https://doi.org/10.1088/0022-3727/44/3/034006.

(72) Keimel, F. A.; Harrington, W. F.; Schultz, J.; Nardin, M.; Packham, D. E.; Chehimi, M. M.; Azioune, A.; Cabet-Deliry, E.; Joanny, J.-F.; Pizzi, A.; Kolluri, O. S.; Walker, P.; DeVries, K. L.; Borgmeier, P. R. *Handbook of Adhesive Technology*, 2nd ed.; Pizzi, A., Mittal, K. L., Eds.; Taylor & Francis, 2003.

(73) Haubrich, J.; Löbbecke, M.; Watermeyer, P.; Wilde, F.; Requena, G.; da Silva, J. Buried Interfaces – A Systematic Study to Characterize an Adhesive Interface at Multiple Scales. *Appl. Surf. Sci.* **2018**, *433*, 546–555. https://doi.org/10.1016/j.apsusc.2017.10.015.

(74) Meng, F.; Liu, Y.; Liu, L.; Li, Y.; Wang, F. Studies on Mathematical Models of Wet Adhesion and Lifetime Prediction of Organic Coating/Steel by Grey System Theory. *Materials (Basel).* **2017**, *10* (7), 1–15. https://doi.org/10.3390/ma10070715.

(75) Roche, A.-A.; Dole, P.; Bouzziri, M. Measurement of the Practical Adhesion of Paint Coatings to Metallic Sheets by the Pull-off and Three-Point Flexure Tests. *J. Adhes. Sci. Technol.* **1994**, *8* (6), 587–609. https://doi.org/10.1163/156856194X00366.

(76) Arrospide, E.; Bikandi, I.; Garcia, I.; Durana, G.; Aldabaldetreku, G.; Zubia, J. Mechanical Properties of Polymer-Optical Fibres. In *Polymer Optical Fibers: Fiber types, materials, fabrication, characterisation and applications*; 2017; pp 201–215. https://doi.org/10.1016/B978-0-08-100039-7.00007-5.

(77) Standard Test Method for Pull-off Strength of Coatings Using Portable Adhesion Testers. American Society for Testing and Materials 1995.

(78) *Adhesion Aspects of Polymeric Coatings.*; 1983.

(79) Bouchet, J.; Roche, A. A.; Hamelin, P. Internal Stresses, Young's Modulus and Practical Adhesion of Organic Coatings Applied onto 5754 Aluminum Alloy. *Thin Solid Films* **1999**, *355*, 270–276. https://doi.org/10.1016/S0040-6090(99)00449-6.

(80) Myers, J. J.; Washer, G. *Structural Steel Coatings for Corrosion Mitigation*; 2010.

(81) Belghazi, A.; Bohm, S.; Sullivan, J. H.; Worsley, D. A. Zinc Runoff from Organically Coated Galvanised Architectural Steel. *Corros. Sci.* **2002**, *44* (8), 1639–1653. https://doi.org/10.1016/S0010-938X(01)00176-7.

(82) Leth-Olsen, H.; Nisancioglu, K. Filiform Corrosion of Aluminium Sheet. I. Corrosion Behaviour of Painted Material. *Corros. Sci.* **1998**, *40* (7), 1179–1194. https://doi.org/10.1016/S0010-938X(98)00026-2.

(83) Brenna, A.; Bolzoni, F.; Beretta, S.; Ormellese, M. Long-Term Chloride-Induced Corrosion Monitoring of Reinforced Concrete Coated with Commercial Polymer-Modified Mortar and Polymeric Coatings. *Constr. Build. Mater.* **2013**, *48*, 734–744. https://doi.org/10.1016/j.conbuildmat.2013.07.099.

(84) Selvaraj, R.; Selvaraj, M.; Iyer, S. V. K. Studies on the Evaluation of the Performance of Organic Coatings Used for the Prevention of Corrosion of Steel Rebars in Concrete Structures. *Prog. Org. Coatings* **2009**, *64* (4), 454–459. https://doi.org/10.1016/j.porgcoat.2008.08.005.

(85) Drozdz, S. A.; Greigger, P. P.; Fruge, R.; Benton, S. D. *Application of Corrosion- and Fire-Resistant Coating Systems on Buildings 227 and 299 at Rock Island Arsenal*; 2009.

(86) Schmidt, H.; Langenfeld, S.; Naß, R. A New Corrosion Protection Coating System for Pressure-Cast Aluminium Automotive Parts. *Mater. Des.* **1997**, *18* (4–6), 309–313. https://doi.org/10.1016/s0261-3069(97)00070-8.

(87) Suay, J. J.; Rodríguez, M. T.; Izquierdo, R.; Kudama, A. M.; Saura, J. J. Rapid Assessment of Automotive Epoxy Primers by Electrochemical Techniques. *J. Coatings Technol.* **2003**, *75* (945), 103–111. https://doi.org/10.1007/bf02720157.

(88) Twite, R. L.; Bierwagen, G. P. Review of Alternatives to Chromate for Corrosion Protection of Aluminum Aerospace Alloys. *Prog. Org. Coatings* **1998**, *33* (2), 91–100. https://doi.org/10.1016/S0300-9440(98)00015-0.

(89) Rosales, B. M.; Di Sarli, A. R.; De Rincón, O.; Rincón, A.; Elsner, C. I.; Marchisio, B. An Evaluation of Coil Coating Formulations in Marine Environments. *Prog. Org. Coatings* **2004**, *50* (2), 105–114. https://doi.org/10.1016/j.porgcoat.2003.12.002.

(90) Mateo, M. P.; Piñon, V.; Nicolas, G. Vessel Protective Coating Characterization by Laser-Induced Plasma Spectroscopy for Quality Control Purposes. *Surf. Coatings Technol.* **2012**, *211*, 89–92. https://doi.org/10.1016/j.surfcoat.2012.01.018.

(91) Lee, S. H.; Oh, W. K.; Kim, J. G. Acceleration and Quantitative Evaluation of Degradation for Corrosion Protective Coatings on Buried Pipeline: Part II. Application to the Evaluation of Polyethylene and Coal-Tar Enamel Coatings. *Prog. Org. Coatings* **2013**, *76* (4), 784–789. https://doi.org/10.1016/j.porgcoat.2012.12.006.

(92) Howard, R. L.; Zin, I. M.; Scantlebury, J. D.; Lyon, S. B. Inhibition of Cut Edge Corrosion of Coil-Coated Architectural Cladding. *Prog. Org. Coatings* **1999**, *37* (1), 83–90. https://doi.org/10.1016/S0300-9440(99)00059-4.

(93) Lei, H.; Francis, L. F.; Gerberich, W. W.; Scriven, L. E. Stress Development in Drying Coatings after Solidification. *AIChE J.* **2002**, *48* (3), 437–451. https://doi.org/10.1002/aic.690480304.

(94) Shimbo, M.; Ochi, M.; Matsuura, N. Shrinkage and Internal Stress in Curing

Process of Epoxide Resins. *Kobunshi Ronbunshu* **1981**, *38* (3), 145–151. https://doi.org/10.1295/koron.38.145.

(95) Kendall, K. The Adhesion and Surface Energy of Elastic Solids. *J. Phys. D. Appl. Phys.* **1971**, *4* (8), 1186–1195. https://doi.org/10.1088/0022-3727/4/8/320.

(96) Reedy, E. D.; Guess, T. R. Comparison of Butt Tensile Strength Data with Interface Corner Stress Intensity Factor Prediction. *Int. J. Solids Struct.* **1993**, *30* (21), 2929–2936. https://doi.org/10.1016/0020-7683(93)90204-K.

(97) Taylor, P.; Singer, I. L.; Kohl, J. G.; Patterson, M. Mechanical Aspects of Silicone Coatings for Hard Foulant Control. *Biofouling J. Bioadhesion Biofilm* **2000**, *16* (2–4), 301–309.

(98) Zhao, F.; Xue, W.; Wang, F.; Sun, J.; Lin, J.; Liu, L.; Sun, K.; Wang, L. Braided Bioresorbable Cardiovascular Stents Mechanically Reinforced by Axial Runners. *J. Mech. Behav. Biomed. Mater.* **2019**, *89* (September), 19–32. https://doi.org/10.1016/j.jmbbm.2018.09.003.

(99) Chen, L.; Li, A.; He, X.; Han, L. A Multi-Scale Biomechanical Model Based on the Physiological Structure and Lignocellulose Components of Wheat Straw. *Carbohydr. Polym.* **2015**, *133* (September), 135–143. https://doi.org/10.1016/j.carbpol.2015.07.002.

(100) Josep, V. K. *Paint and Coating Testing Manual*; 1995. https://doi.org/10.1002/col.5080200415.

(101) Edwards, D. A. A Mathematical Model for Trapping Skinning in Polymers. *Stud. Appl. Math.* **1997**, *99* (1), 49–80. https://doi.org/10.1111/1467-9590.00056.

(102) Naito, K.; Onta, M.; Kogo, Y. The Effect of Adhesive Thickness on Tensile and

Shear Strength of Polyimide Adhesive. *Int. J. Adhes. Adhes.* **2012**, *36*, 77–85. https://doi.org/10.1016/j.ijadhadh.2012.03.007.

(103) Kim, W. S.; Yun, I. H.; Lee, J. J.; Jung, H. T. Evaluation of Mechanical Interlock Effect on Adhesion Strength of Polymermetal Interfaces Using Micro-Patterned Surface Topography. *Int. J. Adhes. Adhes.* **2010**, *30* (6), 408–417. https://doi.org/10.1016/j.ijadhadh.2010.05.004.

(104) Quach, A.; Simha, R. Pressure-Volume-Temperature Properties and Transitions of Amorphous Polymers; Polystyrene and Poly (Orthomethylstyrene). *J. Appl. Phys.* **1971**, *42* (12), 4592–4606. https://doi.org/10.1063/1.1659828.

(105) Mao, X.; Yuk, H.; Zhao, X. Hydration and Swelling of Dry Polymers for Wet Adhesion. *J. Mech. Phys. Solids* **2020**, *137*. https://doi.org/10.1016/j.jmps.2020.103863.

(106) Torres, J. M.; Stafford, C. M.; Vogt, B. D. Elastic Modulus of Amorphous Polymer Thin Films: Relationship to the Glass Transition Temperature. *ACS Nano* **2009**, *3* (9), 2677–2685. https://doi.org/10.1021/nn9006847.

(107) Paik, J. K.; Thayamballi, A. K. *Ship-Shaped Offshore Installations. Design, Building and Operation*; 2007.

(108) Ringsberg, J. W.; Ulfvarson, A. Y. J. On Mechanical Interaction between Steel and Coating in Stressed and Strained Exposed Locations. *Mar. Struct.* **1998**, *11* (6), 231–250. https://doi.org/10.1016/S0951-8339(98)00015-X.

(109) Ringsberg, J. W. A Study on the Influence of Ageing of Coatings on Their Mechanical Properties and Fracture in Ballast Tanks. *Ships Offshore Struct.* **2016**. https://doi.org/10.1080/17445302.2016.1247488.

(110) Fedors, R. F. A UNIVERSAL REDUCED GLASS TRANSITION TEMPERATURE FOR LIQUIDS. *J. Polym. Sci. Polym. Lett. Ed.* **1979**, *17*, 719–722.

(111) Xu, R.; Ouhlal, A.; Schreiber, H. P. Temperature Dependence of Polymer Interaction: Relevance to Adhesion. *J. Adhes.* **2002**, *78* (2), 99–111. https://doi.org/10.1080/00218460210382.

(112) Patrick, R. L.; Brown, J. A.; Verhoeven, L. E.; Rlpling, E. J.; Mostovoy, S. Stress-Solvolytic Failure of an Adhesive Bond. *J. Adhes.* **1969**, *1* (2), 136–141. https://doi.org/10.1080/00218466908078884.

(113) Bonner, M. Controlling Air Temperature to Improve Finish Quality. *Paint & Coatings Industry*. August 2019.

(114) Early, M. R. Quantifying, Understanding, and Modelling Autocatalytic Solventborne Epoxy-Amine Cure of Polymer Films, The University of Southern Mississippi, 2020.